PLASTIC DEFORMATION OF MOLYBDENUM SINGLE CRYSTALS

Thesis Submitted in Supplication
for the Degree
of Doctor of Philosophy

by

Francisco Guiu Giralt

Department of Physical Metallurgy
Imperial College
University of London

April 1965

A B S T R A C T

Molybdenum single crystals have been grown by the electron beam floating zone melting technique in a vacuum of 10^{-6} to 10^{-7} torr. Tensile specimens, with the deformation axis orientated in the <110> and <100> directions, and in a direction near the centre of the unit stereographic triangle, have been prepared by surface grinding. The amount of deformation introduced during the machining of the specimens was carefully controlled.

The effect of orientation on the yield and flow stress of the single crystals is investigated over the temperature range 413°K to 77°K. At temperatures $\leq$ 300°K the proportional limit and work-hardening rate is strongly orientation dependent. At temperatures >300°K the proportional limit is practically independent of the orientation, and the crystals can experience a large uniform elongation. Crystals with the tensile axis orientated in a direction near the centre of the stereographic triangle exhibit three work-hardening stages.

After a study of the active slip systems, at various temperatures, an explanation is suggested for the softening observed at temperatures >300°K.

The temperature and strain rate dependence of the flow stress is investigated for crystals with

⟨100⟩ and ⟨110⟩ orientation. A model is proposed to explain both the effect of the orientation and the temperature and strain rate sensitivity of the yield and flow stress. This model is based on the existence of two simultaneous thermally activated processes. One is the non-conservative movement of jogs in screw dislocations and the other is the overcoming of an intrinsic lattice friction. The magnitude of the lattice friction at $0^{\circ}K$ is of the order of 10 kg/mm^2.

TABLE OF CONTENTS

C H A P T E R 1.

GENERAL INTRODUCTION

Plastic Deformation of b.c.c. Metals

1.1. Preliminary Remarks

It is well known that the main characteristic features of the b.c.c. transition metals are the strong temperature and strain rate dependence of the yield stress, and the large decrease or complete loss of ductility at low temperatures. In fact all of them, with the exception of tantalum, undergo a change from ductile to brittle behaviour when the temperature is lowered.

The problem of the ductile-brittle transition which is believed to be closely related to the rapid increase in the yield stress which preceeds the onset of brittleness, has stimulated in the last decade a considerable amount of research into the mechanisms of yielding and flow of these metals.

Much useful information has been obtained in the past from the study of polycrystalline materials of commercial purity, and the effect of temperature, strain rate, grain size, and impurity content on the yield stress of the b.c.c. metals has now been

clearly established.

However, the study of single crystals of high purity is of the greatest importance when a special knowledge of the actual atomic mechanisms which govern the deformation behaviour is required. Although in the last few years this study has been facilitated by advances in the techniques of preparation of single crystals, the information on the mechanical properties of b.c.c. single crystals is at present scarce and inconsistent.

The present investigation is an attempt to understand some of the discrepancies which have become apparent from a review of the present state of knowledge of the deformation of the transition b.c.c. metals.

1.2. The Yield Point Phenomenon

Both single crystals and polycrystals of b.c.c. metals of low purity exhibit discontinuous yielding, or a pronounced drop in load in the early stages of the deformation. The first explanation of this phenomenon was proposed by Cottrell (1948) and Cottrell and Bilby (1949) in terms of the dislocation-locking effect of certain solute atoms which may migrate to dislocations and form 'atmospheres' about them. Yielding can occur when the stress is high

enough to free the dislocations from their impurity atmospheres, and once the deformation is initiated, a yield point or drop in load can be observed because the stress necessary to keep the free dislocations moving is smaller than the unpinning stress.

This theory has been able to explain satisfactorily the effect of the impurities on the yielding of b.c.c. metals. It was also able to account for the temperature and strain rate dependence of the yield stress, because the unpinning or unlocking process can be thermally aided (Cottrell and Bilby 1949, Yokobori 1952, Fisher 1955, Cottrell 1957).

However, this interpretation was unable to explain the observation that the upper yield stress, the lower yield stress, and the flow stress all exhibit the same temperature and strain rate dependence (Conrad and Schoeck 1960, Hutchison 1963). This suggested that perhaps some mechanism other than unpinning might control both the yielding and subsequent flow.

An alternative view of the yield point phenomenon was put forward by Johnston and Gilman (1959) to explain the behaviour of LiF single crystals, and subsequently the same idea was applied to the b.c.c. metals by Hahn (1962) and Cottrell (1963). This interpretation is based on the dynamic properties of

the dislocations and their rate of multiplication.

The plastic shear strain rate, $\dot{\gamma}$, produced by a number of dislocation segments, moving at an average speed v is given by (Cottrell 1953):

$$\dot{\gamma} = Lbv \qquad (1.1.)$$

where b is the Burgers vector of the dislocations and L is the number of mobile segments per unit volume.

A relationship between the strain rate and the stress can be obtained if the velocity is expressed as a function of the effective stress, τ^*, acting on the dislocation segments. The effective stress is the difference $\tau - \tau_\mu$, between the applied stress, τ, and the long range internal stress, τ_μ, that arises from the presence of other dislocations.

It has been experimentally verified by several authors that for lithium fluoride (Johnston and Gilman 1959), silicon iron (Stein and Low 1960) and tungsten (Schadler 1964) the relation between the stress and velocity is of the form:

$$v = (\tau^* / \tau_o)^m \qquad (1.2.)$$

where τ_o is the effective stress necessary to move the dislocatioms at a unit velocity, and m is a dimention-less constant. The meaning of the stress

which appears in the empirical Equation 1.2. is not altogether clear, and it is even possible that in the case of Si-Fe and tungsten it is not strictly equal to the effective stress τ^* as defined above.

Equation 1.1. can now be written as:

$$\dot{\gamma} = Lb \left(\tau^* / \tau_o \right)^m \qquad (1.3.)$$

If the initial number of mobile dislocations in a crystal (which is being deformed at a constant rate) is small, a large velocity is required to accommodate plastically the imposed strain rate, and the stress increases rapidly at the beginning of the deformation. If there is a sudden increase in the number of mobile dislocations, L, the same plastic strain rate can be maintained with a smaller dislocation velocity, and hence with a smaller stress. It is then possible that a drop in load may occur.

The conditions necessary for a crystal to exhibit a sharp yield point are: a) a rapid increase in the number of mobile dislocations, and b) a small value of m.

It is important to realise that this theory does not exclude the possibility that a yield drop may result as a consequence of a dislocation unpinning process. The conditions which may give rise to different types of yield points have been discussed

by Cottrell (1963).

Equation 1.3. not only explains the yield point phenomenon, but it may also be used to describe the subsequent deformation behaviour if the variation of both L and τ^* with strain is known. On this basis Hahn (1962) has proposed an equation to describe the deformation of the b.c.c. metals. In this approach, the variation of the stress with temperature can also be accounted for if one knows the temperature dependence of the parameters τ_o and m (Orava 1963).

This method has been particularly successful when applied to the deformation of crystals with the diamond structure (Dew-Hughes1961, 1962; Schäfer et al. 1964), because for these crystals Haasen (1957) has proposed an expression that gives explicitly the variation of the velocity, v, with the stress τ^* and the temperature.

It must be pointed out that Hahn's model is merely descriptive, since it is based only on empirical relations.[4] From a fundamental point of view the knowledge of the particular mechanisms which determine the dynamical properties of the dislocations is far more important.

However, one fact that seems to have been clearly established is that the yielding and flow of b.c.c.

---

[4]Dorn and Rajnak (1964) have recently given some theoretical justification to the form of Equation 1.2.

metals is determined by the mobility of the free dislocations. It will be convenient therefore to review the various factors which are responsible for the resistance to dislocation motion and their temperature and strain rate dependence. This will be done in the following sections.

1.3. The Peierls-Nabarro Stress

The force which opposes the movement of a dislocation as it tends to move through an otherwise perfect lattice from one equilibrium position to the next, was originally considered by Peierls (1940) and subsequently studied by other investigators (Nabarro 1947, Ieibfried and Dietze1949). This force, known as the Peierls-Nabarro force was found to be very sensitive to the width of the dislocation (Foreman et al. 1951) and it was also believed that the temperature dependence of the friction stress could be due to the variation of the width of the dislocation with the temperature (Heslop and Petch, 1956).

The calculation of the Peierls-Nabarro force for any particular type of lattice is a rather difficult problem. Kuhlmann-Wilsdorf (1960), after introducing the concept of the 'uncertainty of position of the dislocation axis' has concluded that the Peierls-Nabarro

stress is large for the b.c.c. metals at low temperatures ($T \ll T_M$), and intrinsically temperature dependent.

The overcoming of the Peierls-Nabarro barrier by a dislocation segment is believed to be thermally aided through a process involving the nucleation of a pair of kinks of opposite sign. This concept was introduced by Seeger (1956) to explain the Bordoni peaks of internal friction observed in some f.c.c. metals. According to Seeger (1956) (and Seeger et al. 1957) the pairs of kinks can be formed under the combined action of the thermal fluctuations and the applied stress. The energy of a kink is given by:

$$U_k = (2a/\pi)(2E_o ab\, \tau_o^*/\pi)^{1/2} \qquad (1.4.)$$

where a is the distance between the position of the minima of potential energy, E_o is the line energy of the dislocation, and τ_o^* the Peierls stress at 0^oK. The activation energy for kink formation is:

$$H = U_k \left[1 + \tfrac{1}{4} \ln(16\, \tau_o^*/\pi\tau)\right] \qquad (1.5.)$$

The kinetics of dislocation motion has been discussed on the basis of this model by Lothe and Hirth (1959). More recently Dorn and Rajnak (1964) have reformulated the problem of the nucleation of a pair of kinks. In their model the activation energy

U_n ($U_n \equiv H$) must be calculated by numerical integration, but the ratio $U_n/2U_k$ is given as a function of τ^*/τ_o^* in a simple graphical form. An important difference between Seeger's and Dorn and Rajnak's model is that in the latter the activation energy becomes zero when the applied stress approaches the Peierls stress τ_o^*. However, in both models the energy of a kink pair is intrinsically independent of the temperature. The temperature dependence of the Peierls stress simply arises from the effect of temperature on the rate of nucleation of kink pairs.

1.4. Dissociation of Dislocations into Partials

A lattice friction opposing the motion of screw dislocations can arise in b.c.c. metals as a result of the dissociation of the a/2 $\langle 111 \rangle$ dislocations into partials. Since screw dislocations possess three-fold symmetry with respect to the possible slip planes, Hirsch (1960) has suggested the possibility of the existence of the dissociation:

$$a/2\ [111] \rightarrow a/6\ [111] + a/6\ [111] + a/6\ [111]$$

along the three $\{112\}$ or $\{110\}$ planes of the $[111]$ zone. Sleeswyk (1963), on the other hand, has shown that the dissociation is energetically more favourable if it takes place on two rather than on three planes, and that it is more likely to occur on $\{112\}$ than on

{110} planes. In both cases the movement of a screw dislocation will require the formation of a constriction or fault, and this will result in a friction stress inherent of the b.c.c. lattice. Mitchell et al. (1963) thought that this effect might account for the low mobility of the screw dislocations and for their preferential alignment along <111> directions. at low temperatures (Low and Turkalo 1962, Keh and Weissmann 1963, Lawley and Gaigher 1964).

1.5. The Effect of Impurities

The hardening of crystals produced by the presence of impurities is a well established fact. Since impurities can be present in solution and in the form of precipitates the way in which they can affect the dislocation mobility may be quite different. The pinning of dislocations by atmospheres of interstitial impurity atoms has already been mentioned in Section 1.2., and it will not be repeated here.

The strained regions which arise from the presence of impurity solute atoms randomly distributed in the crystal, act as obstacles to the movement of dislocations. Since the interaction between the dislocation and the strained region is of a short range (i.e. takes place only over a few interatomic distances), thermal fluctuations can help to push the

dislocations through the obstacles. As a result of this, the stress needed to move the dislocations through the impurity solute atoms can be temperature dependent. Cochardt et al. (1955) have estimated that the interaction energy between a dislocation and an impurity atom is of the order of 0.75 e.V.

Fleischer (1962 a, 1962 b, 1963) has studied in detail the interaction between solute atoms and dislocations for a wide range of solution hardening systems, and in particular has considered the hardening effect of those interstitials which produce asymetrical distortions. This type of hardening is specially important because it increases rapidly with the concentration of interstitial impurities and may affect the mobility of both edge and screw dislocations.

The frictional resistance to dislocation motion due to the Snoek effect may be relatively important at temperatures at which the interstitial impurities attain high mobilities. This friction is the result of the ordering of the interstitial impurity atoms (mainly carbon and nitrogen) into preferential positions as a dislocation passes near them. This effect is believed to contribute significantly to the flow stress of iron above room temperature (Schoeck and Seeger 1959).

The resistance that impurity precipitates offer to dislocation motion varies considerably with the size and dispersion of the precipitate particles (Mott and Nabarro, 1940, 1948). A uniform distribution of fine precipitates may give rise to a temperature dependent lattice friction (Mordike and Haasen 1962). On the other hand the obstacles offered by large precipitates cannot be surmounted with the help of thermal fluctuations, and the dislocations must by-pass them either by bulging out or by cross-slip. The kind of hardening arising from this type of obstacle is generally small and temperature indpendent. This should be particularly true for b.c.c. metals, since in these metals dislocations do not seem to be extended (Hirschhorn 1963).

Precipitates can also contribute to the hardening of crystals in an indirect way. It has been observed that, in some metals profuse dislocation tangling takes place in the proximity of the precipitates (Van Torne and Thomas 1963, Lawley and Gaigher 1964), and that at these sites cell structures and long range stress fields subsequently develop (Li 1962).

1.6. The Non-Conservative Movement of Jogs in Screw Dislocations

It has been observed that, in various types of

crystals, edge dislocations have a much higher mobility than screw dislocations (Johnston and Gilman 1959, Low and Guard 1959, Low and Turkalo 1962, Lawley and Gaigher 1964). This was interpreted as being due to the fact that the jogs on screw dislocations exert a dragging force on the dislocations themselves.

A jog in a screw dislocation can move in two different ways: a) by gliding conservatively along the dislocation line (Friedel 1956), and b) by moving non-conservatively with the dislocation and producing point defects ~~or dipole trails~~ (Seeger 1955, Johnston 1962). Since in the latter case additional energy is required to move the screw dislocation, a dragging force is exerted on it. The force necessary to move a screw dislocation is temperature dependent when the production of point defects is thermally aided. This is possible only if the jogs move conservatively whilst they make a non-conservative jump, or if the temperature is high enough for the point defects to diffuse away from the jogs (Seeger 1955).

It is believed that in b.c.c. metals the dislocations may retain a high concentration of jogs when they cool down from high temperatures (Schoeck 1961). Jogs must also exist in the dislocation networks for geometrical reasons (Schoeck 1961), and they can also be formed during the deformation as a result

of dislocation intersections (Cottrell 1953).

1.7. Intersection of Dislocations

The intersection of dislocations in metals with a low stacking fault energy can be a thermally activated process, but this is unlikely to be the case for b.c.c. metals. However, dislocation interactions can still account for an important part of the athermal component of the hardening of b.c.c. metals.

When two dislocations come into contact at more than one point they may form a repulsive junction (Saada 1960), and then a stress is only required to bring them close to each other. On the other hand some dislocations can also interact according to the reaction:

$$a/2\,[111] + a/2\,[1\bar{1}\bar{1}] \rightarrow a[100] \qquad (1.6.)$$

and form an attractive junction (Saada 1961, 1963). This type of junction may be an important source of internal stress, and it originates the hexagonal networks as predicted by Amelinckx and Dekeyser (1959) and observed in many b.c.c. metals (Carrington et al. 1960, Benson et al. 1962, Keh and Weissmann 1963). Under a sufficiently high stress the attractive junctions can be destroyed, leaving a jog on each dislocation, or alternatively they can become unstable producing a chain of point defects (Saada 1963).

The processes mentioned above may result in an athermal contribution to the flow stress.

When the dislocations simply cross each other, a jog is formed on one or both of them (Cottrell 1953), but since the energy of formation of an elementary jog is small (it is proportional to the increase in the dislocation length), the cutting of dislocations that are not extended is a relatively easy process.

1.8. Plastic Deformation as a Thermally Activated Process

The methods for investigating the thermally activated processes which control the mobility of the dislocations and the overall deformation rate, have mostly been based on the theory of rate processes (Eyring 1936). It has been generally accepted that if the mobility of the dislocations is controlled by a single thermally activated mechanism, the mean velocity of a dislocation segment is given by an equation of the form (Orowan 1936):

$$v = p\,\nu_o \left\{\exp(-\Delta G_1/kT) - \exp(-\Delta G_2/kT)\right\} \qquad (1.7.)$$

where ν_o is a frequency factor, p is the distance moved after a successful activation, and ΔG_1 and ΔG_2 are the free energies of activation for motion in the directions favoured and opposed by the local stresses

respectively; k is the Boltzmann constant and T is the absolute temperature.

Similarly, the plastic shear strain rate, $\dot{\gamma}$, at which a crystal deforms is given by:

$$\dot{\gamma} = \nu\left\{\exp(-\Delta G_1/kT) - \exp(-\Delta G_2/kT)\right\} \qquad (1.8.)$$

where $\nu = NAb\nu_0$; N is the number of activated sites per unit volume, A is the area swept by the dislocation segment per successful fluctuation, and b the Burgers vector.

For simplicity the symbol Δ is generally omitted on the understanding that G always represents variations of free energy and not absolute values.

The free energy of activation is:

$$G = H - ST = U - w\tau^* - ST$$

where H is the enthalpy, S is the entropy, U is the internal energy, and $w\tau^*$ is the work done by the effective stress during the activation event. The effective stress, τ^*, has the same meaning as in Section 1.2. ($\tau^* = \tau - \tau_\mu$). τ_μ is the stress required to overcome thermal-insensitive long-range obstacles, and its magnitude is influenced by temperature only through the shear modulus μ.

Equation 1.8. can now be written as:

$$\dot{\gamma} = \nu \left[\exp\left\{-(U-w\tau^*)/kT\right\} - \exp\left\{-(U+w\tau^*)/kT\right\}\right] \quad (1.9.)$$
$$= 2\nu \exp(U/kT) \sinh(w\tau^*/kT)$$

In this equation the entropy term, exp (S/k), is included in the pre-exponential factor ν. The term $w\tau^*$ in the second exponential is positive because it represents the work done against the effective stress during the activation event.

When $w\tau^* \gg kT$, Equation 1.9. takes the form:

$$\dot{\gamma} = \nu \exp\left\{-(U-w\tau^*)/kT\right\} \quad (1.10.)$$

which is the expression usually employed to describe the rate of deformation at low temperatures. It follows from Equation 1.9. that the condition $w\tau^* > kT$ is equivalent to $\dot{\gamma} > 2\nu \exp-(U/kT)$.

In all these equations U, $w\tau^*$, and therefore H can be functions of the temperature and stress.

The Activation Volume

The parameter w can be defined as:

$$w = -(\partial G/\partial \tau^*)_T$$

and if the variation of the entropy is small during the activation event:

$$w = -(\partial H/\partial \tau^*)$$

From Equation 1.10. it follows that if the total energy to overcome the obstacle is not a function of the stress (Conrad 1961a):

$$w = kT \left(\partial \ln \dot{\gamma} / \nu / \partial \tau \right)_T \qquad (1.11.)$$

On the other hand; by definition:

$$w \tau^* = Fd = bL'd \tau^*$$

where F is the force exerted on the obstacle, d is the distance that the dislocation segment moves during the activation event, and L' is the total length of the dislocation segment involved in the activation. Therefore:

$$w = bL'd \qquad (1.12.)$$

w is termed the 'activation volume' and it is in general a function of the effective stress, since both L' and d may be variable with stress.

The Activation Energy

Conrad and Wiedersich (1960) have shown that the enthalpy of activation, H, (which is usually termed 'activation energy') is given by:

$$H(T, \tau^*) = -kT^2 \frac{(\partial \tau / \partial T)_{\dot{\gamma}}}{(\partial \tau / \ln \dot{\gamma} / \nu)_T} = -wT \left(\partial \tau / \partial T\right)_{\dot{\gamma}} \qquad (1.13.)$$

and also by:

$$H(T, \tau^*) = -k \left(\frac{\partial \ln \dot{\gamma} / \nu}{\partial \frac{1}{T}} \right)_{\tau^*} \qquad (1.14.)$$

In writing Equations 1.11., 1.13. and 1.14., it is generally assumed that the variation of τ_μ with τ and

temperature is negligible compared with the variation of the applied stress. However Gibbs (1964) has pointed out that this assumption is not necessary and that the values of w and H calculated from these equations do not need any correction.

If the pre-exponential factor, ν , is constant, Equations 1.11., 1.13. and 1.14., provide a basis for determining experimentally the values of w and H.

In practice the variations of stress with strain rate and temperature, and the variation of the strain rate with temperature at constant stress, are measured at a fixed plastic strain during the course of a test on a single specimen. Thereby the variations of stress, or of strain rate, are obtained for a constant dislocation configuration, and this justifies the assumption that the pre-exponential factor, ν , and the long range internal stress remain constant during the experiment.

The Energy Barrier Characteristics of the Process

When in Equation 1.12. only L' is a function of the stress, U is stress independent and equal to the energy characteristic of the thermally activated process. In this case U can be determined from $U = H + w\tau^*$. However when d, in Equation 1.12., is a function of the stress, U is stress dependent and

the characteristic energy of the process must be obtained by extrapolation of the values of H to zero effective stress. (Christian and Masters 1964).

The Activation Parameters at Low Stresses

When the condition $w\tau^* > kT$ is not satisfied (this will occur when the deformation takes place at high temperatures or small strain rates) Equation 1.10. is not applicable. Then Equation 1.9. approximates to (Alefeld 1962 and Christian 1964):

$$\dot{\gamma} = 2\nu (w\tau^*/kT) \exp (-U/kT) \qquad (1.15.)$$

Alefeld (1962) has shown that under these circumstances Equation 1.11. does not yield the true activation volume of the process, w, but an apparent activation volume, w'. In fact, differentiation of Equation 1.9. yields:

$$(\partial \ln\dot{\gamma}/\partial\tau)_T = \frac{\partial}{\partial\tau^*} (w\tau^*/kT) \coth (w\tau^*/kT) \qquad (1.16.)$$

and therefore the relation between w' and w is given by:

$$w' = w \coth (w\tau^*/kT) \qquad (1.17.)$$

Although w may remain finite at very low stresses, the value of w' tends to infinity when τ^* tends towards zero. Alefeld has pointed out that this may

be the reason why the value of the activation volume obtained experimentally from the strain rate dependence of the applied stress increases sharply at low stresses.

Similarly, when $w\tau^* < kT$ Equation 1.13. gives only an apparent activation energy H' which is related to the true activation energy, $H = U - w\tau^*$ by:

$$H' = U \tanh (w\tau^*/kT) - w\tau^* \qquad (1.18.)$$

This relationship can also explain why the values of the activation energy obtained at low stresses are sometimes very small (Orava 1963). It can also account for the change in slope in the plot of H versus T obtained by various authors (Conrad 1963, Christian and Masters 1964).

1.9. Experimental Evidence for the Rate Controlling Mechanisms in b.c.c. Metals

The method of analysis outlined in the last section has been extensively used to study the nature of the processes controlling the deformation in b.c.c. metals. The experimental evidence obtained in support of the various proposed mechanisms will be briefly reviewed in this section.

From a comprehensive analysis of the existing experimental data, Conrad (1961, 1963) and Conrad and

Hayes (1963) have concluded that the overcoming of the Peierls barrier is a mechanism consistent with the experimental observations for all the b.c.c. metals. They have observed that the values of H and v, and their variation with stress are independent of the impurity content, dislocation structure and of whether yielding or flow is considered. Conrad (1963) suggests that all these facts are not in agreement with any mechanism but that of overcoming the Peierls stress.

A similar conclusion was reached by Basinski and Christian (1960) and Christian and Masters (1964) after an analysis of their results on iron, niobium, vanadium and tantalum.

Furthermore, Conrad (1963) and Christian and Masters (1964) have shown that at low stresses the values of the activation energy are in agreement with those predicted by Seeger's model of kink nucleation.

However, some of the evidence that Conrad (1963) has collected against other specific mechanisms is not substantiated by results obtained by other workers. For example, Mordike and Haasen (1962) found that for iron single crystals both $(d\tau/dT)_{\dot{\gamma}}$ and $(d\tau/d\ln\dot{\gamma})_T$ were increasing functions of the stress (and strain), and therefore structure sensitive. From this observation they concluded that the rate

controlling process could not be the overcoming of an inherent lattice friction. Instead they suggested an explanation based on the overcoming of fine precipitates of carbides or nitrides. But this view has also been subsequently questioned by Nabarro et al. (1964).

It has often been emphasised that jogs in screw dislocations may play an important role in the deformation of b.c.c. metals (Schoeck1961, Low and Turkalo 1962, Lawley and Gaigher 1964), but the actual mechanism which determines the mobility of the jogs is not altogether clear. Mordike (1962) obtained results for tantalum single crystals which he believed were not in complete agreement with the Peierls mechanism, and he favoured the thermally activated conservative movement of jogs in screw dislocations as the rate controlling process. On the other hand, Gregory (1963) and Gregory et al. (1963) have obtained supporting evidence for the non-conservative movement of jogs as the rate controlling mechanism in niobium.

The temperature dependence of the yield stress of molybdenum single crystals (Lawley et al. 1962), tungsten single crystals (Koo 1963), and iron single crystals (Stein et al. 1963) has been found to decrease considerably as the purity of the material is

improved. This effect was interpreted by Stein et al. to mean that the interaction between dislocations and interstitial impurity atoms is the mechanism responsible for the temperature dependence of the yield stress at low temperatures. However, Conrad (1963) and Nabarro et al.(1964) have argued that at very low temperatures the yield stress is independent of the impurity content (Lawley et al. 1962) and that this is again consistent with the mechanism of overcoming the Peierls friction. The different temperature dependences observed at intermediate temperatures would be only due to the fact that the number of sites available for thermal activation varies with the amount of impurities present.

Rose et al. (1962) have investigated the effect of orientation on the yielding and flow of tungsten single crystals and obtained results which are difficult to explain in terms of the Peierls mechanism. The proportional limit of crystals with the tensile axis orientated in the <110> direction was found to be three times higher than that of crystals having the tensile axis in the <100> direction. The subsequent work-hardening rate was also quite different, but the activation energy for yielding was practically independent of the orientation. These authors suggested that the difference in proportional limit

could be a geometrical effect on the mechanism itself, and proposed an explanation based on the properties of the dislocation networks and dislocation jogs in the b.c.c. lattice. Rose et al. did not investigate in detail the effect of temperature and strain rate on the flow stress, and therefore they could not reach any conclusion concerning the nature of the rate controlling mechanism.

1.10. Purpose of the Investigation

After a consideration of the results described in the last section a series of experiments were designed to study the effect of the orientation on the yield and flow stress of molybdenum single crystals. This was done with the purpose of investigating whether the temperature and strain rate dependence of the yield and flow stress could be explained in terms of an inherent isotropic lattice friction or not.

The present work can be divided into three parts.

1. The preparation of single crystals, the machining of single crystal specimens and the auxiliary experimental techniques are described in Chapters 2, 3 and 4 respectively.

2. The effect of the orientation on the deformation

behaviour of the crystals, as determined by conventional tensile tests, is described and discussed in Chapter 5.

3. The effect of temperature and strain rate on the flow stress of crystals with two different orientations is studied in Chapter 6. In this chapter the dislocation mechanisms controlling yielding and flow are also discussed.

CHAPTER 2

THE GROWTH OF MOLYBDENUM SINGLE CRYSTALS

2.1. Introduction

For a long time single crystals of refractory b.c.c. metals were usually grown by strain anneal methods or by the application of a high temperature gradient (Tsien and Chow 1937, Chen et al. 1951). The limitations of purity, size and shape which are inherent in these techniques were not felt until rather recently when crystals of higher purity and perfection have been needed for a better understanding of the mechanical properties of these metals.

The problem of growing large single crystals of refractory and reactive metals of high purity was solved with the use of the floating zone melting technique, applied for the first time by Keck and Golay (1953) to grow single crystals of silicon. The advantage of this method is that the crystal grows without any contact with a crucible, whilst extra purification is achieved as a result of zone refining, and the evaporation of impurities if the process is carried out in vacuum.

In this chapter the growth of molybdenum single crystals by the electron beam zone melting technique

is described after giving a brief account of the growth and purification processes.

2.2. Crystal Growth

When a molten zone is moved along a polycrystalline metallic rod the metal solidifies behind the molten zone in the form of a single crystal, if suitable conditions to avoid the formation of extraneous nuclei ahead of the growing crystal are maintained. This condition is fulfilled by keeping the degree of supercooling of the liquid near the interface to a minimum. To grow a single crystal it is, therefore, necessary to impose a steep temperature gradient in the liquid metal and a slow rate of cooling, i.e. a slow speed of the molten zone. At the same time, if a low dislocation density is desired, the temperature gradient in the recrystallized solid should be small and the growth should be carried out in still conditions.

2.3. Zone Refining

The zone refining process takes place simultaneously with crystal growth. If the metal contains soluble impurities that lower the melting point of the solvent, the impurities will be rejected from the freezing solid and will accumulate in the molten zone. On the contrary, if the soluble impurities raise the

melting point of the solvent metal, they will accumulate in the freezing solid. In the first case, the impurities will travel with the molten zone and will be concentrated at one end of the rod. In the second case, they will accumulate at the other end as a result of being rejected to the solid. In both cases a limiting distribution of impurities is reached after a large number of zone passes in the same direction. The basic theory of zone refining was developed by Pfann (1952) and has been thoroughly reviewed by the same author (Pfann 1957, 1958). Its aim is to predict the impurity distribution profile in terms of the relative zone length, the speed of zoning and the distribution coefficient, k, which is the ratio of solute concentration in the freezing solid to that in the main body of the liquid.

Many of the assumptions that are made in the theoretical solution of the problem are not met in practice and it is always difficult to reproduce the ideal conditions for good zone refining. For instance, in order to ensure a constant relative zone length, very good power control, and a rod of uniform cross-section are needed. The liquid metal should have uniform composition, and this is not achieved unless good stirring or convection action is provided and the zone speed is sufficiently small. Stirring can produce vibrations which are not particularly good for the

perfection of the crystals, but, if on the other hand, a large concentration of solute is built up in the liquid next to the interface a strong constitutional supercooling may result and this will have a deleterious effect on crystal growth. Finally, the condition of negligible diffusion of solute in the solid phase is hardly met in the case of carbon in solution in b.c.c. metals.

In single crystals of some refractory metals grown by floating-zone-melting a slight preferential redistribution of impurities has been detected by resistivity measurements (Buehler and Kunzler 1961, Wernick et al. 1959). Chemical analyses seem to show that, in the case of molybdenum, carbon tends to be carried along with the molten zone (Belk 1959, Belk and Calverley 1961), as one would expect from the phase diagram of the molybdenum-carbon system (Northcott 1956) if zone refining is really effective.

2.4. Evaporation of the Impurities

The evidence that can be obtained from the existing literature (Buehler 1958, Carlson 1959, Schadler and Low 1962, Lawley et al. 1962) and specially from Buehler and Kunzler (1961) and Belk and Calverley (1961) shows that zone refining plays only a minor role in the purification of single crystals of refractory metals, at least for the speeds of growth (about 2mm/min)

used in common practice. The purification is almost entirely due to the evaporation of the impurities when the melting is carried out at pressures of the order of 10^{-5} torr or less. This view has been further confirmed by more recent experiments (Drangel and Murray 1964, Votava 1964). This result is not surprising, since it is known from the principles and experience of vacuum melting, that gaseous impurities and many metallic elements are preferentially volatilised (Wulff 1957, Winkler 1960, Smith 1958). Deoxidation also occurs through evaporation of the metal monoxide (Wulff 1957, Winkler 1960). Carbon is evaporated mainly as CO after combining with the oxygen present in the metal as an impurity (Wulff 1957, Winkler 1960, Hurwitt and Adams 1963). It is expected that carbon will be more effectively removed if the oxygen content of the metal is high, (Hurwitt and Adams 1963). This observation is worth bearing in mind because carbon is always the more difficult interstitial element to eliminate.

2.5. Electron Beam Floating Zone Melting

Radiation heating (Emeis 1954) and induction heating (Buehler and Kunzler 1961, Wernick et al. 1959, Buehler 1958) have been employed in the floating zone melting technique. However, since Davis, Calverley and Lever (1956) described for the first

time the use of electron bombardment, much equipment based on this principle has been built and is now commercially available.

The principle of the electron bombardment method is very simple: the polycrystalline metallic rod is placed vertically in a vacuum chamber and it is surrounded by an incandescent filament. The electrons emitted by the filament are accelerated towards the rod by applying a high voltage between the filament that acts as a cathode and the rod acting as an anode. The electron beam is focused in a narrow zone on the rod where melting takes place. By moving the cathode, the molten zone can be displaced along the rod.

Although this method, in its simplest form, is not suitable for melting metals that have a high vapour pressure at their melting temperature, it has some clear advantages over induction heating. These are:- A) easy construction,

B) very small power requirements,

C) easy power control and the possibility of obtaining a very narrow molten zone.

Practical details of this method can be found in the basic papers by Calverley et al. (1957) and Birbeck and Calverley (1959) and in the review article by Schadler (1963).

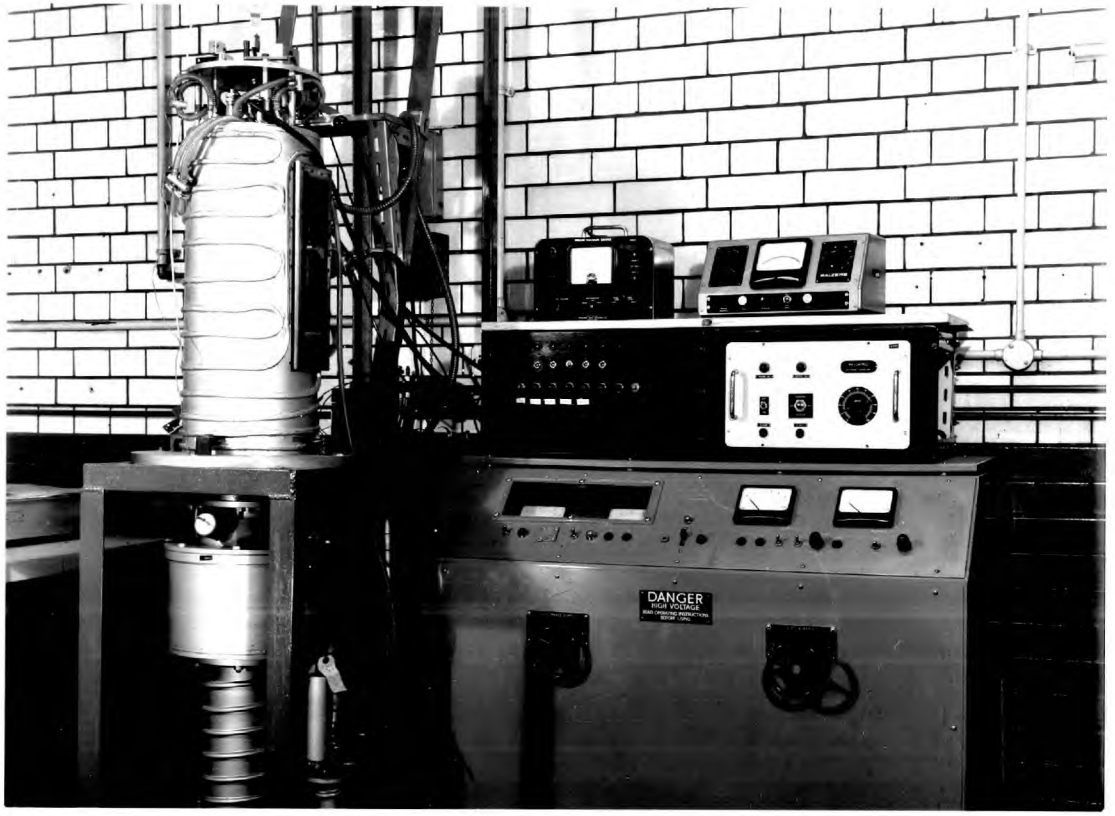

Figure 2.1. General view of the electron beam zone melting equipment.

2.6. Description of the Apparatus Used

Figure 2.1. is a general view of the electron beam zone melting apparatus in which the molybdenum single crystals used in the present investigation have been grown.

2.6.1. Vacuum Parts

The body of the furnace is a cylindrical chamber made of nickel plated mild steel, and is pumped through the bottom by an oil diffusion pump with a capacity of 300 litres/sec. Between the pump and the furnace there is a liquid nitrogen trap to reduce back-streaming of oil vapours into the chamber. There is a thick quartz window shielded by a movable screen and a silica glass plate easy to remove and clean. The pressure is measured by an ionization gauge placed in the side of the chamber. All the internal parts of the furnace are attached to the lid and can be lifted clear of the chamber with a hoist. The electrical power unit can also be seen in Figure 2.1.

2.6.2. Internal Parts

Figure 2.2. is a view of the internal parts of the furnace which are numbered and described in the caption.

The stainless steel liquid nitrogen trap, mounted on the lid, acts as a very effective getter of vapours

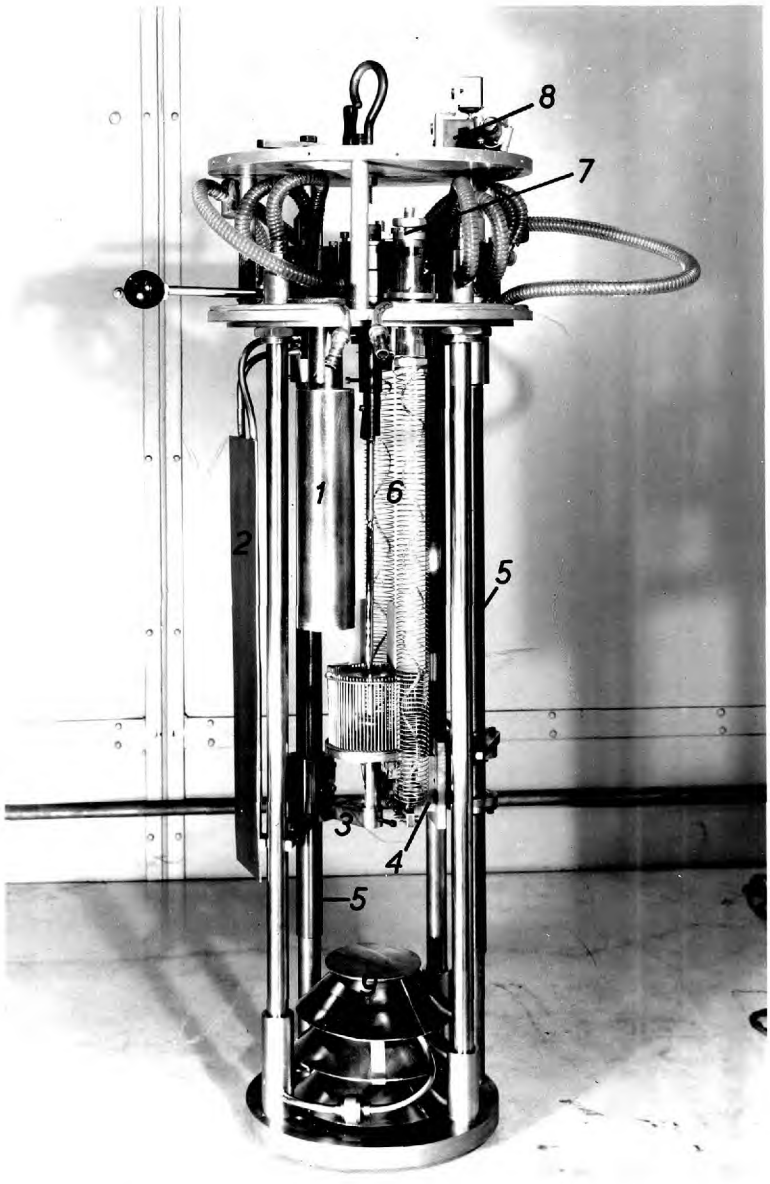

Figure 2.2. Internal parts of the electron beam zone melting furnace.

1. Liquid nitrogen trap. 2. Movable window shield. 3. Lower rod clamp, adjustable in height. 4. Insulating 'pyrophilite' blocks. 5. Water cooled lead screws. 6. Extendible current leads. 7. Vacuum sealed terminals. 8. Reduction gear. 9. Water cooled baffle.

inside the chamber, and helps to improve the ultimate vacuum. It also reduces considerably the frequency of the electrical discharges that normally occur when there is much volatilization of metal.

The cathode is run at a high negative voltage and it is mounted on a lead screw by means of two insulating blocks of "pyrophilite". The rod and all the other parts of the furnace are earthed. The lead screw is driven by a variable speed motor through a reduction gear giving a cathode travel speed variable between zero and 30 mm/min. The "electron gun" is similar to the one developed by Cole et al. (1961) and its components are made of molybdenum. With this type of cathode assembly the filament is hidden from the molten zone and contamination of the crystal with metallic vapours evolved from the filament is avoided. At the same time, the filament does not get coated with metal ejected or evaporated from the molten zone, and its life is increased. In fact, one filament lasts enough to give more than 90 passes. The visibility of the molten zone is also improved. A schematic diagram of the electron gun is shown in Figure 2.3.

The electrostatic screen which deflects the electron beam towards the rod is electrically connected to and is at the same voltage as the filament, although

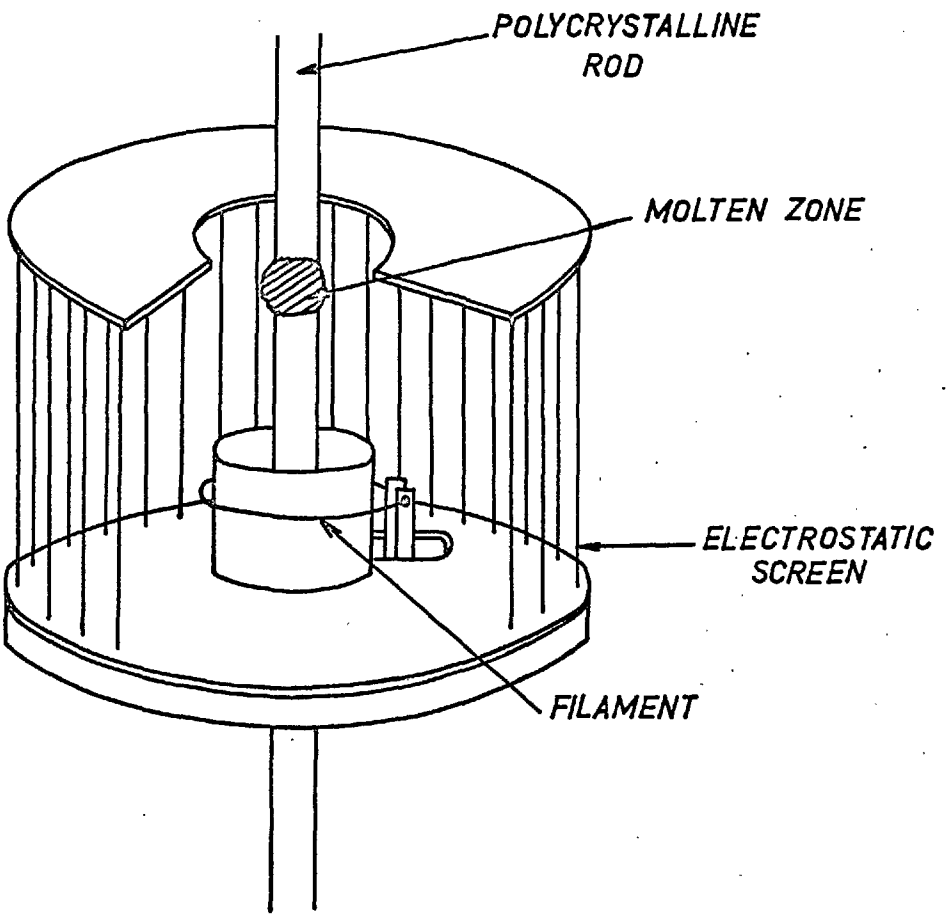

Figure 2.3. Schematic diagram of the electron-gun cut away to show interior parts.

provision has been made to bias it if necessary for focussing purposes. The filament is a loop of tungsten wire of 0.5 mm diameter. The focus of the electron beam can be adjusted by varying the diameter of the filament loop.

The impedance of this type of electron gun is greater than the impedance of the emitter described by Calverley et al. (1957), and Birbeck and Calverley (1959), and is very sensitive to the position of the filament and the diameter of the hole in the top plate.

2.6.3. High Voltage Power Supply

The high Voltage d.c. supply consists of a 10 kV,, 1 Amp. full wave rectifier. It incorporates a trip circuit to prevent overloading and a power control circuit, operated by thyratrons, which regulates the temperature of the filament and therefore the emission current. It is necessary to operate the emitter in the emission limited range to ensure effective regulation. The control circuit is analogous to the one described by Birbeck and Calverley (1959).

The filament voltage is supplied by a high voltage insulated transformer rating 20 Amp. at 50 volt.

2.7. Polycrystalline Material

In the furnace described above, single crystals

have been grown from arc-cast molybdenum, hot swaged to 6 mm diameter rod, and from sintered molybdenum rod of the same diameter.

The arc cast molybdenum was supplied by Mr. J. M. Clyne of the Armaments Research and Development Establishment, Woolwich. A typical analysis of this material is given in Table 2.1. In view of the inconsistencies previously found (Wronski and Johnson 1962) it should be taken as a very rough approximation. The large carbon content is due to the addition of this element for deoxidation during the fabrication process.

The sintered molybdenum rods were supplied by Murex Ltd. In Table 2.1. the analysis of this material is also given.

2.8. Operating Characteristics and Growth Conditions

The ultimate pressure attained, when the furnace is cold is about 4×10^{-6} torr and when the trap inside the chamber is filled with liquid nitrogen, the pressure is further reduced to 10^{-6} torr.

A stable molten zone is established with a voltage of 6.6 kV and an emission current of 100 mA. This means that to melt the 6 mm diameter molybdenum rod a power less than 700 watts is needed. This value may be compared with the figure of 760 watts quoted by

TABLE 2.1.

Analyses of polycrystalline molybdenum, and molybdenum single crystals.

Element	Content in p.p.m. in weight						
	H	O	N	C	Fe	Si	Other Elements
Arc cast molybdenum. Analysis supplied by A.R.D.E., Woolwich.	4	6	12	80	100	20	
Sintered molybdenum. Approximate analysis supplied by Murex Ltd.	1	10	10	40	80		
Sintered molybdenum. Analysis supplied by B.N.F.M.R.A.	0.35	2-3	$\ll 10$	6-7	60		Not detected
Two pass single crystals, grown from sintered molybdenum. Analysis supplied by B.N.F.M.R.A.	<0.01	<1	$\ll 10$	2-3	16 to 60		Not detected

Belk (1959) for similar conditions. This discrepancy is possibly explained by the fact that the voltage measured may include the voltage drop developed in other parts of the circuit. In our case this is only of the order of 100 volts, but when the impedance of the emitter used is smaller, the voltage drop will be much higher. It has been experienced that when the power exceeds 700 watts the molten zone becomes unstable.

With a view to what has been discussed in section 2.3. no attempt has been made to obtain purification by zone refining. It was felt that it would be more important to optimize the conditions for effective evaporation of the impurities and to obtain a uniform solute distribution along the crystal. The maximum power compatible with the stability conditions was therefore used in order to maintain a well superheated molten zone, and the crystals were grown by passing the zone in opposite directions for an even number of passes at a speed of 2.5 mm/min. After each pass, melting was restarted within the single crystal region away from the last freezing zone.

Violent outgassing and spluttering is observed, during the first pass, when sintered molybdenum is melted. This behaviour is not observed if arc cast molybdenum is used. In neither case was solid state

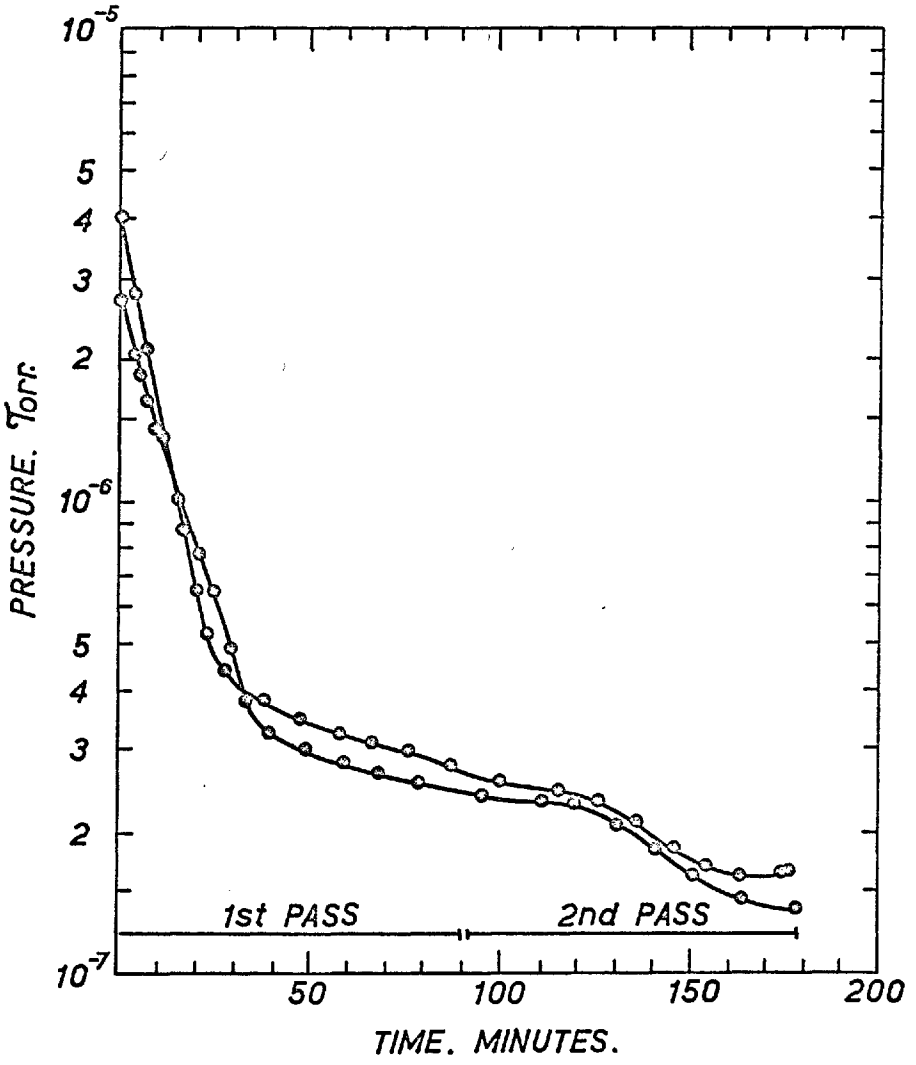

Figure 2.4. Variation of the pressure with time during the growth of molybdenum single crystals.

outgassing necessary.

As soon as melting is started, the pressure in the furnace begins to decrease and continues to do so until it reaches an ultimate value of about 2×10^{-7} torr. A typical variation of the pressure with time during melting is shown in Figure 2.4. The reason for this decrease in pressure is that the molybdenum evaporated from the melting rod deposits in the cold parts of the furnace and this deposit acts as a getter for gases, mainly hydrogen (Hunt et al. 1960). The amount of molybdenum lost by evaporation, with the melting conditions described above, is 8% in weight per pass.

The crystals grow with random orientation, and if a specific orientation of the crystal axis is desired it is necessary to seed them. Any crystal with the right orientation can be used as a seed, but to grow the first oriented crystal the device shown in Figure 2.5. was used. A randomly oriented crystal is cut through a plane normal to the desired direction by the method described in Section 3.3. By screwing this face flat against the horizontal plane of the holder, the seeding direction coincides with the vertical and the axis of the rod. The misorientation of the axis of the crystals grown by this method is less than 2°.

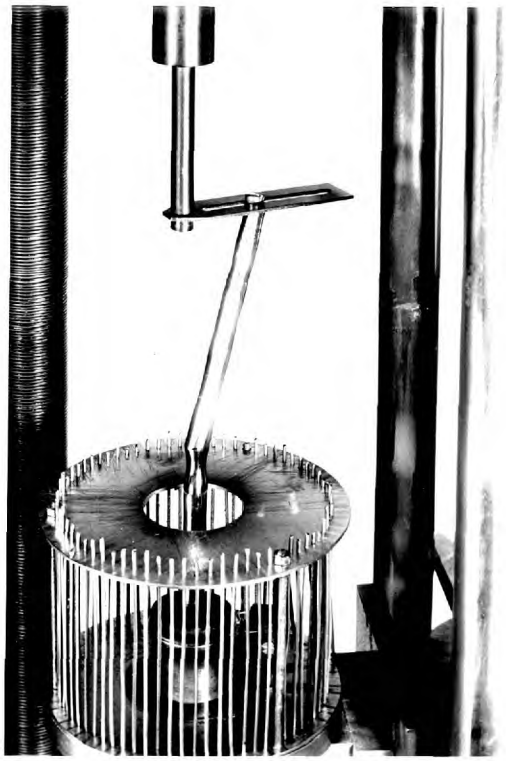

Figure 2.5. Detail of the seed holder

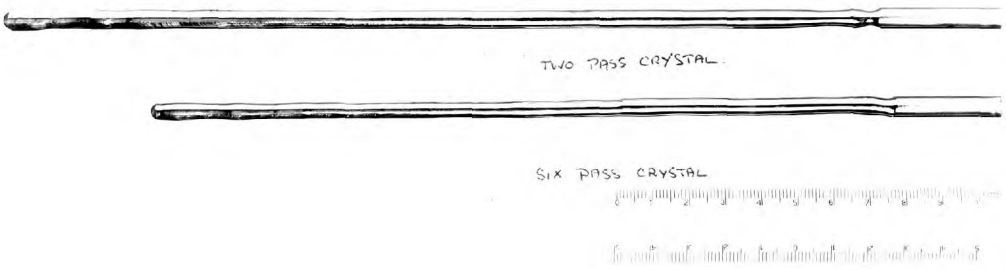

Figure 2.6. Molybdenum single crystals: Scale in cm.

2.9. Perfection and Purity of the Crystals

A molybdenum single crystal grown with two passes of the molten zone and one grown with six passes are shown in Figure 2.6. The two pass crystals have a length of over 20 cm. and a diameter about 5.5 mm. The six pass crystals are slightly shorter and thinner due to the evaporation of metal.

The structure and purity of the crystals grown from sintered molybdenum were found to be very different from those grown from arc cast molybdenum.

2.9.1. Crystals Grown from Sintered Molybdenum

The X-ray Laue photographs of these crystals show always very clear spots, indicating that the misorientation of the subgrains is smaller than 30'. The low angle boundaries and dislocation structure can be seen in the photographs of Section 4.1., all of which are representative of crystals grown from sintered molybdenum rod. The etching technique used to reveal the dislocations is discussed in Section 4.1. The true dislocation density of the as grown crystals is difficult to estimate, because of the peculiar orientation effect which is also described in Section 4.1. The etch pit density of the as grown crystals varies from 10^5 pits/cm^2 on $\{100\}$ planes to 10^8 pits/cm^2 on planes that make an angle of 30° with

{100}. The substructure and density of etch pits, as it appears on {113} planes, compares favourably with that of other refractory metallic single crystals grown by the same technique (Schadler and Low 1962).

The different mechanisms of dislocation nucleation during crystal growth have been summarily reviewed by Tiller (1963). In view of the conditions in which the present crystals have been grown, it is believed that the major part of the dislocations have been introduced by thermal and mechanical stresses. Thermal stresses are expected to be important because the focus of the electron beam on the surface of the rod is not very uniform, and therefore the shape of the solid liquid interface can be very irregular. The mechanical stresses are produced by the vibrations of the system.

Chemical analyses of the crystals grown with two passes of the molten zone, have been made by B.N.F.M.R.A. and the results are listed in Table 2.1. Accurate determination of the impurities by ordinary analytical methods is very difficult, for it is not unusual that in the single crystals grown by floating zone melting the impurity content is below the limit of detection.

To obtain an idea of the impurity distribution along the crystal, microhardness and Vickers hardness measurements were made on {100} faces of slices cut

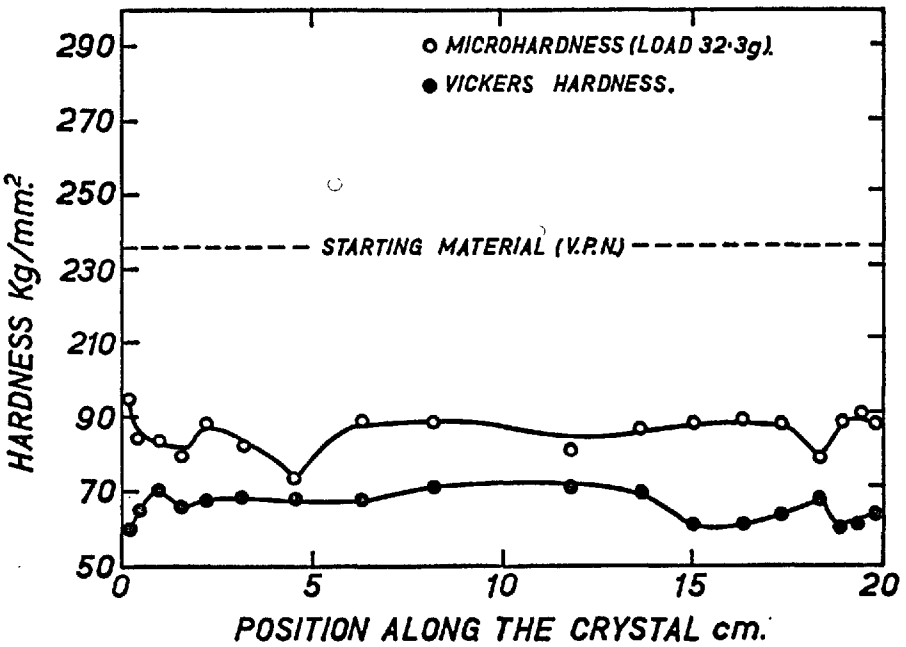

Figure 2.7. Variation of the hardness along the length of a molybdenum single crystal grown from sintered rod.

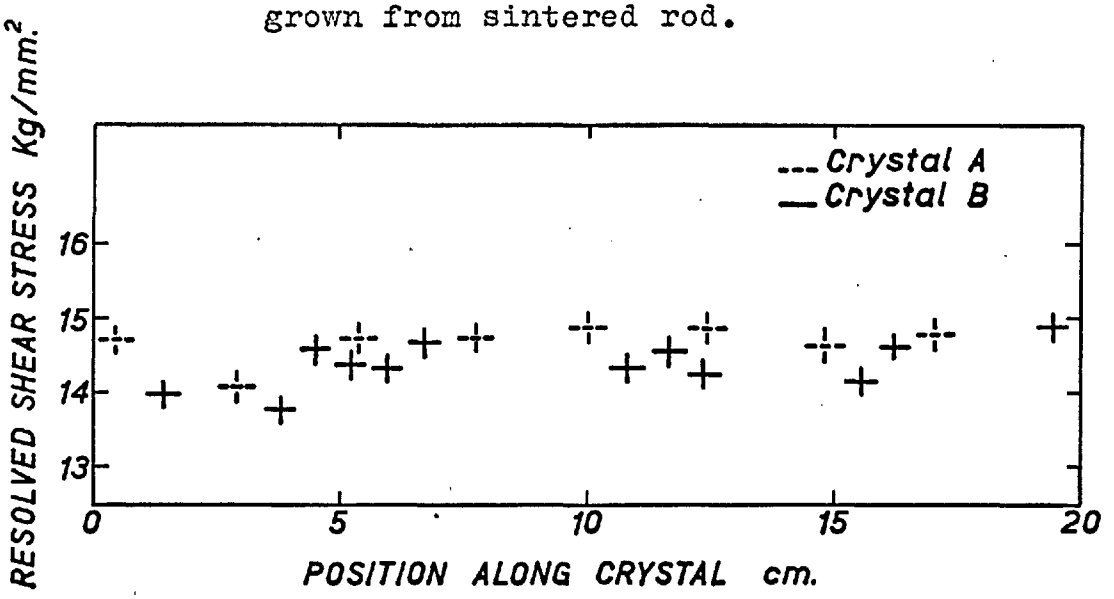

Figure 2.8. Proportional limit of compression specimens with axis in the ⟨110⟩ direction, machined from different parts of two molybdenum single crystals grown from sintered rod.

from different parts of a two pass crystal. The results of these measurements are shown in Figure 2.7. To check the results of the hardness measurements, the proportional limit of compression specimens machined from different parts of two crystals was also measured. The specimens were machined as described in Chapter 3, and with the compression axis in the ⟨110⟩ direction. The values of the proportional limits are plotted in Figure 2.8.

From these results, it can be concluded that the distribution of interstitial impurities more likely to influence the mechanical properties of the single crystals is uniform enough to make any two specimens cut from different parts of the rod mechanically indistinguishable. It also became evident, from the results obtained in the course of the present investigation, that all the crystals grown in similar conditions have the same mechanical properties.

Although single crystals with four and six passes of the molten zone have also been grown by the same method, an assessment of their impurity content and distribution has not been made, because they were not used in the present investigation.

2.9.2. Crystals Grown from Arc-Cast Molybdenum

The X-ray Laue photographs of these crystals

show very often double and triple spots which indicate the presence of sub-grains with misorientations between 1^{o} and 2^{o}. The mean etch pit density of the crystals grown from arc-cast molybdenum is not substantially different from that of crystals grown from sintered molybdenum. There is, nevertheless, a great difference in the dislocation arrangement. Figure 2.9. shows the etch pit pattern on a {113} plane of a crystal grown from arc-cast molybdenum. Clouds of dislocation etch pits surround what are believed to be precipitate particles of Mo_2C (Lawley and Gaigher, 1963). This seems to be a typical example of dislocation nucleation by differential thermal stresses around inclusions, produced during cooling. It can also be seen in Figure 2.9. that the precipitates tend to segregate to the sub-boundaries.

Chemical analyses of these crystals have not been made. There is, however, strong evidence to believe that their carbon content is greater than that of the crystals grown from sintered molybdenum; first, because of the greater amount of carbon in the starting material, and secondly, because of the presence of the large precipitates.

The proportional limit of compression specimens oriented in the <110> direction and machined from different parts of a two pass crystal has been

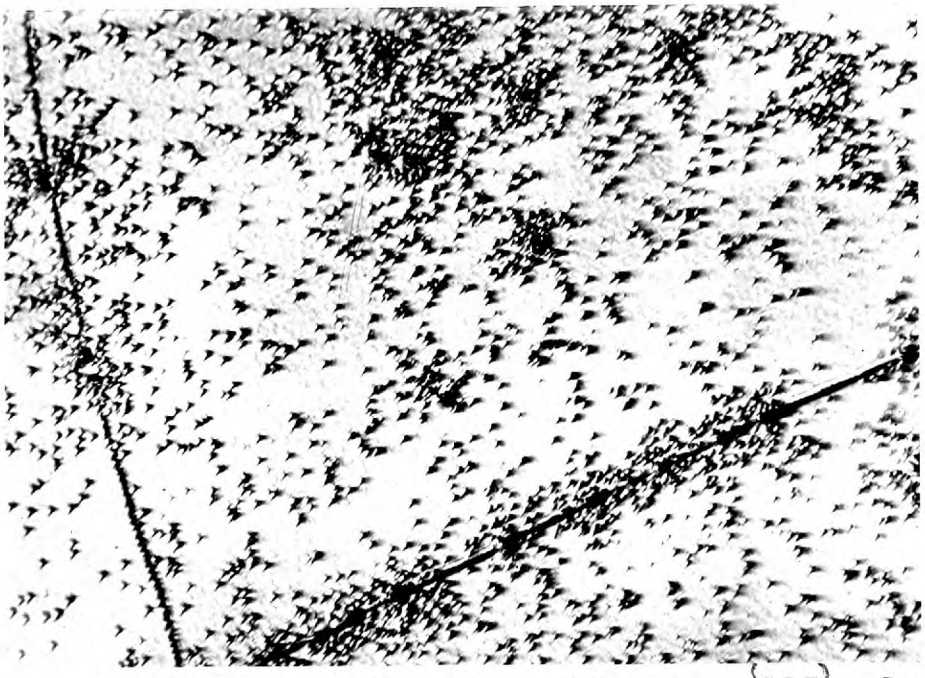

Figure 2.9. Dislocation etch pits on a {113} plane of a single crystal grown from arc cast rod.

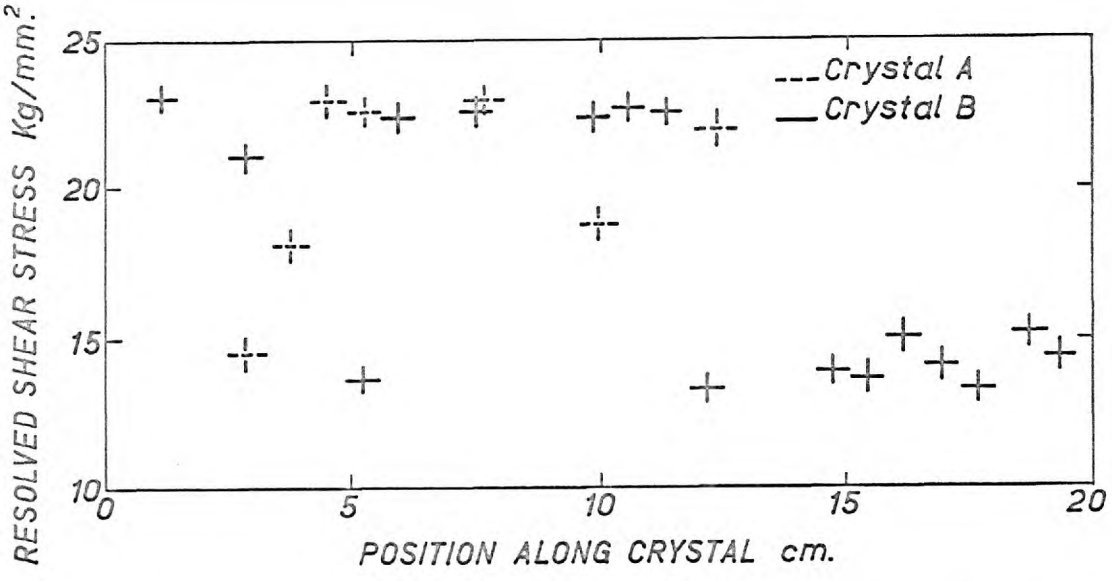

Figure 2.10. Proportional limit of compression specimens with axis in the ⟨110⟩ direction, machined from different parts of two single crystals grown from arc cast rod.

measured. The results, shown in Figure 2.10., suggest a very inhomogeneous distribution of impurities. Specimens from different parts of the crystal show not only different proportional limits, but also quite different stress-strain curves. The softer specimens yield smoothly, the harder ones show a pre-yield region followed by a yield point. This non-uniform distribution of impurities is not believed to be the result of zone refining, but rather to be the effect of an inhomogeneous distribution in the starting material.

CHAPTER 3

PREPARATION OF THE SPECIMENS

3.1. Introduction

The methods usually employed to prepare strain-free specimens of single crystals fall in two main categories;

a) Machining that does not introduce any deformation, such as chemical attack and electro-machining (Farmer and Glaysher 1953, Avery et al. 1958, Young and Wilson 1961, Titchener and Davies 1963).

b) Machining that produces a thin deformed layer which has to be subsequently removed by chemical or electrolytic polishing (Cole et al. 1961).

The choice of the method of preparation for any particular case has to be, quite often, a compromise between perfection and practicability. If a specimen is desired that does not contain any "fresh" dislocations it would be advisable to use chemical or electrolytic machining. Spark erosion, as well as careful mechanical machining are possible methods if the main concern is only the absence of asterism in the X-ray Laue back-reflection photographs.

It is possible, sometimes, to estimate the depth of the cold worked layer by more sensitive methods than

the X-ray Laue technique, as for instance by dislocation etch pitting, but it would be unrealistic to think that a specimen without any fresh dislocations can be prepared by spark erosion or mechanical machining. It is possible to reduce the free, and even total, dislocation density after machining by an adequate annealing of the specimen. In this case, precautions should be taken to make sure that the final purity of the crystal is not endangered.

Single crystalline specimens of b.c.c. metals have been prepared sometimes by electro-machining (Schadler and Low 1962, Lawley et al. 1962), as well as spark erosion (Mitchell et al. 1963), and centerless grinding (Ferris et al. 1962, Koo 1963). Electro-machining and spark erosion are relatively slow methods, and they are only practical when the specimens can be machined from single crystalline rods of small and very uniform diameter. The molybdenum single crystals that have been obtained by the method described in Chapter 2 have a rather large diameter, and as a result of having been grown in superheated conditions their shape is in many cases not very uniform. To machine specimens out of these crystals it is necessary to remove a considerable amount of material, and consequently a method relatively fast and reliable had to be developed.

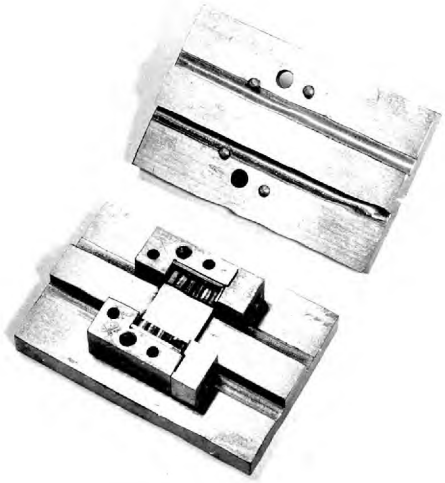

Figure 3.1. Jig for holding the tensile specimens during the grinding operation.

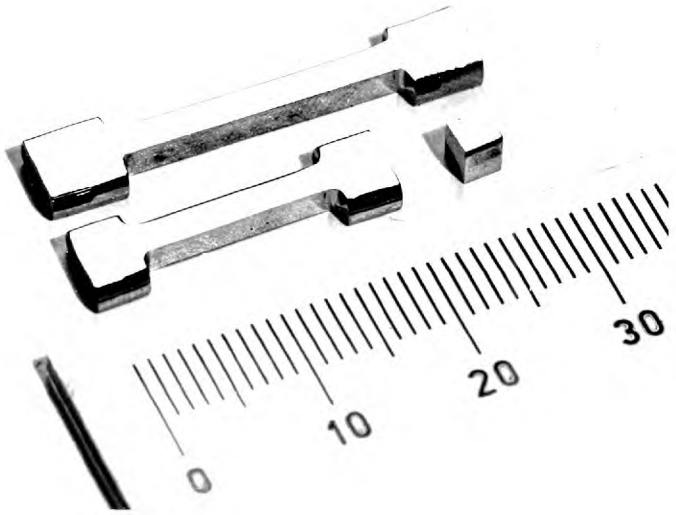

Figure 3.2. Single crystal specimens.

3.2. Machining of Tensile Specimens

The tensile specimens were machined by surface grinding. A few preliminary experiments were necessary to investigate the amount of deformation introduced by this method and to establish the most convenient machining conditions.

The oriented single crystalline rods are cut with a carborundum slitting wheel into 21 mm. lengths. These pieces are held in a steel tray, encased in Wood's alloy, and they are machined into slabs about 2.5 mm. thick by surface grinding. A self cleaning alumina grinding wheel is used for this operation. The slabs thus obtained are clamped in a special device, shown in Figure 3.1. in batches of six, and the specimens are finally shaped by grinding across the length of the slabs. A harder alumina wheel is used for this final operation and during the last cuts a small fillet radius is introduced in the shoulder of the specimen. Throughout the grinding process only cuts 0.0012 mm. deep are used, but in the final stages the cutting rate is reduced to one cut for every four passes of the wheel.

The specimens thus obtained have rectangular cross section of dimensions 2.55 x 2.7 mm., a total length of 21 mm. and a gauge length of 12.5 mm. A typical specimen, after it has been electropolished,

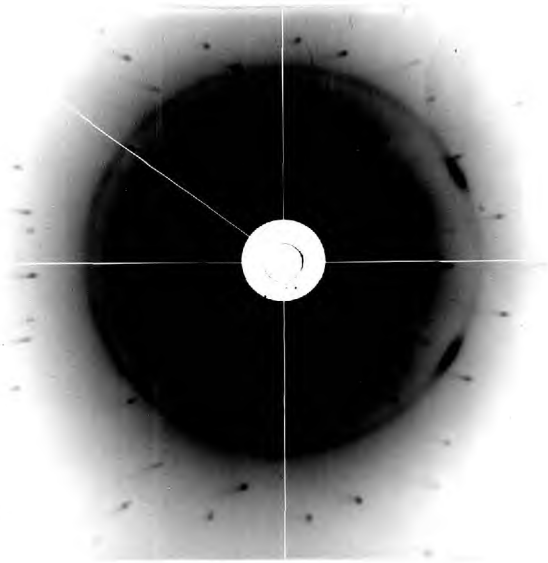

Figure 3.3. X-ray Laue picture of a specimen in the as machined condition.

is shown in Figure 3.2., together with a longer tensile specimen, machined by the same procedure, and a compression specimen.

The flat faces of these specimens are highly suitable for slip line and etch pit observations, as they can be made to coincide with specific crystallographic planes.

The deformed layer introduced during the machining is subsequently removed by electropolishing the specimen in concentrated H_2SO_4. The depth of this deformed layer was estimated by X-ray Laue back-reflection photographs and by observing the dislocation etch pit density at different depths below the machined surface.

An X-ray Laue picture of the machined surface shows a faint Debye ring on a background of clear spots which exhibit slight asterism (Figure 3.3.), but after removing a layer 0.040 mm. thick, the asterism and ring have disappeared and the picture is typical of a crystal in the as grown condition.

The sequence of photographs of Figure 3.4. show the dislocation etch pit structure at different depths below the machined surface. The density of pits decreases with increase in depth and after a layer 0.120 mm. thick has been removed from the machined surface, it reaches an almost constant value. It appears from this result that the thickness of the deformed layer

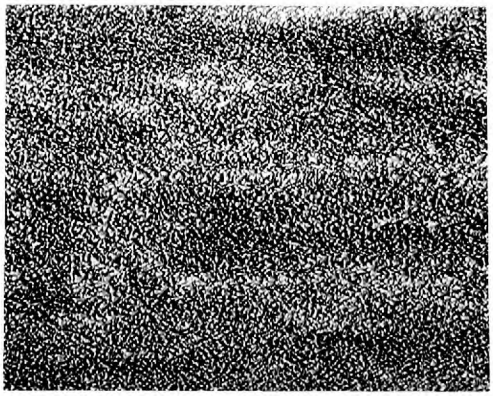

a

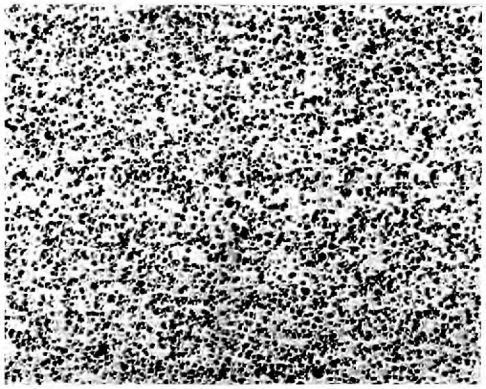

b

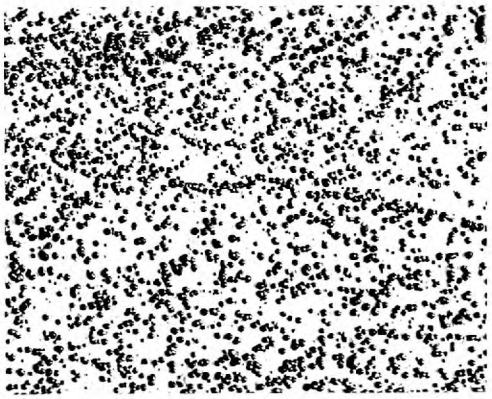

c

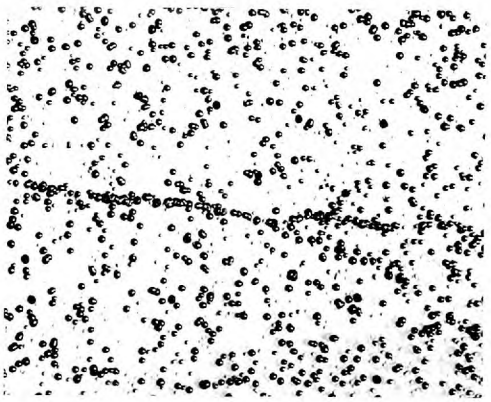

d

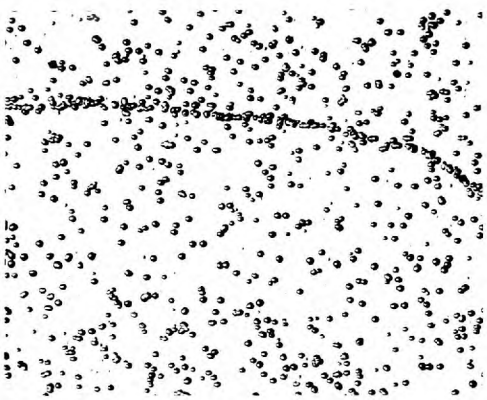

e

Figure 3.4.
Dislocation etch pits at different depths below the machined surface of a tensile specimen. (Mgn. x 200)
a. 0.030 mm. b. 0.065 mm.
c. 0.090 mm. d. 0.120 mm.
e. 0.180 mm.

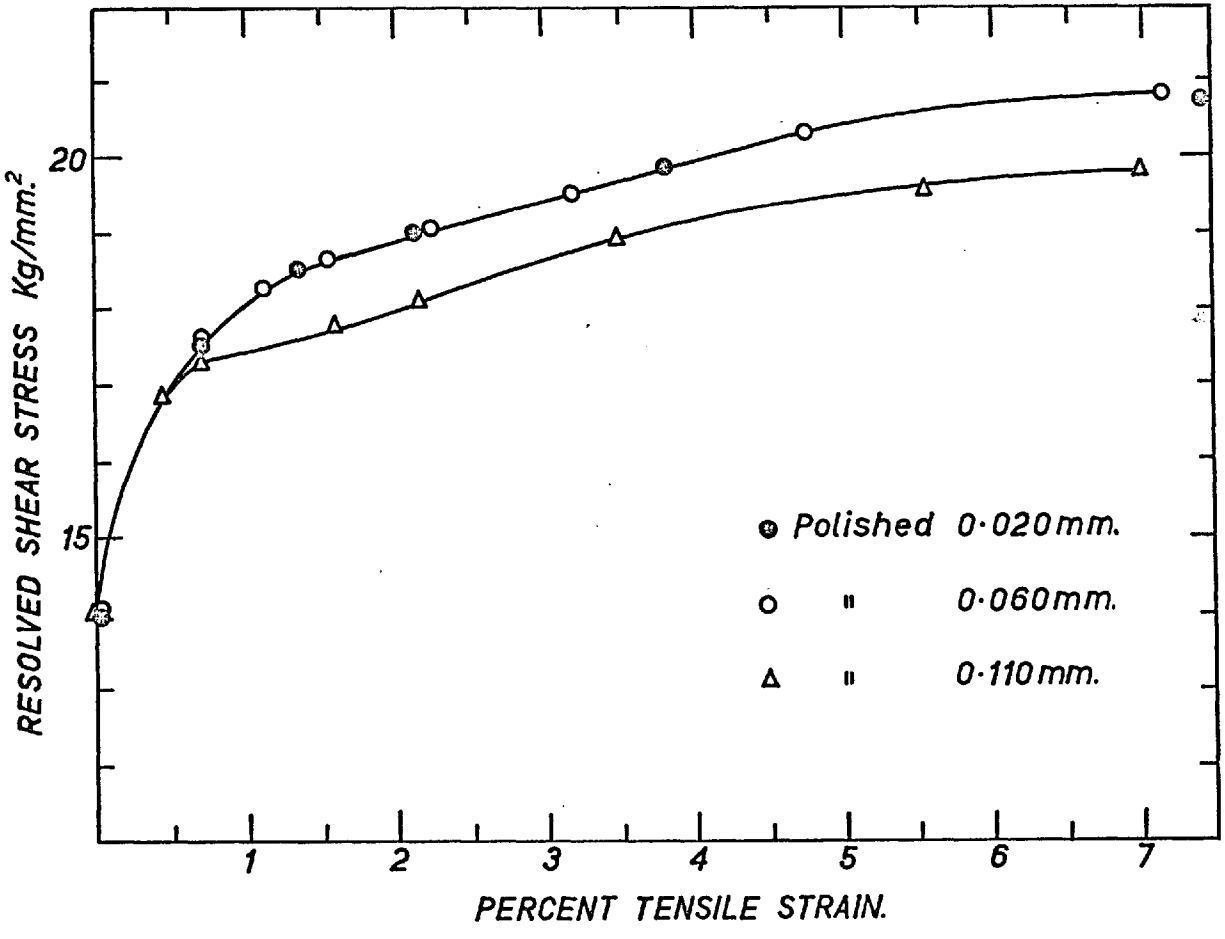

Figure 3.5. The influence of the cold-worked layer on the stress-strain curve of tensile specimens.

is not less than 0.100 mm. and therefore much greater than revealed by the X-ray Laue photographs.

The effect of the cold worked layer on the mechanical properties of the crystals was investigated by testing, in the same conditions, specimens that were polished different amounts. The results of these tests, shown in Figure 3.5., indicate that the specimens retaining the larger amount of deformation have a greater work-hardening capacity. However, all the specimens tested exhibited the same proportional limit.

3.3. Machining of Compression Specimens

Prismatic compression specimens with the compression axis oriented in any desired crystallographic direction were machined by slitting the single crystalline rods with a carborundum disc turning at high speed.

The rod is clamped in a two stage goniometer (Figure 3.6.) designed to fit in both the X-ray bench and the magnetic table of the slitting machine. The crystal is conveniently oriented to be cut into slices with faces perpendicular to the direction chosen as the compression axis. These slices, that have accurate parallel faces, are held in the jig shown in Figure 3.7., and finally cut into prisms. The dimensions of the specimens, before electropolishing, are

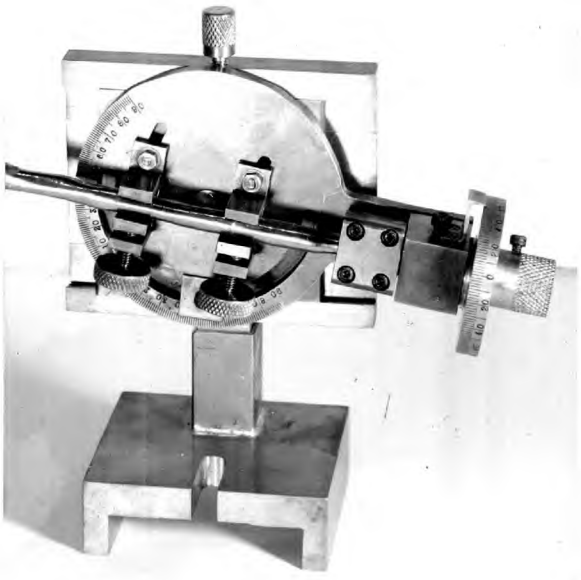

Figure 3.6. Two stage goniometer.

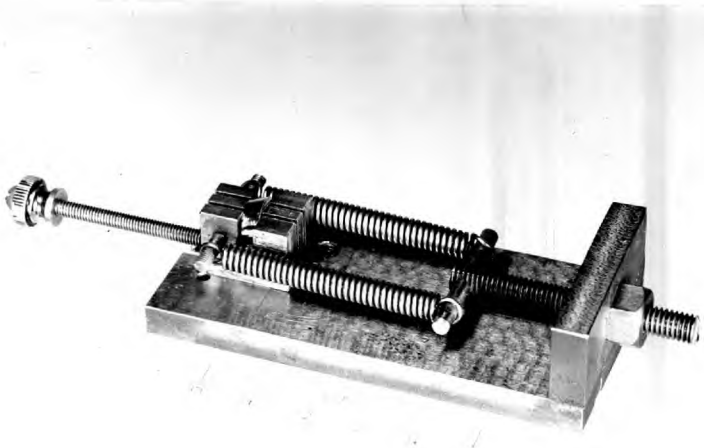

Figure 3.7. Jig for holding the compression specimens during the slitting operation.

3.55 x 3.00 x 3.00 mm. approximately. The compression axis is parallel to the larger dimension.

The deformed layer introduced during cutting is subsequently removed by electrolytic polishing in concentrated H_2SO_4.

After the specimens have been electropolished, its faces do not remain perfectly flat. The compression faces have been finally flatened by polishing with grade 500 silicon carbide paper. This operation introduces a cold-worked layer of 0.020 mm. that does not affect the mechanical characteristics of the crystal. This cold worked layer can also be removed with a very light electropolish.

The variation of the etch pit density with depth below the cold-worked surface was investigated in a specimen that had been annealed in vacuum at 1600°C for one hour. A slight recrystallization took place at the surface of the specimen, but at a depth of 0.025 mm. no recrystallization was observed and below 0.150 mm. the etch pit pattern and density was found to be already similar to that of an unstrained crystal. The asterism of the Laue spots disappeared completely after a layer of 0.040 mm. was removed from the machined surface.

The effect of the deformed layer on the mechanical properties of the compression specimens is shown

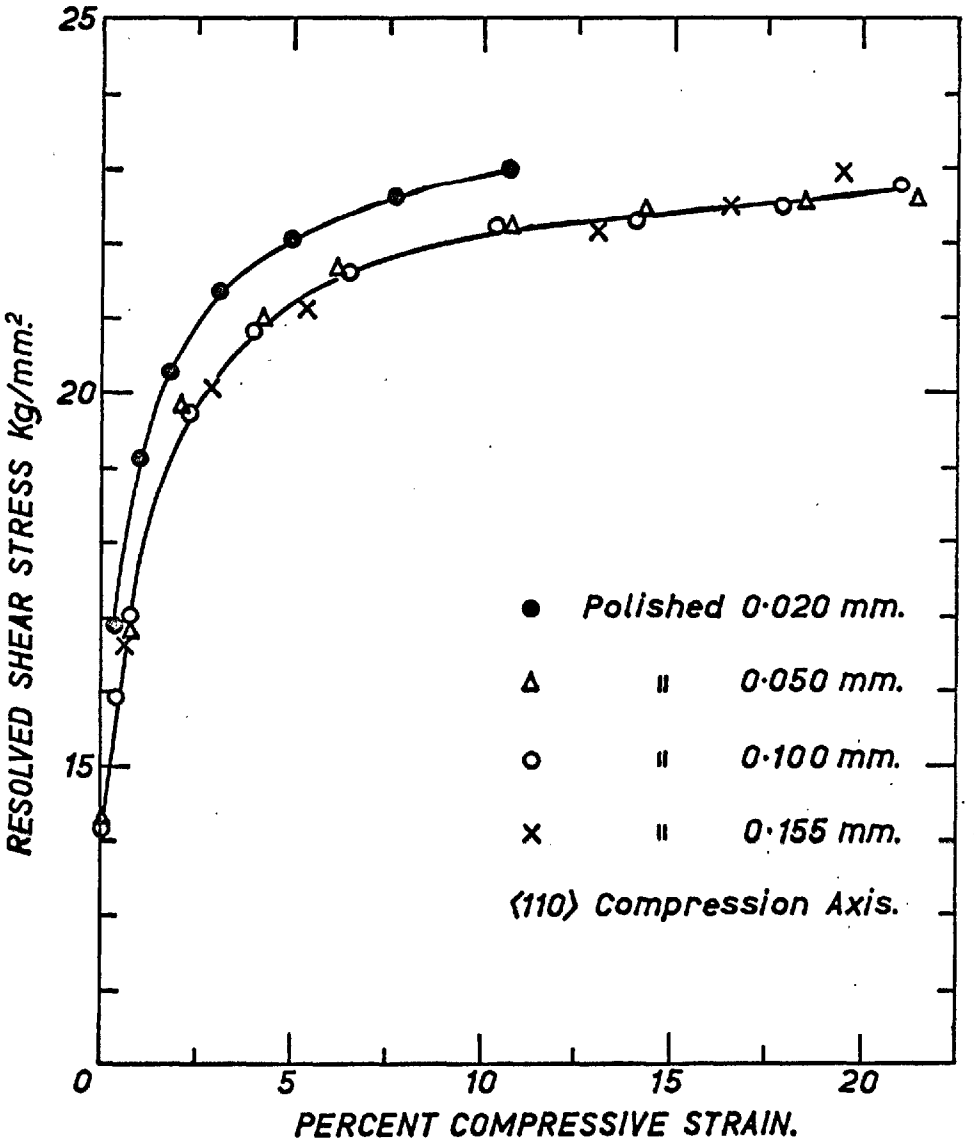

Figure 3.8. Effect of the cold-worked layer on the stress-strain curve of compression specimens.

in Figure 3.8. The results obtained in this case are rather similar to those obtained with the tensile specimens. The cold worked layer does not seem to affect the proportional limit of the crystals, but it increases their work-hardening capacity.

It appears that the criterion of the absence of asterisms in the Laue photographs is equivalent to the absence of surface damage that affects the work-hardening characteristics of the crystals, but both criteria seem to underestimate the thickness of the deformed layer introduced by careful mechanical machining.

CHAPTER 4

EXPERIMENTAL TECHNIQUES

4.1. Dislocation Etch Pits in Molybdenum

4.1.1. Etching Reagents

Although several reagents to etch molybdenum were known when this investigation was started, (Metals Handbook A.S.M. 1948) it appears that only Aust and Maddin (1956) had previously used some of them to reveal dislocation sub-boundaries in molybdenum. Following their work a series of tests were carried out to try to establish a simple and reliable dislocation etching procedure for molybdenum. Good etching characteristics were obtained with the following etchants.

a) Chemical etching in a 1:1 aqueous solution of HNO_3.

b) Chemical etching in a solution of 10 gms. $K_3Fe(CN)_6$, 10 gms. KOH, or NaOH, and 100 ml. H_2O.

c) Electro-etching in a 0.0025 M solution of $(COOH)_2$ with a voltage of 2V. and current density of 2 mA/cm^2.

The concentrations of the etchants were chosen so as to give a conveniently slow rate of attack and etching times easy to control. The four etchants reveal fresh dislocations without any previous decoration,

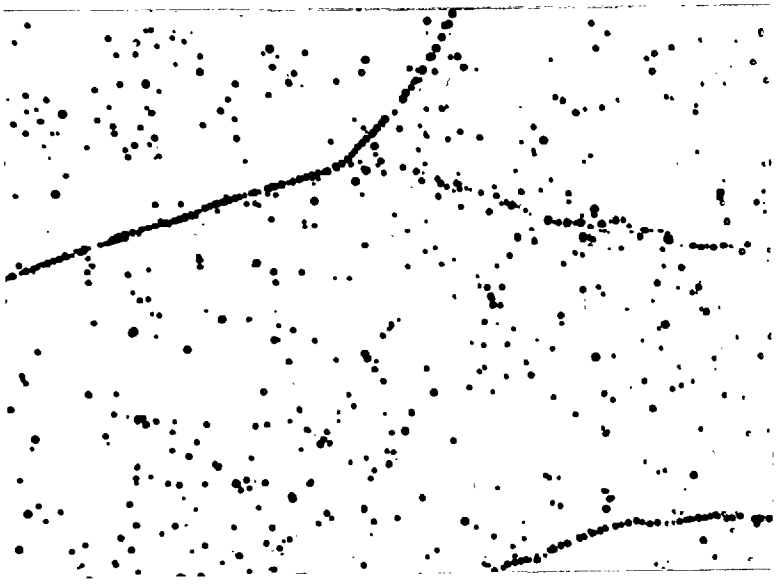

(a)

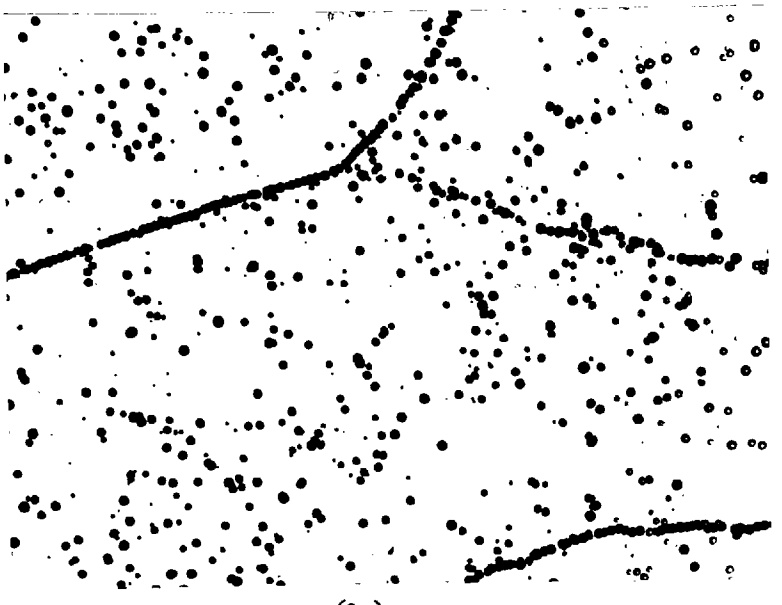

(b)

Figure 4.1. Dislocation etch pits on a {100} plane after etching times of (a) 20 seconds and (b) 40 seconds. Etchant c) x 250.

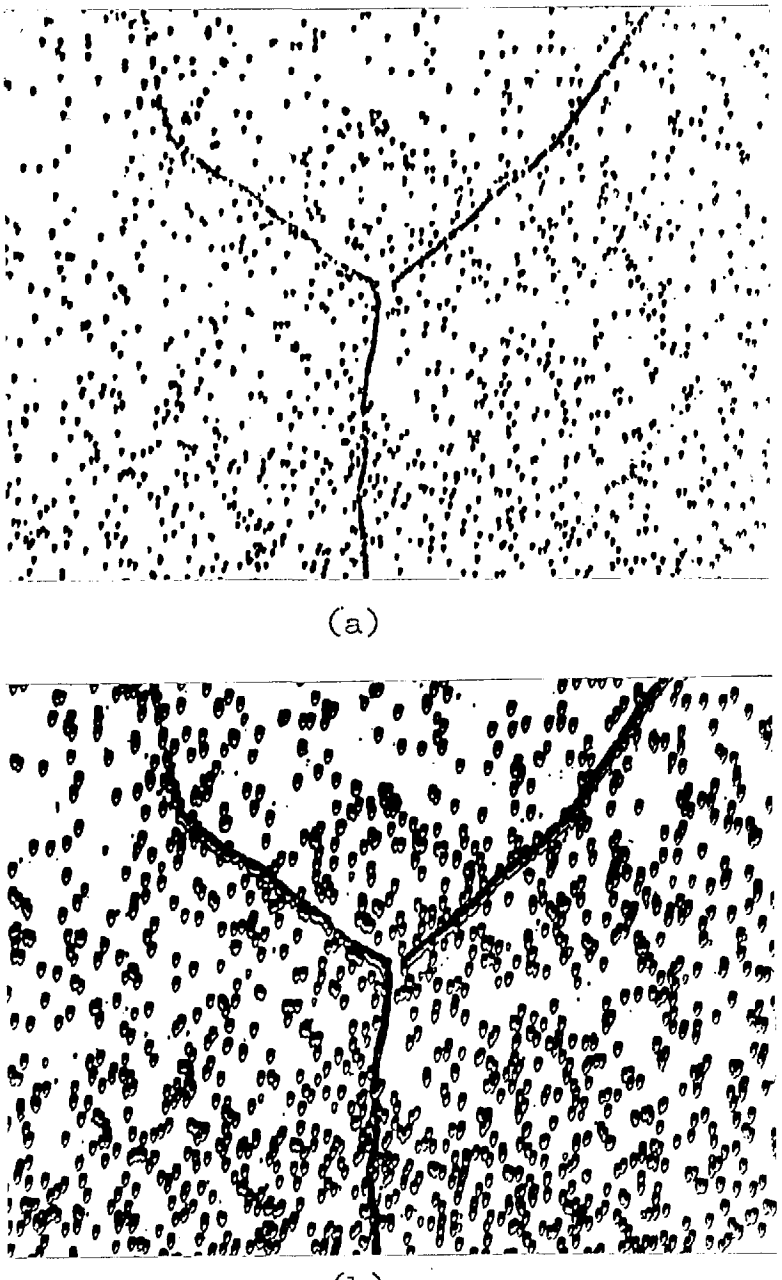

(a)

(b)

Figure 4.2. Dislocation etch pits on a {113} plane after etching times of (a) 20 seconds and (b) 75 seconds. Etchant c) x 500.

and they appear to be active on the same crystallographic planes, as they produce pits of similar shape. The rate of attack of etchant a) was found to be very sensitive to the temperature of the solution, and the best results were obtained with the last three which have exactly the same characteristics and have all been used in the etch pit studies described in this thesis.

4.1.2. Etching Characteristics

The etch pits produced on {100} planes appear almost conical, but they have really degenerated from pyramidal pits of a square base. As the plane of observation deviates from {100} the pits become more elongated. Figure 4.1. and Figure 4.2. show the dislocation etch pits on {100} and {113} planes respectively. It can be observed that the size of the pits increases with the etching time, whilst their density remains almost constant. The pits have a more regular size on {113} planes than on {100} planes.

The shape and orientation of the pits suggests that their faces are made of {110} planes. Similar etch pits are also produced in tungsten by the etching solution b) and detailed studies of their geometry have been made by Schadler (1962), and Berlec (1962).

Etch pits revealing the fresh dislocations produced

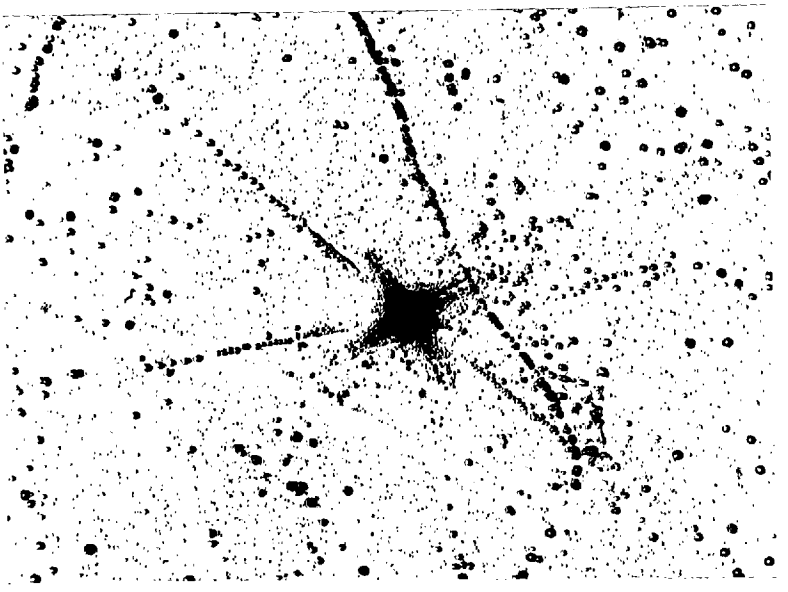

Figure 4.3. Etch pits revealing the fresh dislocations produced by a microhardness indentation on a {100} plane. Etchant c) x 200.

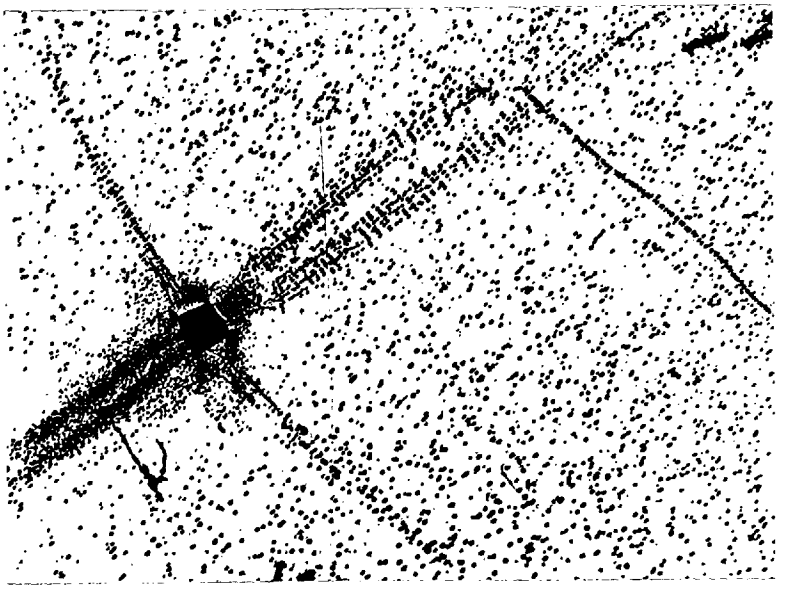

Figure 4.4. Etch pits revealing the fresh dislocations produced by a microhardness indentation on a {113} plane. Etchant c) x 200.

by a microhardness indentation on a {100} and on a {113} plane are shown in Figures 4.3 and 4.4. It was observed that when a scratch or indentation is made on a {100} plane, which had been previously etched, a subsequent etching does not reveal the fresh dislocations introduced by the deformation. It seems, therefore, that the surface becomes passivated as a result of etching. However, when the same experiment is repeated on a {113} plane, the fresh dislocations are revealed as small etch pits, superimposed on the background of the larger pits corresponding to the original dislocations.

4.1.3. Variation of the Etch Pit Density with the Plane of Observation

A very peculiar characteristic of all the etchants investigated is that the density of the etch pits formed on a certain plane increases with the angle that this plane makes with {100}, on which the density is a minimum. In order to illustrate this effect, a series of photographs were taken of an etched cylindrical specimen with its axis in the <110> direction. The variation of the etch pit density with the observation plane is shown in Figures 4.5. and 4.6. The pits could not be revealed on {112} planes; not even after having reduced the dislocation density by

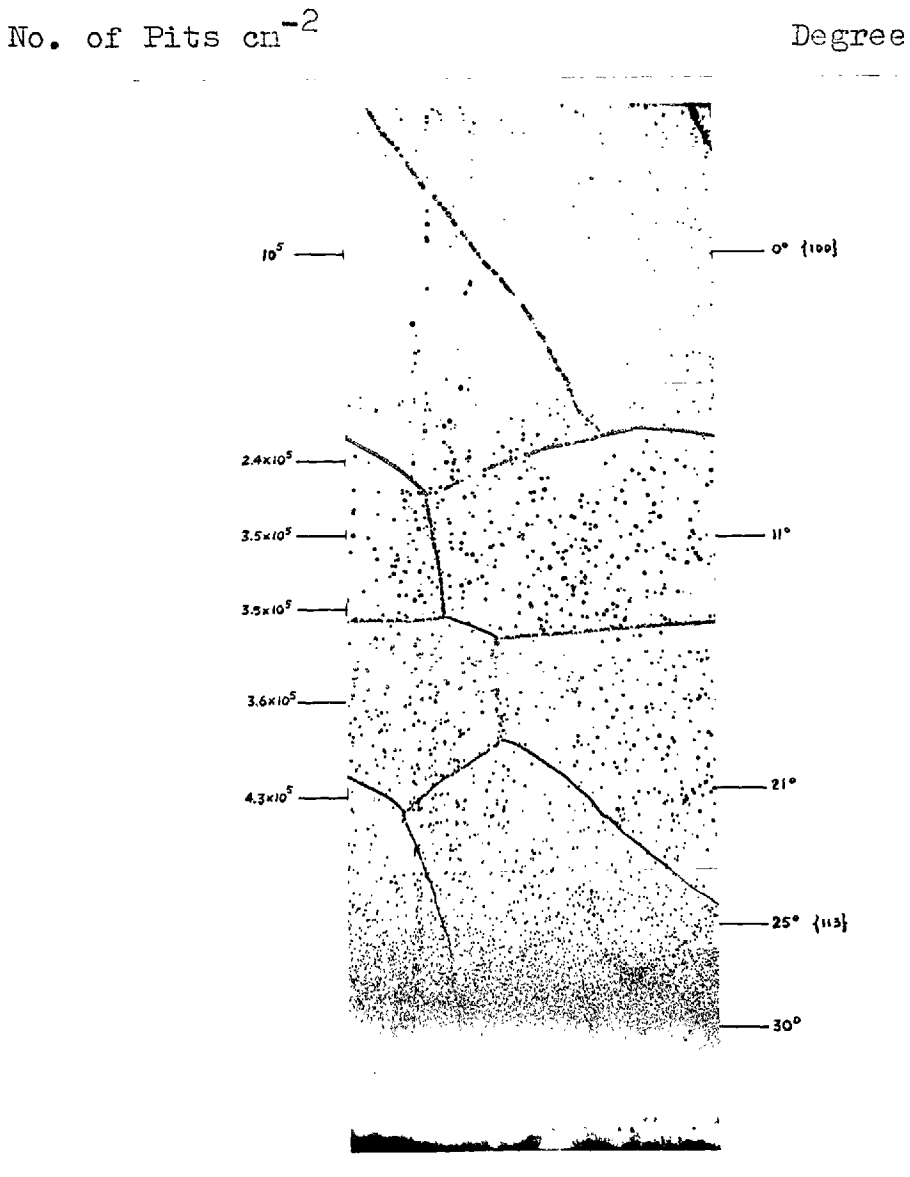

Figure 4.5. Variation of the etch pit density with the plane of observation. Etchant c) x 80.

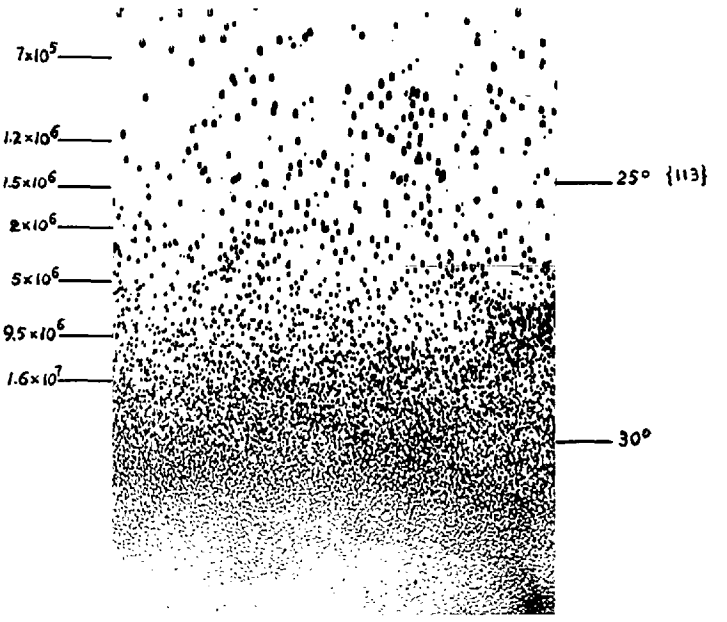

Figure 4.6. The {113} region of Figure 4.5 at a higher magnification. x 200

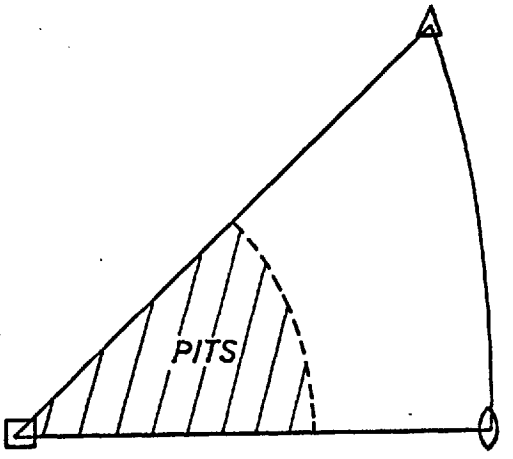

Figure 4.7. Orientation of the planes on which the etch pits can be formed.

a prolonged annealing of the crystal near the melting temperature. The region of the unit stereographic triangle containing the poles of the planes that can be effectively etched is shown in Figure 4.7. This effect cannot be the result of a preferential dislocation arrangement in the crystal, because it is a characteristic of all the planes of the same form and not of a particular set of planes.

In view of this result, it would be pointless to try to establish a one to one correspondence between etch pits and dislocations. It is surprising that Aust and Maddin (1956), and Duan et al. (1963) claim to have verified such a correspondence, using etchant c).

No further investigation was conducted to elucidate either the effect of the orientation of the observation plane on the etch pit density or the apparent passivation of the {100} planes.

The limitations of the etching procedure for quantitative studies are obvious, and a conclusion of practical importance is that planes other than {100} are the most convenient for etch pit observations.

4.2. Testing Techniques and Equipment

4.2.1. Single Crystal Specimens

All the experiments described in this thesis were

conducted with 'two pass' crystals grown by the technique described in Chapter 2, where details of their purity and structure are given.

The preparation of the tensile and compression specimens is described in Chapter 3. After machining, a layer between 0.001 and 0.015 mm. thick was removed from the machined surface by electropolishing. The final dimensions of the specimens are approximately as follows:

Compression specimens:

Cross section: 2.8 x 2.8 mm^2.

Gauge length: 3.3 mm.

Tensile specimens:

Cross section: 2.1 x 2.3 mm^2.

Gauge length: 12.7 mm.

Fillet radius of the shoulder: 0.5 mm.

A few tensile specimens of the same cross section and gauge length of 18.0 mm. were occasionally used.

4.2.2. Testing Machine and Accesories

The tests were conducted in an Instron machine Model TT-CM, and 500 as well as 5000 kg. capacity load cells were used. With this machine, discretely variable cross-head speeds between 0.005 and 50 cm/min can be obtained. The automatic load recorder has a ¼ second full scale response.

For tests at other than room temperature a frame made of nickel plated mild steel, mounted on the bottom of the mobile cross head, was used. This frame can be immersed in a liquid during the test. Its lower part is shown in Figure 4.8. holding the jig that was used for the compression tests. The compression plates, made of hardened steel, were ground and lapped.

Special grips were designed to fit the tensile specimens used.

The compliance of the system composed of testing machine, load cell, universal coupling and grip adapters is 0.0011 mm/kg at a load of 50 kg, and 0.00075 mm/kg at a load of 500 kg. When the frame for low and high temperature tests is incorporated in the system, the compliance is 0.0013 mm/kg at a load of 50 kg, and 0.0008 mm/kg at a load of 500 kg.

4.2.3. Methods of Obtaining Test Temperatures

The different testing temperatures were obtained by immersing the frame and the specimen in liquid baths contained in a Dewar flask. For the temperatures below 20°C the following coolants were used:

-20°C - Mixture of ice and NaCl

-30°C - Boiling liquid CCl_2F_2 (Isceon 12)

-78°C - Sublimation of solid CO_2 in acetone, or

Figure 4.8. Frame for carrying out tests in a constant temperature liquid medium. (Compression jig in position).

CCl_3F (Isceon 11) cooled with liquid N_2.

$-120^{\circ}C$ - Isceon 12 cooled with liquid N_2

$-196^{\circ}C$ - Boiling liquid N_2.

These temperatures were maintained constant within $\pm$ $1^{\circ}C$ during the test.

Temperatures above $20^{\circ}C$ were obtained by heating a silicone oil bath with an electric resistance placed in the bottom of the Dewar flask. The temperature was stabilised within $\pm$ $0.5^{\circ}C$ by adjusting the heating voltage with a variable transformer.

The temperatures were measured with pentane and mercury immersion thermometers placed close to the specimen.

CHAPTER 5

THE EFFECT OF ORIENTATION ON THE YIELDING AND FLOW OF MOLYBDENUM SINGLE CRYSTALS

5.1. Introduction

When the present investigation was started, no information was available on the effect of orientation on the deformation characteristics of molybdenum single crystals. Therefore some preliminary tests were conducted with compression specimens in order to establish which orientations are the most significant to examine for providing a full picture of the deformation properties of the single crystals. As a result of these tests, it was decided to investigate the mechanical properties of the crystals with their deformation axis in the ⟨110⟩, ⟨100⟩, and ⟨111⟩ directions, and also in a direction lying near the centre of the unit stereographic triangle.

The results of these investigations are described and discussed in the following sections.

5.2. Deformation Axis in the [011] Direction

Typical stress-strain curves of crystals deformed under a stress applied in the [011] direction at various temperatures and cross-head speeds are shown

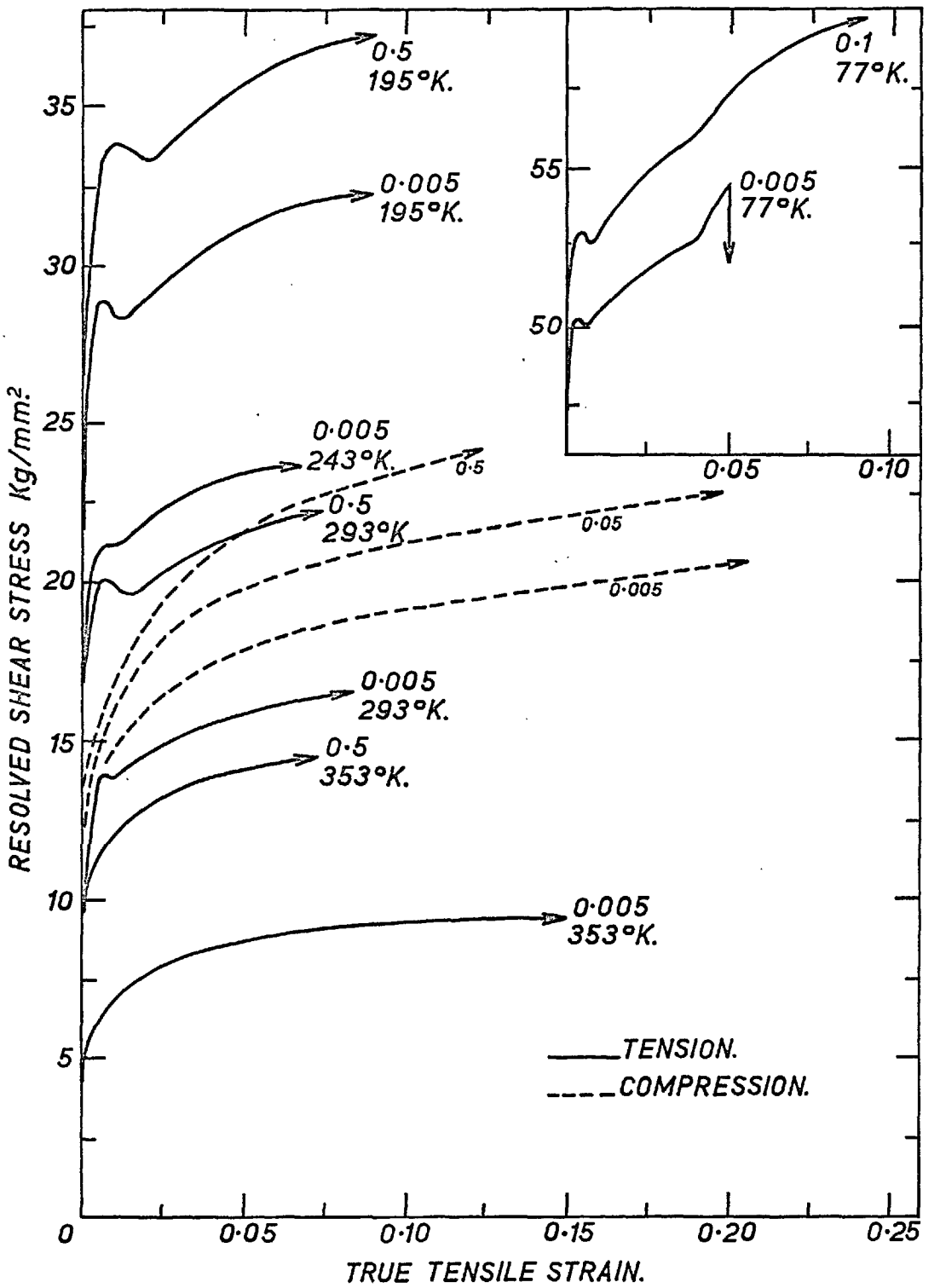

Figure 5.1. Stress-strain curves of crystals with the deformation axis in the ⟨110⟩ direction. The numbers, 0.5, 0.1, 0.05, and 0.005 refer to the cross-head speeds in cm/min.

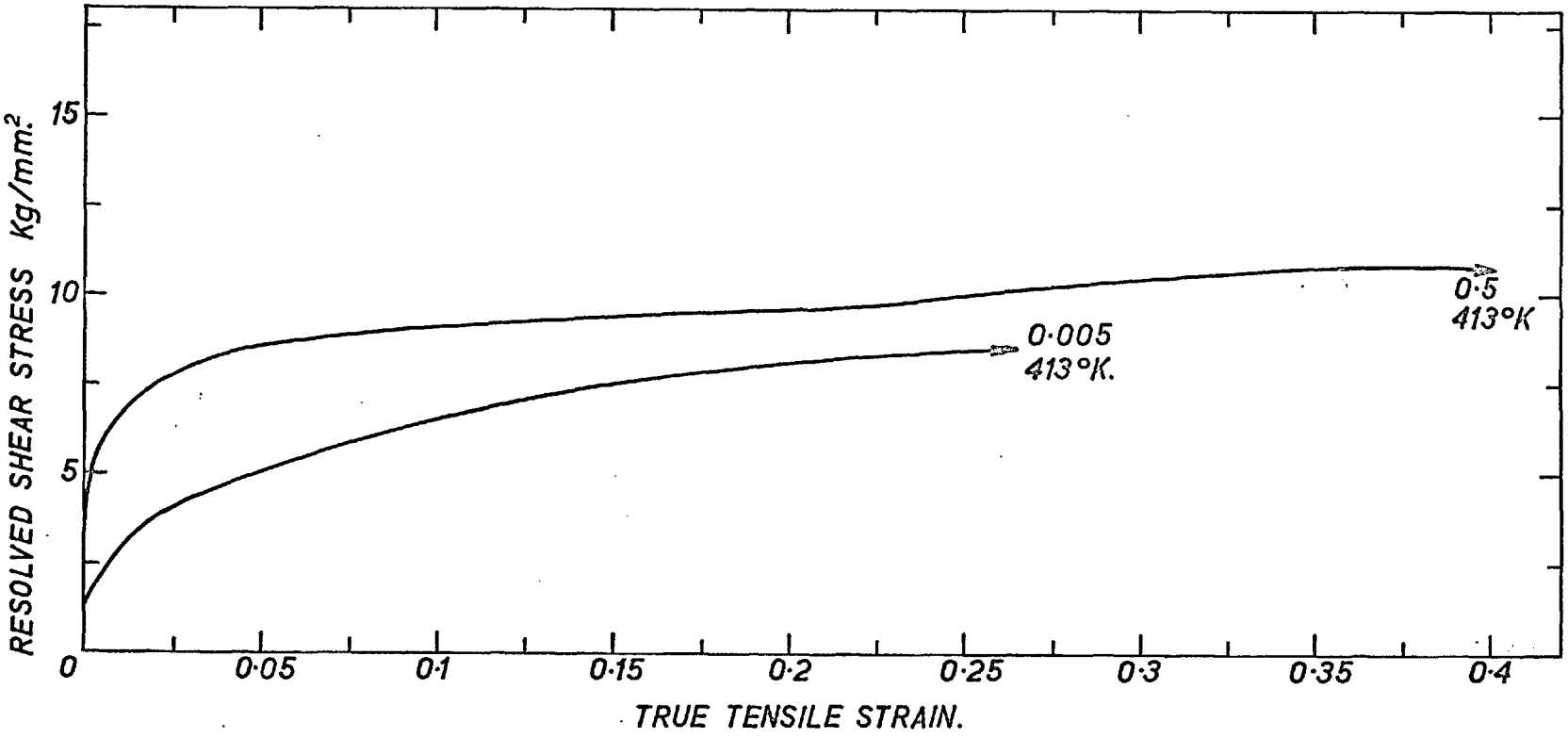

Figure 5.2. Stress-strain curves of crystals with the deformation axis in the ⟨110⟩ direction. The numbers, 0.5 and 0.005 refer to the cross-head speeds in cm/min.

in Figures 5.1. and 5.2. The values of the proportional limits and yield stresses are summarised in Table 5.1. The proportional limit is defined as the value of the stress at which the first departure from linearity is observed in the load-elongation curve. When a yield drop is present, the lower yield stress is used as the yield stress, and in the absence of a yield drop the extrapolated value of the flow stress on to the elastic slope of the stress-strain curve is taken.

A pre-yield region followed by a smooth yield drop is observed in the crystals deformed at and below room temperature. The subsequent work-hardening rate is rather low and almost insensitive to temperature. However, at 353^{o}K the yield drop disappears and as the temperature is further increased the crystal can experience a large uniform elongation.

Unless otherwise stated, the curves of Figures 5.1. and 5.2. are plotted up to the onset of necking. The necking is always very localised and fracture occurs after 100% of reduction in area, giving rise to a perfect type of 'chisel' fracture clearly visible in Figure 5.3. where it can also be observed that the reduction in area has taken place only in one direction.

At 77^{o}K some specimens fractured prematurely by cleavage at the shoulder, and in one case the fracture

TABLE 5.1.

Proportional limit and yield stress of single crystals with the deformation axis in the [011] direction.

	Temperature ^{o}K	Cross-head speed cm/min	Proportional limit kg/mm^2	Yield stress kg/mm^2
Tensile Tests	413	0.005	1.1	2.5
		0.100	1.5	4.0
		0.500	3.5	6.0
	353	0.005	4.1	6.0
		0.100		10.0
		0.500	8.9	10.8
	293	0.005	11.2 ± 0.7	13.9 ± 0.2
		0.010	11.5	
		0.100	13.4	17.2 ± 0.5
		0.500	16.6	19.6 ± 0.7
		1.000	15.0	18.5
	243	0.005	16.6	21.2
		0.100	20.0	25.0
	195	0.005	21.5	28.3
		0.100		31.2 ± 0.2
		0.500	26.6	33.5
	77	0.005	47.2	50.1
		0.100	51.0	52.6

TABLE 5.1. Continued.

	Temperature ^{o}K	Cross-head speed cm/min	Proportional limit kg/mm^2	Yield stress kg/mm^2
Compression Tests	293	0.005	10.7 ± 0.3	
		0.010	10.7 ± 0.3	
		0.020	12.7 ± 0.2	
		0.050	13.5 ± 0.5	
		0.100	14.2 ± 0.2	
		0.200	15.0	
		0.500	16.7 ± 0.7	

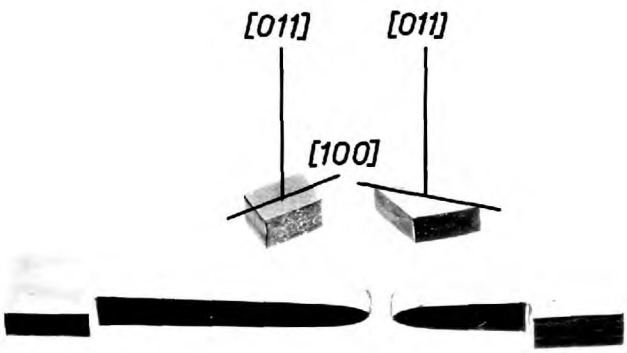

Figure 5.3. The appearence of the tensile and compression specimens after having been deformed.

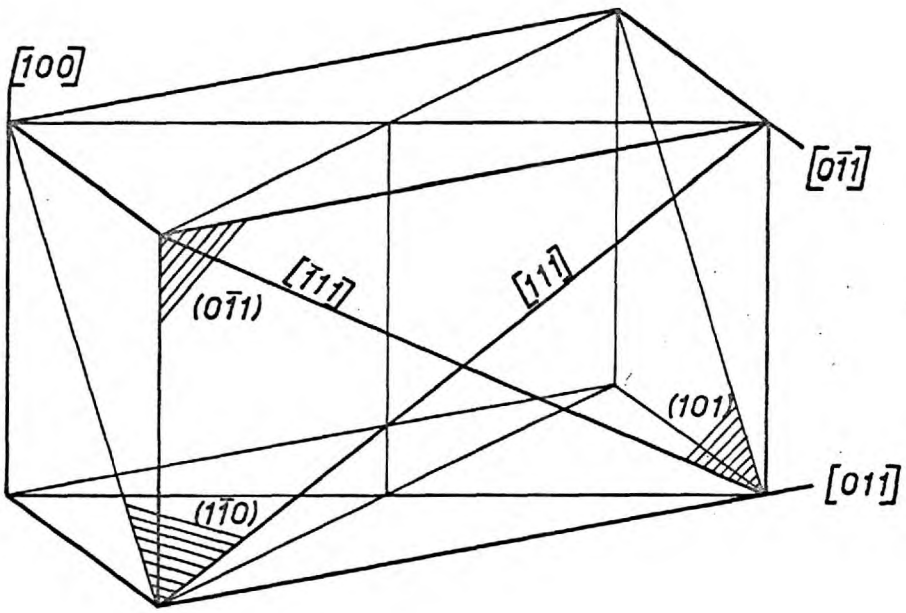

Figure 5.4. Geometrical relationship between the deformation axis and the slip directions

was accompanied by twinning.

The results of a few compression tests, carried out at room temperature, are also included in Table 5.1. The corresponding stress-strain curves are shown in dotted lines in Figure 5.1. It is not surprising that these curves do not show any yield drop, since yield drops are difficult to obtain in compression tests, and even more in the present case where no extra care was taken to ensure perfect axial loading. Furthermore, rather short compression specimens were used for these tests, and the effect of friction between the specimen and compression plates should be rather important. This is possibly the reason why the flow stress in compression is so much higher than the corresponding flow stress in a tensile test performed at a similar strain rate.

The compression experiments show more clearly the unidirectional deformation of the crystals which has already been pointed out when describing the necking of the tensile specimens. Two deformed compression specimens are shown in Figure 5.3. It can be observed that only one of the dimensions of their cross section has increased. This effect results from the fact that when a stress is applied in the [011] direction there are only two active slip directions, which at the same time are coplanar with the deformation

axis. This situation is illustrated in Figure 5.4. When the [100] direction is a diagonal of the cross section a deformed compression specimen assumes a rhombohedral shape, as shown in Figure 5.3.

The values of the Schmid factor (i.e. ratio between resolved shear stress and applied tensile or compressive stress) for the possible slip systems involving {110} and {112} type planes when the deformation axis is in the [011] direction are given in Table 5.2.

TABLE 5.2.

Schmid factors for different slip systems when the deformation axis is in the [011] direction.

Slip Direction	Slip Plane	Schmid Factor
$[\bar{1}11]$	(211)	0.4714
	(101)	0.408
	(110)	0.408
	$(1\bar{1}2)$	0.236
	$(12\bar{1})$	0.236
[111]	$(\bar{2}11)$	0.4714
	$(\bar{1}10)$	0.408
	$(\bar{1}01)$	0.408
	$(11\bar{2})$	0.236
	$(1\bar{2}1)$	0.236

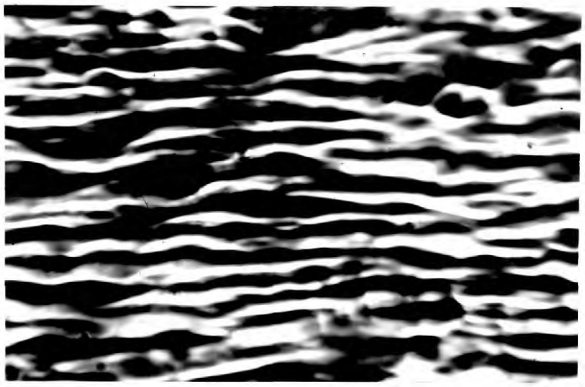

Figure 5.5. Wavy slip lines on the (100) plane after 25% compressive strain at 293°K. x 140.

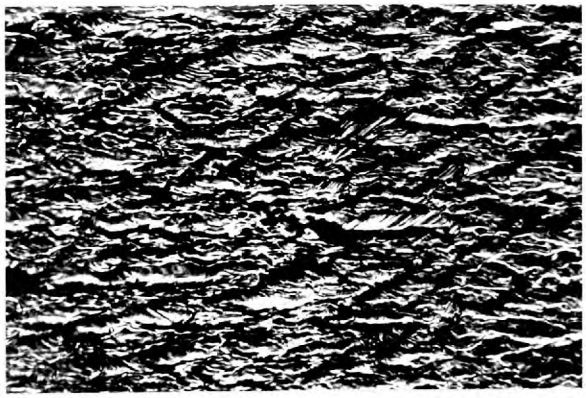

Figure 5.6. Wavy slip lines on the (100) plane after 30% tensile strain at 353°K. x 200

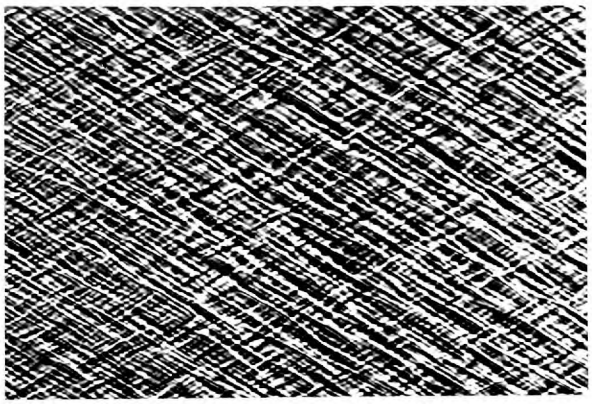

Figure 5.7. Straight slip lines on the $(0\bar{1}1)$ plane after 30% tensile strain at 353°K. x 200

From the distortion of the compression specimens and from the chisel aspect of the fracture of the tensile specimens it could be inferred that slip takes place symmetrically with respect to the two-fold [011] symmetry axis. On the other hand, X-ray Laue back-reflection photographs of specimens deformed at various temperatures showed no rotation of the deformation axis and this result confirms that, in fact, symmetrical operative slip systems are equally strained throughout the deformation at all the temperatures investigated.

5.2.1. Slip Line Observations

The slip lines are usually very difficult to resolve with the optical microscope after deformations smaller than 6% tensile strain. In the specimens strained at and below room temperature the slip lines are only clearly defined in the region of the neck. The aspect of the slip lines when viewed on a surface near the (100) plane, after heavy deformation, is very wavy (Figure 5.5. and 5.6.) but they are straight and long on planes nearly parallel to the slip directions (Figure 5.7. and 5.8.). Similar observations were reported much earlier by Vogel and Brick (1953) in iron and by Maddin and Chen (1954) in molybdenum.

The unambiguous identification of the slip planes

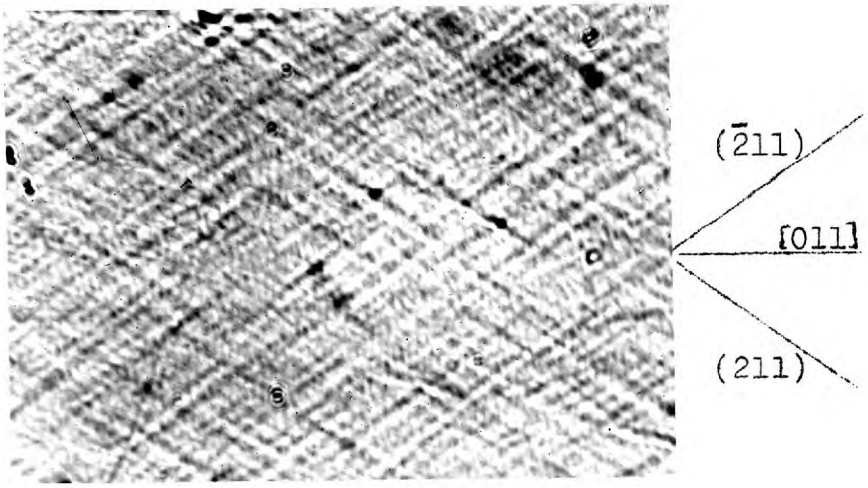

Figure 5.8. Slip lines on the $(2\bar{5}5)$ plane after 7% tensile strain at 293°K. x 200.

Figure 5.9. Slip lines on the $(5\bar{1}1)$ plane after 7% tensile strain at 293°K. x 500.

by means of the slip traces observed on surfaces nearly parallel to the slip directions is very difficult. For this reason, clear evidence of slip in {110} type planes could not be obtained, and only in one case could the slip lines be identified with the traces of $(\bar{2}11)$ and (211) planes. These traces are shown in Figure 5.7. The observation was made on a $(2\bar{5}5)$ plane of a tensile specimen strained 7% at room temperature. On the $(51\bar{1})$ face of the same specimen the slip lines in regions away from the neck appear as shown in Figure 5.9. These lines which are traces of $(11\bar{2})$ and $(12\bar{1})$ planes were also observed in many of the specimens deformed at different temperatures.

5.2.2. Dislocation Etch Pit Observations

Several specimens were etched after being strained different amounts in order to observe the development of the etch pit pattern in the early stages of the deformation. Although a general increase in the number of dislocation etch pits was always observed, the arrangement of the pits did not conform to any significant pattern. The variation of the etch pit density with the shear stress in specimens deformed at two different temperatures is shown in Figure 5.10. A significant increase in the number of etch pits is observed in the region of the

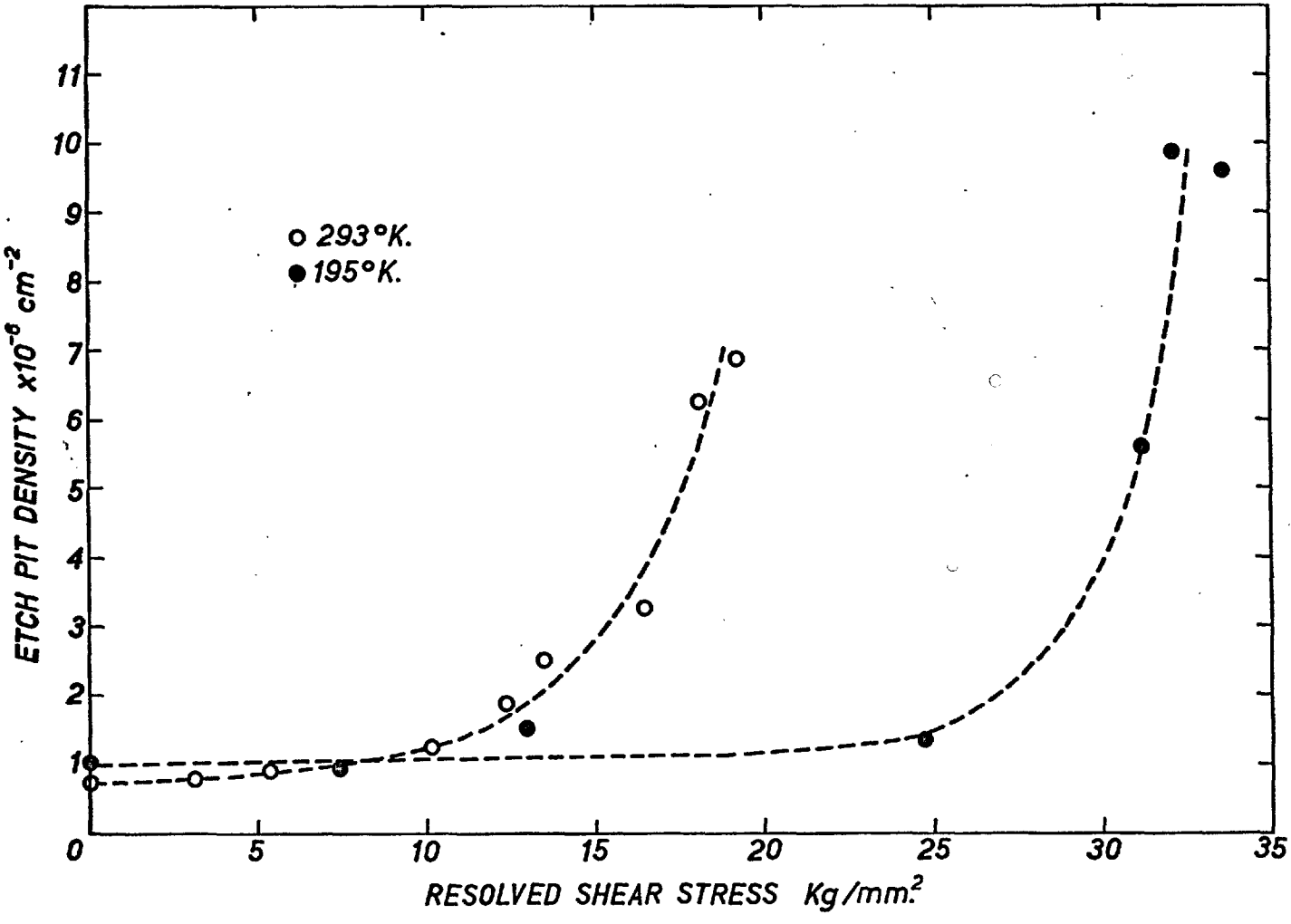

Figure 5.10. Variation of the etch pit density with the applied stress. Deformation axis in the ⟨110⟩ direction.

proportional limit. The homogeneous distribution of the pits after different amounts of strain is shown in Figure 5.11.

The general features of the etch pit pattern and the failure to observe dislocation arrays are in good agreement with the wavy aspect of the slip lines that appear on the same surfaces after heavier deformations. These results give support to the idea that the waviness of the slip lines is the result of profuse cross-slip or 'composite slip' (Maddin and Chen 1954). This is consistent with the fact that the dislocations intersecting the faces where these lines are observed have a predominantly screw component, and that in the present case the conditions for cross-slip of the screw dislocations between (101) and (110) planes, and ($\bar{1}$10) and ($\bar{1}$01) planes are optimum.

The dislocations that intersect the surfaces where the slip lines are straight have a predominant edge component and well defined arrays of dislocations are more likely to exist there. Unfortunately they cannot be revealed with the etchant that has been used because it is only effective on planes near {100}.

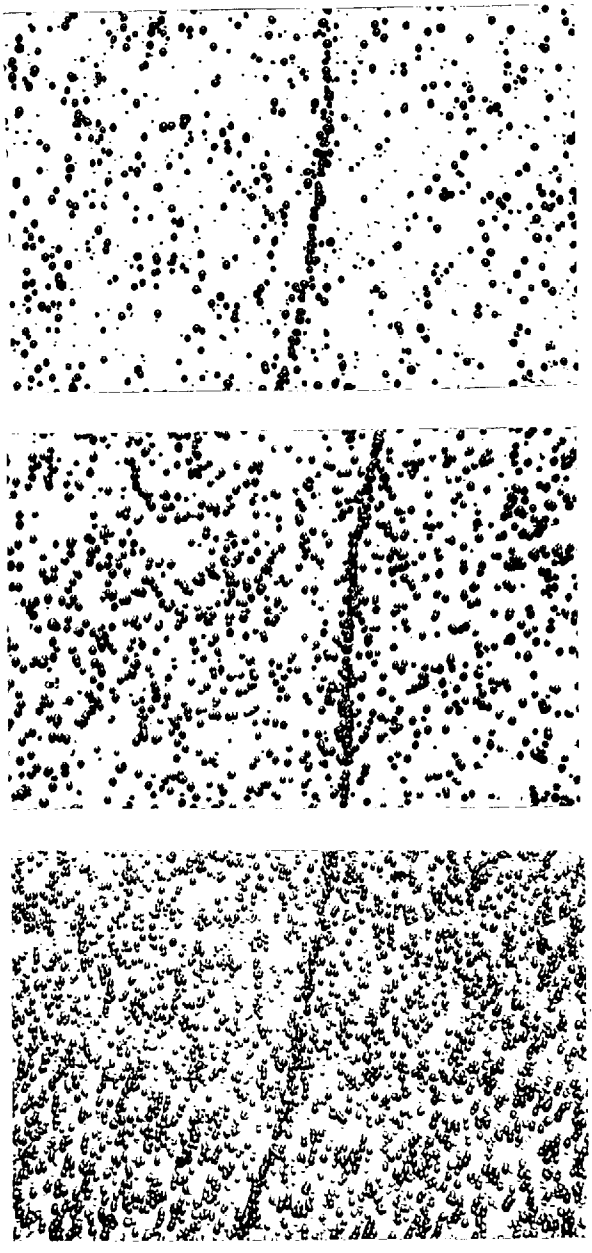

Figure 5.11. Dislocation etch pits on a plane near (100) after different amounts of strain. Deformation axis in the [110] direction. x 200.

5.2.3. Asterism of the Laue Spots

The asterism of the Laue spots usually observed in the X-ray back-reflection photographs of deformed crystals is believed to be produced by the rotation of the slip planes around an axis which is perpendicular to both the slip direction and the pole of the slip plane (Chen and Maddin 1951). From a stereographic plot of this asterism it is possible, in some cases, to determine the operative slip plane, (Chen and Maddin 1951, Maddin and Chen 1953) and this method has been used in the present investigation.

Figure 5.12. shows the asterism of a specimen deformed in tension at 413°K. The stereographic plot of Figure 5.14. indicates that slip has taken place in $(\bar{2}11)$ planes and, by symmetry, also in (211) planes. The same planes were found to be active in specimens deformed in compression at room temperature.

The determination of the axis of rotation of the crystallographic planes in the case of specimens deformed at 77°K was not so simple. When the asterism of the Laue spots (Figure 5.13.) was plotted stereographically a unique axis of rotation was not found. The plot of Figure 5.14. shows that this result can be explained by simultaneous slip on (211), (110) and (101) planes.

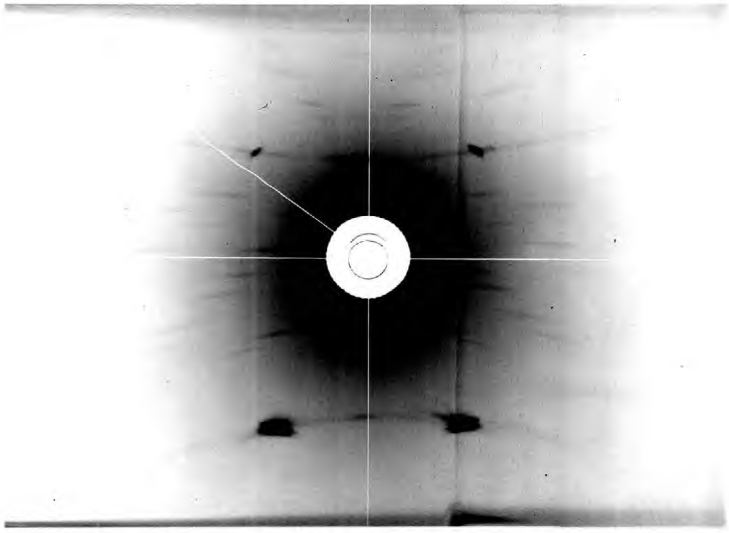

Figure 5.12. Asterism of the Laue spots for a crystal deformed 36% at 413°K. The [100] direction is perpendicular to the plane of the photograph.

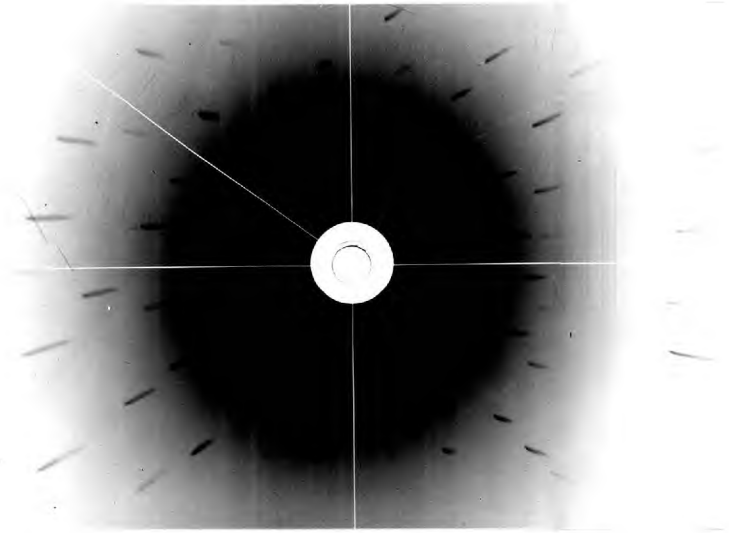

Figure 5.13. Asterism of the Laue spots for a crystal deformed at 77°K. The [100] direction is almost perpendicular to the plane of the photograph.

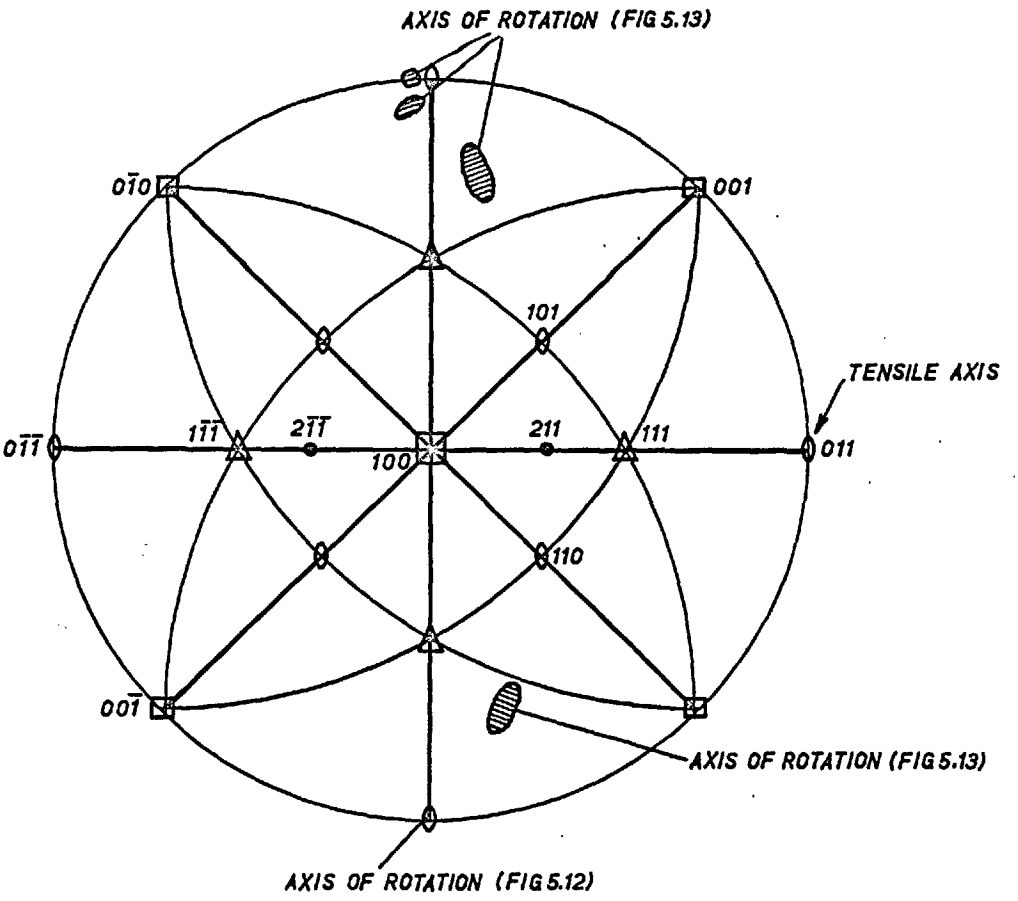

Figure 5.14. Stereographic representation of the asterism of Figures 5.12 and 5.13.

5.2.4. Twinning and Cleavage Fracture

Twinning and simultaneous cleavage fracture occurred near the shoulder of one specimen tested at 77°K. The photographs of Figures 5.15. (a, b and c) show some of the twin traces on a $(\bar{3}11)$ plane. The twinning planes responsible for these traces are $(11\bar{2})$ and $(12\bar{1})$ which, together with the directions $[111]$ and $[\bar{1}11]$ respectively, correspond to the twin systems 7 and 11 in the notation of Schmid and Boas (1950). Slip lines following the traces of $(12\bar{1})$ planes can also be observed in Figure 5.15(a), and this indicates that slip occurred prior to twinning.

From the aspect of the twins near the fractured surface, and from the presence of a great number of cracks crossing the twins, it can be concluded that twinning occurred prior to fracture, and there is good reason to believe that fracture was nucleated by twinning itself.

The type of crack nucleating twins commonly observed to cause cleavage fracture in b.c.c. metals are those that intersect along a $\langle 110 \rangle$ direction (Honda 1961). Some authors (Hull 1960, Gleeswyk 1962) find it more convenient to express the same condition by saying that these types of twin intersect on $\{100\}$ planes, if they have finite thickness and meet at their tips. The explanations that are given to this

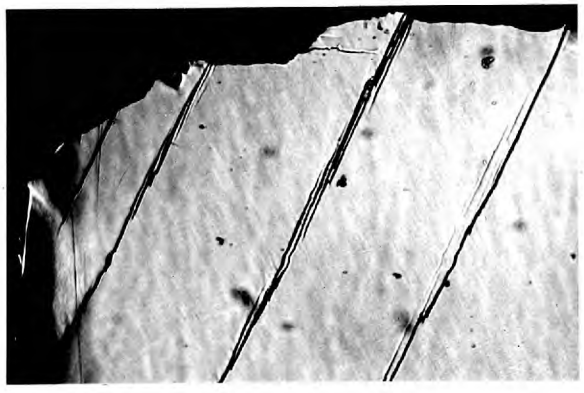

(a)

x 200

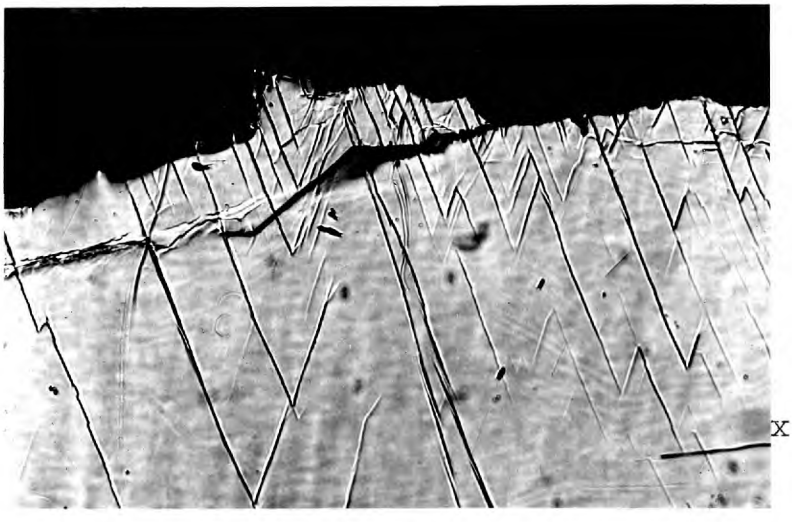

(b)

x 80

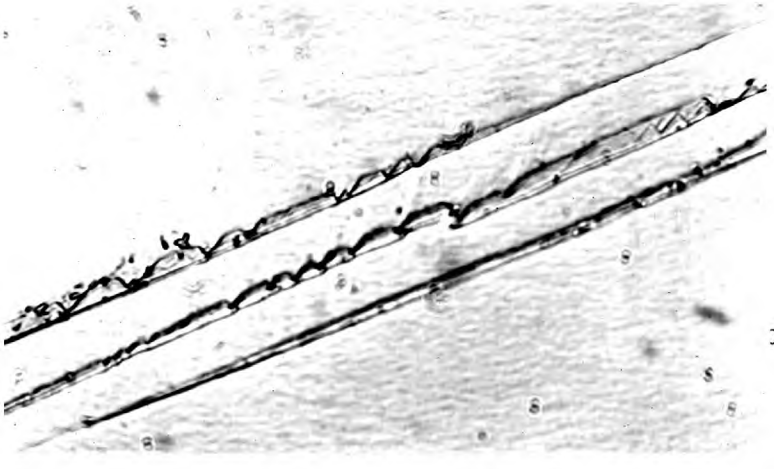

(c)

x 1000

Figure 5.15. Twins observed on the $(\bar{3}11)$ plane of a crystal deformed in the [011] direction at 77°K. The horizontal cracks are on (011) planes.

experimental fact are based on the idea that cleavage in b.c.c. metals is only possible on {100} planes. From this it follows, irrespective of the crack nucleating mechanism involved, that it is impossible to create micro-cracks leading to brittle fracture by twin intersection under a tensile stress in the ⟨110⟩ direction (Sleeswyk 1962). However the present case constitutes an interesting exception.

If the twins observed in this case have a finite thickness and meet at their tips, they intersect on a (011) plane. It can be observed in Figure 5.15(b) that the twins here involved are of 'non-crossing' type, i.e. they are arrested when they meet another twin. Therefore the formation of a crack in the plane of intersection of the twins can be considered in terms of the strain concentration at the tip of the stopped twin (Honda 1961, Hull 1961). This mechanism is regarded as more plausible than the formation of a sheet of holes in the (110) plane as a result of the dislocation reaction $a/6\ [111] + a/6\ [1\bar{1}\bar{1}] \rightarrow a/3\ [100]$ proposed by Hull (1960). Nor is the emissary dislocation reaction $\frac{a}{2}[111] + \frac{a}{2}[\bar{1}11] \rightarrow a[011]$ energetically favourable (Sleeswyk 1962). The idea of a cleavage crack on the (011) plane opening under the action of the applied stress, normal to that plane, is consistent with the appearence of the

fracture. In fact, cracks on (011) planes are clearly visible in Figures 5.15 (a) and 5.15 (b), although the fracture deviated subsequently towards the (001) and (010) planes which formed the major part of the fractured surface.

Cleavage in {110} type planes has been reported in the past in silicon iron (Honda, 1961), tantalum (Barrett and Bakish, 1958).and niobium (Churchman 1960); and more evidence of this type of cleavage has been found in other specimens during the present investigation.

5.3. Deformation Axis in the [001] Direction

Typical stress-strain curves of crystals deformed in the [001] direction at various temperatures and cross-head speeds are shown in Figures 5.16. and 5.17. The crystals tested in this orientation yield smoothly at relatively low stresses and show a large initial work-hardening rate. As a result of this, it was difficult in some cases to detect accurately the deviation from the elastic region in the load-elongation curve, and therefore a large relative error may be involved in the determination of the proportional limit. Values of the proportional limits of crystals tested under different conditions are given in Table 5.3.

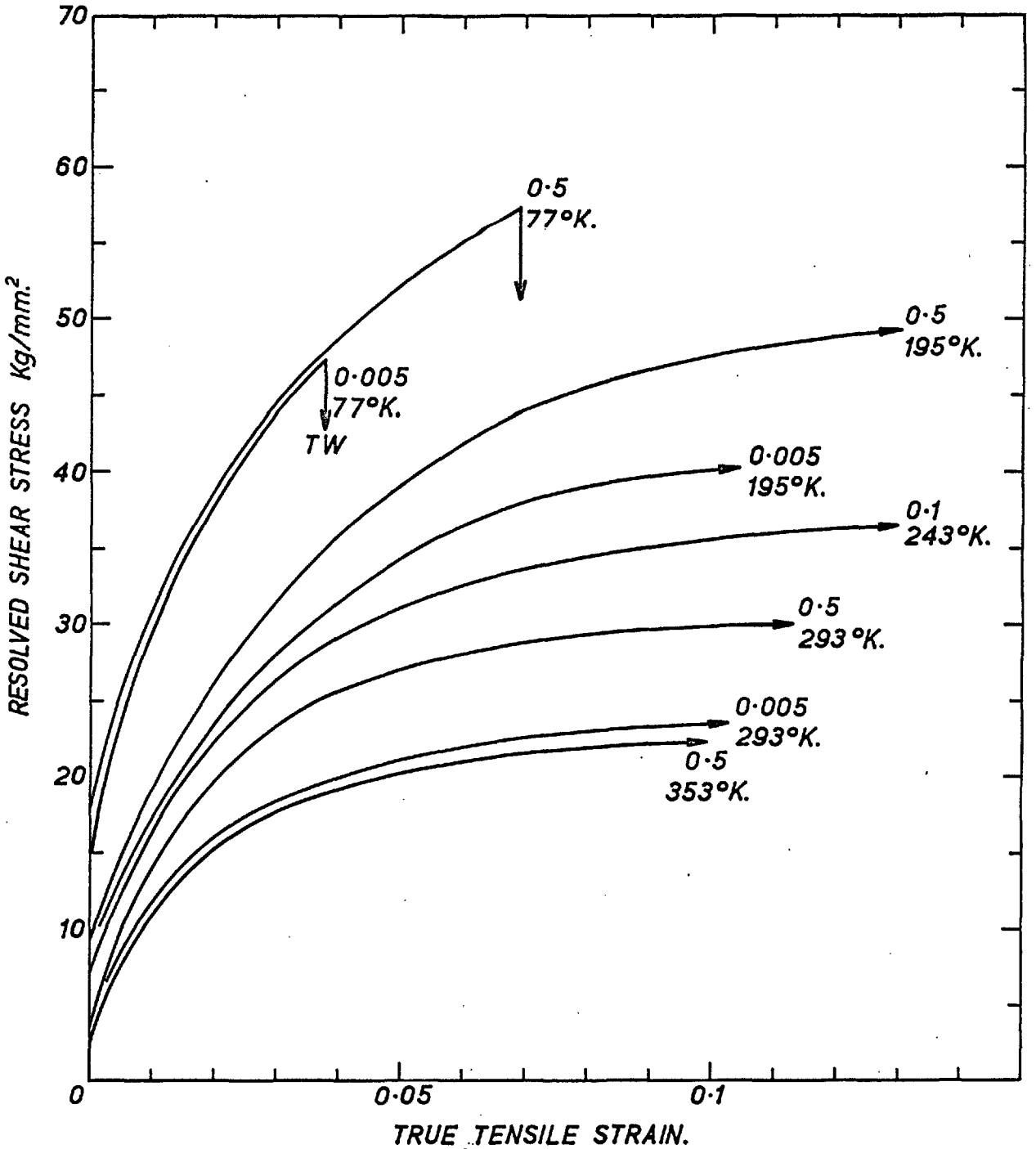

Figure 5.16. Stress-strain curves of crystals with tensile axis in the ⟨100⟩ direction. The numbers 0.5, 0.1, and 0.005 refer to the cross-head speeds in cm/min.

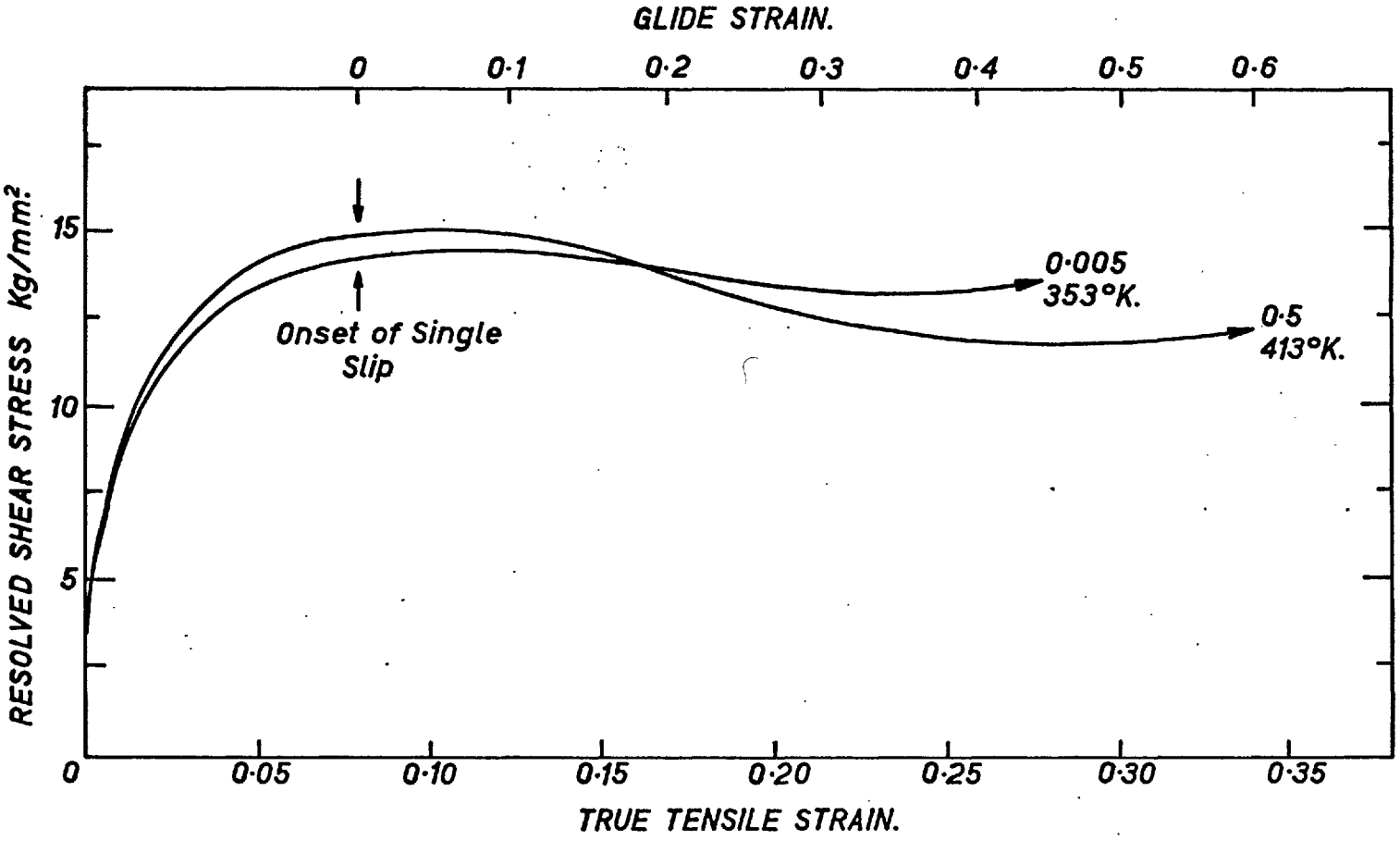

Figure 5.17. Stress-strain curves of crystals with the tensile axis in the ⟨100⟩ direction. The numbers 0.5 and 0.005 refer to the cross-head speeds in cm/min.

TABLE 5.3.

Proportional limit of single crystals with the tensile axis in the [001] direction.

Temperature ^{o}K	Cross-head speed cm/min	Proportional limit kg/mm^2
413	0.005	2.6
	0.500	
353	0.005	3.4
	0.500	3.0
293	0.005	3.4
	0.100	3.9
	0.500	4.2 - 5.1
195	0.005	
	0.500	11.0
77	0.005	15.0
	0.500	17.4

The curves of Figures 5.16 and 5.17 show that the work-hardening rate increases with increasing strain-rate and decreasing temperature, in all the range of temperatures investigated. The crystals tested at a slow cross-head speed, at 353°K, and those tested at 413°K exhibited a peculiar behaviour. After the onset of plastic instability and localised necking, the specimen continued deforming uniformly and experienced a large elongation. The crystals fractured ultimately by shear with practically a 100% reduction in area.

The crystals tested at and below room temperature fractured by cleavage after a considerable reduction in area which was about 50% at 293°K and decreased with temperature. Twinning occurred in some of the specimens deformed at 77°K. Other specimens tested at the same temperature fractured prematurely at the shoulder.

Typical stress-strain curves of crystals deformed in compression are shown in Figure 5.18. The large stresses at which these crystals deformed cannot be explained entirely in terms of the strain rate dependence of the stress. They are possibly due to friction occurring between the specimen and the compression plates. No peculiar distortion of the specimens was observed in this case, and this is in

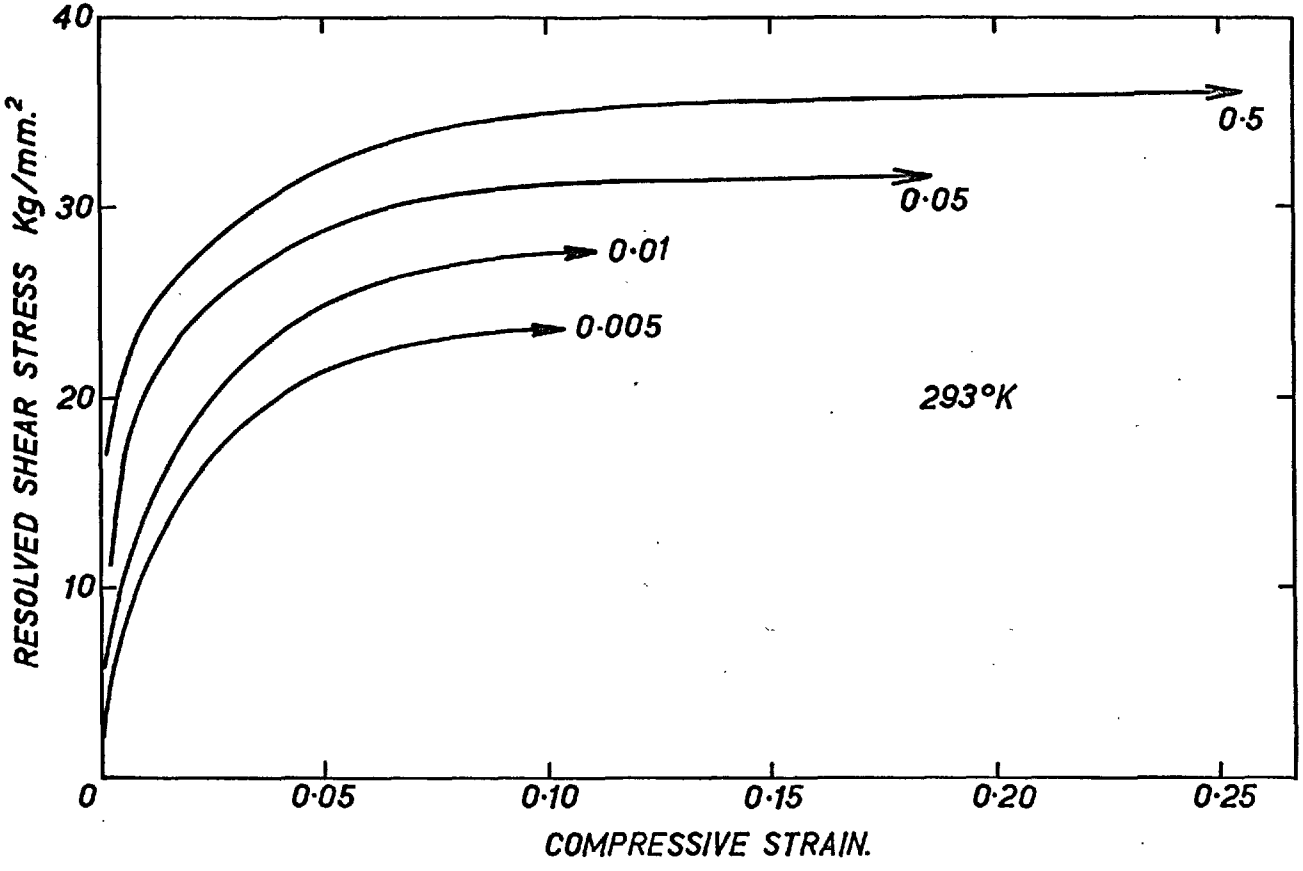

Figure 5.18. Stress-strain curves of crystals with the compression axis in the ⟨100⟩ direction. The numbers 0.5, 0.05, 0.01, and 0.005 refer to the cross-head speeds in cm/min.

agreement with the symmetrical character of the slip elements with respect to the compression axis.

5.3.1. Slip Systems

The possible slip systems involving $\{110\}$ and $\{112\}$ type planes together with the corresponding Schmid factors are given in Table 5.4.

X-ray Laue back-reflection photographs of the deformed specimens have shown that the symmetry of the deformation axis is maintained up to the onset of necking and this indicates that symmetrical and equivalent slip systems are equally strained throughout the deformation.

The orientation of the tensile axis of the specimens that were deformed above room temperature, and which experienced a large elongation becomes unstable at the first onset of necking, because at that moment the crystals start deforming by single slip in the $(\bar{1}12)$ $[1\bar{1}1]$ system. This type of deformation is initiated in the region of the neck and gradually propagates along the whole gauge length of the specimen. The operative slip system was determined by the rotation of the tensile axis and the orientation of the slip lines.

TABLE 5.4.

Schmid factors for different slip systems when the deformation axis is in the [001] direction.

[111]	(10$\bar{1}$)	0.408
	(0$\bar{1}$1)	0.408
	(11$\bar{2}$)	0.4714
	($\bar{2}$11)	0.236
	(1$\bar{2}$1)	0.236
[$\bar{1}$11]	(0$\bar{1}$1)	0.408
	(101)	0.408
	(1$\bar{1}$2)	0.4714
	(12$\bar{1}$)	0.236
	(211)	0.236
[1$\bar{1}$1]	(011)	0.408
	(10$\bar{1}$)	0.408
	($\bar{1}$12)	0.4714
	(121)	0.236
	(21$\bar{1}$)	0.236
[11$\bar{1}$]	(011)	0.408
	(101)	0.408
	(112)	0.4714
	(2$\bar{1}$1)	0.236
	($\bar{1}$21)	0.236

Figure 5.19. The appearence of the slip lines and fracture profile on a {100} plane of a crystal deformed in the ⟨100⟩ direction at 195°K. x 200.

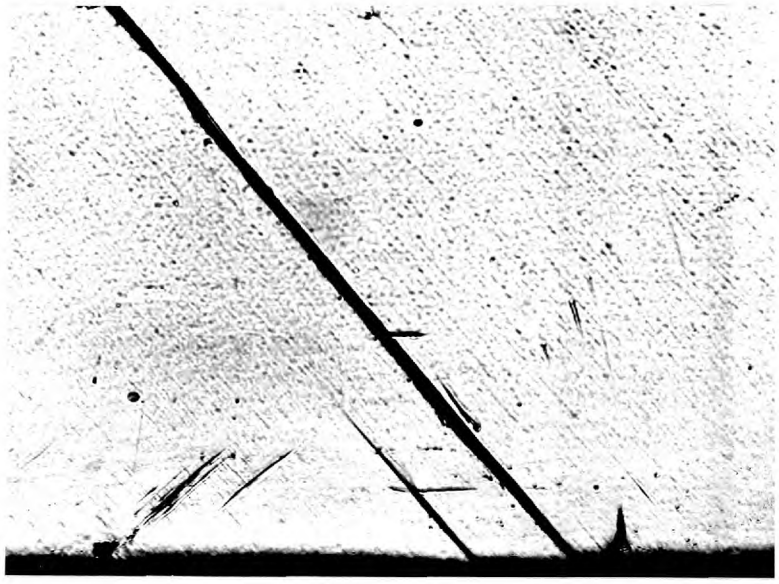

Figure 5.20. Slip lines on a {100} plane of a crystal deformed in the ⟨100⟩ direction at 353°K. x 200.

5.3.2. Slip Line Observations

In the specimens deformed below room temperature the slip lines are only clearly visible in the proximity of the neck and they are very fine (Figure 5.19). In the crystals deformed at and above room temperature similar traces can be observed as well as a few very sharp and long slip lines that produce a high step on the surface and that sometimes run almost across the face of the specimen (Figure 5.20). The latter are preferentially nucleated at scratches and at the edge of the specimen and they seem to have developed progressively rather than suddenly, otherwise a load drop would probably have been observed in the load-elongation curves. It is not surprising that sharp slip lines leaving high steps on the surface were never observed in crystals deformed in the [011] direction, since in that case the slip directions were almost parallel to the surface of the specimen.

The faces of the specimens where the observations were made deviate slightly from (100) and (101) planes. The fine slip lines which form an angle of 45° with the tensile axis (Figure 5.19) have been invariably observed at temperatures lower than $353^{\circ}K$ and they coincide with traces of {110} planes, or {112} type planes with a Schmid factor of 0.236. Only on one occasion have a few sharp slip lines that

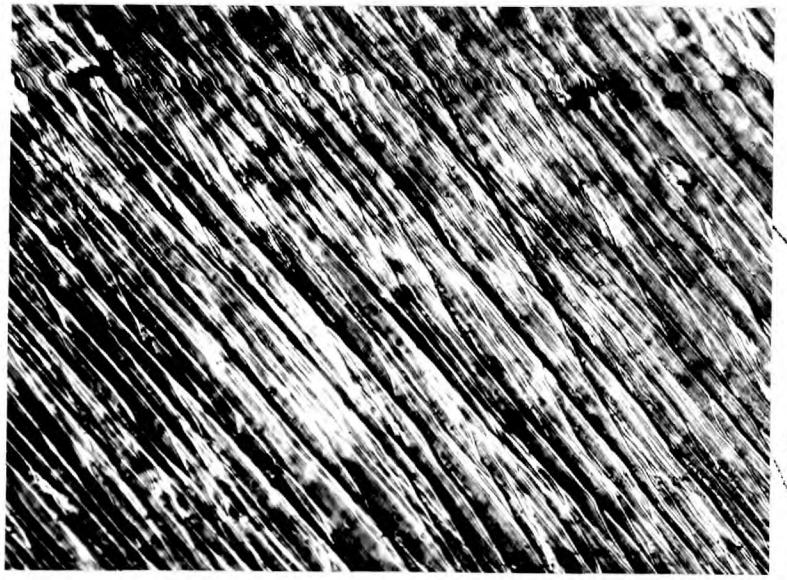

(a)

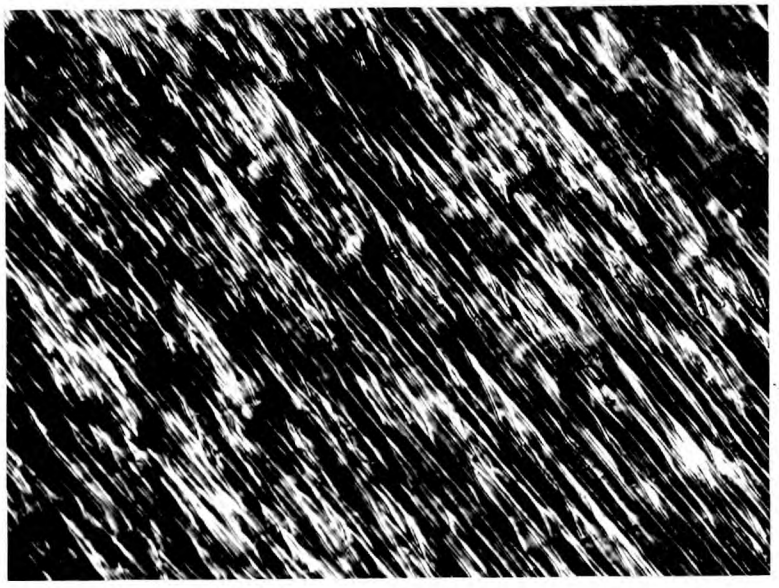

(b)

Figure 5.21. Slip lines on surfaces near the (100) and the (010) planes after 35% tensile strain at 413°K. Deformation axis in the [001] direction. x 200.

could be unambiguously identified with traces of {112} planes with a Schmid factor of 0.4714 been observed at 353°K.

The slip lines on the specimens that deformed by single slip above room temperature are very distinct and they are shown in Figures 5.21 (a) and 5.21 (b). They are the result of slip in $(\bar{1}12)$ planes. A few connecting slip lines that appear to be traces of $(\bar{2}13)$ planes are also visible in Figures 5.21 (a) and 5.21 (b).

5.3.3. Dislocation Etch Pit Observations

Dislocation etch pit observations similar to those described in Section 5.2.2. were also made in specimens deformed in the [001] direction. Arrays of etch pits were never observed in the early stages of the deformation at any temperature (Fig. 5.22). In some specimens deformed at 413°K and 195°K and given strains of the order of 7% or 10% it was possible to detect a rough alignment of the pits in directions at 45° to the tensile axis (Figure 5.23). The dislocations intersected by both the (100) and (101) planes, where these observations were made, have a small predominant edge component and consequently they cannot cross-slip easily. This is the reason why short arrays of dislocations in the direction of

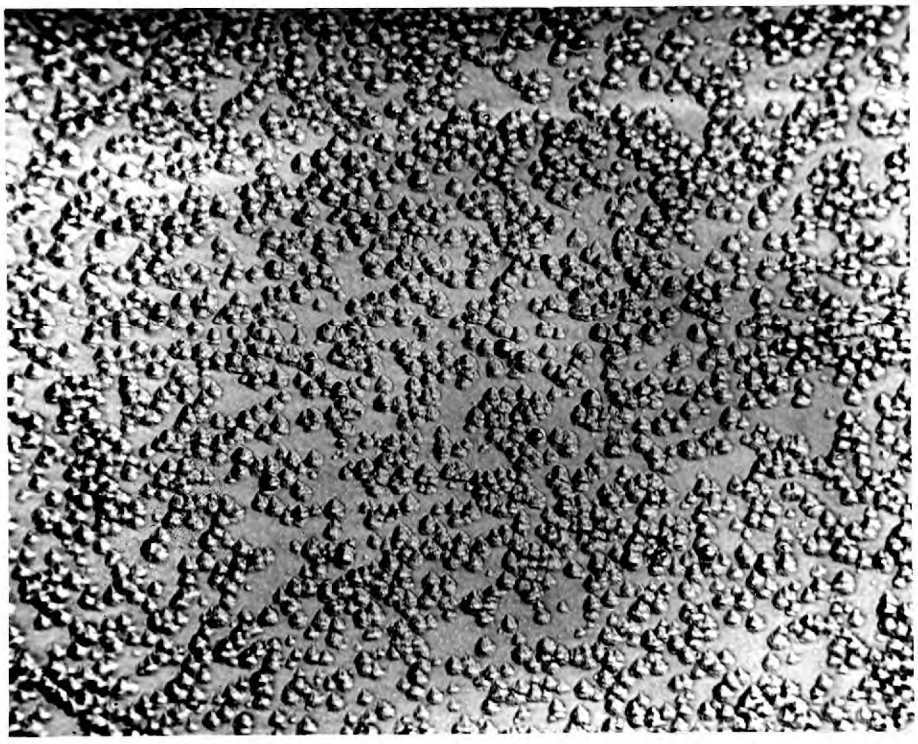

Figure 5.22. Dislocation etch pits on a surface near the {100} plane after 1% tensile strain at 353°K. Deformation axis in the ⟨100⟩ direction. Etchant b).

x 600

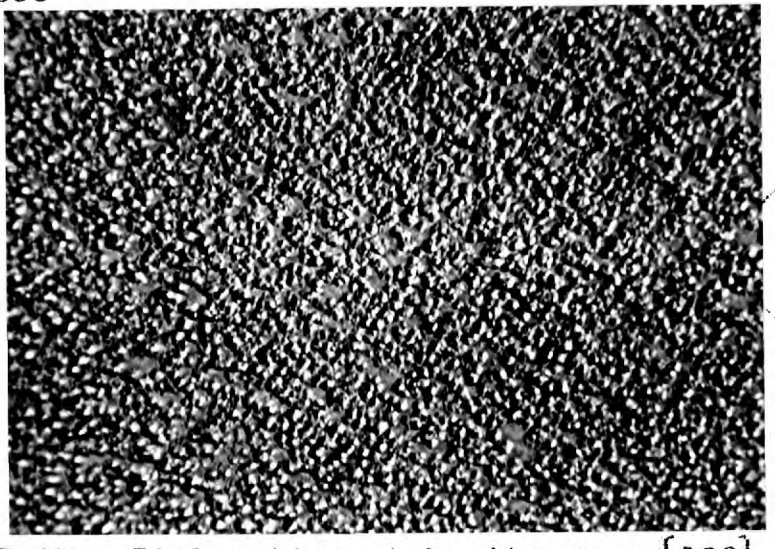

Figure 5.23. Dislocation etch pits on a {100} plane after 7% tensile strain at 195°K. Deformation axis in the ⟨100⟩ direction. Etchant b). x 800.

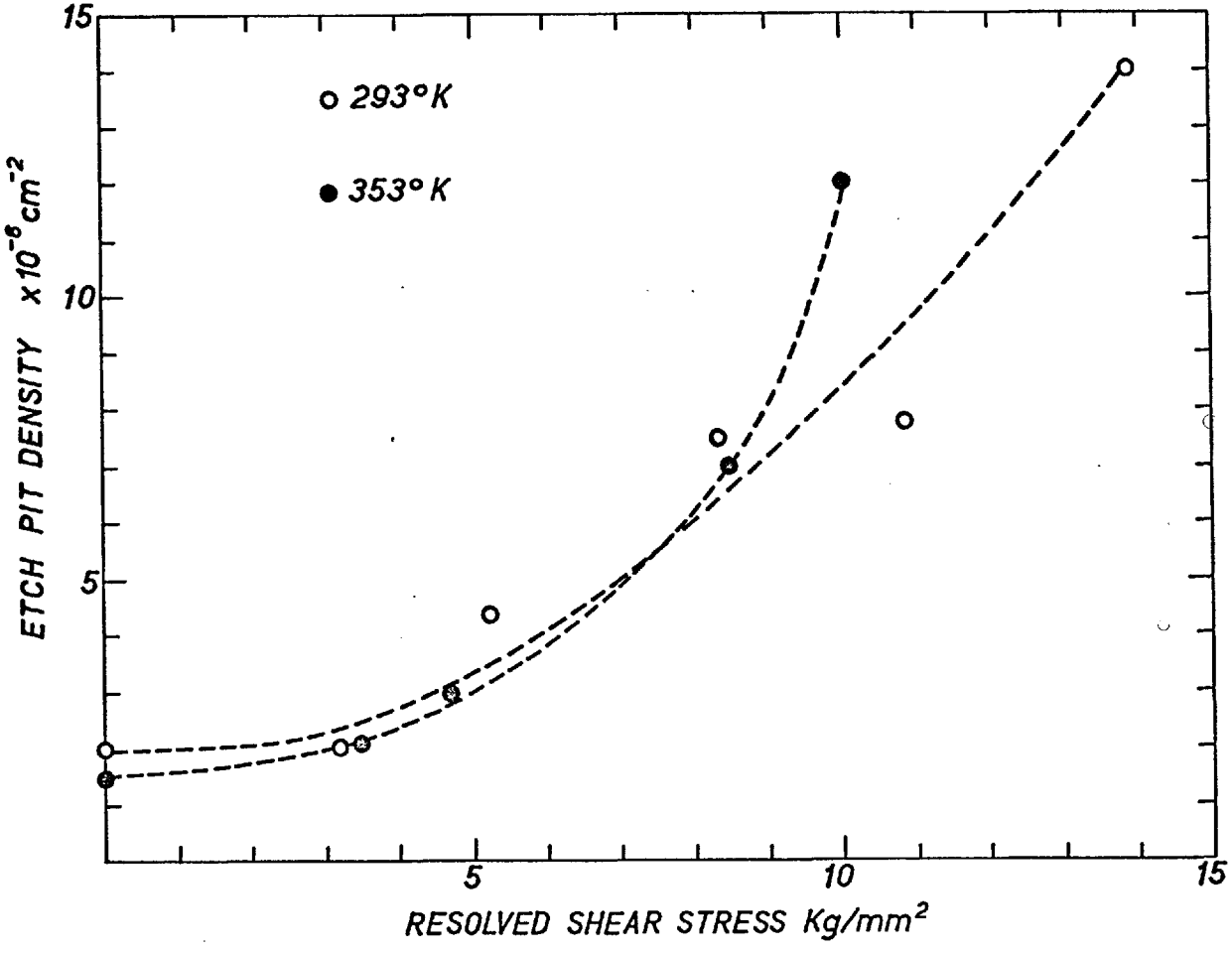

Figure 5.24. Variation of the etch pit density with the applied stress. Deformation axis in the ⟨100⟩ direction.

the slip lines are observed in this case.

The variation of the etch pit density with the shear stress, at two different temperatures, is shown in Figure 5.24. A substantial increase in the number of etch pits occurs in the region of the proportional limit.

5.3.4. Asterism of the Laue Spots

The Laue spots of X-ray back-reflection photographs of specimens deformed at and below room temperature showed splitting and multiple asterism as a result of multiple slip. This made the analysis of the asterism practically impossible. Only in those specimens that deformed by single slip above room temperature was the asterism of the Laue spots clear, (Figure 5.25) and in this case the stereographic representation (Figure 5.26) served to confirm that slip was confined to the $(\bar{1}12)$ planes, as previously determined by means of the slip line traces.

5.3.5. Twinning and Cleavage Fracture

With the exception of the specimens that deformed by single slip, which fractured by shear in the $[1\bar{1}1]$ direction, all the others fractured by cleavage on the (001) plane, normal to the specimen axis. The fracture was generally initiated on the surface and edges of the specimen, probably at points of high

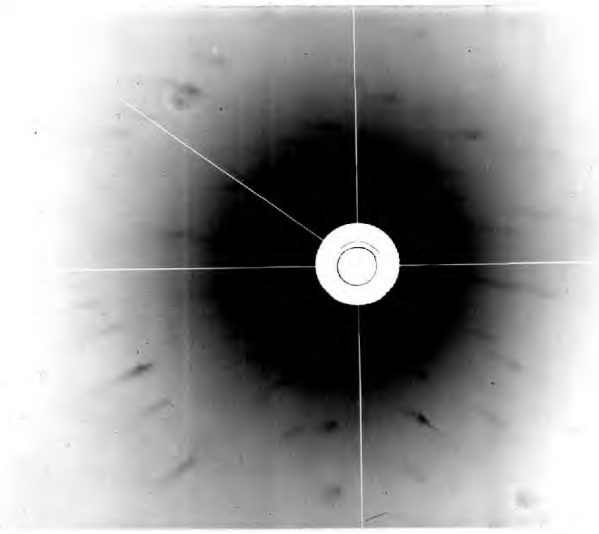

Figure 5.25. Asterism of the Laue spots for a crystal deformed 34 % at 413° K. ~~The [100] axis is perpendicular to the plane of the photograph.~~

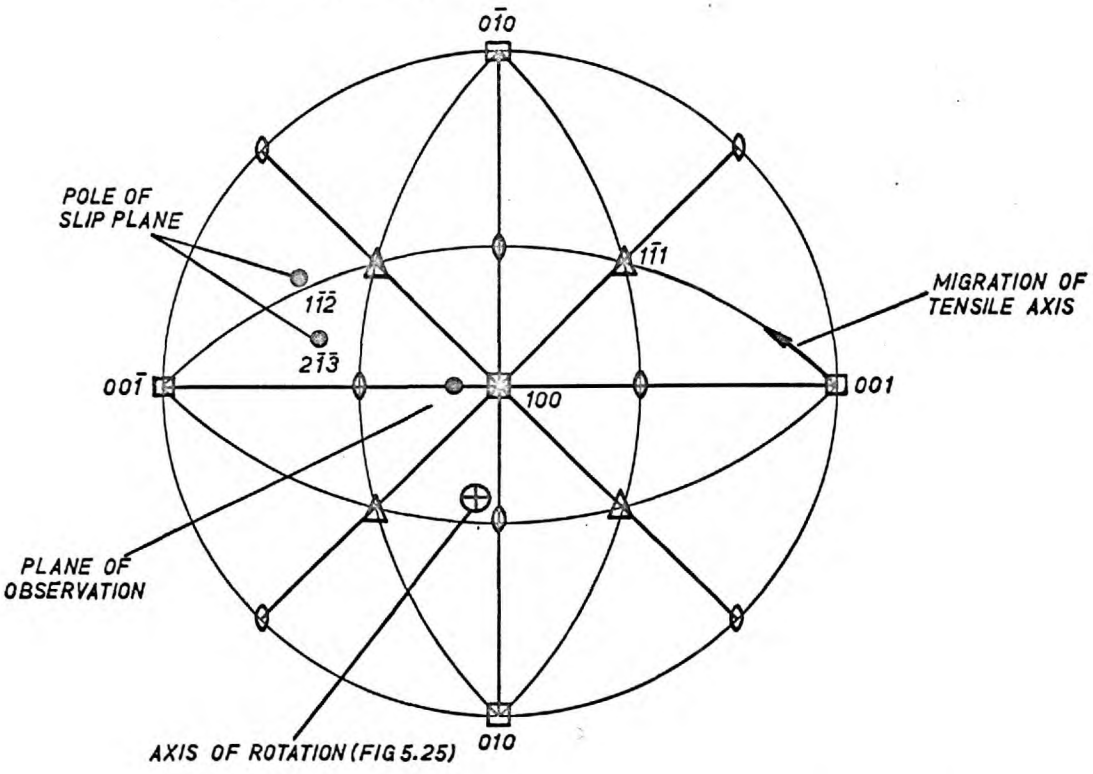

Figure 5.26. Stereographic representation of the slip traces of Figures 5.21 (a) and (b), the rotation of the tensile axis, and the asterism of Figure 5.25.

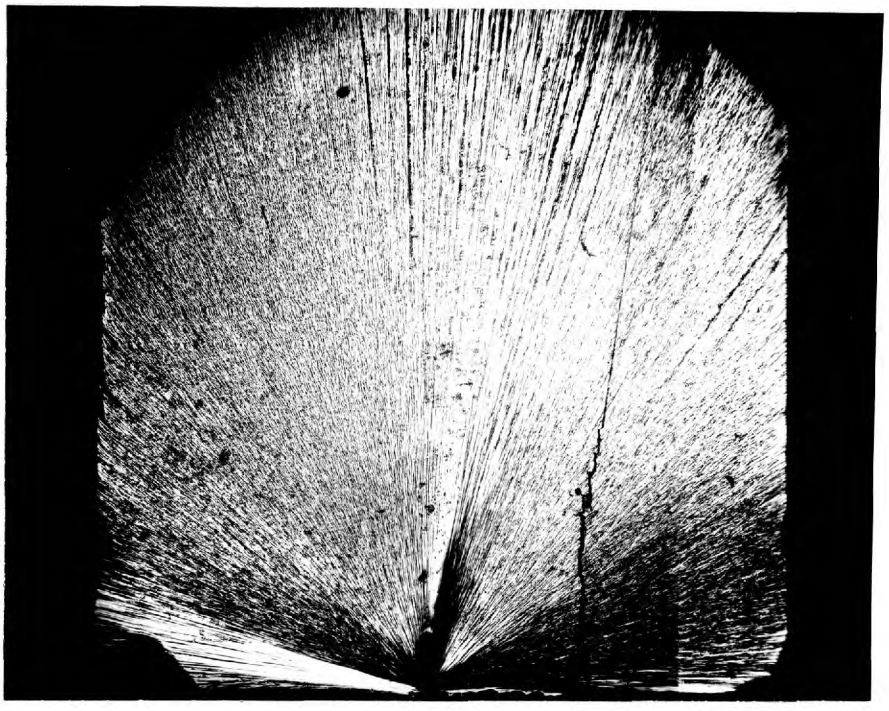

Figure 5.27. Cleavage fracture surface of a crystal deformed at 243°K in the ⟨100⟩ direction. x 50.

Figure 5.28. Fracture propagated along a twin boundary in a crystal deformed at 77°K in the ⟨100⟩ direction. Surface etched with etchant b). x 200.

stress concentration, such as scratches. The cleavage surface of a specimen fractured at 243°K, is shown in Figure 5.27. A fracture profile with a cleavage step on a {110} plane is shown in Figure 5.19.

Twinning occurred in the specimens tested at 77°K and at a cross-head speed of 0.005 cm/min. The fracture was always subsequent to twinning but no evidence of 'crack nucleating' twin intersections was found. In some cases the fracture propagated along the twin interface, as shown in Figure 5.28.

5.4. Deformation Axis in the [111] Direction

The deformation of crystals under a stress applied in the [111] direction was not investigated in detail, and only a few compression tests were conducted at room temperature and at various cross-head speeds.

The mechanical characteristics of the crystals were found to be rather similar to those of the crystals with deformation axis in the [001] direction. The stress-strain curves of Figure 5.29 show that the only difference is that, in the present case, the crystals have a higher proportional limit and a smaller work-hardening rate. These differences were not considered to be sufficiently important to justify a thorough investigation, and it was felt that

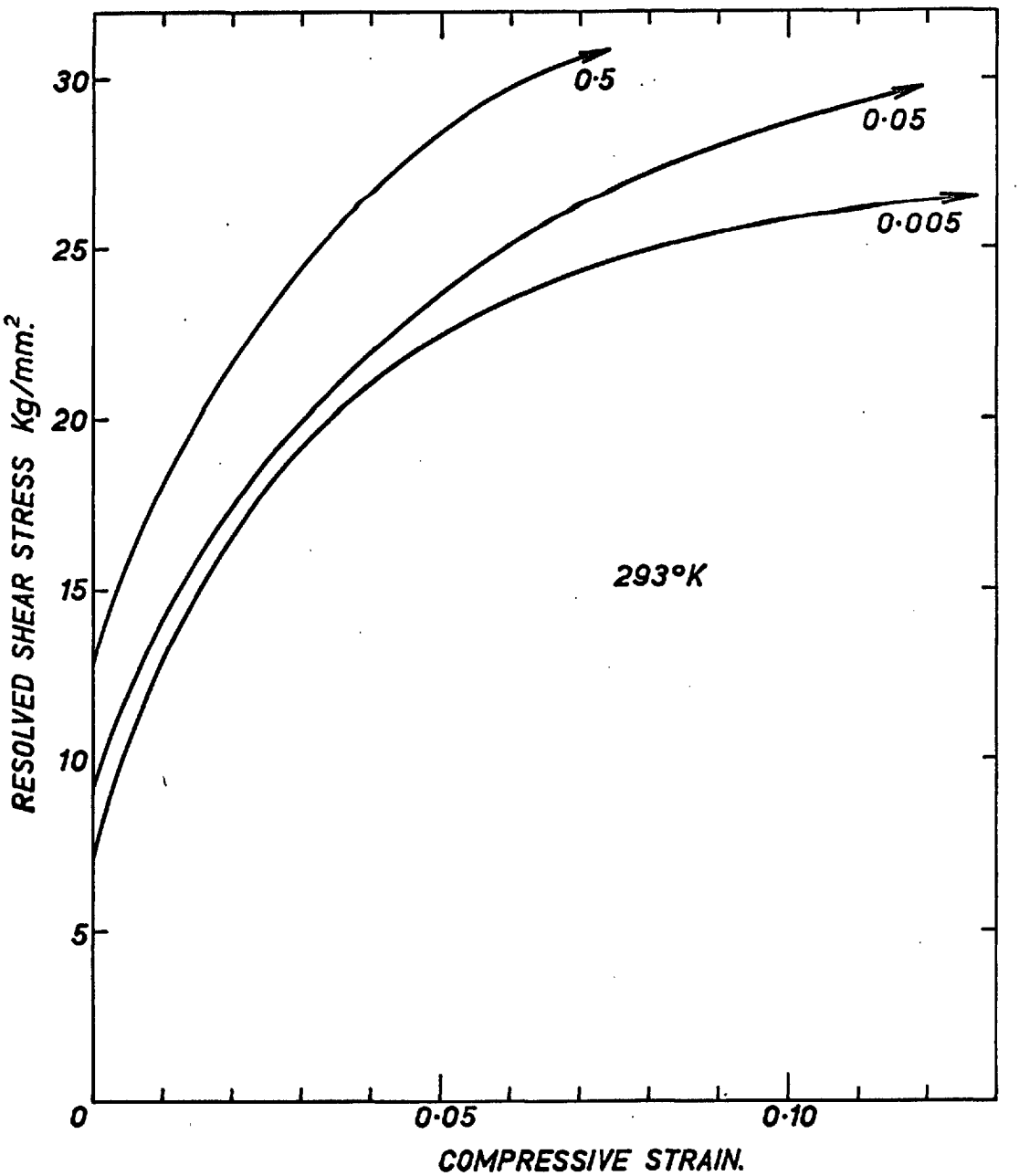

Figure 5.29. Stress-strain curves of crystals with the compression axis in the ⟨111⟩ direction. The numbers 0.5, 0.05, and 0.005 refer to the cross-head speeds in cm/min.

more information would be obtained by concentrating on the study of the other orientations.

5.5. Deformation Axis in a Direction Near the Centre of the Unit Stereographic Triangle

Several crystals with the tensile axis in a direction near the centre of the stereographic triangle, as shown in Figure 5.30, were deformed at various temperatures and cross-head speeds.

The crystals deformed at and below room temperature have a large initial work-hardening rate, and generally behave in a very similar way to those extended in the [001] direction. In the present case, however, the proportional limit is higher and it can be determined more accurately. Values of the elastic limits of crystals deformed under different conditions are given in Table 5.5.

The specimens deformed below 293°K fractured by cleavage after considerable necking, but at 77°K some specimens fractured prematurely at the shoulder. Twinning was observed in some specimens deformed at low speed, at 77°K.

The stress-strain curves shown in Figure 5.30 may be compared with those obtained by other workers (Lawley et al. 1962, Lawley and Gaigher 1964) for molybdenum single crystals of similar orientation

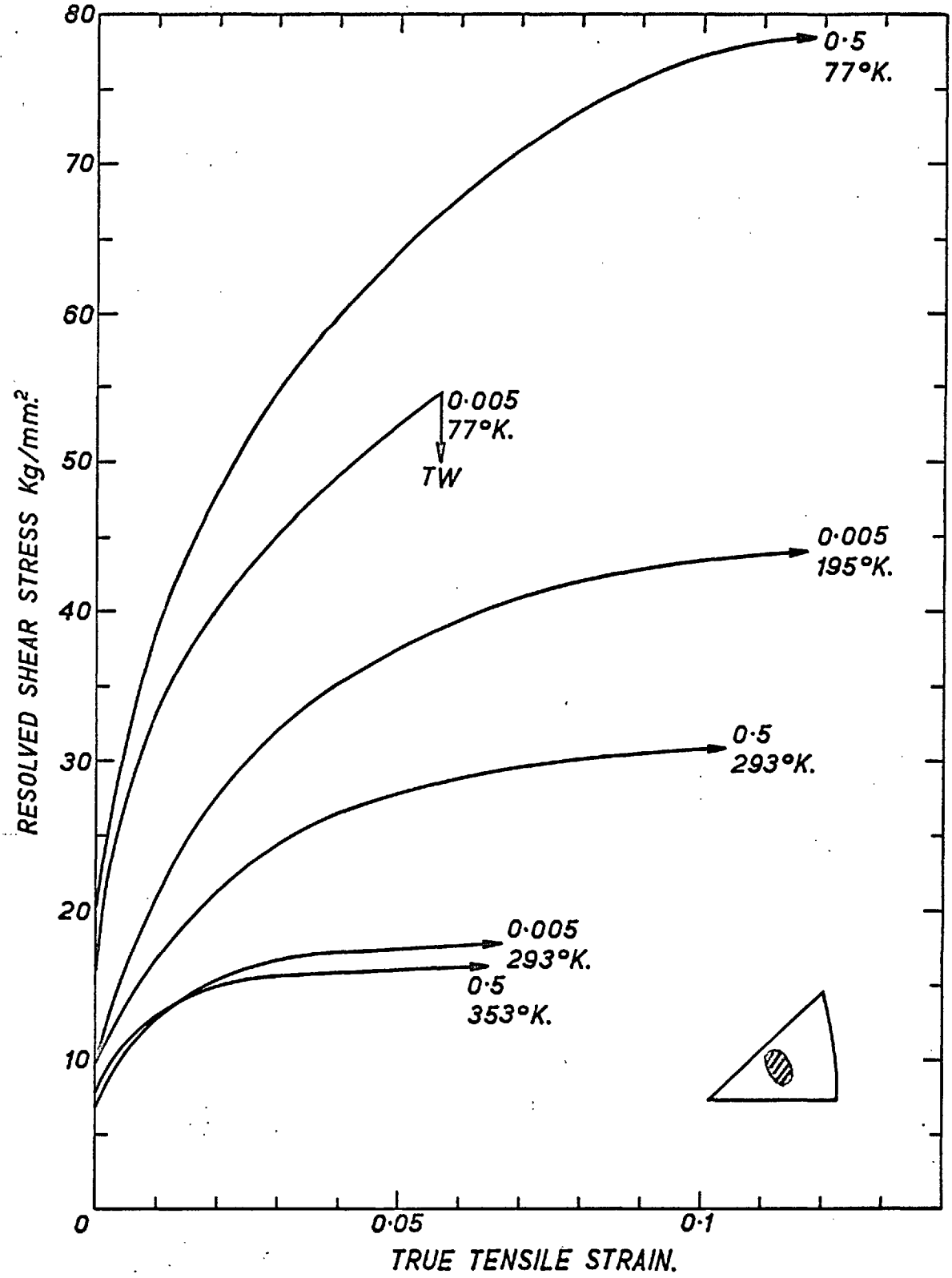

Figure 5.30. Stress-strain curves of crystals with the tensile axis in a direction as shown in the stereographic triangle. The numbers 0.5 and 0.005 refer to cross-head speeds in cm/min.

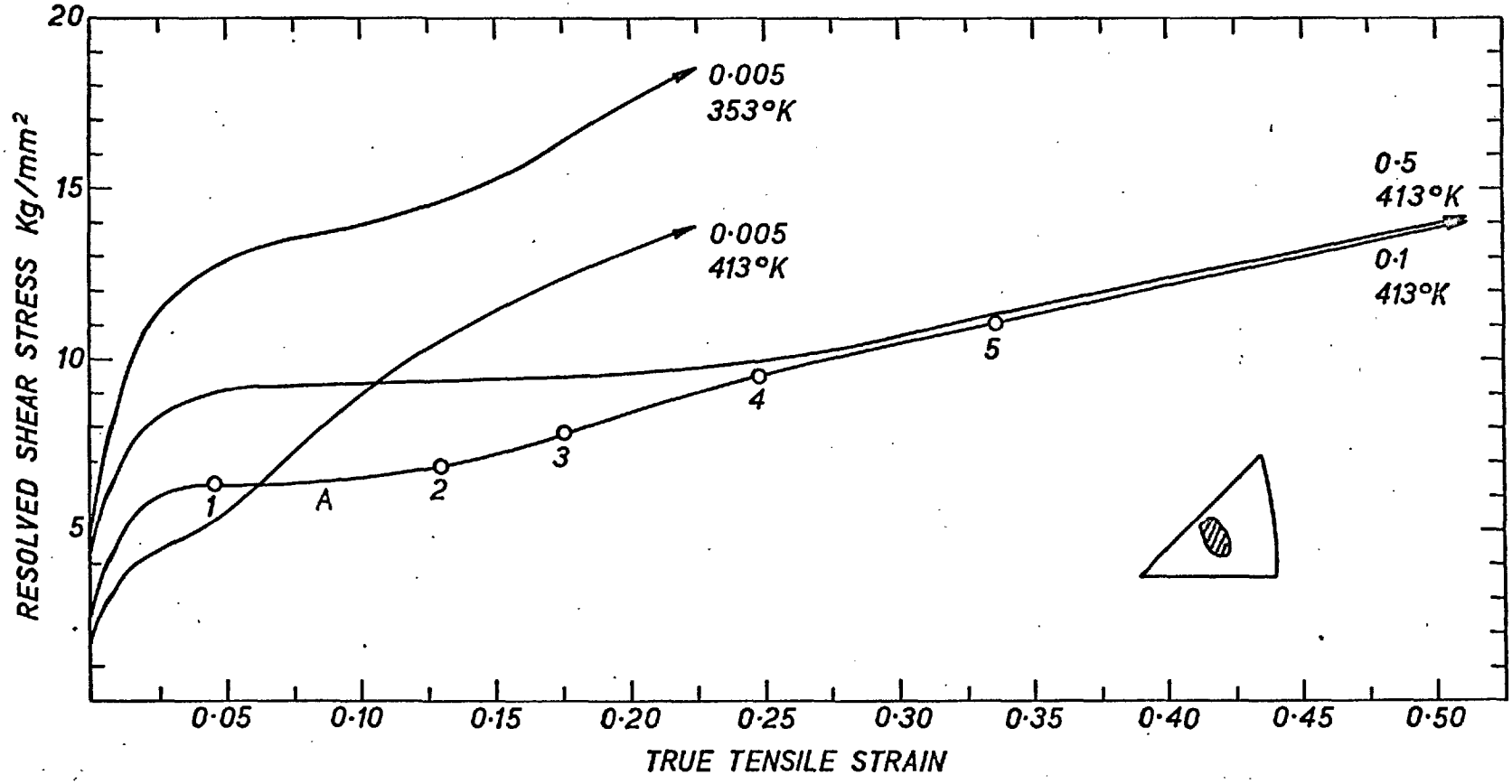

Figure 5.31. Stress-strain curves of crystals with the tensile axis in a direction as shown in the stereographic triangle. The numbers 0.5, 0.1, and 0.005 refer to cross-head speeds in cm/min.

TABLE 5.5.

Proportional limit of crystals with the tensile axis in a direction near the centre of the stereographic triangle.

Temperature ^{o}K	Cross-head speed cm/min	Proportional limit kg/mm^2
413	0.005	4.4
	0.500	1.7
	0.100	2.4
353	0.005	4.7
	0.500	7.7
293	0.005	5.6 - 6.8
	0.500	10.2
195	0.005	9.3
77	0.005	15.3 ± 1.3
	0.500	23.2 ± 0.3

grown also by electron beam floating zone melting. The proportional limit of the crystals used in the present investigation is of the same order, or lower, than that of the 'six pass' and 'three pass' crystals tested by these authors under similar conditions. By constrast, our crystals exhibit a higher initial work-hardening rate and a different trend in the relation between the maximum uniform elongation and temperature. A possible explanation for the difference in the work-hardening rate may be the method of preparation of the specimens. Lawley and Gaigher (1964) prepared their specimens by electro-machining and therefore they possibly had a lower dislocation density than our specimens which were machined by surface grinding. Up to what an extent the initial dislocation density really affects the work-hardening characteristics is something that cannot be discussed without a good understanding of the work-hardening mechanisms, which, at this point, is still lacking.

The specimens deformed at 353°K (and at low speed) and 413°K behaved quite differently. They experienced a very large uniform elongation, and in the corresponding stress-strain curves shown in Figure 5.31, it is possible to distinguish three work-hardening stages. These stages are not as pronounced

as in the case of f.c.c. crystals but they are similar to those observed in other b.c.c. metal single crystals (Mitchell et al. 1963, Keh 1963), and they had never before been observed in molybdenum.

Mitchell et al. (1963) showed that the different work-hardening stages that they observed in niobium were the result of single and double glide processes, as in f.c.c. metals, and they believed that the same behaviour should be found in all the b.c.c. metal single crystals provided they were tested under suitable conditions. The results obtained with the molybdenum single crystals cannot be compared in detail with those of Mitchell et al. because in the present case not enough systematic tests have been made covering a wide range of orientations, strain rates and temperatures.

5.5.1. Slip Systems

Although not all the crystals tested had the tensile axis in exactly the same orientation, the Schmid factor for the possible slip systems involving {110} and {112} type planes does not differ greatly from one crystal to another. A list of the glide systems that have the largest Schmid factor is given in Table 5.6.

The X-ray Laue back-reflection photographs of

TABLE 5.6.

Schmid factors for different slip systems when the tensile axis is in a direction in the middle of the unit stereographic triangle.

Slip Direction	Slip Plane	Schmid Factor
$[\bar{1}\bar{1}1]$	(011)	0.500
	(101)	0.206
	($\bar{1}$21)	0.455
	(112)	0.455
$[\bar{1}11]$	(0$\bar{1}$1)	0.472
	(101)	0.296
	(1$\bar{2}$1)	0.366
	(11$\bar{2}$)	0.433
[111]	($\bar{1}$01)	0.321
	(0$\bar{1}$1)	0.186
	($\bar{1}\bar{1}$2)	0.290
	($\bar{2}$11)	0.258

specimens deformed at low temperatures showed that the tensile axis wanders around its initial position but it does not migrate steadily towards any direction. This indicates that, in this case, at least three different slip directions must be operating. However the axis of the specimens that show the three stage hardening was found to rotate towards the $[11\bar{1}]$

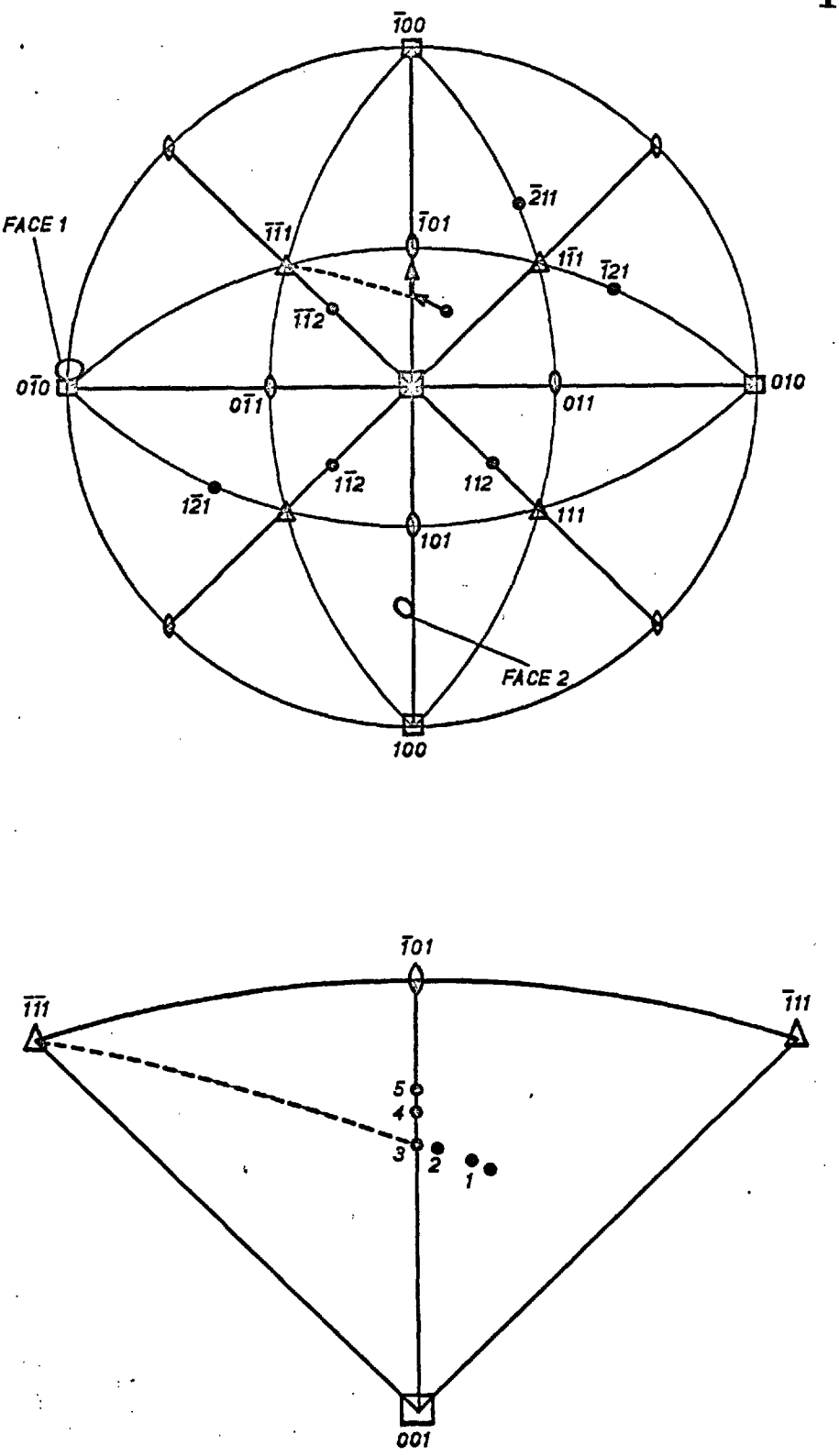

Figure 5.32. Rotation of the tensile axis in crystals deformed above 353° K, and orientation of the observation planes.

direction until it reached the [001] - [$\bar{1}$01] symmetry boundary. Then it moved towards [$\bar{1}$01] as a result of equal amounts of slip in the [11$\bar{1}$] and [$\bar{1}$11] directions.

The migration of the tensile axis during the straining of a crystal at 413°K is illustrated in Figure 5.32. The values of the strain corresponding to the different positions of the axis are shown in the curve A of Figure 5.31. It can be observed that the end of 'easy glide' and the onset of the second stage of work-hardening takes place before the tensile axis reaches the [001] - [$\bar{1}$01] symmetry line.

5.5.2. Slip Line Observations

A detailed observation of the slip lines was made in several specimens deformed at 353°K and 413°K. Although the results reported here refer to a single specimen they are representative of all the specimens deformed at these temperatures and which exhibit three stage hardening. The average orientation of the planes on which the slip lines were observed is indicated in Figure 5.32. The observation faces are referred to as Face 1 and Face 2.

After a tensile strain of 0.045 (point 1 in the curve of Figure 5.31) the slip lines on Face 1 (Figure 5.33(a)) became composed of short wavy segments and they define traces of (112) and (011) planes which both

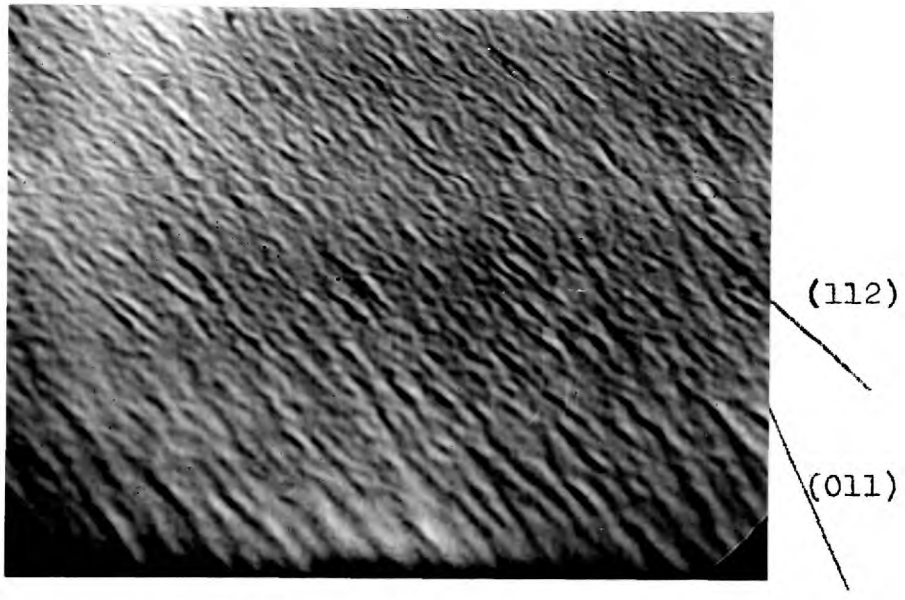

(a) x 500

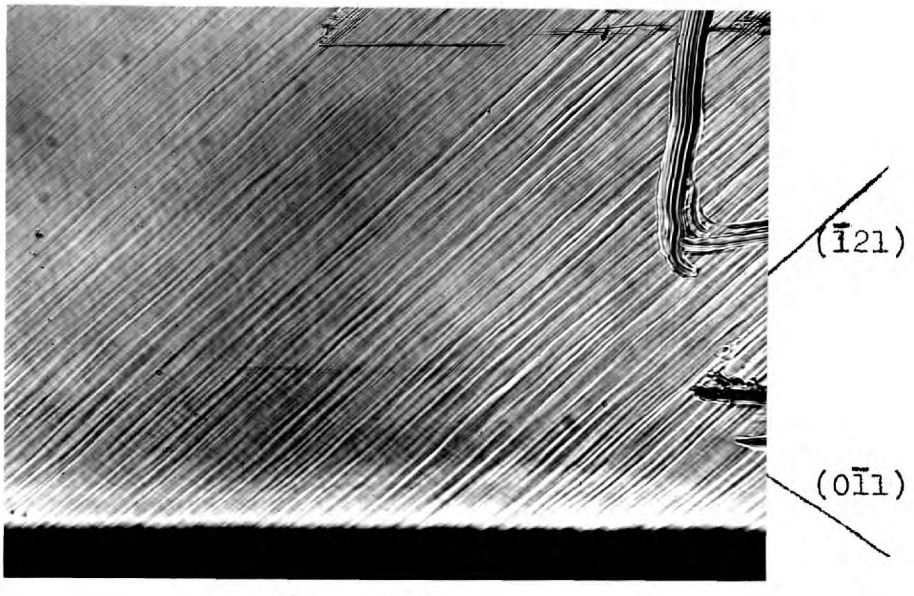

b) x 140

Figure 5.33. Slip lines on (a) Face 1, and (b) Face 2 after 4.5% tensile strain.

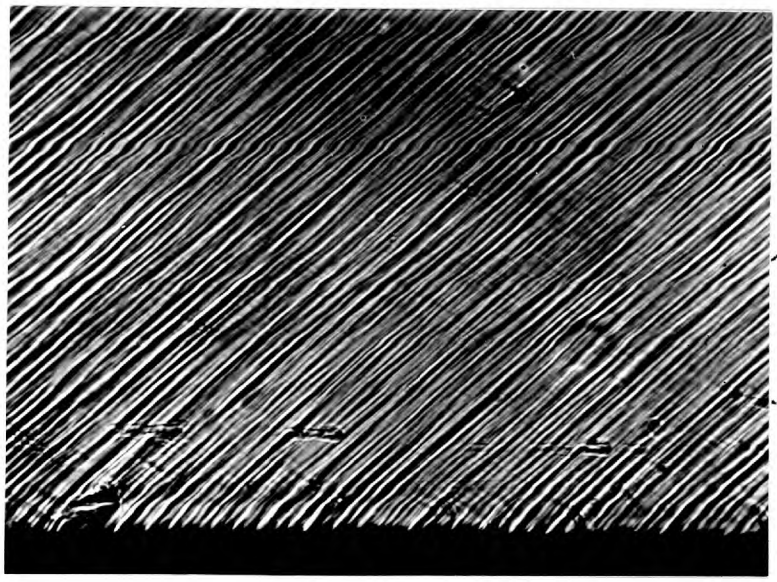

a) x 140

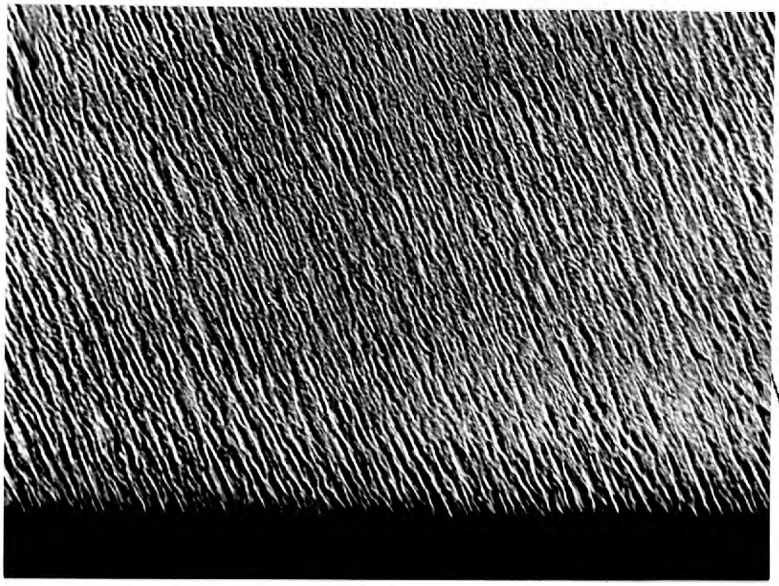

b) x 140

Figure 5.34. Slip lines on (a) Face 2, and (b) Face 1 after 13% tensile strain.

belong to the $[11\bar{1}]$ zone. Long and straight traces of $(\bar{1}21)$ planes can be observed on Face 2 (Figure 5.33(b)) where some fine slip lines that coincide with traces of $(0\bar{1}1)$ planes are also visible. This seems to constitute evidence of slip in the $[\bar{1}11]$ direction, which on the other hand can not have contributed significantly to the total strain because a net rotation of the axis towards the $[11\bar{1}]$ direction is clearly observed.

The aspect of the slip lines on Face 2 has not changed after a strain of 0.13 (Figure 5.34(a)), but on Face 1 the traces of (112) planes are not clearly visible (Figure 5.34(b)).

As deformation proceeds, glide bands formed as a result of slip in $(\bar{1}21)$ planes, appear on Face 1, (Figure 5.35).

In order to observe more clearly the traces of secondary slip which was expected to take place when the tensile axis reached the symmetry boundary, the specimen was polished and the slip traces were observed after a total deformation of 0.175. On Face 1 the segments defining traces of (011) planes have shortened and the $(\bar{1}21)$ bands appear well developed (Fig. 5.36). On Face 2 traces of primary slip in $(\bar{1}21)$ planes and secondary slip in (110) planes are clearly observed (Fig. 5.37).

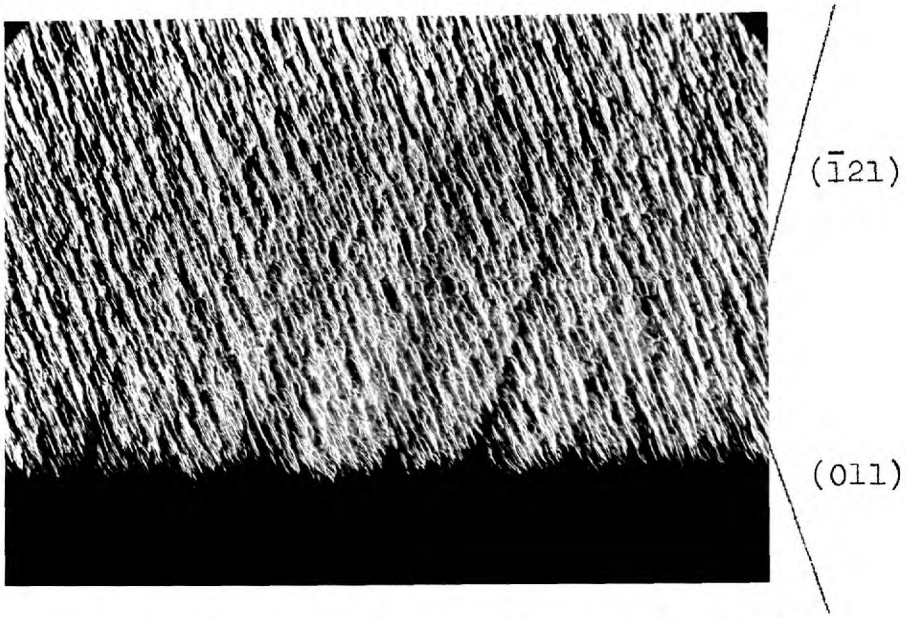

Figure 5.35. Slip lines on Face 1 after 15% tensile strain. x 140.

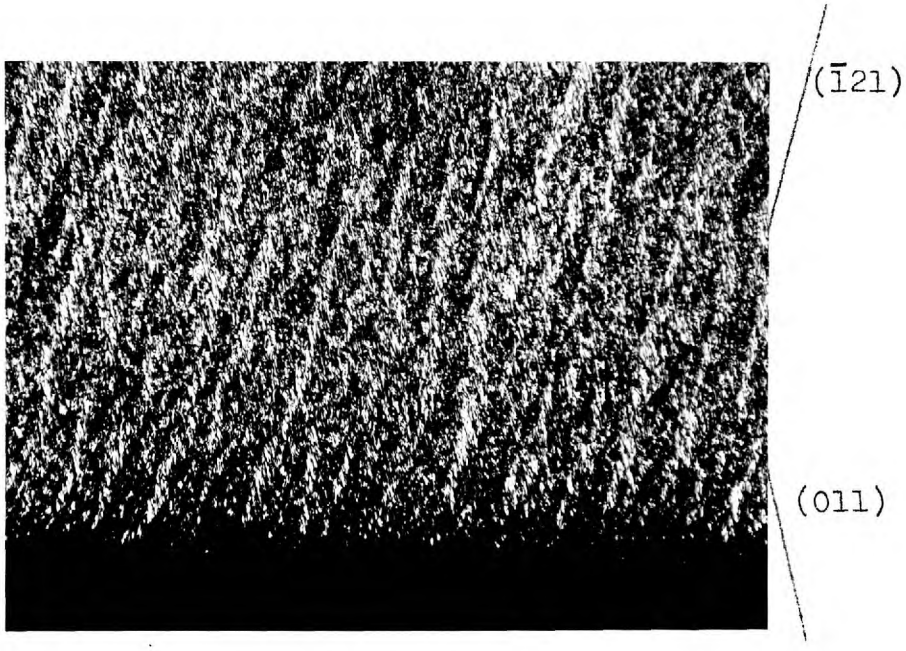

Figure 5.36. Slip lines on Face 1 after 17.5% tensile strain. x 80.

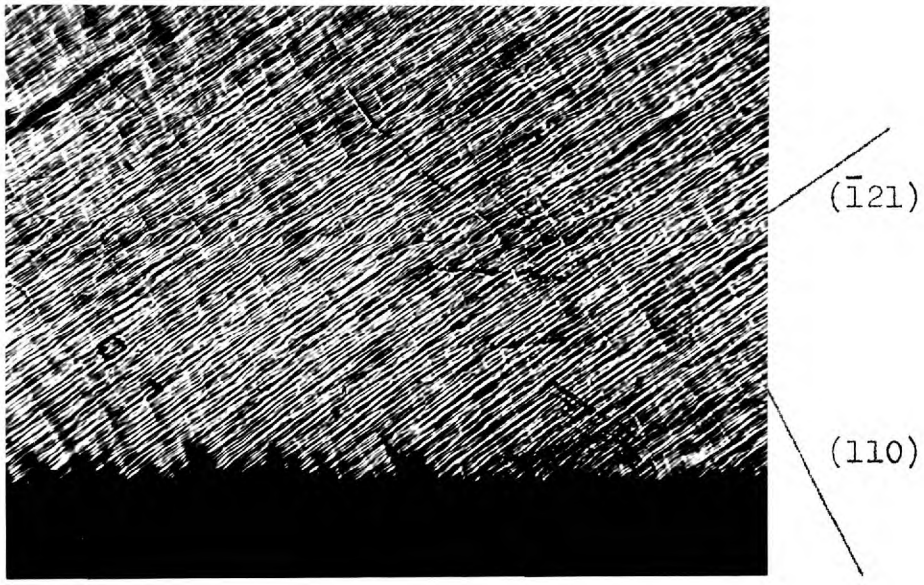

Figure 5.37. Slip lines on Face 2 after 17.5% tensile strain. x 80.

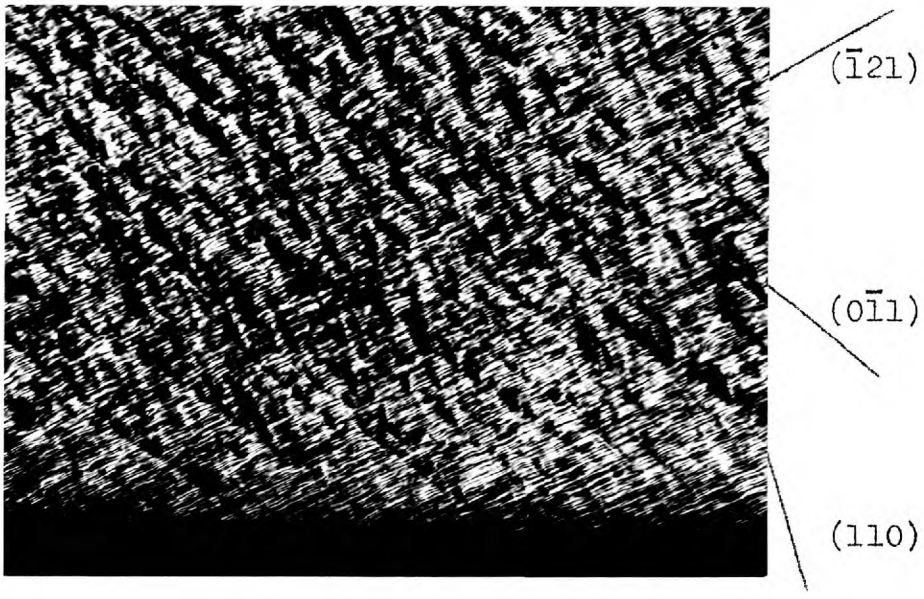

Figure 5.38. Slip lines on Face 2 after 33.5% tensile strain. x 80.

Finally, the last observation was made after a strain of 0.335 and no change in the appearance of the lines was observed on Face 1. However, on Face 2 the traces of primary slip are broken into very short segments and bands of secondary slip in (110) and ($0\bar{1}1$) planes can be clearly observed (Figure 5.38.).

The observations reported here have many similarities with the results that Mitchell et al (1963) obtained in the study of the work-hardening of niobium single crystals. An important common feature is, for example, that in both metals slip in more than one plane of the same zone is observed. This fact makes it possible to interpret the wavy aspect of the slip lines as the result of cross-slip of the screw dislocations between two planes of the same zone (as explained in Section 5.2.2.). According to this interpretation, the waviness of the slip lines on Face 1 results from the predominant screw component of the dislocations intersected by this face and the ease with which they can cross slip between (112) and (011) planes. The resolved shear stress is larger on (011) planes on which slip is predominant. Slip in (112) planes acts as 'connecting slip' between (011) planes.

5.6. Discussion

5.6.1. The Slip Systems

Since the early work of Taylor and Elam (1926, 1928), it has been known that in b.c.c. metals slip takes place in the $\langle 111 \rangle$ close packed direction and on more than one crystallographic plane. In fact, slip on $\{110\}$, $\{112\}$, and $\{123\}$ type planes has been repeatedly observed by many investigators. (For a review see Maddin and Chen 1954).

The first attempt to correlate the operative slip systems with the testing conditions was made by Andrade and Chow (1940), but a great deal of evidence showing the inaccuracy of this correlation has been subsequently gathered. More recent investigations have shown that slip predominates in $\{110\}$ and $\{112\}$ type planes and it appears that $\{112\}$ planes are preferentially active at high temperatures (Schadler and Low, 1962, Erickson, 1962).

The results reported in the preceding sections of this chapter also support this view. Evidence of $\{110\}$ and $\{112\}$ slip planes was obtained at temperatures lower than 293°K . At temperatures above 293°K only slip on $\{112\}$ planes was observed for certain orientations of the deformation axis. When the tensile axis is oriented in the centre of the unit stereographic triangle, slip on $\{110\}$ planes also

occurs at high temperatures and this shows that the resolved shear stress acting on each system is an important factor in deciding the activity of the slip plane.

A peculiar observation has been described in Section 5.2.1., namely the presence of slip on $(11\bar{2})$ and $(12\bar{1})$ planes, on which the resolved shear stress is only one half of that on the $(\bar{2}11)$, (211) and other $\{110\}$ type planes. This anomaly would be readily explained if slip in planes other than $\{110\}$ is really the result of 'pencil glide' or composite slip on non-parallel $\{110\}$ planes. However, any explanation based on this idea which was put forward by Elam (1935) and has been shared by other authors (Greninger 1937, Maddin and Chen, 1954) should be regarded as speculative, since direct evidence of such a mechanism has never been obtained.

5.6.2. Calculation of the Shear Stresses and Glide Strains

The multiplicity of slip which has been almost invariably observed during the present investigation complicates the problem of the calculation of the shear stresses and glide strains.

To be consistent with the theory of composite slip the shear stress should always be resolved on $\{110\}$ planes. However, this criterion has not been

followed here and the shear stresses have been resolved on the system for which these were the larger. The reason for doing this was that at high temperatures, slip was only observed on {112} planes with the maximum resolved shear stress. On the other hand, as the values of the proportional limits are in many cases very small, it was preferable to work with values of the stress which would represent an upper limit, and that in any case would only be 15% larger than if the stresses had been resolved on {110} planes.

In all the cases where no rotation of the deformation axis was observed the shear stress was calculated by the formula (Schmid and Boas, 1950):

$$\tau = \frac{P\,(1+\epsilon)}{a_o} \cos\varphi_o \cos\lambda_o \qquad (5.1.)$$

Where P is the load, ϵ the tensile strain (taken as negative in compression), a_o the original cross-sectional area, φ_o the angle between the deformation axis and the normal to the slip plane, λ_o the angle between deformation axis and the slip direction. The subscripts, zero, indicate the values for the undeformed crystal. The term $(1+\epsilon)$ accounts for the variation in cross-sectional area (assuming constant volume) because φ and λ remain constant.

The shear stress in the region of single slip of crystals in the [001] direction (Section 5.3.) was

calculated by using the expression (Schmid and Boas, 1950):

$$\tau = \frac{P \cos\chi_o}{a_1}\sqrt{1 - \frac{\sin^2 \lambda_o}{[1+(\epsilon-\epsilon_1)]^2}} \qquad (5.2.)$$

where a_1 and are the cross-sectional area and the tensile strain at the onset of single slip.

The shear stresses for the specimens that deformed by single and double glide (Section 5.4.) were calculated by the expressions for single glide (Eq. 5.2.) and double glide (Mitchell et al. 1953):

$$= \frac{P\,(1+\epsilon)}{a_o\sqrt{3}} \cos\beta \cos(45 - \beta) \qquad (5.3.)$$

where β is the angle between the [I01] direction and the tensile axis, and is related to its value β_o for the undeformed crystal by:

$$\sin\beta = (1+\epsilon)\sin\beta_o.$$

The calculation of the glide strains is practically impossible because, except in one case, in all the conditions investigated more than one active slip plane was observed. Even when the rotation of the tensile axis obeys the single and double glide conditions: $1+\epsilon = \sin\lambda_o/\sin\lambda$ and $1+\epsilon = \sin\beta_o/\sin\beta$, as in the case of the crystals that show the three stage hardening, the glide strain cannot be calculated unless the amount of slip on each of the active planes is known.

In the case of single slip observed at high temperatures in the crystals with an [001] orientation, the rotation of the tensile axis was found to obey the single glide condition within an accuracy of 10%. If any possible slip on $(2\bar{1}3)$ planes is neglected the glide strain in the $(1\bar{1}2)$ $[\bar{1}11]$ system may be calculated by the formula (Schmid and Boas, 1950):

$$\gamma = \frac{1}{\sin\varphi_o}\left(\sqrt{\epsilon^2 - \sin^2\lambda_o} - \cos\lambda_o\right) \qquad (5.4.)$$

Glide strains calculated in this way are represented in Figure 5.17. from the onset of single glide.

The reasons for having plotted the stress-strain curves in terms of the true tensile strain (defined as, $\ln[1 + \epsilon]$) are obvious. It is also evident that the values of the work-hardening rate obtained from the stress-strain curves would only have a conventional meaning.

5.6.3. The Effect of the Orientation on the Proportional Limit

It has been shown in the previous sections that the proportional limit and work-hardening rate of molybdenum single crystals is very strongly orientation dependent. The results reported so far are very similar to those obtained by Rose et al. (1962) with single crystals of tungsten. In both cases the highest proportional limit is exhibited by crystals

with ⟨110⟩ orientation and the lowest by crystals deformed in the ⟨100⟩ direction. The yield drop and low work-hardening rate characteristic of the ⟨110⟩ orientation is also observed in tungsten. By contrast, niobium (Mitchell et al. 1963, Votava 1964), tantalum (Ferris et al. 1962) and iron (Allen et al. 1956, Edmondson 1961) appear to behave differently.

The orientation dependence of the yield stress can neither arise from differences in the resolved shear stress nor from differences in the impurity content of the crystals. Other factors such as method of preparation of the specimens and condition of the surface were also considered and ruled out by Rose et al. (1962). The yield drop cannot be an impurity effect, because it is observed only in crystals with one specific orientation.

It appears, therefore, that the effect of the orientation is essentially of a crystallographic or geometrical nature and it was on this basis that Rose et al. interpreted their results on tungsten. Although the same geometrical and crystallographic considerations will apply in the case of molybdenum, a different interpretation of this effect will be attempted here.

It is becoming generally accepted that free dislocations or dislocations generated at points of very

high stress concentration become mobile in the metallic lattice at very low stresses, well below the detectable proportional limit (Brown and Ekvall 1962, Lawley and Gaigher 1964, Shaw and Sargent, 1964 . Additional evidence in support of this view will be given in Chapter 6). The amount of plastic strain which is produced at these stresses is very small, either because the dislocations become immobile as soon as they meet an obstacle (exhaustion hardening) or because they experience the effect of very strong and rapid interaction hardening. When the stress is high enough to free the dislocations from the obstacles, or to cause dislocation multiplication, a proportional limit which corresponds to the onset of a detectable plastic strain is observed. It seems therefore, that in order to explain the variation of the proportional limit with the direction of the applied stress it will be necessary to know how the nature and number of the obstacles in the 'micro-strain' region varies with the orientation.

As a result of a consideration of the type of obstacles that arise from the dislocation interactions discussed in Chapter 1, it can be shown that the mobility of screw dislocations may be strongly orientation dependent.

Crystals with [110] Orientation

When a crystal is deformed under a stress applied in the [011] direction, the jogs produced by the intersection of mobile dislocations will have $[\bar{1}11]$ and $[1\bar{1}1]$ Burgers vectors. These jogs, and many others of the 'intrinsic' type (Schoeck 1961), lie on the $(0\bar{1}1)$ plane on which the resolved shear stress is zero, and therefore it will be difficult for them to glide conservatively. As a result of this, the screw components are expected to become strongly locked in the micro-strain region. In Sections 5.2.2. and 5.3.3. it was shown that the number of dislocations increases when the proportional limit is reached. Since any multiplication mechanism involves the movement of the screw dislocations over large distances (Low and Turkalo 1962) macroscopic yielding is believed to occur as soon as the jogs become mobile. Rose et al. (1962) supposed that this would happen when, as a result of slight misorientations, the stress on the jogs reached a value large enough to move them conservatively. However our interpretation will stress the fact that the screw dislocations may become mobile when the jogs move non-conservatively producing point defects.

The high proportional limit of the crystals with <110> orientation would be explained in the following

way.

If the temperature is low enough for the thermal diffusion of the defects to be negligible and the jogs do not glide conservatively, the energy, U_f, to create a defect and the energy, U_m, to move the jog away from it must be entirely supplied by the applied stress (Seeger 1955). If the jogs in the dislocations are long, dipole trails will be created instead of point defects and the energy required to form the trails would also have to be supplied by the applied stress (Johnston and Gilman 1960). The type of jogs that produce vacancies will be the easiest to move, because the energy of formation of a vacancy is smaller than the energy of formation of an interstitial (Broom and Ham 1958), although, from the geometrical configuration of the glide elements (Figure 5.4.) it appears that the jogs produced by screw-screw intersections would mainly lead to the formation of interstitials (Cottrell 1957a).

If some of the jogs glide conservatively under the influence of internal stress fields, the yielding process can be thermally activated. Since the jogs move away from the point defects as soon as the latter are created, the activation energy for such a process would be $U_f - \tau^* l b^2$, (Seeger 1955), where l is the jog spacing. As the conservative

movement of jogs in screw dislocations is a difficult process in crystals with ⟨110⟩ orientation, there will be in general very few places available for thermal activation. Therefore, the pre-exponential factor in the rate equation which describes the process will be small and a relatively large stress will be needed to maintain a given strain-rate. This stress will be, however, smaller than $(U_m + U_f)/lb^2$, which is the stress required when the process is not thermally activated.

Dislocation multiplication takes place as soon as the screw dislocations become mobile, and since this happens at a stress when the strain rate sensitivity is high, (see Figure 5.40.) a rapid increase in the number of mobile dislocations can give rise to the yield drop observed in the crystals with ⟨110⟩ orientation.

Crystals with ⟨100⟩ Orientation

The low proportional limit of crystals with ⟨100⟩ orientation can be explained on the grounds of the same dislocation interactions previously discussed. The main difference is that in crystals with this orientation a stress of the same order as that acting on the dislocations is acting also on the jogs. These jogs will glide conservatively very easily, and they may become attached to an edge

component or may annihilate by meeting jogs of opposite sign. As a result of this, the screw dislocations will be able to move under relatively low stresses for two main reasons. The first is because there will be a large number of jogs available for thermal activation, and the second is because the mean jog spacing will be larger than that for deformation in the ⟨110⟩ direction.

For any orientation other than those two considered before the situation will be an intermediate one, and intermediate values of the proportional limit are to be expected according to this interpretation. This is indeed in close agreement with all the results obtained in the present investigation.

5.6.4. The Temperature and Strain Rate Dependence of the Yield Stress

If the deformation is carried out at a temperature high enough for the diffusion of the vacancies to be important, yielding may occur with the help of thermal activation on a large number of sites, even in the case of deformation in the ⟨110⟩ direction. The activation energy of this process would be $U_f + U_m - \tau^* lb^2$. However, the deformation of crystals with ⟨100⟩ orientation would require only an activation energy equal to $U_f - \tau^* lb^2$, because in

this case the vacancies do not need to diffuse away from the jogs.

When the number of sites available for thermal activation is large, the crystals deformed in the ⟨110⟩ direction may not exhibit a yield drop because the transition between the micro-strain region and macroscopic flow occurs through a gradual increase of the number of mobile dislocations. In this case yielding takes place much in the same way as for the other orientations.

The temperature and strain rate dependence of the proportional limit for the orientations that have been studied are shown in Figures 5.39. to 5.43. The plastic strain rates at any point of the stress-strain curve were calculated by using Equation 26 of the Appendix. The curves of Figures 5.41. and 5.42. do not include much experimental data because of the difficulties in determining the proportional limit already explained in Section 5.3.

The temperature and strain rate dependence of the yield stress is larger for the ⟨110⟩ orientation than for the other orientations. Data from the work of Lawley and Gaigher (1964) have also been included in Figure 5.43. It can be observed that the proportional limit increases very sharply between 77 and 42°K and there are reasons to expect a similar

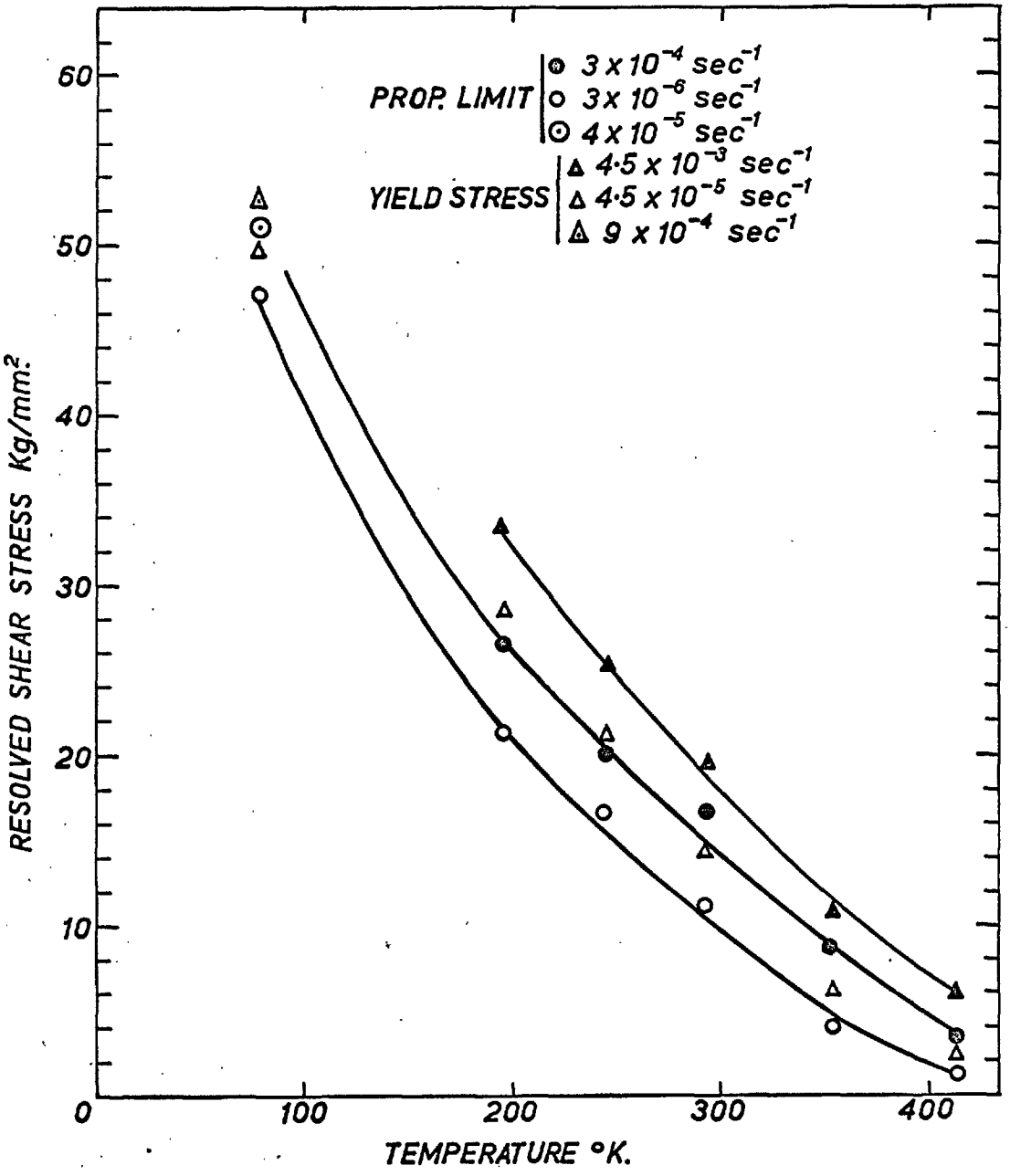

Figure 5.39. The effect of temperature on the proportional limit and yield stress of crystals with the deformation axis in the ⟨110⟩ direction.

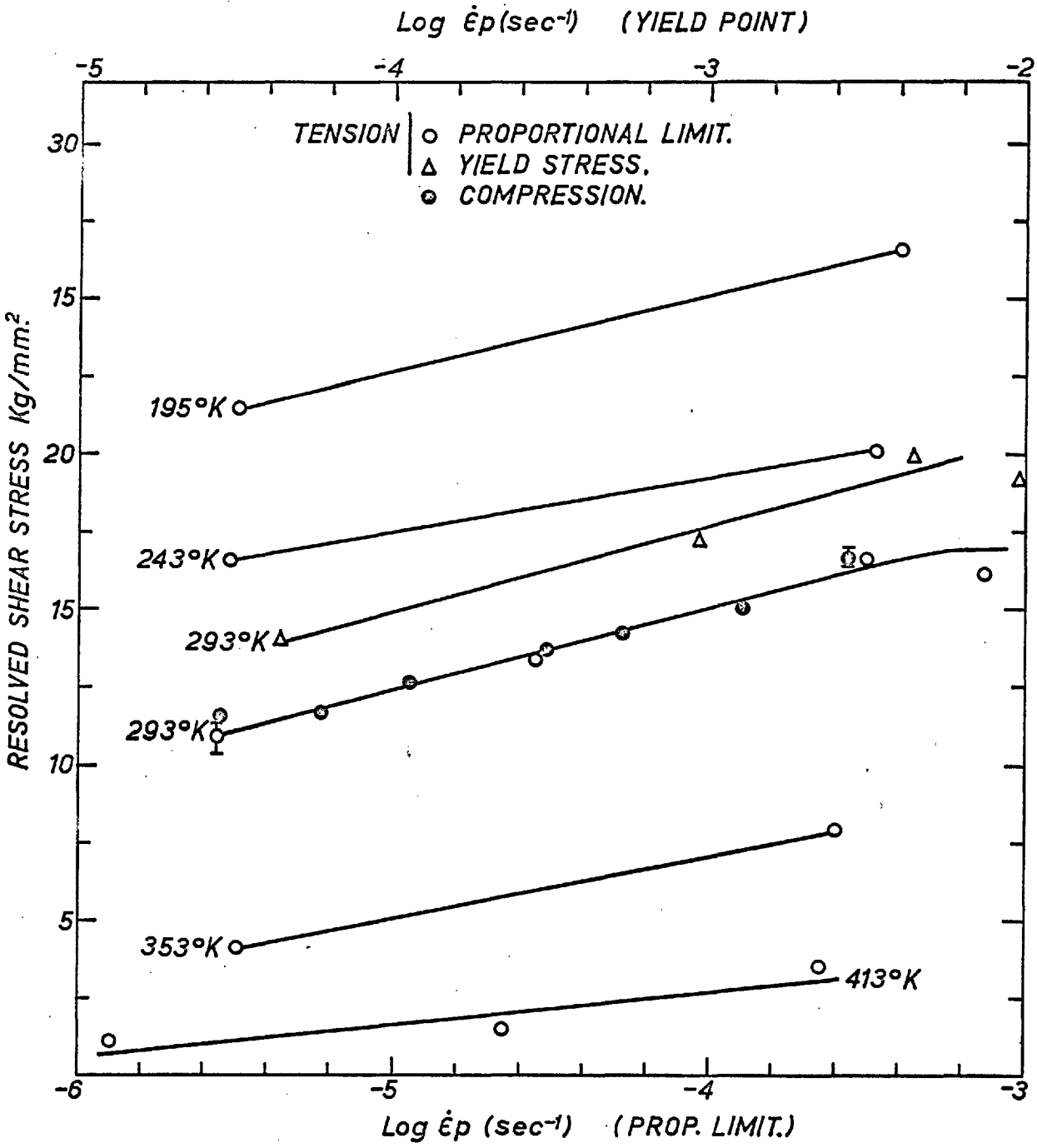

Figure 5.40. The effect of strain rate on the proportional limit and yield stress of crystals with the deformation axis in the ⟨110⟩ direction.

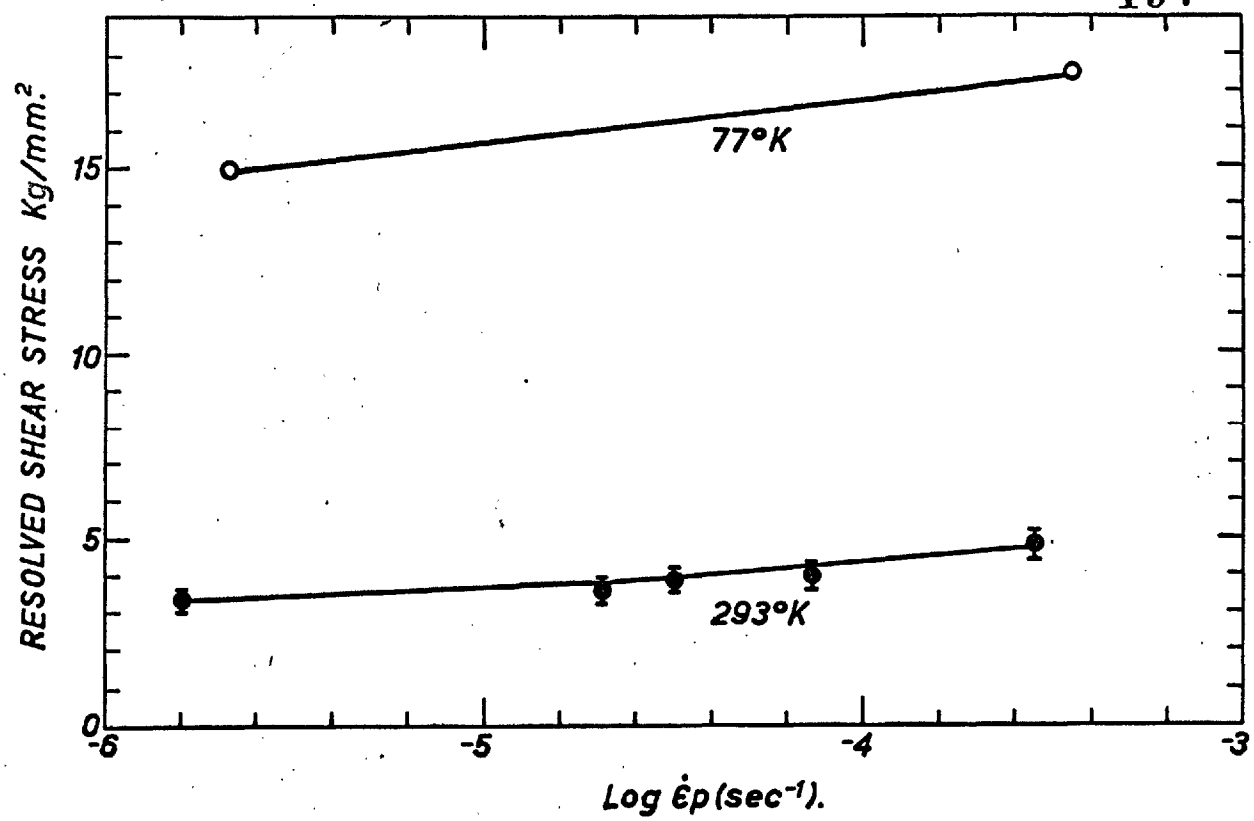

Figure 5.41. The effect of strain rate on the proportional limit of crystals with the tensile axis in the ⟨100⟩ direction.

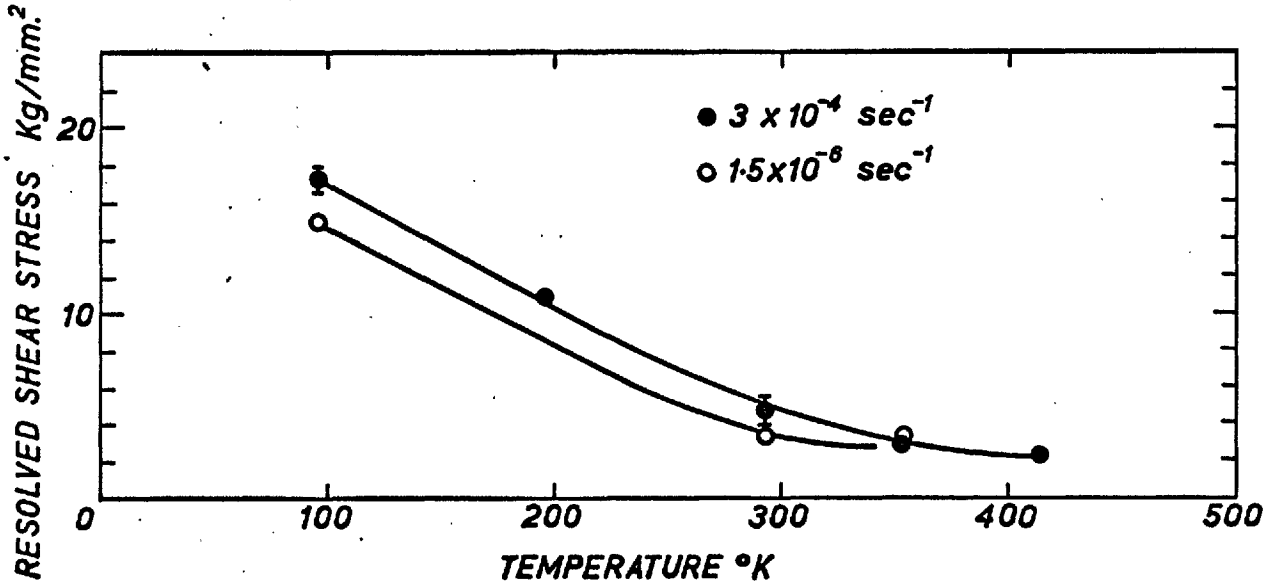

Figure 5.42. The effect of temperature on the proportional limit of crystals with the tensile axis in the ⟨100⟩ direction.

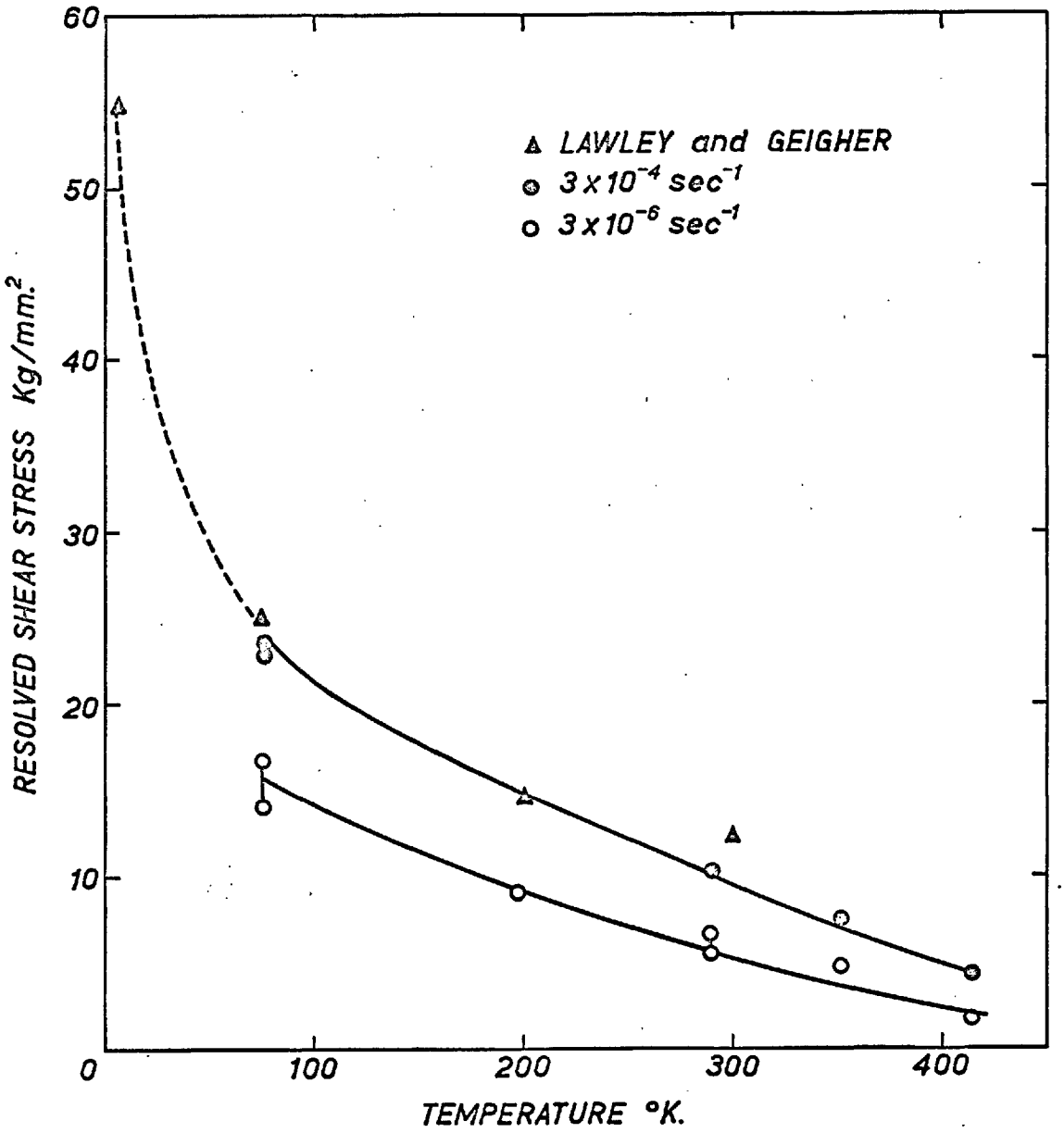

Figure 5.43. The effect of temperature on the proportional limit of crystals with the tensile axis in a direction near the center of the unit stereographic triangle.

behaviour from the crystals tested in the <100> direction. It appears therefore that the effect of the orientation tends to disappear at temperatures near $0^{\circ}K$ and above $400^{\circ}K$.

This result is consistent with the predictions of the mechanism proposed to explain the effect of the orientation. The different proportional limits of crystals with different orientation arises from the different numbers of jogs available for thermal activation, and hence from the differences in the pre-exponential factor in the corresponding rate equations. When the temperature of the deformation approaches $0^{\circ}K$ the influence of the pre-exponential factor is negligible compared with that of the exponential term, and therefore in order to maintain a given strain rate, $\dot{\gamma}$, a large difference in the pre-exponential factor, ν, is compensated by an insignificant difference in τ^*. This is clearly shown by the relationship:

$$- kT\, d(\ln \nu) = lb^2\, d\tau^*$$

obtained by differentiation of the rate equation. For example, if at a temperature of $4.2^{\circ}K$ a stress of 50.0 kg/mm^2 is necessary to give a strain rate of 10^{-4} sec^{-1}, when ν has the value of 10^{12} sec^{-1}, then an increase in stress of 0.1 kg/mm^2 is all that is necessary to maintain the same strain rate at the

same temperature even when the value of ν decreases by a factor of 10^6 sec^{-1}.

The reasons why at high temperatures no orientation dependence is observed have already been given.

The arguements developed so far cannot be claimed to constitute a complete model of the yielding phenomenon. Even if the non-conservative movement of jogs is responsible for the orientation dependence of the yield stress, it is possible that other mechanisms are involved in the process. For example, so far nothing has been said about the effect of the friction stress arising from the interaction between dislocations and impurity atoms, or about the effect of the Peierls stress of the lattice. These will be considered later.

5.6.5. The Activation Parameters

Values of the activation energy and activation volume involved in the yielding of crystals with ⟨110⟩ and ⟨100⟩ orientations have been calculated using the data of Figures 5.39. to 5.42., and Equations 1.11 and 1.13. The use of these equations is entirely justified, because in this case the product $w\tau^*$ is ten times larger than the product kT. The calculated values are given in Table 5.7.

It is important to realise that the values

TABLE 5.7.

Values of the Activation Parameters at the Proportional Limit (P.L.) and at the Yield Point (Y.S.).

Orientation	Temp. °K	Strain rate $\dot{\epsilon}$, sec^{-1}	Applied stress kg/mm^2	H(±15%)		w(±10%)		$U=H+w\tau^*$ e.V.	ν sec^{-1}
				10^{-12}erg	e.V.	$10^{-22}cm^3$	b^3		
<110>	195	3×10^{-6}	24(P.L.)	0.79	0.49	2.6	13	0.96	5×10^{6}
	293	3×10^{-6}	11(P.L.)	1.17	0.73	3.4	17	0.94	4×10^{6}
	273	3×10^{-6}	2.5(P.L.)	1.24	0.77	7.5	37	0.84	3×10^{4}
	293	4.5×10^{-6}	19.5(Y.S.)	1.17	0.73	3.4	17	1.1	5×10^{9}
<100>	293	3×10^{-5}	4.0(P.L.)	1.36	0.85	13.6	67	1.1	5×10^{9}

$\tau = \tau_\mu + \tau^*$

τ_μ = 1.0 kg/mm^2 at the proportional limit.

τ_μ = 4.0 kg/mm^2 at the yield point.

obtained for the activation energies are too small to be in agreement with the idea that yielding is controlled by the non-conservative movement of jogs in screw dislocations. If the work done by the effective stress, $w\tau^*$, is added to the activation energy, ΔH, the total energy obtained is still much smaller than the energy for vacancy formation (U_f = 3.6 eV, Peacock 1961) in molybdenum.

Although the importance of the non-conservative movement of jogs in screw dislocations on the yielding of b.c.c. metals has been discussed and emphasised by many authors (Schoeck 1961, Mordike 1962, Gregory 1963, Gregory et al. 1963, Lawley and Gaigher 1964), there has always been great difficulty in obtaining experimental evidence in favour of this mechanism which requires a large activation energy. Only on one occasion have activation energies of the order of 3 or 4 eV. been obtained for niobium (Gregory 1963, Gregory et al. 1963) and even in this case the interpretation of the results is not unquestionable.

Mordike (1962) has suggested that the low value of the activation energy found in tantalum is in agreement with the activation energy for the conservative motion of interstitial jogs in screw dislocations. (Hirsch 1962). It is difficult, however, to imagine how this mechanism would apply to metals that do not

contain extended dislocations.

Other Mechanisms

The overcoming of the Peierls-Nabarro stress is a mechanism which would be in better agreement with the values of the activation parameters determined here. The activation energies and activation volumes of Table 5.7. would fit very well into the unified picture of yielding and flow of b.c.c. metals proposed by Conrad (1963). The main difficulty that this mechanism faces is that it is unable to explain the orientation dependence of the proportional limit, which is the main concern of the present discussion.

The interaction energy of an interstitial atom with a screw dislocation is of about the same order as the activation energies measured in the present case (Cochardt et al. 1955, Koo 1963). However not too much significance should be attached to this agreement because no orientation effect would arise from such an interaction.

On the other hand the strengthening due to interstitial solute atoms would be rather small. For instance the temperature independent strengthening due to the Snoek ordering (Snoek, 1941) can be calculated from Schoeck and Seeger's (1959) formula:

$$\frac{\partial \tau}{\partial p} = 0.65 \text{ kg/mm}^2 \text{ . at. conc. \% .} \quad (5.5.)$$

A concentration of carbon in molybdenum of 10 p.p.m. in weight is equivalent to an atomic concentration of 10^{-4}. If all the carbon is assumed to be in solution, one obtains from Equation 5.5. that $\tau = 0.65$ Kg/mm^2, which only has significance at very high temperatures.

The increase in shear stress at 0°K produced by the solute atoms causing tetragonal distortion in the <100> direction is, according to Fleischer (1963):

$$\tau = \mu \frac{\Delta e}{3} \sqrt{c} \quad (5.6.)$$

where c is the atomic concentration of solute and Δe is a measure of the tetragonality. For iron $\Delta e = 0.4$ (Cochardt et al. 1955) and as the lattice parameter of molybdenum is 10% larger than iron, Δe can roughly be taken as 0.36. The value of μ is, from the data by Bolef and de Klerk (1962), $\mu = 1.5 \times 10^{12}$ dyne/cm^2. Equation 5.6. then gives $\tau = 15$ kg/mm^2. which is only one fourth of the stress at 77°K.

Although the solubility of carbon in molybdenum at room temperature is 40 p.p.m. by weight, (Northcott 1956) it is possible that the actual concentration of carbon in solution is smaller than has been assumed. In fact Lawley and Gaigher (1963) have observed fine precipitates of Mo_2C in single crystals

of molybdenum of a similar purity. These precipitates were seen to act as obstacles to dislocation motion, but their contribution to the yield stress is impossible to estimate in the present case because nothing is known about their size and distribution.

The friction stress arising from the dissociation of screw dislocations into partials lying on {112} planes may be significant in b.c.c. metals with a relatively low stacking fault energy, but its importance in the case of molybdenum is difficult to assess. This effect is not likely to give rise to an orientation dependent friction stress, because for the ⟨110⟩ and ⟨100⟩ orientations the distribution of the resolved shear stresses on the {112} slip planes is the same.

Since none of the mechanisms considered above provides a satisfactory explanation of the experimental results it is possible that the interpretation of the yielding phenomenon cannot be given in terms of a single mechanism. This situation merits a more comprehensive study and although at this stage a detailed treatment will not be attempted, certain considerations should be made.

5.6.6. The Existence of a 'Rate Controlling Mechanism'

Whenever yielding is the result of several different indepentent and parallel processes, it is

possible for the easiest one (i.e. that with the smallest activation energy) to be rate controlling, (Conrad et al. 1961). In such a situation the calculation of the activation parameters by means of Equations 1.11 and 1.13 is justified. However the problem is not so straightforward when the dislocation motion is controlled by two or more almost simultaneous mechanisms, and such a situation might well exist in the present case.

If both the dragging of jogs and the Peierls-Nabarro stress affect significantly the mobility of the screw dislocations, the stress, τ, necessary to keep a dislocation moving at a constant speed is, in the simplest case, the sum of the stresses required by each one of these two mechanisms independently. The variation in stress $(\Delta\tau)_{\dot{\epsilon}}$ necessary to maintain a constant strain rate when the temperature of the deformation is changed is the sum $(\Delta\tau_j)_{\dot{\epsilon}}+(\Delta\tau_p)_{\dot{\epsilon}}$ of the variation required by both of these two mechanisms. Similarly, the increment $(\Delta\tau)_T$ necessary to produce an increase in the plastic strain rate at a constant temperature is $(\Delta\tau_j)_T+(\Delta\tau_p)_T$.

Since the value of the activation energy, H, is calculated from the temperature and strain rate dependence of the stress through the ratio $(\Delta\tau)_{\dot{\epsilon}}/(\Delta\tau)_T$, it turns out that in general, this calculation will

not give the activation energy of any of the two processes involved.

Yet, if a situation such as that described above is to be investigated in more detail, the effect of the pinning points on the rate of nucleation of double kinks should also be considered (Celli et al. 1963). The problem is still further complicated if the interaction between dislocations and interstitial impurities or precipitates is taken into account.

It seems therefore, that the results obtained when considering that the deformation is determined by a unique rate controlling process should not be accepted without reservation. Further consideration to this problem will be given in Chapter 6.

5.6.7. The Effect of Orientation on the Work-Hardening Rate

It is possible that the orientation dependence of the work-hardening rate observed at temperatures lower than 300°K is actually larger than it appears when the curves of Figures 5.1. and 5.16. are compared with each other. The reason is that in the case of deformation in the <100> direction there are probably twice as many active slip systems as for deformation in the <110> direction. However, the magnitude of the work-hardening rate is rather unimportant here,

because a quantitative discussion cannot be attempted on the grounds of the experimental evidence obtained.

The nature of work-hardening in b.c.c. metals has been so little investigated in the past that it would be premature to aim at a reasonable understanding of the orientation dependence of the work-hardening rate without more extensive and precise information than that so far obtained. It seems, however, important to realise that it is possible to correlate the larger work-hardening rate of crystals with a ⟨100⟩ orientation with the comparatively larger number of obstacles arising from dislocation interactions in crystals of this orientation.

Let us consider the barriers formed by the $a\langle 001\rangle$ dislocations that result from the reaction 1.6. When the deformation axis is in the [011] direction, and if only the planes with the maximum resolved shear stress are considered to be active, the $a\langle 001\rangle$ dislocations may lie in three different directions on each slip plane.

When the deformation axis is in the [001] direction there are four active slip directions and the $a\langle 100\rangle$ dislocations may be formed as a result of six different reactions of the same type as 1.6. At the same time on every slip plane (if only planes with the maximum resolved shear stress are considered to be

active) these dislocations may lie in five or six different directions, depending whether the slip plane is of {110} type or of {112} type.

One would expect that in the last case a denser network of obstacles is built on each slip plane. By analogy with the role of Cottrell-Lomer sessile dislocations in the hardening of f.c.c. metals, this would result in a more profuse dislocation tangling, (Benson et al. 1962, Ohr and Beshers 1964) a denser cell structure and a stronger long range stress field (Li, 1962).

The dislocation etch pit arrangement shown in Figure 5.22. constitutes a small piece of evidence in favour of the mechanism of cell formation. This arrangement is somewhat similar to that observed by Livingston (1962) in copper single crystals in that it indicates regions of low dislocation density (cells) separated by high density areas (cell boundaries).

A dense cell structure will produce an effect which is similar to forming within the lattice roughly defined sub-boundaries (Li 1963, McLean 1962). The multiple splitting of the Laue spots, mentioned in Section 5.3.4., may be an indication that this effect is present in the crystals deformed in the ⟨100⟩ direction.

The behaviour of crystals with ⟨110⟩ orientation

is more difficult to explain satisfactorily in terms of the cell structure and the long range internal stress, since the work-hardening rate exhibited by these crystals is high in the pre-yield region and it changes suddenly to a lower value after the yield point. It would be pure speculation to discuss the present results in context with other theories of work-hardening (for a review see Nabarro et al. 1964), and further comments should be deferred until the results of a more detailed study of the flow stress are presented in Chapter 6.

5.6.8. The Temperature Dependence of the Work-Hardening Rate

The most significant effect of temperature on the work-hardening rate of molybdenum single crystals is the 'recovery transition' observed at about 350°K. The large uniform elongation that the crystals experience above this temperature is interpreted as the result of a decrease in the work-hardening capacity of the slip systems in which the deformation is initiated. For this reason, only the planes with the maximum resolved shear stress are active, and cross-slip on other planes is less prominent. At lower temperatures the higher work-hardening rate of the initially active slip systems probably induces slip on other planes with a smaller resolved shear stress.

Thus, the work-hardening effect is enhanced.

Lawley and Gaigher (1964) thought that the absence of single slip in molybdenum single crystals, deformed at room temperature, could be explained in terms of the solubility of interstitial impurities. They suggested that the presence of precipitate particles would shorten the dislocation mean free path and enhance their multiplication rate, and that this would produce a parabolic hardening. This suggestion demands further investigation since the argument as it stands is not likely to explain the softening observed above room temperature and it does not account for the strain hardening prior to recovery.

The fact that in all the orientations investigated the deformation is initiated by slip in more than one plane, and that the softening takes place after an initial stage of a comparatively larger work-hardening rate, suggests that the recovery may be due to a collapse or destruction of obstacles created in the first stages of the deformation. This would happen more easily at points of high stress concentration (for instance in the region of the neck of the tensile specimens, as observed in crystals with ⟨100⟩ orientation) and it would also result in a sudden increase of the number of mobile dislocations. The softening observed in the ⟨100⟩ orientation should

be more pronounced for the following reasons:

a) The amount of pre-strain is larger and therefore a larger number of obstacles collapse.

b) The destruction of barriers to dislocation motion occurs at the front of a propagating region of single slip where the stress concentration is possibly high.

c) The deformation takes place by single slip and therefore any hardening produced by dislocation interaction is small.

The collapsing of obstacles appears to be a thermally activated process, since the transition temperature for recovery is strain rate dependent. Since recovery takes place just above the temperature at which the yield point in crystals with a ⟨110⟩ orientation disappears, one is tempted to think that it might be associated with the diffusion of point defects. A supersaturation of point defedts may be built up in the first stage of the deformation and the migration of these defects to dislocation lines may induce climb of the edge segments and the pinching-off of dipole trails.

However, in the present case the recovery cannot be controlled by the normal diffusion of vacancies through the lattice, because the mobility of vacancies at temperatures near 400°K is very small. In fact,

a rough calculation shows that the mean jump frequency, j, of a vacancy at this temperature is about 10^{-2} sec^{-1}. A more detailed study of the processes by which point defects can promote recovery is required in order to check the ideas presented above. While this is being done, it is useful to consider other methods that may help to gain a better understanding of the recovery phenomenon. One of these is the examination by transmission electron microscopy of the deformation structures produced before and after the recovery transition. The other method is the comparative study of the deformation characteristics of group VA and group VIA b.c.c. metals, and their temperature dependences. The first of the two methods is simply mentioned as a suggestion for future work. The second approach is discussed in more detail in the next Section.

5.6.9. Comparison of the Mechanical Properties of Different b.c.c. Metals

It is well known that the refractory b.c.c. metals of Group VIA, molybdenum and tungsten, have similar chemical and mechanical properties, and in the present investigation some of their mechanical similarities have been emphasised. These metals have a higher critical resolved shear stress than niobium and

tantalum. The latter belong to Group VA of the Periodic table and experience much larger uniform elongations in a tensile test. Some results have been reported in this thesis which show that the mechanical properties of molybdenum and niobium single crystals are not so different from each other as has been thought. When molybdenum single crystals are tested above 350°K, they exhibit a behaviour very similar to that of niobium single crystals tested above 200°K. Compare, for example, the lower curve of Figure 5.2. with curve 17 of Figure 5 in the paper of Mitchell et al (1963); and the curves of Figure 5.31. in this thesis with the curves of Figure 7 in the same paper. Niobium and molybdenum also behave similarly when deformed at temperatures lower than 200°K and 350°K respectively. For example, niobium single crystals, with the orientation of the tensile axis in the centre of the stereographic triangle, do not exhibit any three stage hardening when tested at 175°K.

All these observations suggest that the main difference in the deformation characteristics of these two metals is that the 'softening' or 'recovery' transition occurs in niobium at a lower temperature than that in molybdenum. If this is a correct interpretation, it should be expected that the proportional limit and work-hardening rate of single crystals of niobium,

tested at temperatures below 200°K, would show the same orientation dependence as that of molybdenum. Also, one would expect tungsten single crystals to exhibit a recovery transition at temperatures higher than 350°K.

As there is no data on the recovery transition for tantalum single crystals, a comparison with this metal is not possible at present. It will also be extremely interesting to extend this comparison to iron if results for this metal become available.

The above discussion leads one to believe that the solution to the problem of the recovery transition would have to explain the detailed mechanism in both molybdenum and niobium. It would also have to account for the different transition temperatures of these two metals. It is therefore possible that this phenomenon may be further understood if the deformation of the b.c.c. metals is investigated in a unified manner.

CHAPTER 6

DEFORMATION MECHANISMS IN MOLYBDENUM SINGLE CRYSTALS

6.1. Introduction

In the last chapter the deformation characteristics of molybdenum single crystals were discussed after an analysis of the results obtained from conventional tensile tests at various temperatures and strain rates. A more detailed study of the variation of the stress with temperature and strain rate, in the micro-strain and flow region, is described in the present chapter where, at the same time, an attempt will be made to understand more fully the mechanisms involved in the deformation of single crystals with the tensile axis orientated in the ⟨110⟩ and ⟨100⟩ directions.

6.2. The Relaxation Test

A stress relaxation method particularly useful for calculating the strain rate sensitivity of the stress has been developed during the present investigation. The interpretation of the relaxation phenomenon and the analysis of the test are described in detail in the Appendix, and for this reason they will be only briefly outlined here.

When a solid is plastically deformed in a hard

tensometer and the movement of the cross-head is arrested, a continuous decrease of load with time is observed. This effect is due to the continuous deformation of the solid at a decreasing stress and strain rate. Since the amount of strain that occurs during the relaxation is small, the long range internal stress, τ_μ, is assumed to be constant, and the relaxation process is interpreted as the variation of the effective stress, τ^*, with time. The solid reaches the equilibrium state, $\dot{\epsilon} = \dot{\tau} = 0$, when $\tau^* = 0$.

If the values of τ during the relaxation are plotted against log (t+c) (where t is the time, and c is a conveniently chosen constant) a straight line is obtained. The positive value of the slope of this line, λ, is the strain rate sensitivity of the stress. Thus:

$$\lambda = \frac{d\tau}{d \log \dot{\epsilon}} = \frac{d \tau^*}{d \log \dot{\epsilon}} \qquad (6.1.)$$

Therefore, in the interval of t during which the linear relationship between τ and log (t+c) is experimentally satisfied the equation of the relaxation curve is:

$$\tau - \tau_o = \lambda \log c - \lambda \log (t+c) \qquad (6.2.)$$

Such an equation is justified by the fact that a suitable integration of the rate equation yields a linear relationship of the same type as (6.2.). It

must be noticed, however, that in order to perform such an integration the pre-exponential factor, the internal energy, and the activation volume in the rate equation have to be constant. The values of λ can be measured from the semi-logarithmic plot with an absolute error smaller than ± 0.05 kg/mm^2.

The main advantages of the relaxation method over the strain rate cycling test are as follows:

a) Values of λ can be obtained in parts of the stress-strain curve that show a very large work-hardening rate.

b) If the strain rate sensitivity is strongly stress dependent, with the relaxation test one obtains true values of λ instead of mean values.

c) The amount of strain introduced in the determination of λ is very small, and it is therefore possible to determine simultaneously the strain rate dependence and the temperature dependence of the flow stress.

The importance of these advantages will become clear later.

6.3. Experimental Results Obtained at 293°K

The parameter λ was determined at various points on the stress-strain curves during the deformation of crystals with ⟨110⟩ and ⟨100⟩ orientation. Strain rate cycling tests as well as relaxation tests were

used for this determination. The different types of experiments performed at 293^{o}K will be described separately in the following sections.

6.3.1. Relaxation Tests During Deformation at a Constant Cross-head Speed

The values of λ obtained by the relaxation method during the deformation of crystals with the tensile axis in the $\langle 110 \rangle$ and $\langle 100 \rangle$ directions are plotted as a function of the applied stress in Figures 6.1. and 6.2. Finite values of λ were obtained at a stress as low as 1 kg/mm^{2}, and this indicates that the specimens undergo plastic deformation at that stress. However, the fact that deformation may start at points of high stress concentration should not be overlooked if any consideration is to be given to this result.

In the crystals deformed in the $\langle 110 \rangle$ direction, λ increases very sharply near the proportional limit, but remains constant after the specimen has yielded macroscopically. By contrast, in the crystals with $\langle 100 \rangle$ orientation λ increases continuously, and after the proportional limit has been reached the Cottrell-Stokes law, $\Delta\tau/\tau$ = constant (Cottrell and Stokes 1955), is closely obeyed.

The strain rate at which the specimens are deformed has also some influence on the value of λ. It can be observed in Figures 6.1. and 6.2., that for

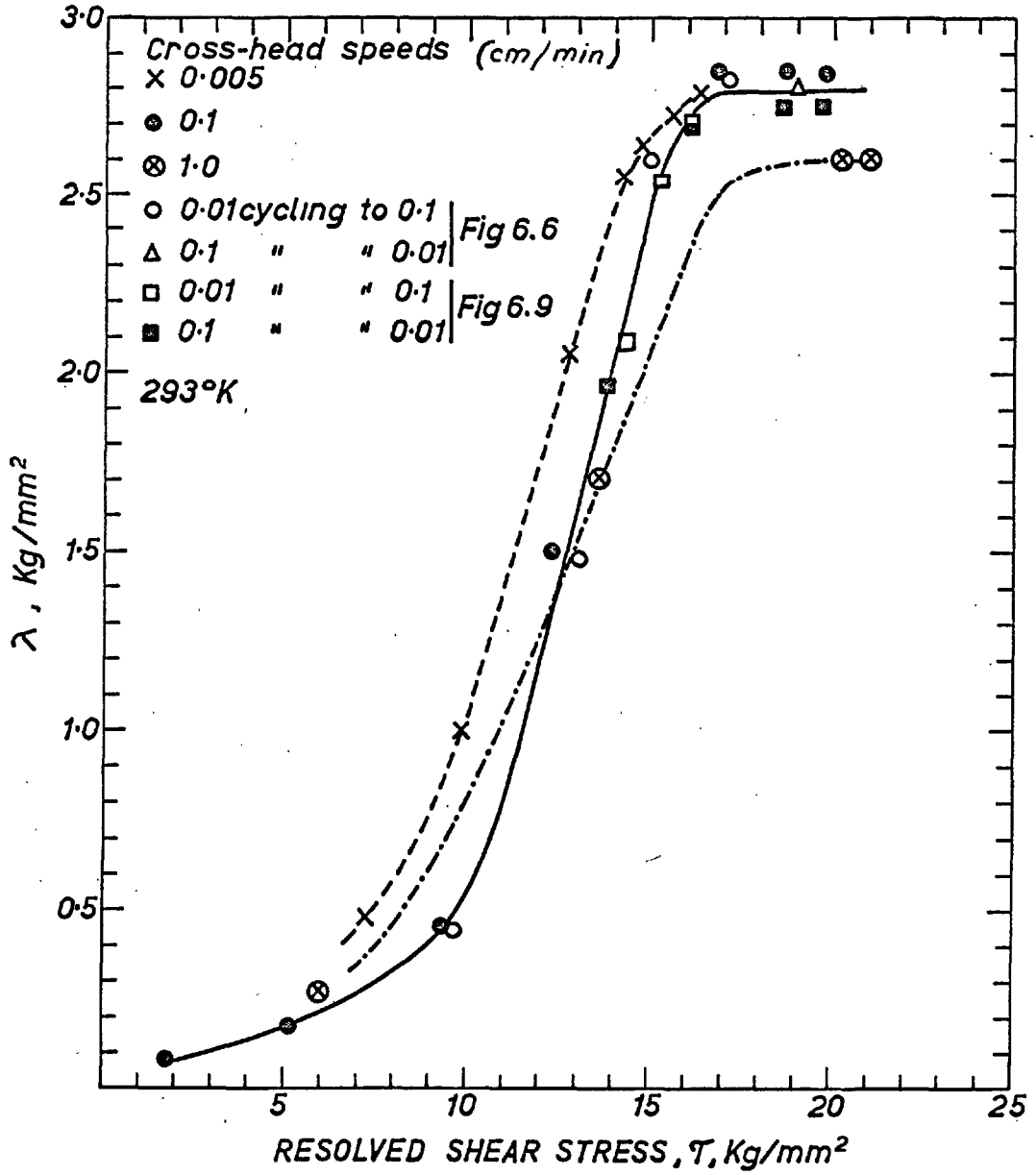

Figure 6.1. Variation of the strain rate sensitivity with stress at 293°K for crystals with ⟨110⟩ orientation.

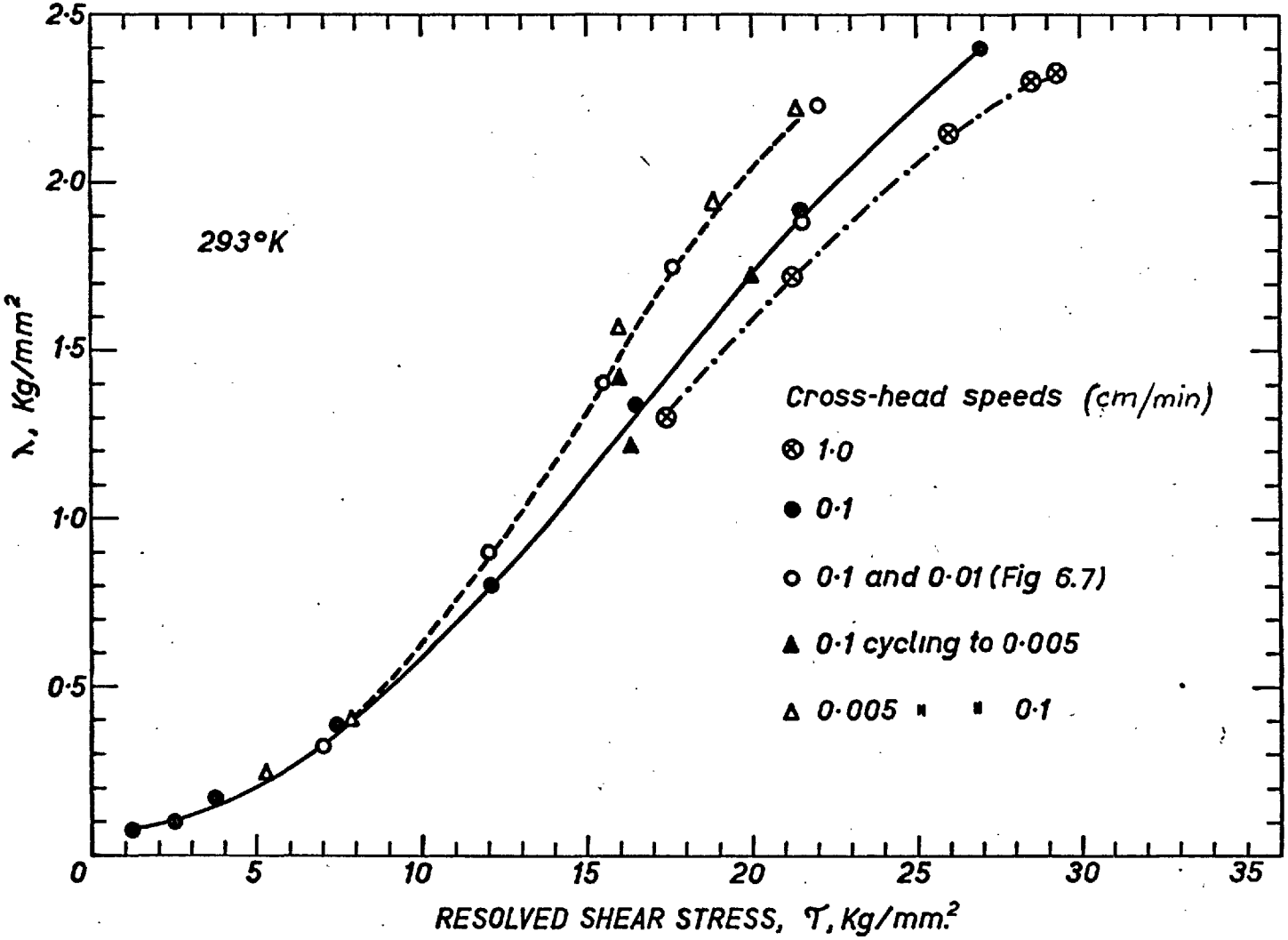

Figure 6.2. Variation of the strain rate sensitivity with stress at 293°K for crystals with <100> orientation.

the same stress, λ is larger when the crystals are deformed at a smaller strain rate.

6.3.2. Determination of the 'Relaxed Flow Stress'

According to the interpretation given to the relaxation phenomenon, it should be possible to measure the value of the long range internal stress, τ_μ, by allowing the specimen to relax until the equilibrium state $\dot{\epsilon} = \dot{\tau} = 0$ is reached. Unfortunately the determination of the stress at which this equilibrium is attained is in some cases very difficult. For instance, in the case of molybdenum single crystals deformed at room temperature it was found that the equilibrium is not reached even after 14 hours of relaxation, and this makes the determination of τ_μ not only impractical, but also unreliable. It is possible that by leaving the specimen under stress for such a long time some recovery process may take place, and therefore the value of the equilibrium stress may not be a true measure of τ_μ at the stress at which relaxation was started.

In order to avoid these difficulties the following method for determining τ_μ was tried. The specimens were loaded up to succesively increasing values of the stress, and the amount of relaxation taking place in one or two minutes was recorded at each stress level. The maximum stress that the specimen can withstand

without relaxing during this time was tentatively taken as an approximation to the stress at which the equilibrium is attained.

Since it is impossible to know a priori how close an approximation this is, it is also impossible to know how accurately the value of τ_f can be determined. For this reason, it will be convenient to designate the stress measured by this method by the more general term 'relaxed flow stress'. This term was already used by Bell and Bonfield (1964), and it will be represented hereafter by the symbol τ_r.

Conventional stress-strain cruves, and curves of τ_r versus strain, for crystals with ⟨110⟩ and ⟨100⟩ orientation are shown in Figures 6.3. and 6.4. The values of $\tau - \tau_r$ versus strain are also shown in the same figures. For the crystals with the deformation axis in the ⟨110⟩ direction the difference $\tau - \tau_r$ increases in the micro-strain region, and beyond the proportional limit (16 kg/mm^2) it remains constant and equal to 10 kg/mm^2. The strain-hardening is then exclusively due to an increase in τ_r.

For the crystals deformed in the ⟨100⟩ direction, both τ_r and $\tau - \tau_r$ increase throughout the deformation.

6.3.3. Strain Rate Cycling Tests.

Simultaneous strain rate cycling tests and relaxation tests were performed in the following way.

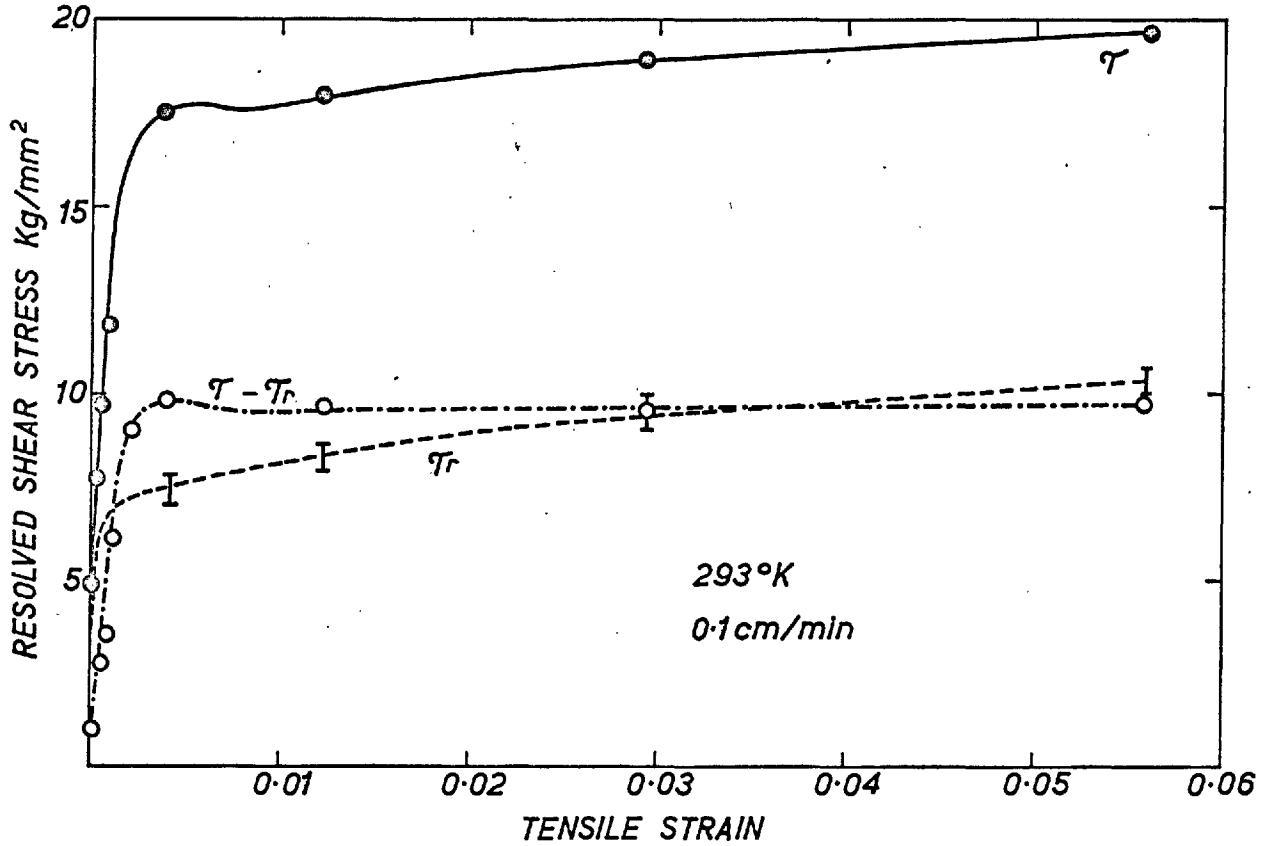

Figure 6.3. Variation of τ, τ_r, and $(\tau - \tau_r)$ with strain for a crystal with the tensile axis in the ⟨110⟩ direction.

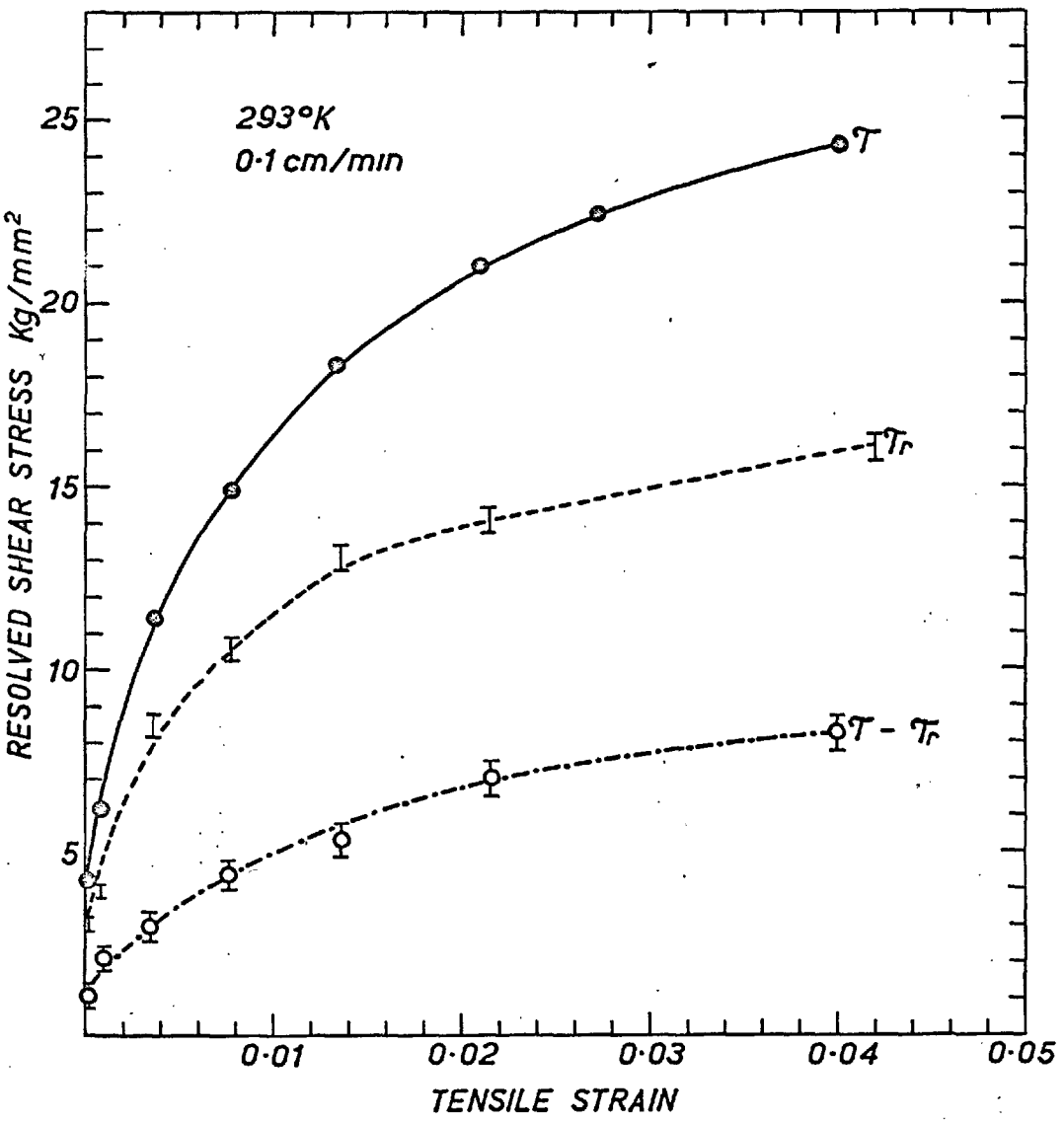

Figure 6.4. Variation of τ, τ_r, and $(\tau - \tau_r)$ with strain for a crystal with the tensile axis in the ⟨100⟩ direction.

The crystals were strained at a cross-head speed of 0.1 cm/min up to a stress τ_1 where relaxation was carried out. After partially unloading the specimen, straining was continued at a cross-head speed of 0.01 cm/min up to the same stress τ_1 where relaxation was carried out again. This process was repeated at increasing values of the stress, and after the specimen yielded plastically, conventional strain rate cycling tests were also performed. In this way, it was possible to obtain in the same test the stress increments corresponding to a variation of the plastic strain rate by a factor of 10.

Figures 6.6. and 6.7. show two typical strain rate cycling and relaxation experiments conducted with crystals with ⟨110⟩ and ⟨100⟩ orientation respectively. In these figures the continuous line represents the conventional stress-strain curve and the dotted line indicates the variation of stress with time during the relaxation. The values of the plastic strain rate at the beginning of the relaxation test, and the parameters, λ and c, are given in the figures. The plastic strain rates that occur after certain relaxation times are also indicated.

The plastic strain rates were calculated by the three methods described in the Appendix. By estimating the errors inherent in each one of these methods, the

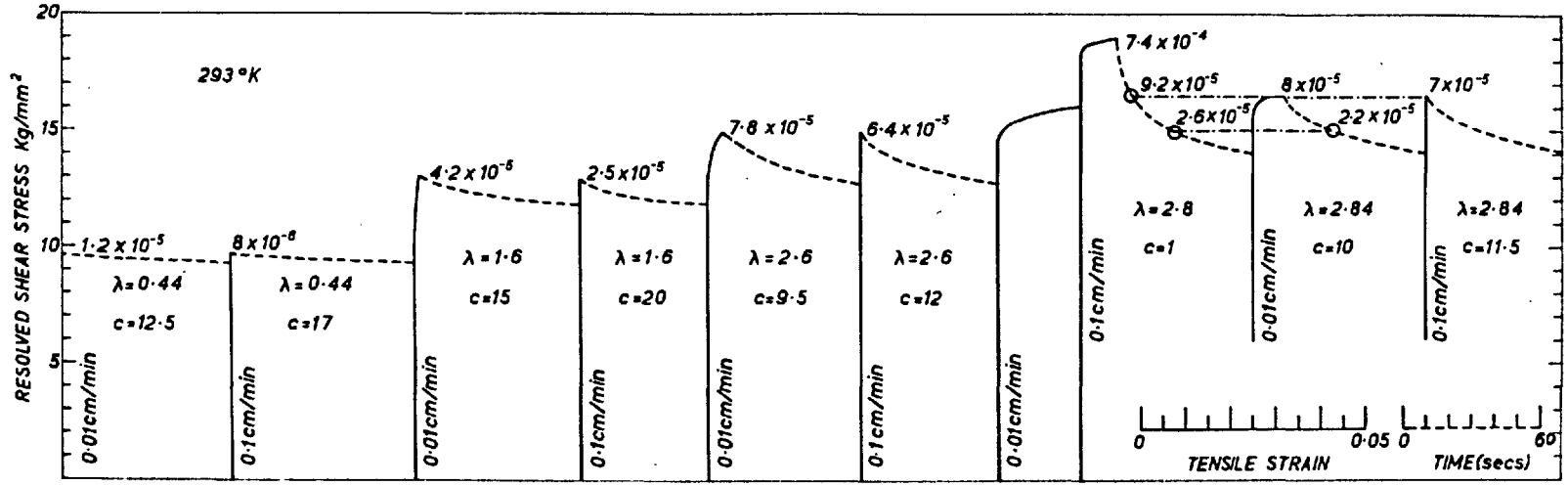

Figure 6.6. Results of a strain rate cycling and relaxation test for a crystal with ⟨110⟩ orientation. Values of the strain rate are given in sec^{-1}, values of λ in kg/mm^2, and values of c in sec.

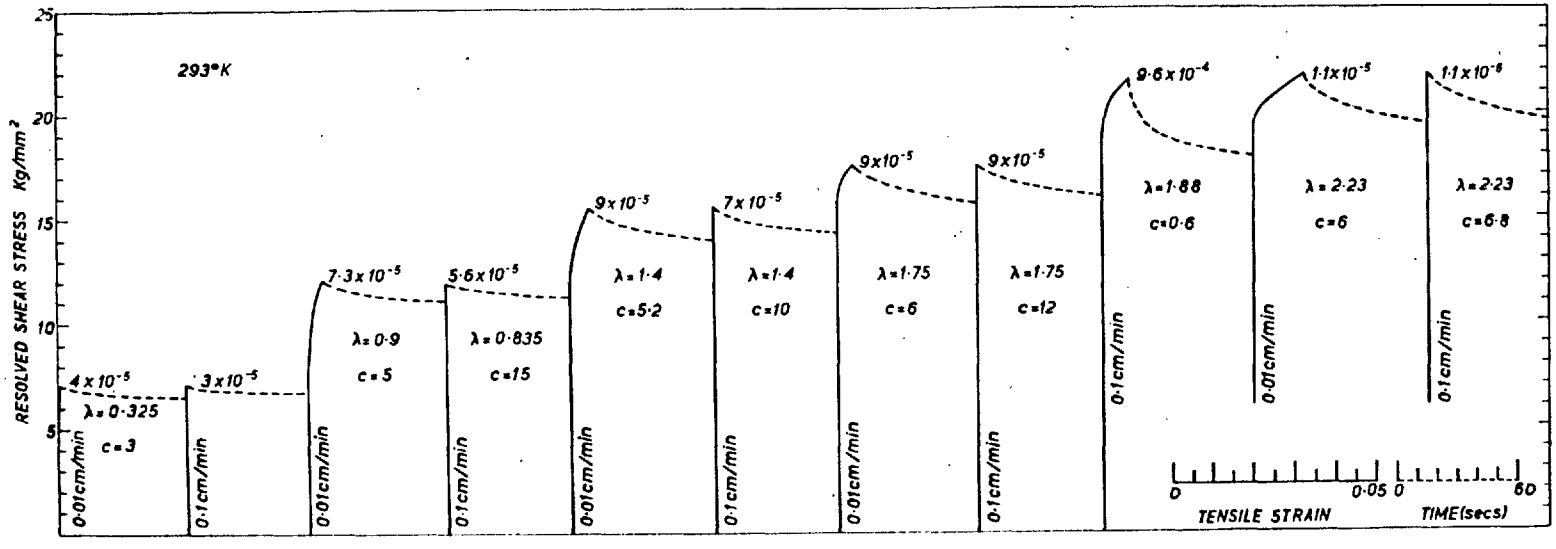

Figure 6.7. Results of a strain rate cycling and relaxation test for a crystal with ⟨100⟩ orientation. Values of the strain rate are given in sec^{-1}, values of λ in kg/mm^2, and values of c in sec.

most reliable value was obtained. The accuracy depends on the cross-head speed at which the crystals are deformed, and on the slope of the load-elongation curve. The values of $\dot{\epsilon}_p$ given in the figures have an error of $\pm$ 10%, when the cross-head speed is 0.1 cm/min, and an error of $\pm$ 5% when the cross-head speed is 0.01 cm/min.

The values of λ determined by the relaxation method were always in perfect agreement with those calculated from the ratio $\Delta\tau / \log (\dot{\epsilon}_1 / \dot{\epsilon}_2)$ obtained from the strain rate cycling experiments. This agreement is better illustrated in Figure 6.8., which shows the results of a cycling test between the cross-head speeds of 0.005 and 0.1 cm/min.

The curves of Figures 6.6. and 6.7. show a very interesting result. When the work-hardening rate is small, the plastic strain rate at which the crystals deform is a function of the applied stress alone. It is irrelevant whether the specimen has yielded or not, and whether the stress is increasing or decreasing. Observe, for example, in Figure 6.6. that at a stress of 16.2 kg/mm^2, the plastic strain rate is $(8 \pm 1) \times 10^{-5}$ sec^{-1} and at a stress of 15 kg/mm^2, it is $(2.4 \pm 0.2) \times 10^{-5}$ sec^{-1} irrespective of the manner in which the stress was achieved.

When the crystals deform in a region of a high

work-hardening rate, the plastic strain rate is not only a function of the applied stress, but also depends on the amount of strain. This could be interpreted to mean that the small amount of deformation introduced during the relaxation and subsequent straining produces a significant increase in the work-hardening component of the stress, or in other words, that a very small strain modifies considerably the dislocation configuration.

The fact that, at constant temperature, the plastic strain rate is only a function of the dislocation configuration and effective stress is already expressed by Equations 1.3. and 1.10.

Figure 6.8. shows the result of a strain rate cycling and relaxation experiment in which the machine cross-head speed was varied from 0.005 cm/min to 0.1 cm/min. The dotted lines indicate the amount of strain introduced by the relaxation. The values of λ obtained by the relaxation method are compared with those obtained from the strain rate cycling test, in the upper part of Figure 6.8. They have also been plotted as a function of the applied stress in Figure 6.2. During this test the value of the relaxed flow stress was also determined at different strains and at the two strain rates involved in the experiment. The results indicate that within the accuracy of the

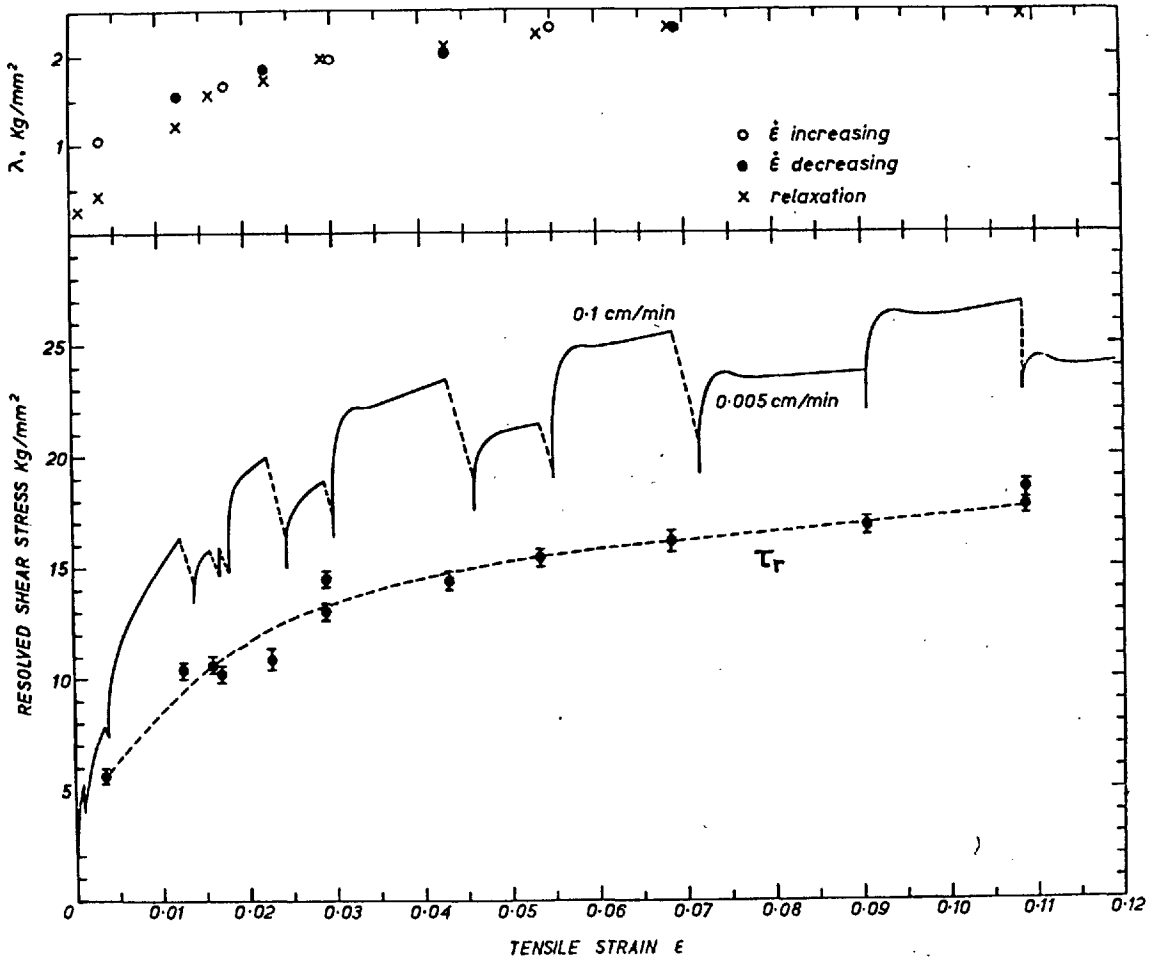

Figure 6.8. Results of a strain rate cycling and relaxation test for a crystal with ⟨100⟩ orientation.

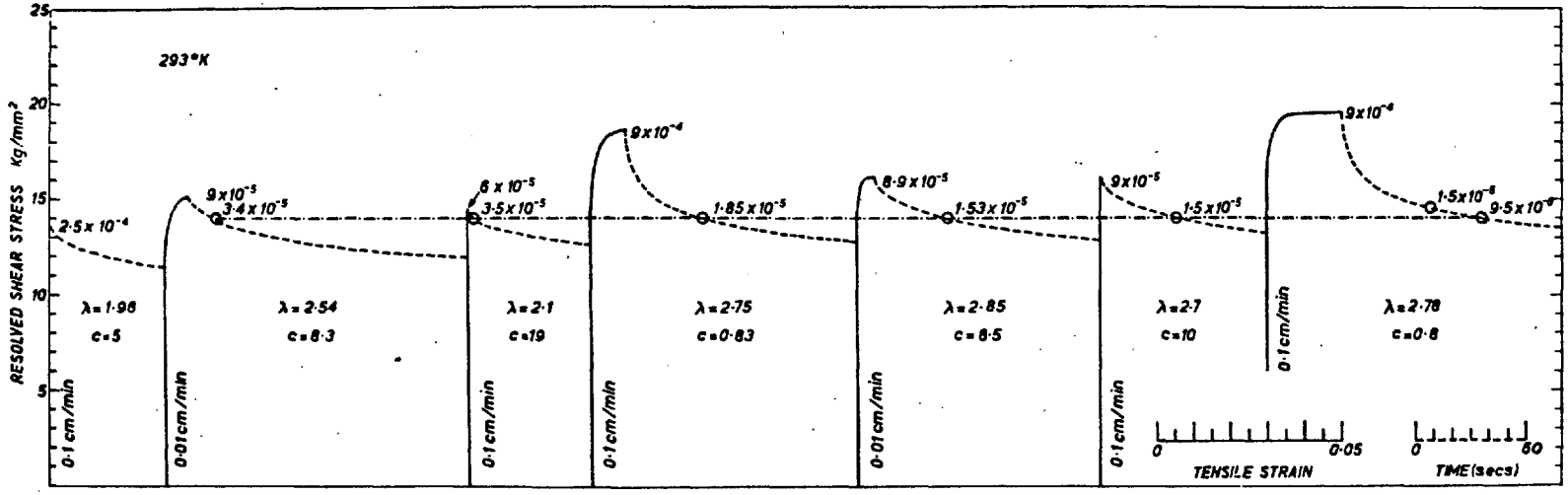

Figure 6.9. Results of a strain rate cycling and relaxation test for a crystal with ⟨110⟩ orientation. Values of the strain rate are given in sec^{-1}, values of λ in kg/mm^2, and values of c in sec.

measurements, τ_r does not vary when the strain rate is changed.

Another strain rate cycling test which illustrates the variation of λ with the applied stress in crystals with ⟨110⟩ orientation is shown in Figure 6.9. In this experiment, the first straining of the specimen was conducted using a machine cross-head speed of 0.1 cm/min. The plot of the values of λ versus τ obtained from this test (Figure 6.1.) indicates that at constant temperature the strain rate sensitivity is a function of τ alone, and that for values of $\tau > 14$ kg/mm^2 it is independent of the previous amount of strain.

If a similar test is performed with crystals orientated in the ⟨100⟩ direction, it is found that the strain rate sensitivity is not only a function of the applied stress, but also depends on the amount of previous strain.

6.4. The Strain Rate Sensitivity of the Stress at Temperatures Other than 293°K

When the relaxation tests were carried out at temperatures other than 293°K, special precautions had to be taken. Since both the specimen and the frame for low and high temperature experiments, had to be immersed in a temperature controlled bath, it was

necessary to wait for a time long enough for all the parts of the frame to be in thermal equilibrium. If this precaution were neglected, a variation of the load with time could be observed as a result of the different rates of cooling, or heating, of the various parts of the frame. This variation of the load is small, and it is negligible in an ordinary tensile test, but it can be very significant during a relaxation experiment when small variations of load are measured. Relaxation tests have been performed during the straining of crystals with ⟨110⟩ and ⟨100⟩ orientation at a cross-head speed of 0.1 cm/min and at various temperatures. The values of λ obtained from these tests are plotted against the applied stress in Figures 6.10. and 6.11.

Figure 6.10. shows that for crystals with ⟨110⟩ orientation λ increases rapidly at stresses just below the proportional limit. When the crystals are deformed at 413°K, λ exhibits a maximum value at a stress $\tau = 8$ kg/mm^2. As the stress is increased and when the crystals experience a large uniform elongation (a characteristic of this temperature), λ decreases.

Figure 6.11. shows that in the crystals with a ⟨100⟩ orientation the strain rate sensitivity increases continuously with the applied stress except when the

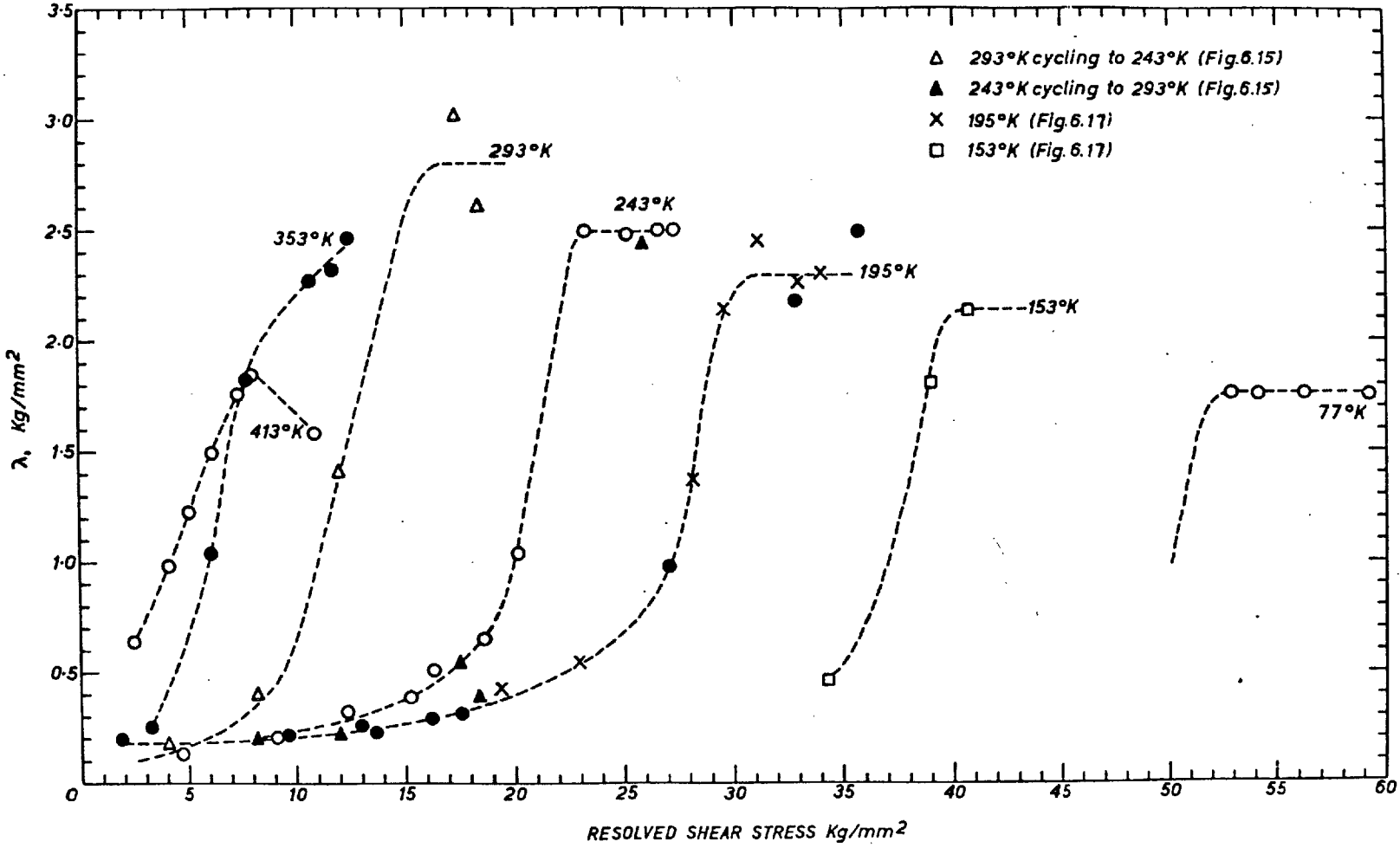

Figure 6.10. Variation of the strain rate sensitivity with stress at various temperatures for crystals with ⟨110⟩ orientation.

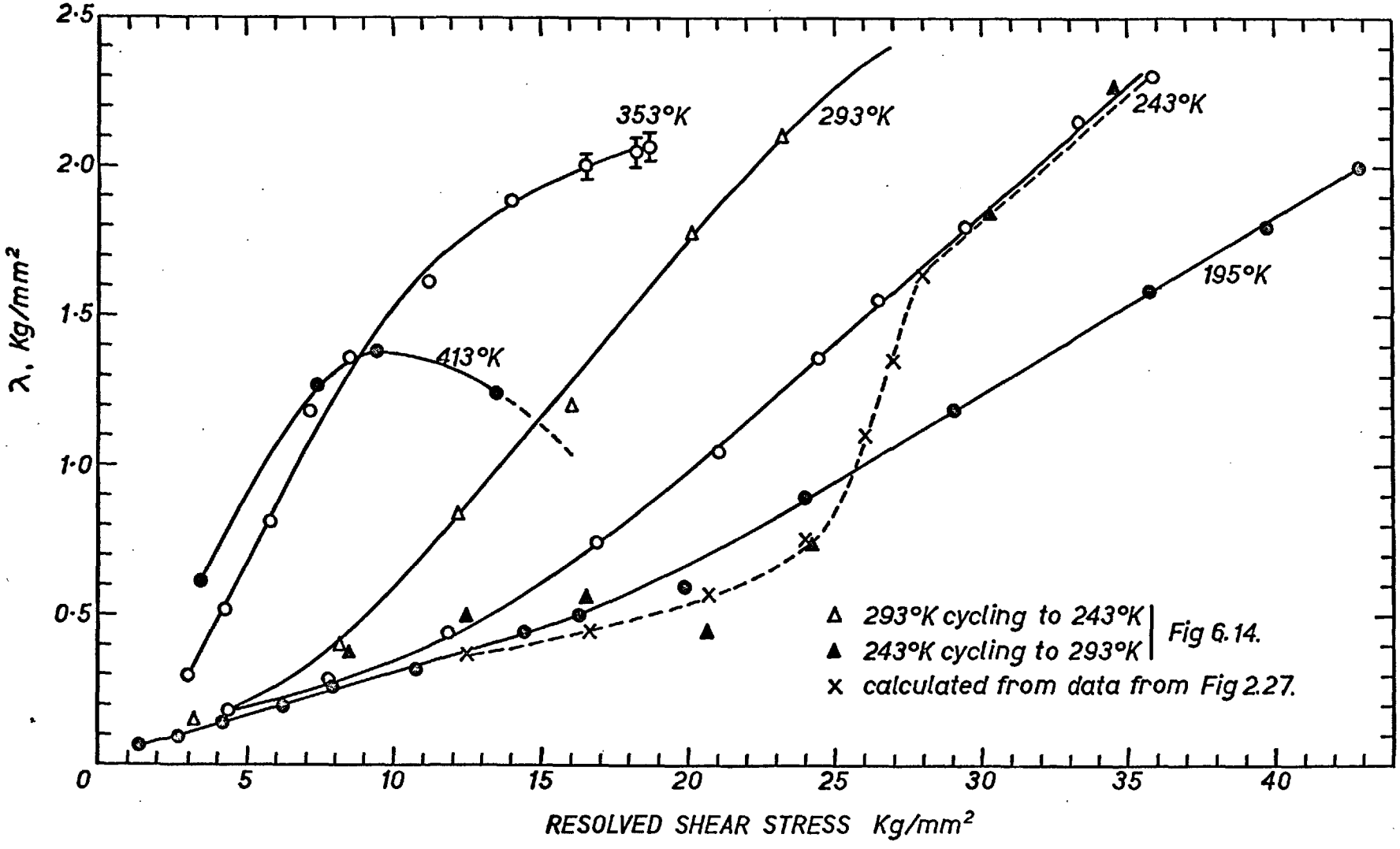

Figure 6.11. Variation of the strain rate senstivity with stress at various temperatures for crystals with ⟨100⟩ orientation.

temperature is 413°K. In this case the curve of λ versus stress exhibits a maximum value at $\tau = 10$ kg/mm^2.

6.5. Determination of the Relaxed Flow Stress at Temperatures Other than 293°K

The value of the relaxed flow stress was determined for crystals with both the ⟨110⟩ and ⟨100⟩ orientations. The tests were performed at a cross-head speed of 0.1 cm/min and at various temperatures. The method described in Section 6.3.2. was also used in this case, and extreme care was taken to stabilize the temperature of the bath and testing frame in order to avoid random variations of the load during the determination.

The results of some of these experiments are shown in Figure 6.12. and in Figures 6.13(a) and (b). It is clear, from these results, that τ_r increases considerably by decreasing the temperature, and more striking is the fact that at temperatures lower than 300°K the difference $\tau - \tau_r$, at a given strain, is independent of the temperature. The increase in the flow stress produced by lowering the temperature is entirely due to the increase in τ_r. However, when the crystals are deformed at 353°K, the value of both τ_r and $\tau - \tau_r$ at a given strain are smaller than the corresponding values in crystals deformed at 293°K. Therefore, when the temperature is increased

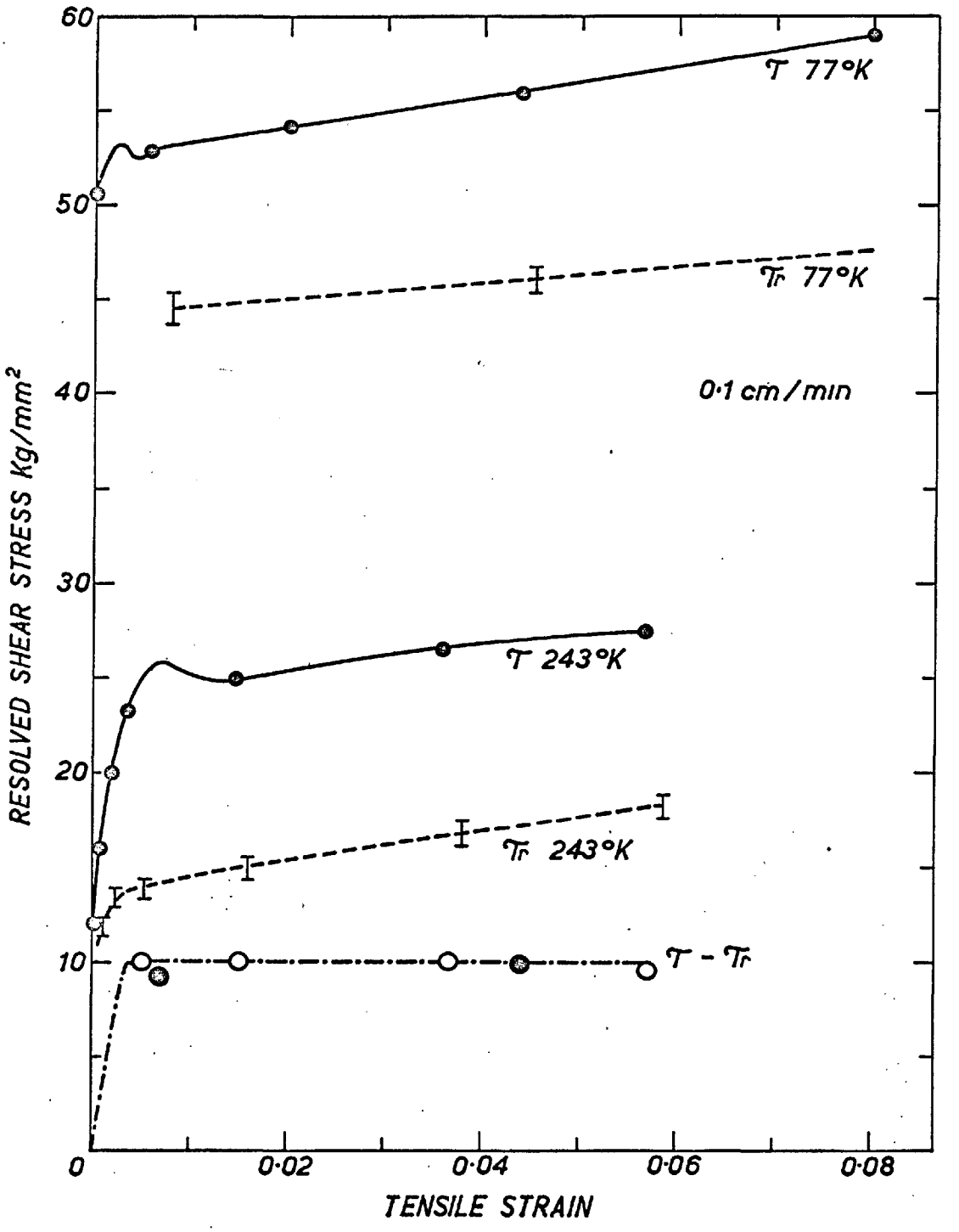

Figure 6.12. Variation of τ, τ_r, and $(\tau - \tau_r)$ with strain at two different temperatures, for a crystal with the tensile axis in the $\langle 110 \rangle$ direction.

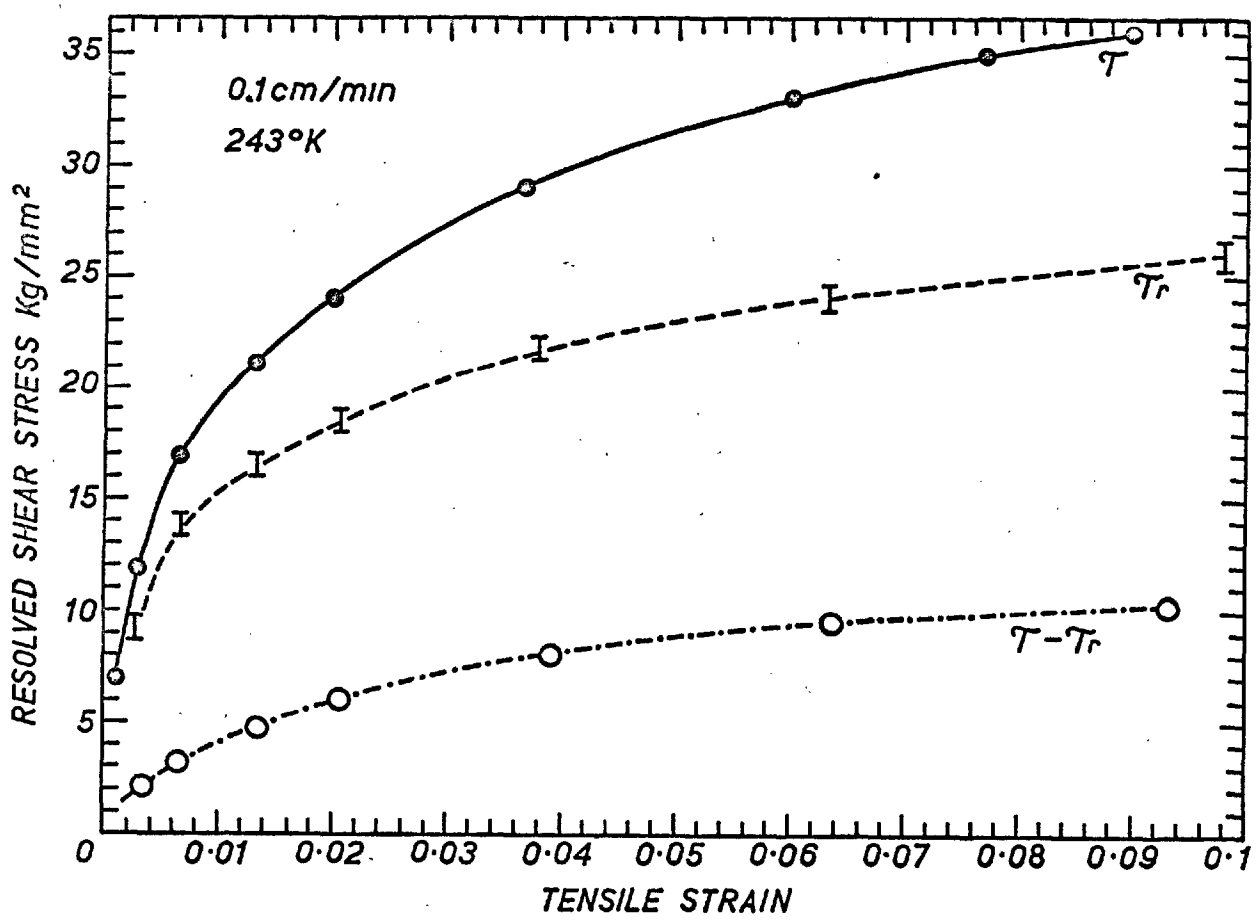

(a)

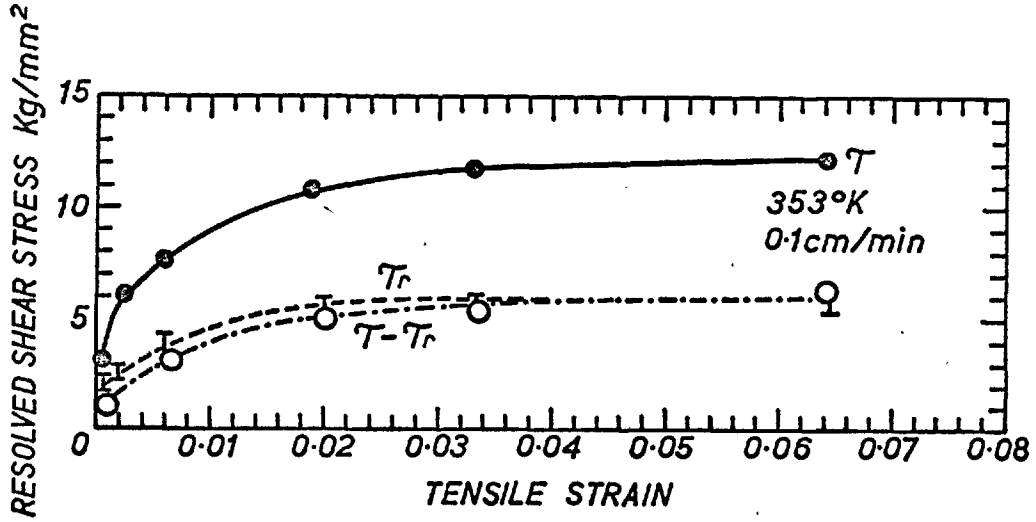

(b)

Figure 6.13. Variation of τ, τ_r, and $\tau - \tau_r$ with strain for crystals with ⟨100⟩ orientation. (a) at 243°K (b) at 353°K.

above 293°K, the decrease in the flow stress is due to the decrease of both τ_r and $\tau - \tau_r$.

6.6. Temperature Cycling Experiments

Temperature cycling experiments were performed with crystals of the ⟨110⟩ and ⟨100⟩ orientations. At the same time, relaxation tests were carried out at the two temperatures involved in the experiment, and thus the strain rate sensitivity of the stress could be measured in the same test. The results of these experiments will be described with the help of Figures 6.14. and 6.15.

Figure 6.14. shows the results of a test performed in the following way: A crystal, with its tensile axis orientated in the ⟨100⟩ direction, was strained at the basic temperature of 293°K and at a cross-head speed of 0.1 cm/min, up to a stress $\tau = 8$ kg/mm^2 when relaxation was carried out. The specimen was then partially unloaded, and the temperature changed to 243°K. The crystal was restrained at the same cross-head speed and up to the same value of the stress where a relaxation test was again performed. This process was repeated at successively increasing values of the stress until the region of low work-hardening rate was reached. At this point the crystal was given larger strains than previously,

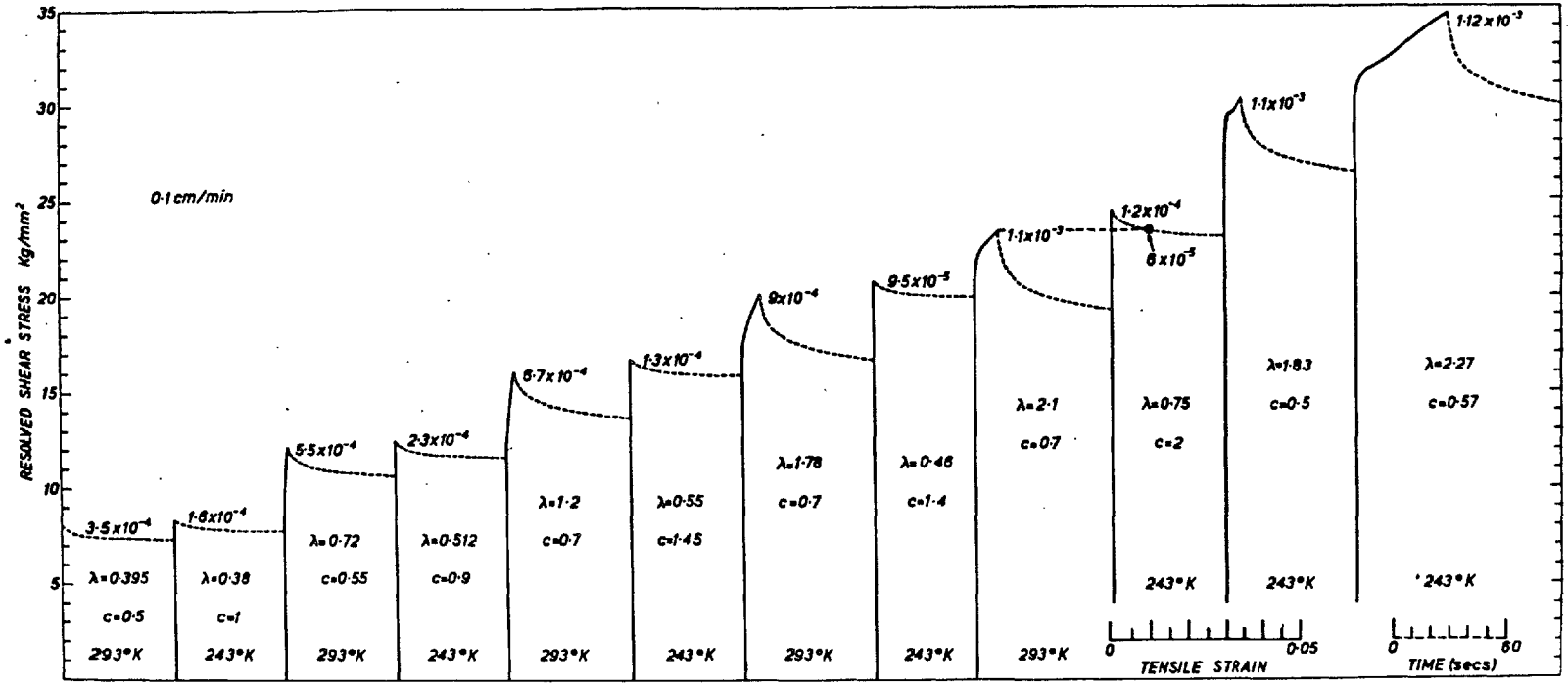

Figure 6.14. Results of a temperature cycling and relaxation test for a crystal with ⟨100⟩ orientation. Values of the strain rate are given in sec^{-1}, values of λ in kg/mm^2, and values of c in sec.

at the low temperature, and a conventional temperature cycling test was thus conducted. The relaxation parameters λ and c, and the plastic strain rates at the points chosen for relaxation are indicated in Figure 6.14. The test illustrated in this figure is also similar to a creep test, since the variation of the plastic strain rate produced by a change in temperature at a constant stress can be measured.

It is interesting to observe that the strain rate sensitivity, λ , at a constant stress, is a function of the temperature and that the ratio $\lambda_{293^{\circ}K}/\lambda_{243^{\circ}K} \simeq 3$ is not equal to the ratio of the temperatures, 293/243 = 1.2. This means that the activation volume, $w = 2.3\ k\ T/\lambda$, at constant stress, varies with the temperature.

The values of λ obtained from this experiment are plotted in Figure 6.11. In this figure it can be seen that λ is not a function of the applied stress and temperature alone, but depends also on the history of the crystal and on whether the specimen is being deformed in the 'micro-strain' region or in the 'flow' region.

Figure 6.15. shows the results of a similar temperature cycling experiment performed with a crystal with the tensile axis orientated in the $\langle 110 \rangle$ direction. The values of the relaxation parameters and

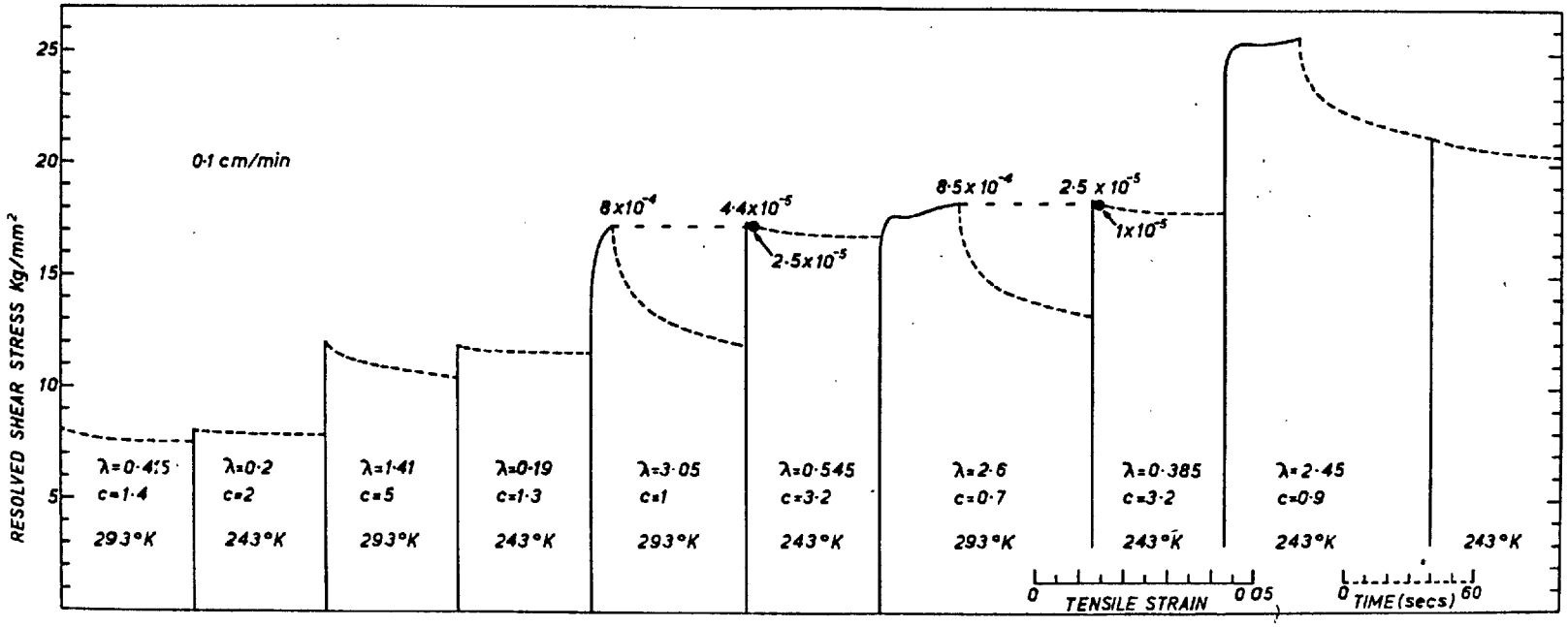

Figure 6.15. Results of a temperature cycling and relaxation test for a crystal with ⟨110⟩ orientation. Values of the strain rate are given in sec^{-1}, values of λ in kg/mm^2, and values of c in sec.

plastic strain rates are also given in the figure. The observations to be made here are similar to those made with reference to the test of Figure 6.14. The activation volume at constant stress is a function of the temperature, because the ratio $\lambda_{293^{\circ}K}/\lambda_{243^{\circ}K} \simeq 6$ is not equal to the ratio of the temperatures 293/243 = 1.2. The values of λ obtained from this test are plotted in Figure 6.10. In this case, the strain rate sensitivity is a function of the stress and temperature alone; it is independent of the history of the crystal. In fact, all the values of λ obtained at 293°K fall on a unique curve. Also, all the values of λ obtained at 243°K fall on a single curve, irrespective of both the way in which the stress is reached, and of the actual strain rate at which the specimen deforms, and independent of any previous straining at other temperatures.

6.6.1. Determination of the Relaxed Flow Stress During Temperature Cycling

Figure 6.16. shows the results of a temperature cycling test, between 293°K and 243°K, conducted with a crystal whose tensile axis is orientated in the ⟨100⟩ direction. The relaxed flow stress was measured during this test at each one of the temperatures involved. The results of Figure 6.16. show that when

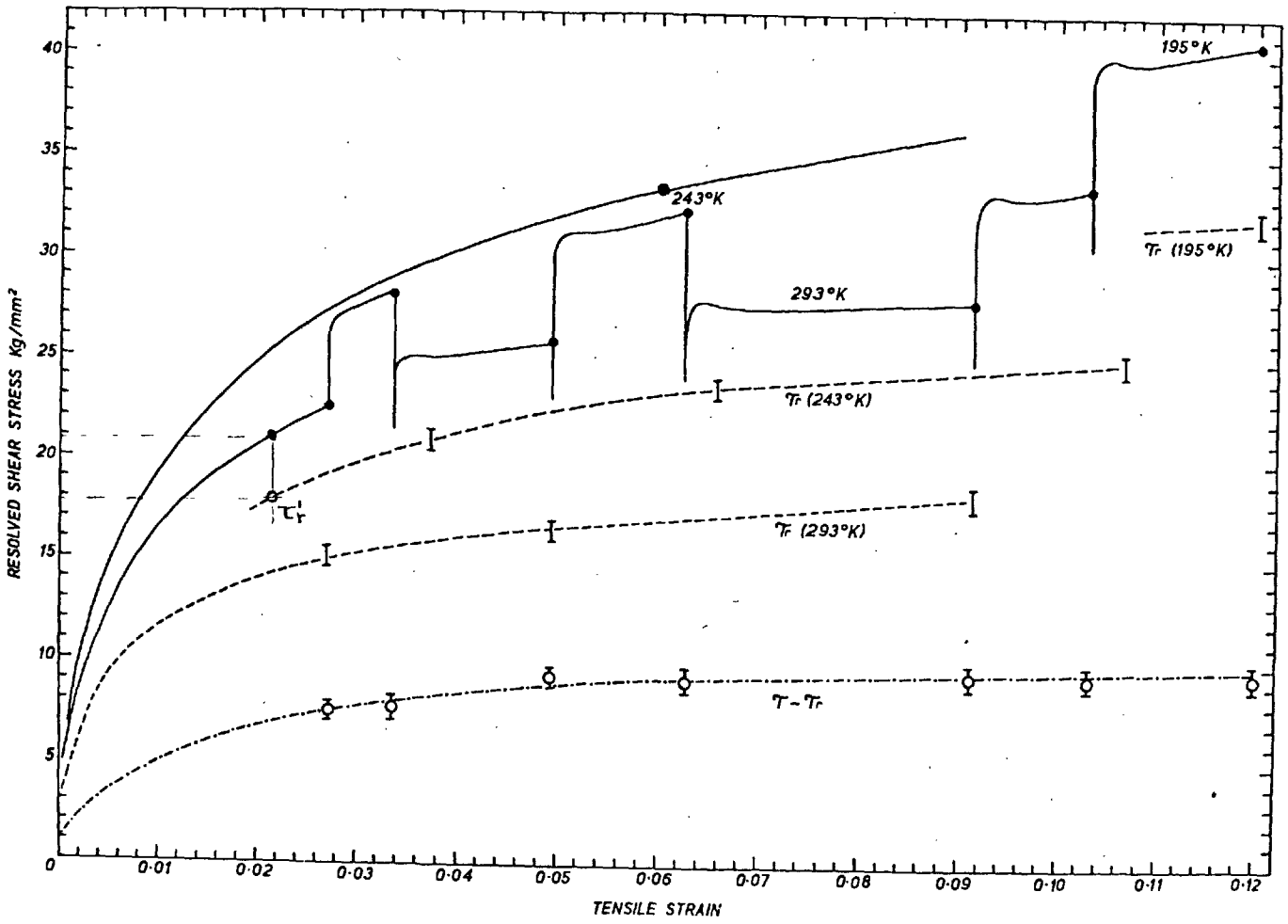

Figure 6.16. The effect of strain and temperature on the magnitude of τ, τ_r, and $(\tau - \tau_r)$ for a crystal with a ⟨100⟩ orientation.

the temperature is lowered τ_r increases, and that by raising the temperature to its original reference value, τ_r decreases. The variation of τ_r with temperature is reversible, and is equal to the variation of the applied stress, τ, with temperature. The difference $\tau - \tau_r$ remains constant and its value at a given strain is equal to that obtained during the continuous straining of the crystal at a constant temperature of 293°K or 243°K. (cf. Figures 6.4. and 6.13(a)).

The stress-strain curve of Figure 6.13(a) is also plotted on Figure 6.16. to show that the straining at 293°K during the temperature cycling test produces an irreversible dynamic recovery (Cottrell and Stokes 1955) in the crystal. In fact the stress necessary to deform the specimen to a given strain is lower for the specimen that is temperature cycled than for the crystal which is deformed constantly at the same temperature. It is also evident that this difference in stress is equal to the difference in the relaxed stress τ_r.

For the crystal deformed at constant temperature, the strain rate sensitivity at a stress $\tau = 33.3$ kg/mm^2 is $\lambda = 2.15$ kg/mm^2, (see Figure 6.11.). For the crystal that is subjected to temperature cycling λ has a value of 2.25 kg/mm^2 at the stress $\tau = 33.5$ kg/mm^2.

This observation suggests that λ is a function of the stress, but independent of strain.

Figure 6.16. also shows a final temperature change from 243°K to 195°K. The variation of the flow stress corresponding to this decrease in temperature is equal to the variation of τ_r. The difference $\tau - \tau_r$ remains constant and approximately equal to 10 kg/mm^2.

A temperature cycling experiment between 195°K and 153°K was carried out with a crystal with its tensile axis orientated in the ⟨110⟩ direction. The results of this test are shown in Figure 6.17. The specimen was strained at the initial temperature of 243°K and the relaxed flow stress was determined at various strains. After a tensile strain of 0.044 the temperature was decreased to 153°K, and the relaxed flow stress was measured without any further straining, that is to say, at the same strain of 0.044. The value of τ_r was found to increase by 5.6 kg/mm^2. This increment was equal, within the errors of the measurement, to the increase experienced by the applied stress when the crystal was subsequently strained at the low temperature. The difference $\tau - \tau_r$ remained constant after the proportional limit, and its value, is the same as that for the crystals deformed at 293°K (cf. Figure 6.3.).

Figure 6.18. shows the results of a temperature

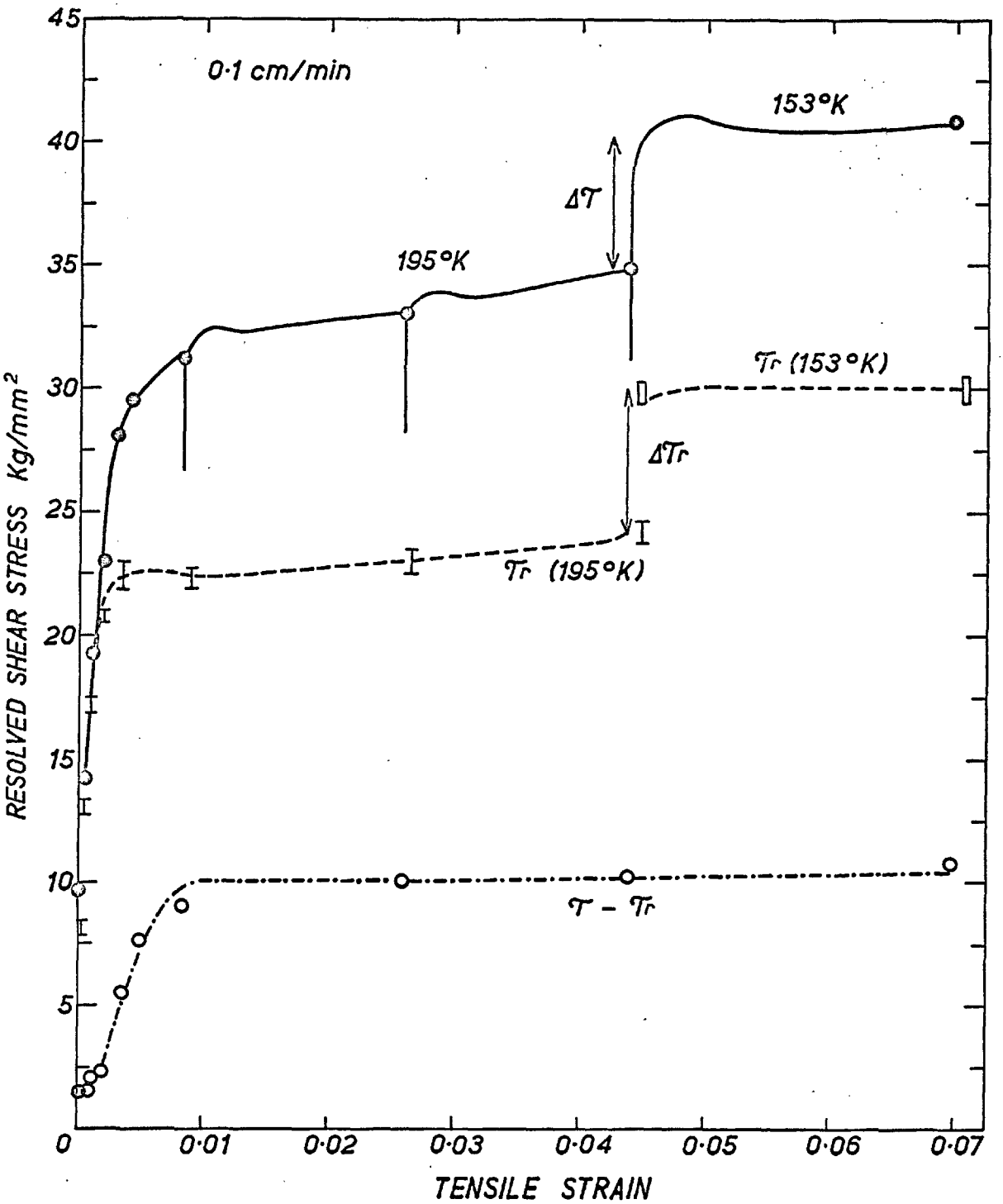

Figure 6.17. The effect of strain and temperature on the magnitude of τ, τ_r, and $(\tau - \tau_r)$ for a crystal with the tensile axis in the $\langle 110 \rangle$ direction.

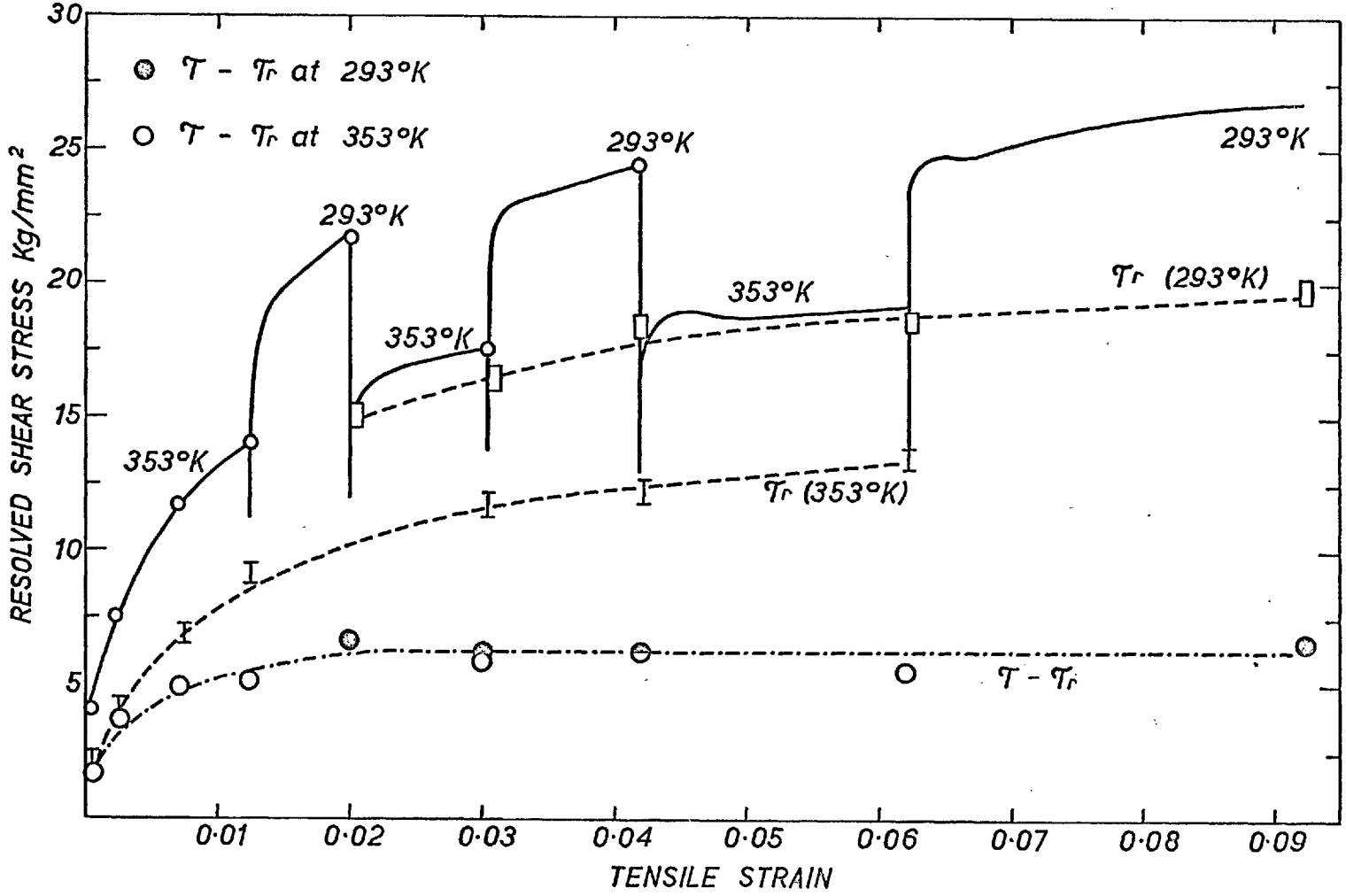

Figure 6.18. The effect of strain and temperature on the magnitude of τ, τ_r, and $(\tau - \tau_r)$ for a crystal with the tensile axis in the $\langle 100 \rangle$ direction.

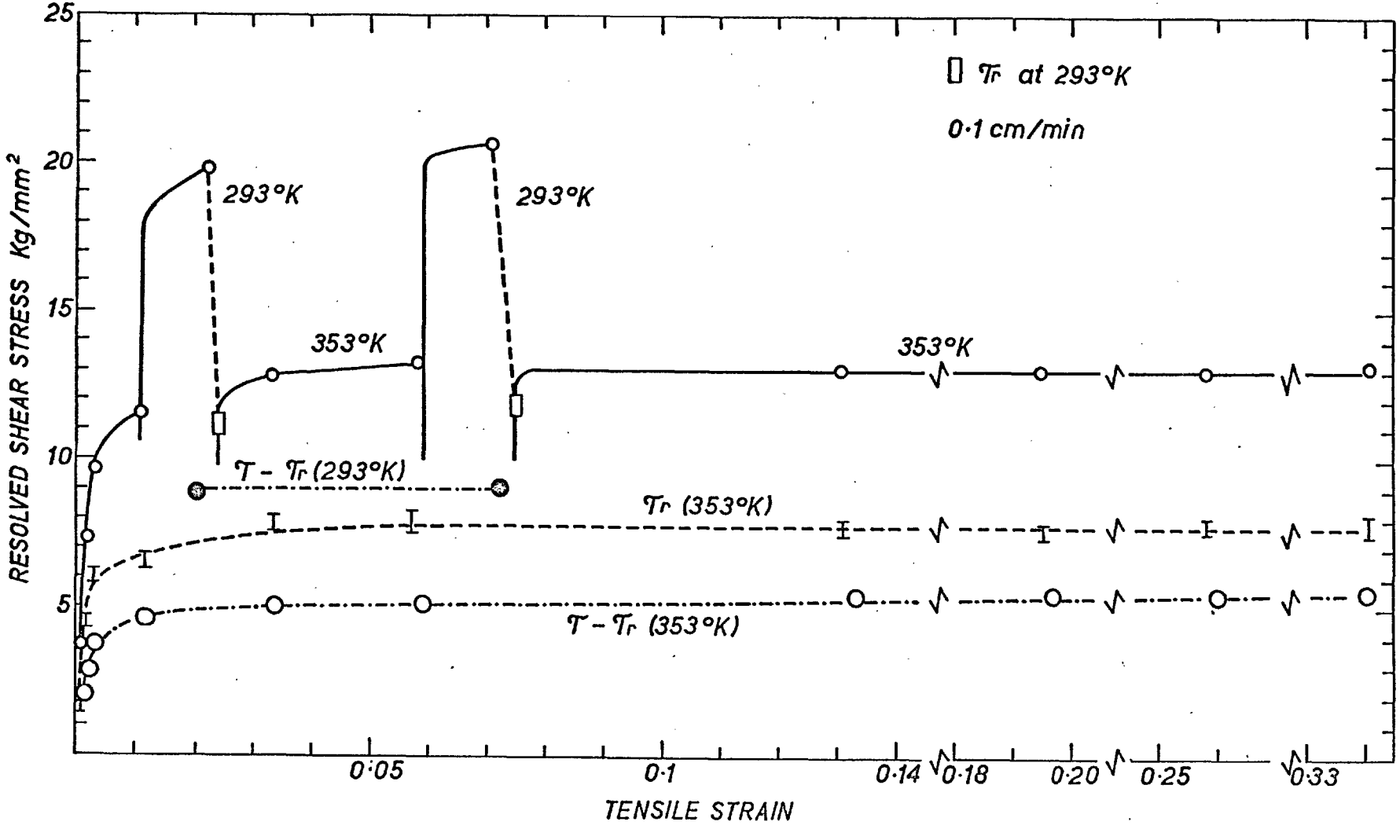

Figure 6.19. The effect of strain and temperature on the magnitude of τ, τ_r, and $(\tau - \tau_r)$ for a crystal with the tensile axis in the ⟨110⟩ direction.

cycling experiment between 353°K and 293°K carried out with crystals whose tensile axis is orientated in the ⟨100⟩ direction. It can be observed that the reversible variation of applied stress with temperature is almost equal to the variation of τ_r. However, the difference $\tau - \tau_r$ is in this case smaller than that obtained when the crystals are continuously deformed at 293°K. (cf. Figure 6.4.).

The results of a temperature cycling test between 353 and 293°K performed with a crystal with a ⟨110⟩ orientation are shown in Figure 6.19. As a result of the change in temperature there is a variation in both τ_r and $\tau - \tau_r$. The difference $\tau - \tau_r$ at 293°K is 9 kg/mm^2, in fact slightly smaller than in the case of continuous deformation at the same temperature.

Figures 6.20. and 6.21. show the results of two temperature cycling tests between 413°K and 343°K conducted with crystals with ⟨110⟩ and ⟨100⟩ orientations respectively. It can be observed that both the relaxed flow stress τ_r and the difference $\tau - \tau_r$ are variable and reversible with temperature. After a strain of about 0.20 the difference $\tau - \tau_r$ decreases, and it seems important to notice that there is a connection between the decrease of $\tau - \tau_r$ and a decrease in the strain rate sensitivity. (See Figures 6.10. and 6.11., where the values of λ obtained during

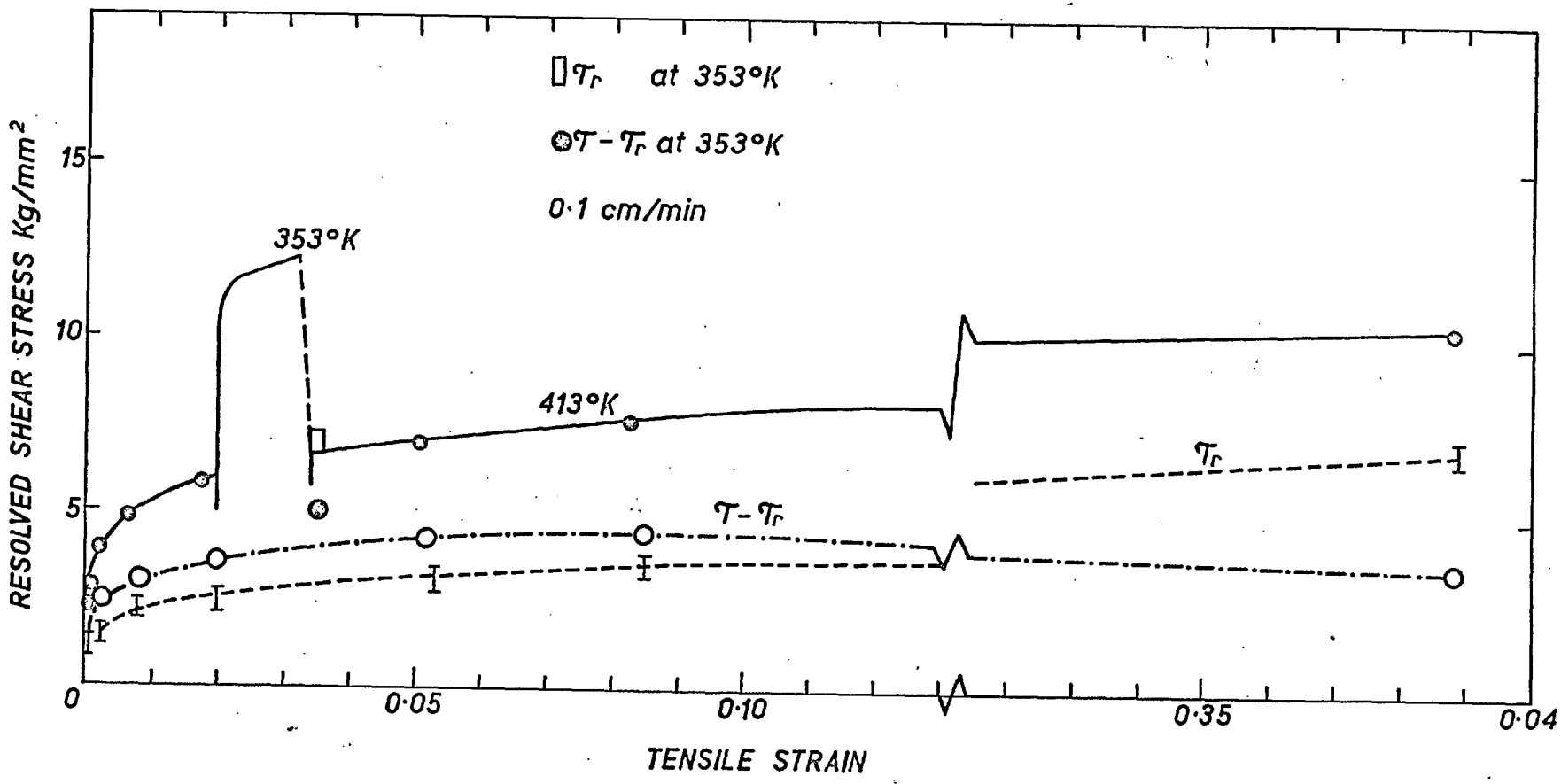

Figure 6.20. The effect of strain and temperature on the magnitude of τ, τ_r, and $(\tau - \tau_r)$ for a crystal with the tensile axis in the ⟨110⟩ direction.

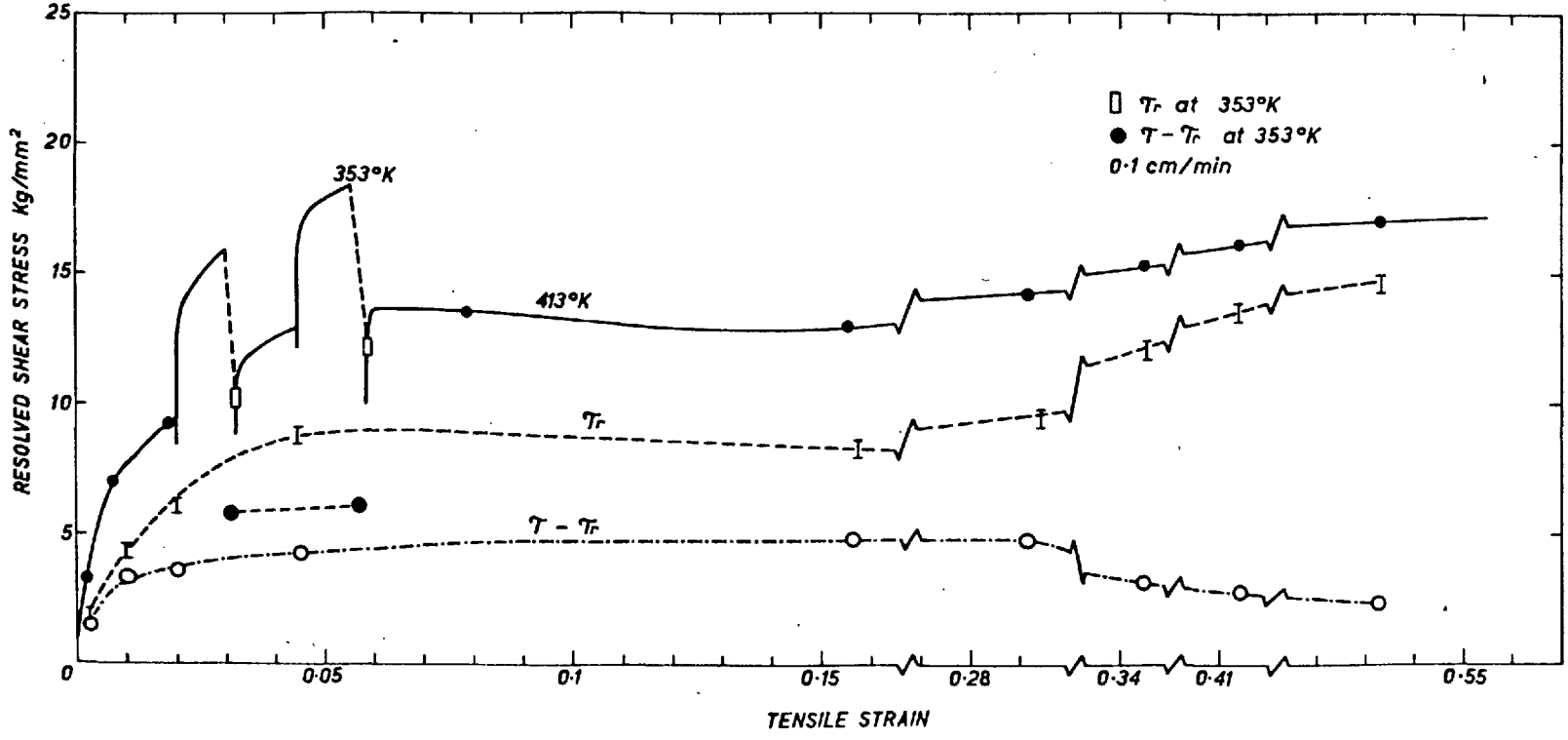

Figure 6.21. The effect of strain and temperature on the magnitude of τ, τ_r, and $(\tau - \tau_r)$ for a crystal with a ⟨100⟩ orientation.

the tests shown in Figures 6.20. and 6.21. are plotted).

6.6.2. Summary of Results of the Temperature Cycling Experiments

The results obtained during the temperature cycling tests conducted with crystals with ⟨110⟩ and ⟨100⟩ orientation are summarised in Tables 6.1. and 6.2. These tables show the variation of the flow stress with temperature, at constant strain rate, and the effedt of temperature on the plastic strain rate when the applied stress is constant.

Figure 6.22. shows the effect of temperature on both the flow stress, τ, and the relaxed flow stress, τ_r, at 2% strain, for crystals with ⟨110⟩ orientation.

Figure 6.23. shows the effect of temperature on both the flow stress and the relaxed flow stress, at the U.T.S., for crystals with ⟨100⟩ orientation.

TABLE 6.1.

Summary of results of the temperature cycling tests for crystals with ⟨110⟩ orientation.

ϵ	τ	Basic Temperature T_1	$\Delta T = T_1 - T_2$	$\Delta\tau$	$\frac{\Delta\tau}{\Delta T}$	$\dot{\epsilon}_1/\dot{\epsilon}_2$	$\ln \dot{\epsilon}_1/\dot{\epsilon}_2$
0.02	6.0	413	60	5.40	0.090	1	0
0.01	11.5	353	60	7.02	0.117	1	0
0.06	13.2	353	60	7.20	0.118	1	0
0.026	18.3	293	50	7.03	0.14	1	0
0.026	18.31	293	50	0	0	86	4.45
0.044	34.0	195	42	5.06	0.12	1	0

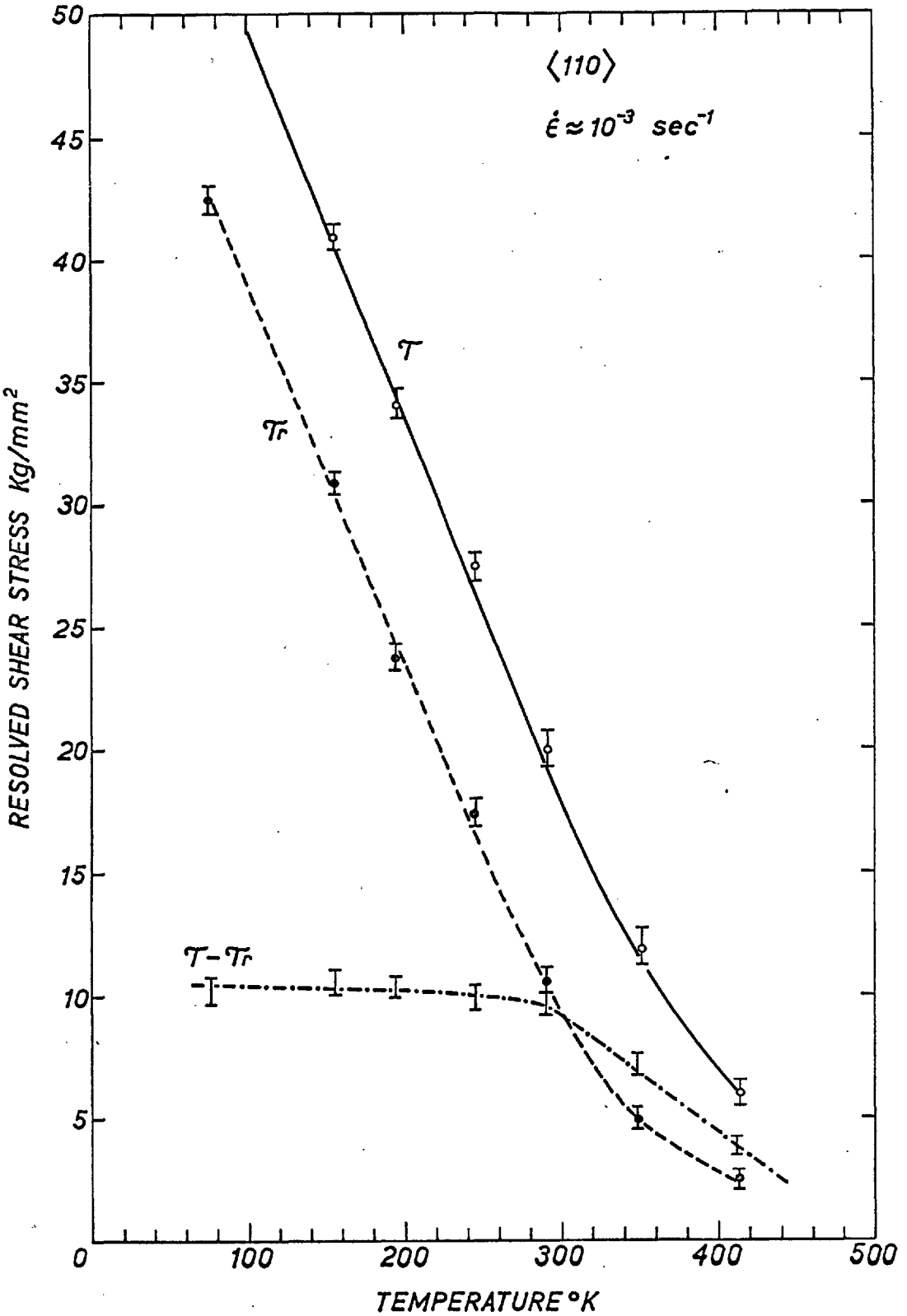

Figure 6.22. The effect of temperature on τ, and τ_r at 2% strain for crystals with ⟨110⟩ orientation.

TABLE 6.2.

Summary of results of the temperature cycling tests for crystals with ⟨100⟩ orientation.

ϵ	τ	Basic Temperature T_1	$\Delta T = T_1 - T_2$	$\Delta\tau$	$\frac{\Delta\tau}{\Delta T}$	$\frac{\dot{\epsilon}_1}{\dot{\epsilon}_2}$	$\ln \frac{\dot{\epsilon}_1}{\dot{\epsilon}_2}$
0.02	9.20	413	60	4.80	0.08	1	0
0.045	12.90	413	60	4.40	0.075	1	0
0.015	14.00		60	5.16	0.086	1	0
0.033	17.65	353	60	5.27	0.088	1	0
0.065	19.1		60	5.1	0.085	1	0
0.027	22.57		50	4.38	0.0875	1	0
0.049	25.7	293	50	4.40	0.088	1	0
0.091	27.8		50	4.6	0.092	1	0
0.035	23.27	293	50	4.7	0.094	1	0
0.035	23.27	293	50	0	0	200	5.3
0.103	33.45	243	48	5.9	0.123	1	0

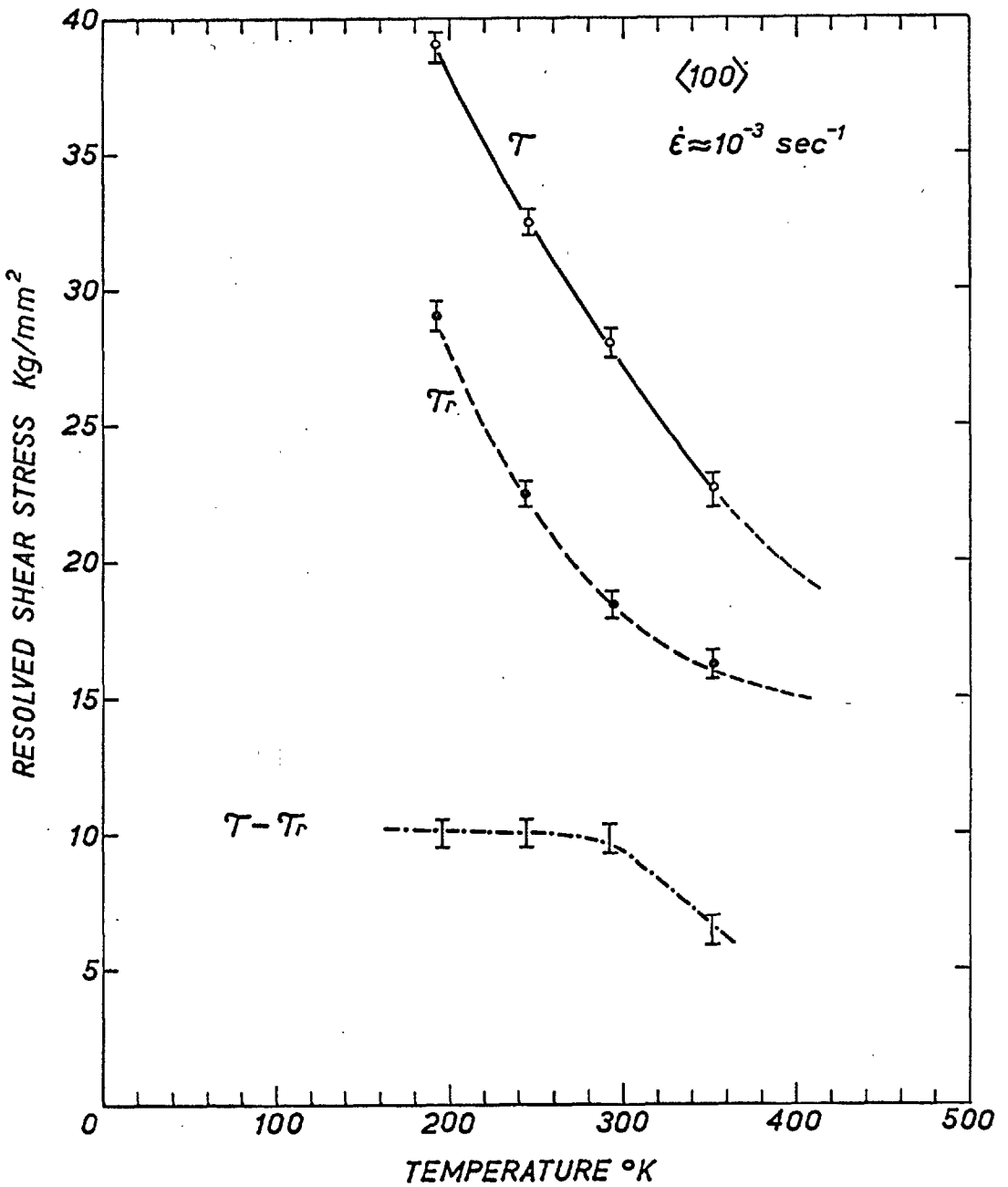

Figure 6.23. The effect of temperature on τ, and τ_r at the U.T.S. for crystals with ⟨100⟩ orientation.

6.7. Discussion

6.7.1. The Relaxed Flow Stress

As a consequence of the interpretation which was given to the relaxation phenomenon it was tentatively assumed in Section 6.3.2. that the long range internal stress, τ_μ, could be determined by measuring the value of the relaxed flow stress. Now, in view of the results described in the subsequent sections serious doubt arises as to the validity of such an assumption. The long range internal stress should vary with temperature through the variation of the shear modulus only; however, the experimental results show that the relaxed flow stress has a much larger temperature dependence and that the difference $\tau - \tau_r$ is sometimes independent of the temperature.

In order to understand the nature of the relaxed flow stress it is essential to realise that when the stress τ_r is applied to the crystals they may still deform at a finite strain rate. The fact that no relaxation is observed during a period of one or two minutes indicates only that the plastic strain rate is too small to produce any detectable deformation in that interval of time.

An upper limit of the plastic strain rate $\dot{\epsilon}_r$ at which the crystals deform under the stress τ_r can be obtained by an extrapolation of the relaxation

plot obtained at a higher stress. If the plot of τ versus log (t+c) is extrapolated to the stress τ_r (assuming that λ remains constant throughout) a value of $(t+c)_r$ is obtained. Then the plastic strain rate at the stress τ_r is calculated by substitution of λ and $(t+c)_r$ in Equation (13) of the Appendix. Since the extrapolation is made assuming that λ is constant an upper limit for τ_r is actually obtained. By this method it has been found that $\dot{\epsilon}_r$ must be smaller than 10^{-7} sec^{-1}.

This limit can also be estimated from the sensitivity of the load recording device. Since the variation in load can be measured with an accuracy of only 0.1 kg. (Section 4.2.2.), a deformation of the specimen smaller than 10^{-4} mm will not produce any detectable relaxation. For a specimen with a length of 18 mm, the strain rate necessary to produce a deformation smaller than 10^{-4}mm in the interval of one minute will be:

$$\dot{\epsilon}_r < \frac{10^{-4}}{60 \times 18} < 10^{-7} \text{ sec}^{-1}$$

The Variation of τ_r with Temperature

Since the deformation of the crystals at strain rates smaller than 10^{-7} sec^{-1} may still be controlled by a thermally activated process, it should not be surprising to find that the relaxed flow stress is

temperature dependent. An expression for the effective relaxed flow stress, $\tau_r^* = \tau_r - \tau_\mu$, may be obtained from Equation 1.9.(Alefeld 1962)

$$\tau_r - \tau_\mu = \frac{U}{w} - \frac{kT}{w} \ln (\nu/\dot{\gamma}_r) + \frac{kT}{w} \ln \tfrac{1}{2} \left[1 + \sqrt{1 + \left(\frac{2\nu \exp -(U/kT)}{\dot{\gamma}_r} \right)^2} \right] \qquad (6.3.)$$

Then assuming the activation volume remains constant if the temperature is changed by ΔT, the variation in stress necessary to maintain the same strain rate, $\dot{\gamma}_r$, is:

$$\Delta \tau_r = - \frac{k \Delta T}{w} \ln (\nu/\dot{\gamma}_r) + \text{correction term} \qquad (6.4.)$$

where the correction term arises from the third term of the right hand side of Equation 6.3.

The variation of the relaxed flow stress predicted by Equation 6.4. may be large at relatively low temperatures when the correction term is negligible, i.e. when $\dot{\gamma}_r > 2\nu \exp -(U/kT)$. This variation will become smaller at high temperatures, when the correction term may be significant.

Although this result seems to be in agreement with the experimental observations, a major difficulty in the interpretation of the relaxed flow stress arises when one tries to determine the magnitude of the difference $\tau_r - \tau_\mu$.

The Magnitude of the Effective Relaxed Flow Stress

Equation 6.3. is of very little practical use for the determination of the effective relaxed flow stress, because neither the value of $\dot{\gamma}_r$ nor the activation parameters of the mechanism which determines τ_r are known. However, the experimental results described in Section 6.6. provide good reasons to believe that the effective relaxed flow stress is very small.

For example, Figure 6.15. shows that during the deformation of the crystals at 243°K, the strain rate sensitivity, λ , increases from 0.4 kg/mm^2 to 2.4 kg/mm^2 when the stress is increased from 18.5 to 25.8 kg/mm^2. It has also been found in the course of other experiments that λ, at any given strain, decreases very rapidly with the applied stress, and that it assumes a very small value when the stress approaches τ_r. This means that the activation volume increases by at least a factor of 6 as the stress decreases towards τ_r, and such a large variation of the activation volume can only be explained if the effective stress is assumed to be very small. In order to clarify this point the magnitude of τ_r^* will now be calculated from the relationship between the activation volume and the effective stress given by Equation 1.17.

Although the apparent activation volume, w' (in this case the activation volume at the stress τ_r) cannot be experimentally measured, it is sufficient to realise that the strain rate sensitivity at the stress τ_r, at 243°K, is smaller than 0.4 kg/mm^2.

Therefore the apparent activation volume w' must be:

$$w' = 2.3\ kT/\lambda > 2.7 \times 10^{-21}\ cm^3.$$

On the other hand the maximum value of λ at this temperature is 2.5 kg/mm^2, and hence the activation volume w is:

$$w = 2.3\ kT/\lambda = 4.3 \times 10^{-22}\ cm^3.$$

From Equation 1.17. it follows that:

$$2.7 \times 10^{-21} < 4.3 \times 10^{-22} \coth(w\,\tau_r^*/kT)$$

and therefore:

$$\coth(w\,\tau_r^*/kT) > 6\ ,\ \text{and}\ \ w\,\tau_r^*/kT < 0.17$$

Hence:

$$\tau_r^* < 1.0\ kg/mm^2$$

At the temperature of 293°K the maximum value of λ is 2.8 kg/mm^2, and if the strain rate sensitivity at the stress τ_r is assumed to be 0.4 kg/mm^2, as before, one obtains at this temperature:

$$\coth(w\,\tau_r^*/kT) > 7,\ \text{and}\ \ w\,\tau_r^*/kT < 0.14$$

Therefore:

$$\tau_r^* < 0.9 \text{ kg/mm}^2.$$

If there is a genuine variation of the activation volume with stress, Equation 1.17. should not be used, for then it is necessary to know the real variation of w with τ^*. The relationship between w and τ^*/τ_o^* obtained by Dorn and Rajnak (1964) (see Figure 6.24.) might be used in this case. If the activation volume has a certain value, W, when the ratio τ^*/τ_o^* is about 0.5.(for example τ_o^* = 50 kg/mm^2, and τ^* = 25 kg/mm^2 are conservative figures) then the activation volume could only be six times larger than W providing that $\tau_r^*/\tau_o^* = 0$, that is to say, only when the effective relaxed flow stress is practically zero.

If the variation of the activation volume with the stress is due to both a real and an apparent effect, then one should take smaller values of w in the above calculations. If the values of w used before are divided by two one obtains:

At 243°K

$$\coth (w\tau_r^*/kT) > 3, \text{ and } \tau_r^* < 1 \text{ kg/mm}^2,$$

and at 293°K

$$\coth (w\tau_r^*/kT) > 3.5, \text{ and } \tau_r^* < 1 \text{ kg/mm}^2.$$

These calculations show that the effective relaxed

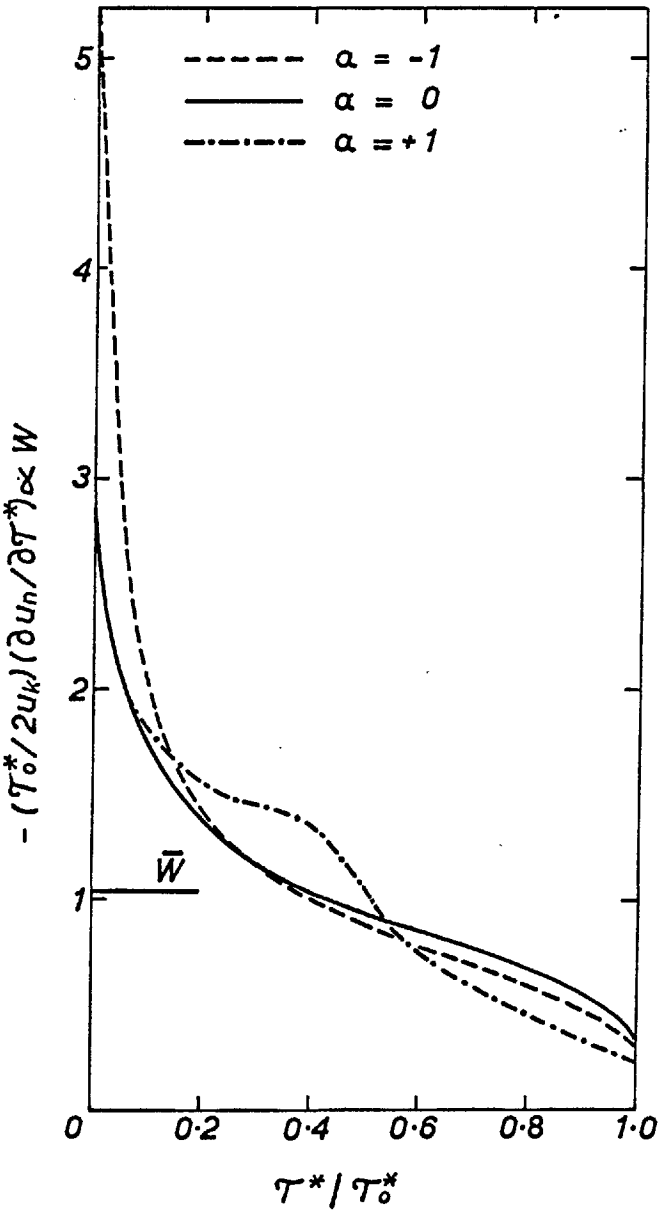

Figure 6.24. Variation of the activation volume with the effective stress after Dorn and Rajnak (1964).

flow stress, is possibly very small and that it does not vary with the temperature.

After careful consideration of the implications of these results it was believed that a consistent interpretation could be given in terms of the existence of two thermally activated mechanisms.

Interpretation of the Results

The possibility that the deformation of molybdenum single crystals could be controlled by more than one thermally activated process was already suggested in Chapter 5. The same view will now be adopted here, and an attempt will be made to interpret the nature of the relaxed flow stress accordingly.

If one considers the simplest case of the deformation being controlled by two simultaneous thermally activated mechanisms, the value of the relaxed flow stress might be controlled by that with the largest activation energy. Physically this would mean that at the stress τ_r the mobility of the dislocations is practically nil, because the stress is not high enough for them to overcome the most difficult obstacles (although it might be sufficiently high to overcome the easy ones if the dislocations were mobile). As the stress increases above τ_r the difficult obstacles could become surmounted at an increasing rate, and then the movement of the

dislocations would be controlled by both mechanisms.

According to this interpretation, the mechanism that would determine the magnitude of the relaxed flow stress should meet the following requirements:

a) It should have a large activation energy.

b) It should involve the overcoming of discrete obstacles in order to account for the variation of τ_r with strain.

c) It should be thermally activated at temperatures as low as $77^{\circ}K$ (and possibly $4.2^{\circ}K$). Therefore the activation energy, U, the activation volume, w, and the relaxed flow stress, τ_r^*, should satisfy the relationship:

$$w\,\tau_r^* < U \qquad (6.5.)$$

even at very low temperatures.

The non-conservative movement of jogs in screw dislocations is the mechanism that was proposed in Chapter 5 to explain the effect of the orientation on the deformation of single crystals, and it is the one that should be favoured if this interpretation of the relaxed flow stress is to be accepted. This mechanism obviously satisfies the requirements (a) and (b), and a simple calculation will show that it is also consistent with the requirement (c). Equation 6.5. can be written in terms of the mean jog spacing, $\bar{l}$, and for very low temperatures:

$$l \simeq U/b^2 \, \tau_r^* \qquad (6.6.)$$

and taking U = 3.6 eV and $\tau_r^* = 50$ kg/mm^2, one obtains for the mean jog spacing, $l \simeq 50$ b, which is a very reasonable value (Schoeck 1961).

6.7.2. The Non-conservative Movement of Jogs and the Peierls Stress

The idea that the deformation may be controlled by more than one thermally activated process will now be considered in more detail.

It will be assumed that the overall rate of flow is controlled by the mobility of the screw dislocations (Gilman 1960)+, and that these can only move by dragging the jogs non-conservatively, as explained in Section 5.6.4. If at the same time a strong lattice friction opposes the movement of the dislocation segments lying free between the jogs, the stress, τ^* necessary to move the jogged screw dislocations at a steady macroscopic rate may be resolved into two components, τ_j^*, and τ_p^*. This can be explained as follows:

The component τ_j^* is the stress necessary to bow out the dislocation segments lying free between the

---

+This assumption is justified by the fact that the mobility of the screw dislocations is much smaller than that of the edge dislocations (Lawley and Gaigher 1964).

jogs. The magnitude of the stress τ_j^* is determined by the force, F, needed to move the jogs at a certain rate, and by the jog spacing, l, and it is given by:

$$\tau_j^* = Fb/w = F/bl$$

The component τ_p^* is equal to the lattice friction that the bowed dislocation segments must overcome in order to be able to move at the same speed as the jogs.

Although this argument is based on a very idealised model, it serves well the purpose illustrating physically the fact that the effective stress τ^* can be expressed as:

$$\tau^* = \tau_j^* + \tau_p^*$$

The same result could be obtained from a consideration of the energy necessary to move a jogged screw dislocation over a certain distance in a given time.

Now it is possible to see that from the mean jog spacing obtained before ($l \simeq 50b$), and from the stress observed at 4.2°K (τ_r = 50 kg/mm^2) a value of the right order of magnitude is obtained for the line tension of the dislocation line. Since at 4.2°K the non-conservative movement of jogs is still a thermally activated process, the jog spacing, l, should be smaller than twice the radius of curvature of the bowed dislocation lines, r. Thus:

$$l \simeq 50b < 2r$$

The line tension of a bowed dislocation line is given by (Cottrell 1953):

$$T = \tau_r br$$

Therefore:

$$T > 1.3 \times 10^{11} b^2 \text{ dyne/cm}^2$$

On the other hand, T can also be calculated from (Cottrell 1953):

$$T \simeq 0.5 \mu b^2$$

and with $\mu \geqslant 10^{12} \text{dyne/cm}^2$ (Bolef and Klerk 1962) one obtains:

$$T \geqslant 5 \times 10^{11} b^2 \text{ dyne/cm}^2$$

and this is in agreement with the value of T obtained before.

<u>The Variation of τ_j^* and τ_p^* with the Strain Rate</u>

The magnitude of τ_j^* and τ_p^*, and its variation with the temperature and the strain rate, are the points that must now be investigated.

In order to simplify the argument, the effect of the conservative movement of jogs will not be considered, and instead it will be assumed that an equilibrium distribution of jogs, with a mean spacing l exists in the screw dislocations. The contribution of the interstitial impurity atoms to the mobility of the jogs and to the lattice friction will also be neglected. For the moment, the lattice friction

stress will be considered to be due solely to the Peierls stress.

For a crystal to deform at a small strain rate, of the order of 10^{-7} sec^{-1} a stress, τ_r^*, (which at low temperatures may be very large) is necessary. If the activation energy for the non-conservative movement of jogs is large compared with that for the Peierls mechanism, it is possible that (mainly at low temperatures) the greater part of the stress τ_r^* will be needed to move the jogs non-conservatively, and only a very small part of τ_r^* is required to overcome the Peierls barrier. If the stress τ_p^* is very small, the activation volume, w_p, for the Peierls mechanism will be very large, namely of the order of $50b^3$ (Dorn and Rajnak, 1964). This activation volume is of the same order of that for the non-conservative movement of jogs, w_j, (Equation 6.6. gives $w_j \simeq 50b^3$). It is not surprising, therefore, that at the stress τ_r a large activation volume ($w' = 2.7 \times 10^{-21}$ $cm^3 \simeq 100b^3$) is obtained.

For the crystal to be deformed at a faster strain rate (e.g. $\dot{\epsilon} = 10^{-3}$ sec^{-1}) an effective stress τ^* is required. The stress necessary to move the jogs at this fast strain rate is not much greater than before, because the activation volume for this process is large, and practically constant at low temperatures.

The variation in stress with strain rate in this case is given by:

$$\Delta\tau_j^* = \frac{kT}{w_j}\,\Delta \ln \dot{\gamma}$$

and when the strain rate varies by a factor of 10^4 sec^{-1}, $\Delta\tau_j^*$ is approximately equal to T/100 kg/mm^2, for $T < 300^oK$. It is possible that at temperatures higher than 300^oK $\Delta\tau_j^*$ may be smaller than T/100 kg/mm^2, for when 'recovery' occurs (Section 5.6.8.) the equilibrium jog spacing may increase, and the activation volume may be greater than has previously been assumed.

However the stress needed to overcome the Peierls barrier must increase considerably with the strain rate, because the activation volume for this mechanism decreases rapidly with increasing stress. For this process the variation in stress with strain rate is given by:

$$\Delta \ln \dot{\gamma} = \frac{1}{kT}\int_{\tau}^{\tau+\Delta\tau} w_p(\tau_p^*)\, d\tau_p^* = \frac{\bar{w}_p(\tau_p^*)}{kT}\Delta\tau_p^*$$

where $\bar{w}_p(\tau_p^*)$ is the mean value of the activation volume. This value can be roughly estimated by graphical integration of the function $w_p(\tau^*/\tau_o^*)$, given in Figure 6.24. It is then found that when $\Delta\dot{\gamma} = 10^4$ sec^{-1} at 293^oK, $\Delta\tau_p^* = 9$ kg/mm^2.

Therefore when the crystal deforms at a

relatively high strain rate the lattice friction is relatively large, and this may be the reason why small values of w are then experimentally determined.

The Variation of τ_j^* and τ_p^* with Temperature

According to the model now being proposed the relaxed flow stress is approximately equal to the stress necessary to move the jogs non-conservatively, and the difference between the flow stress and the relaxed flow stress is approximately equal to the stress necessary to overcome the lattice friction. Thus:

$$\tau_r - \tau_\mu \simeq \tau_j^*, \text{ and } \tau - \tau_r \simeq \tau_p^*$$

The variation of τ_j^* and τ_p^* with the temperature may be obtained from the variation of τ_r and τ, (see Figures 6.22. and 6.23.).

The merit of the preceeding argument is not only that it gives a consistent interpretation of the relaxed flow stress, but also that it is in agreement with the explanation of the effect of the orientation proposed in Chapter 5. Furthermore a basis for analysing the various experimental results is now established, and in the following sections it will be shown that most of these results may be explained by the existence of the two thermally activated mechanisms discussed above.

6.7.3. The Magnitude of the Lattice Friction Stress

The experimental results reported in this chapter show that when the strain rate is of the order of 10^{-3} $sec.^{-1}$, and the temperature is higher than 293°K, both τ_j^* and τ_p^* vary with temperature. However, at temperatures lower than 293°K only τ_j^* is temperature dependent and τ_p^* has a value which is constant and equal to 10 kg/mm^2. This suggests that the overcoming of the lattice friction is almost temperature independent below 293°K, when the crystals are deformed at a strain rate $\simeq 10^{-3}$ sec^{-1}, and that the Peierls stress at 0°K in the crystals investigated would be of the order of 10 kg/mm^2.

Lawley and Gaigher (1964) using an extrapolation method obtained a value of about 10 kg/mm^2 for the friction stress of molybdenum single crystals of similar purity. They also found that the friction stress was almost constant at temperatures lower than 293°K. A similar result was also obtained by Kosscwsky and Brown (quoted by Lawley and Gaigher 1964).

It seems convenient now to summarise some of the implications of this result.

1) Below 293°K, and at strain rates of the order of 10^{-3} sec^{-1} (and possibly at lower strain rates as the temperature decreases below 293°K), the variation

of the flow stress with temperature is mostly due to the variation of τ_j^* (see Figure 6.22.).

2) At temperatures above 293°K and at strain rates of the order of 10^{-3} sec^{-1} (and possibly at higher strain rates as the temperature increases above 293°K), both the non-conservative movement of jogs and the overcoming of the lattice friction are thermally activated processes. Then the variation of the flow stress with temperature is due to a variation in both τ_j^* and τ_p^*, (Figure 6.22.).

3) The stress τ_p^* should not increase by increasing the strain rate above 10^{-3} sec^{-1}, at temperatures lower than 293°K. This conclusion seems to be supported by some results which are discussed in the next section.

6.7.4. The Strain Rate Sensitivity of the Stress

If the strain rate sensitivity of both the proportional limit and the yield stress obtained from Figure 6.1. is compared with the slope of the plot of τ versus $\log \dot{\epsilon}$ shown in Figure 5.40., good agreement is found to exist for the crystals deformed at strain rates within the range of 10^{-3} sec^{-1} to 5×10^{-5} sec^{-1} (cross-head speeds of 0.1 to 0.005 cm/min). The prameter λ has a maximum value of 2.8 kg/mm^2 when the strain rate is about 10^{-3} sec^{-1}. By increasing the strain rate from 10^{-3} sec^{-1} to

10^{-2} sec^{-1} the strain rate sensitivity decreases slightly, whilst both the proportional limit and yield stress remain constant (Figure 5.40.). Since the scatter involved in the determination of the proportional limit and the yield stress at the strain rate of 10^{-2} sec^{-1} has not been determined, it would be premature to draw any conclusion from this result.

However, it is important to realise that no increase in the value of τ_p^* should be expected as a result of increasing the strain rate from 10^{-3} to 10^{-2} sec^{-1}. This result seems to be in agreement with the fact that λ never becomes greater than 2.8 kg/mm^2.

Now the question arises of how strain rates faster than 10^{-3} sec^{-1} can be accommodated. Although it is possible to imagine that more dislocation segments may become mobile at the higher rates of strain, the way in which this occurs is a problem which demands further investigation.

6.7.5. The Variation of λ with Temperature and Stress

The effect of temperature on the strain rate sensitivity of the yield stress for crystals with $\langle 110 \rangle$ orientation is shown in Figure 6.25. The values of λ at the U.T.S. for crystals with $\langle 100 \rangle$ orientation have also been plotted as a function of

temperature in this figure. In both cases the strain rate sensitivity was measured at a strain rate of the order of 10^{-3} sec^{-1}.

The shape of the curves shown in Figure 6.25. is characteristic of all the b.c.c. metals (Basinsky and Christian 1960, Conrad and Frederick 1962, Mordike 1962, Sleeswyk and Helle 1963, Christian and Masters 1964), and Christian and Masters (1964) have pointed out that this type of dependence may be a consequence of the almost linear relationship which exists between λ/T and τ^*. They also indicated that the linear relationship between λ/T and τ^* could provide an argument in favour of the Peierls mechanism as the rate controlling process in the deformation of b.c.c. metals. Figure 6.26. shows that, in the case of molybdenum single crystals, a plot of λ/T against τ^* does not give a straight line, and this is by no means an exceptional result. Similar non-linear plots have also been obtained for other b.c.c. metals (Mordike 1962, Christian and Masters 1964). For example, the results of Christian and Masters for polycrystalline tantalum have been replotted in Figure 6.26. in order to show that the relation between λ/T and τ^* for this metal is similar to that obtained for the molybdenum single crystals.

In an attempt to rationalize the variation of

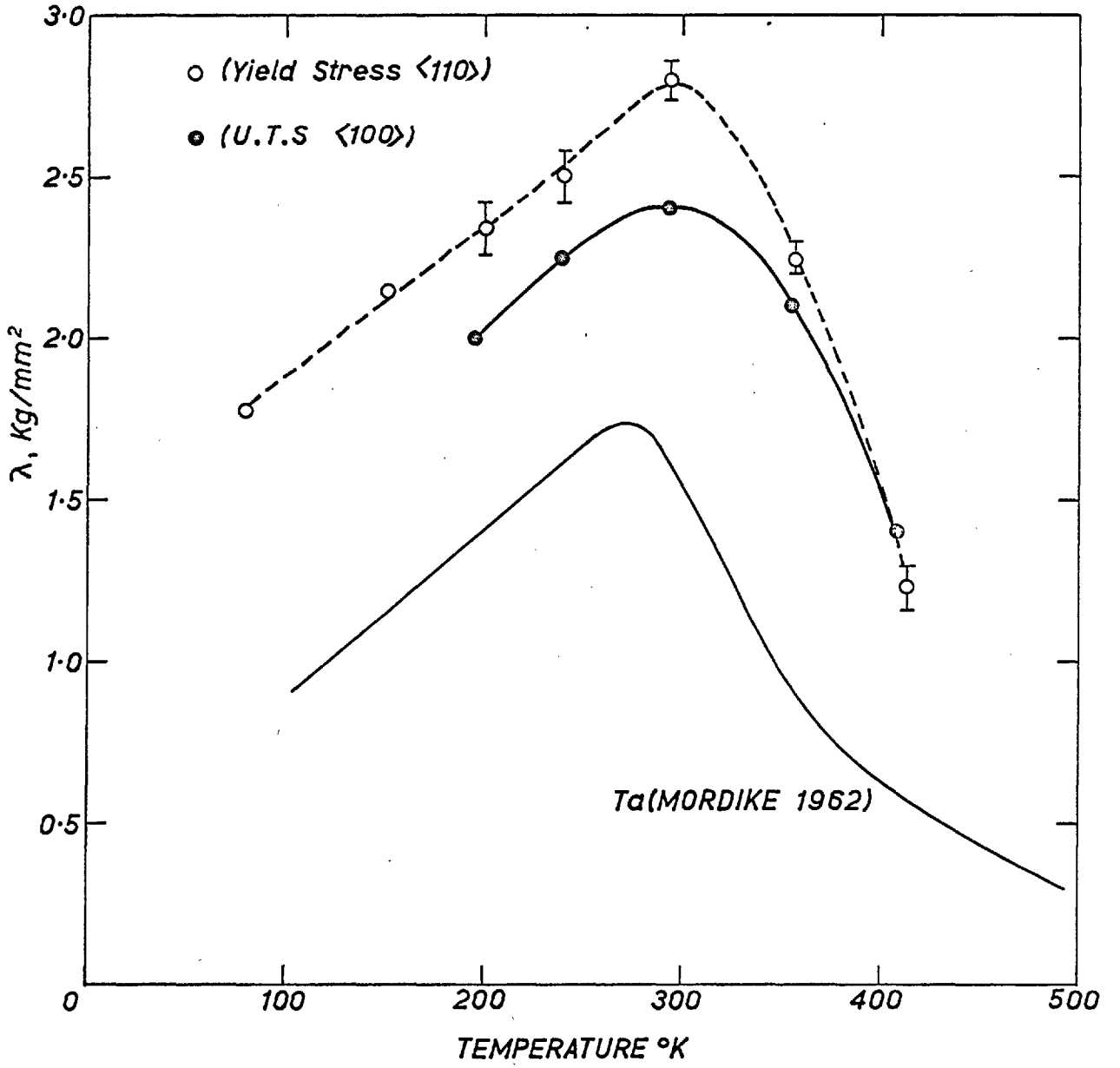

Figure 6. 25. The effect of temperature on the strain rate sensitivity of the stress for molybdenum single crystals, and tantalum single crystals (after Mordike 1962).

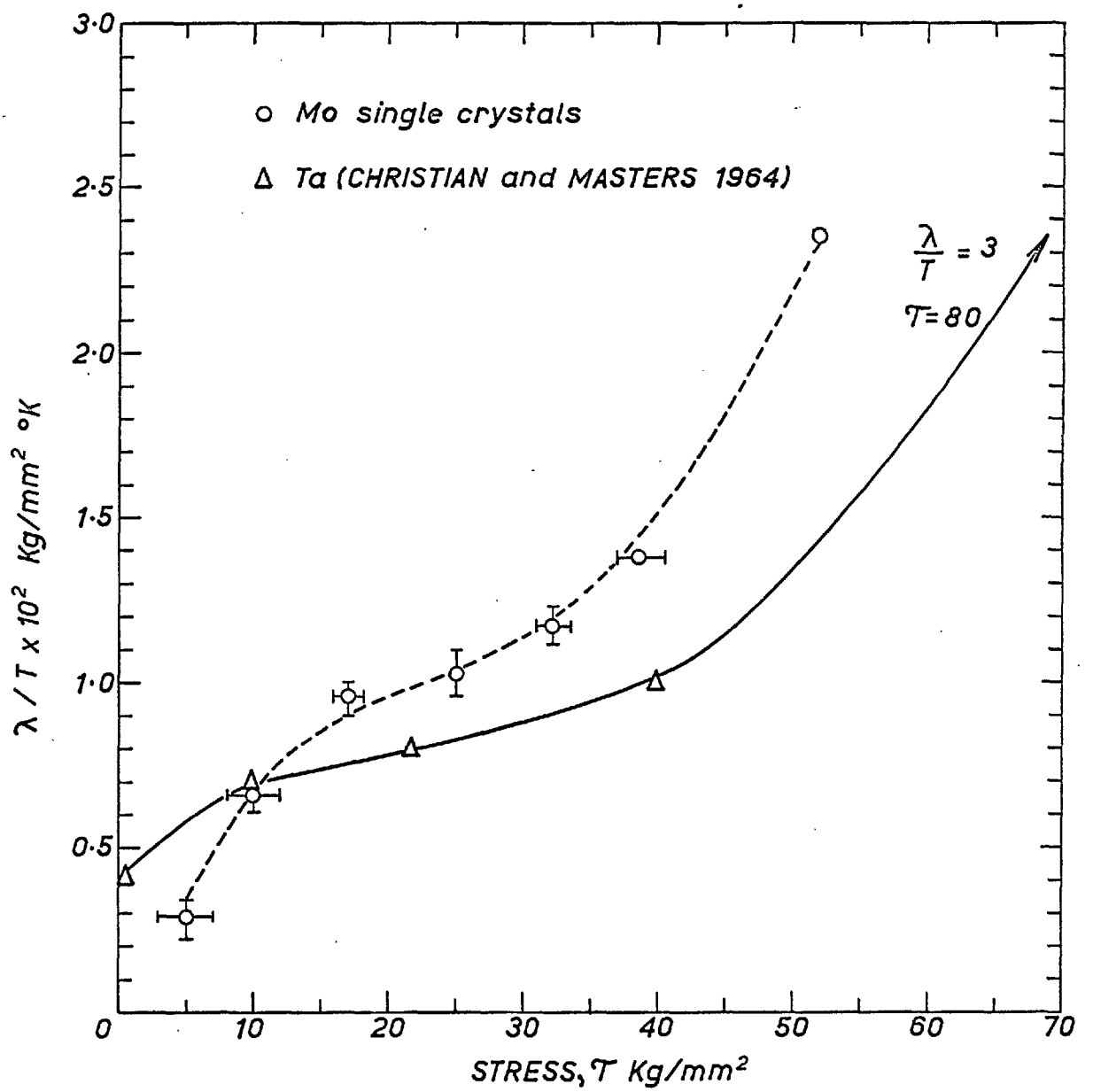

Figure 6.26. The variation of λ/T with the applied stress. The zero in the stress axis is chosen arbitrarily.

the strain rate sensitivity with stress, the values of λ/T, obtained at various temperatures for the two orientations investigated, have been plotted against $\tau - \tau_r$ in Figure 6.27. It can be observed from this plot that all the data fall in a single curve. This result seems to be in agreement with the relation $\tau - \tau_r \simeq \tau_p^*$, since it would indicate that the measured activation volumes are only a function of the stress τ_p^*, and independent of the strain, temperature and orientation.

If it is assumed that the stress τ_p^* does not increase when the temperature decreases below 293°K, a multiplicity of values of λ/T is obtained for $\tau_p^* = 10$ kg/mm^2. However, it does not seem justified to give such a precise limit to the value of τ_p^*; in the first place because of the error involved in the determination of τ_r, and secondly, because of the approximation in the relation $\tau - \tau_r \simeq \tau_p^*$. It is possible (and more satisfactory from a physical point of view) that the stress τ_p^* still increases slightly when the temperature decreases below 293°K, and therefore the dotted curve of Figure 6.27. is probably a closer approximation to the real variation of λ/T with τ_p^*.

The activation volume has been plotted as a function of τ_p^* in Figure 6.27. Although the values

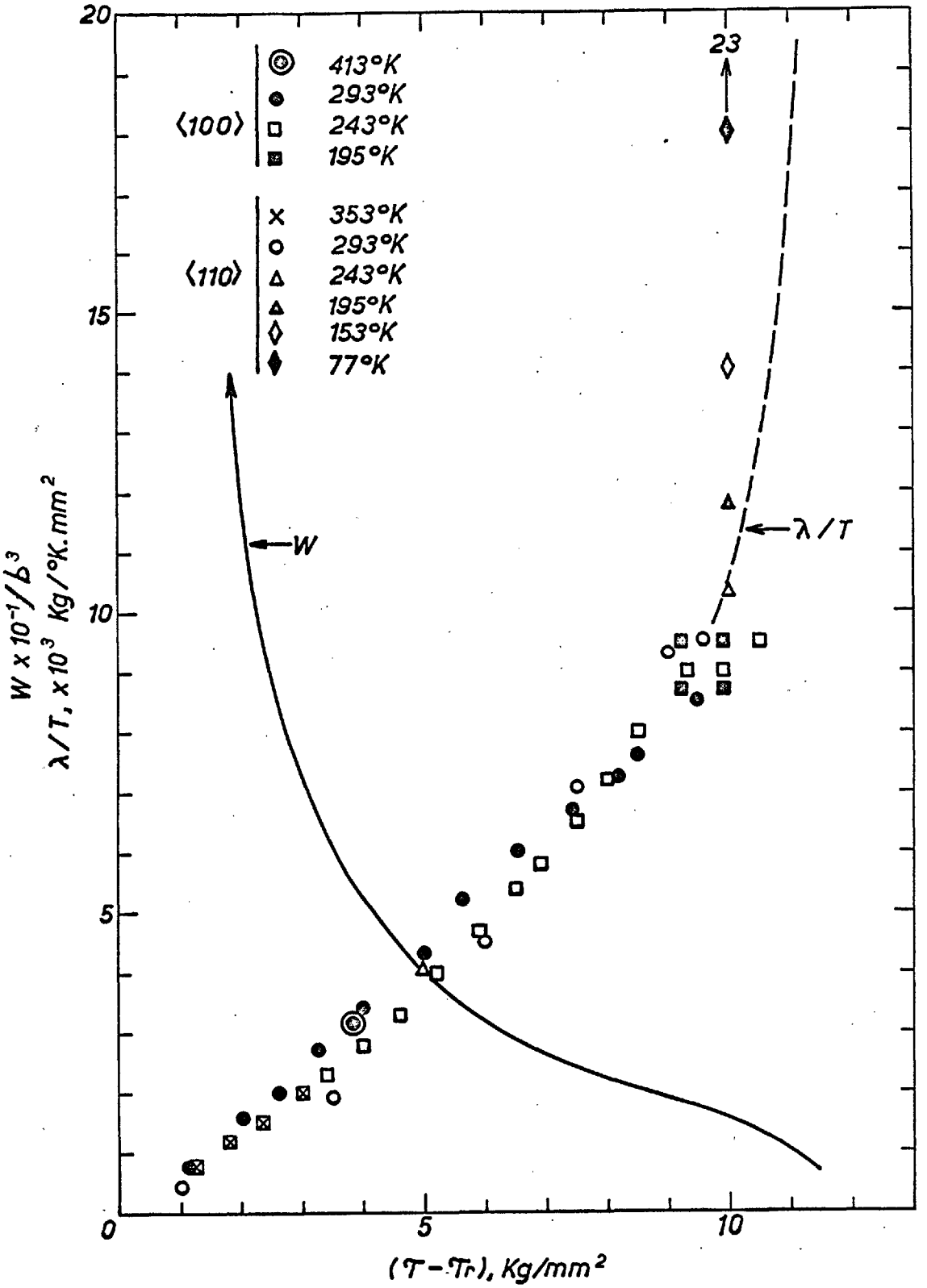

Figure 6.27. The variation of the activation volume and λ/T with $\tau - \tau_r$.

of λ/T increase rapidly when the temperature decreases below $293^{\circ}K$, the corresponding variation of the activation volume is small, and it is in qualitative agreement with the theoretical calculation of Dorn and Rajnak (1964). Compare, for example, the curve of Figure 6.27. with those of Figure 6.24.

6.7.6. The Equation of State for Crystals with ⟨110⟩ Orientation

The yield and flow stress of crystals deformed in the ⟨110⟩ direction in the temperature range between $300^{\circ}K$ and $77^{\circ}K$ obey an equation of state of the type:

$$\tau = \tau (\epsilon , \dot{\epsilon} , T,),$$

This statement has been derived from a consideration of the following experimental results.

1) The work hardening-rate is independent of the temperature in the range $300^{\circ}K$ to $77^{\circ}K$.

2) The yield and flow stress have the same temperature dependence (Figure 5.1. and Table 6.1.).

3) The strain rate sensitivity of the yield and flow stress are equal (Figure 6.10.).

Now, λ can be expressed as a function of τ_p^* and temperature alone (Figure 6.27.):

$$\lambda = \lambda (\tau_p^* , T) = \lambda (\tau - \tau_r, T) \quad . \quad . \quad (6.7.)$$

Since for crystals with ⟨110⟩ orientation the variation of τ_r with strain is rather small, one can make the

approximation $\tau_r = \tau_r(T)$, in the range of strain rates investigated. Therefore Equation 6.7. can be written as: $\lambda \simeq \lambda (\tau, T)$

This last equation explains the results already described in Section 6.6., namely that the strain rate sensitivity obeys an equation of state of the variables τ and T, for stresses greater than τ_r.

6.7.7. The Failure of an Equation of State for Crystals with <100> Orientation

The flow stress of crystals deformed in the <100> direction does not obey an equation of state. This is clearly shown by the results reported in Figure 6.16.

In Section 6.6. it has also been pointed out that the strain rate sensitivity of the flow stress is not only a function of stress and temperature, but that it also depends on the history of the crystal. This behaviour can now be understood by means of the relationship between λ/T and τ_p^* given in Figure 6.27.

Let us examine, for example, the results obtained during the temperature cycling experiment shown in Figure 6.14. The values of λ obtained during this test are plotted as a function of the applied stress in Figure 6.11.

At the stress $\tau = 20$ kg/mm^2 and at 293°K, λ is

equal to 1.75 kg/mm^2. When the temperature is decreased to 243°K and the crystal is reloaded up to the stress τ = 20.7 kg/mm^2 the strain rate sensitivity has decreased to λ = 0.47 kg/mm^2. This has happened not only because the temperature has been lowered, but possibly also because the value of τ_r has increased. In fact, the higher value of τ_r at 243°K can be obtained from the data given in Figure 6.16. There one finds τ_r' = 17.7 kg/mm^2. Therefore, after the temperature change has been made and when the applied stress is 20.7 kg/mm^2, the difference $\tau - \tau_r' \simeq \tau_p^*$ is only 3.0 kg/mm^2. Now the value of λ/T that would correspond to τ_p^* can be determined in Figure 6.27. There one finds, $\lambda/T = 2.2 \times 10^{-3}$ kg/mm^2.°K, so that λ = 0.53 kg/mm^2. This is in good agreement with the value of λ experimentally measured.

The strain rate sensitivity, λ, at 243°K has been determined by the same method for each point of the stress-strain curve where the temperature change was made. The values thus obtained are plotted in Figure 6.11., and it can be observed that they are in very good agreement with those determined by experiment.

The previous argument also explains why the ratio $\frac{\lambda 293^\circ K}{\lambda 243^\circ K}$ is not equal to the ratio 293/243, (see Section 6.6.).

6.7.8. The Activation Parameters

The results of the present investigation have been mainly discussed in terms of two thermally activated mechanisms. However, one should not ignore the fact that other authors, when analysing similar types of results, have found reasons to believe that the deformation of b.c.c. metals could be explained by the existence of a single rate controlling process. These reasons were mainly based on the values of the activation parameters determined from the temperature and strain rate dependence of the applied stress. In this section it will be shown that some of the present results are not consistent with this view.

Activation Parameters for a Single Rate Controlling Mechanism

The activation parameters calculated from the data given in Tables 6.1. and 6.2., and from the values of λ given in Figures 6.10. and 6.11., are shown in Tables 6.3. and 6.4. Equations 1.13. and 1.14. were used for this calculation. Figure 6.28. shows graphically the variation of the activation energy with the applied stress.

The first observation to make is that the values of the activation energies obtained here are of the same order as those obtained by other authors for polycrystalline molybdenum (Conrad 1963). It must

TABLE 6.3.

Activation energies for crystals with ⟨110⟩ orientation.

Mean Stress	Mean Temperature	H ± 1%		From tests at constant strain rate.
		erg x 10^{-12}	e.V.	
8.7	383	2.15	1.49	
14.5	323	1.49	0.93	
16.8	323	1.44	0.90	
21.8	268	1.22	0.76	
36.5	174	0.522	0.325	
18.3	268	0.72 ± 0.03	0.45	From tests at constant stress.

TABLE 6.4.

Activation energies for crystals with ⟨100⟩ orientation.

Mean Stress	Mean Temperature	H ± 3%		
		erg x 10^{-12}	e.V.	
11.6	383	2.33	1.45	From tests at constant strain rate
15.1	383	2.18	1.36	
16.6	323	1.62	1.02	
20.3	323	1.42	0.88	
21.6	323	1.31	0.82	
24.8	268	1.15	0.72	
25.6	268	1.13	0.70	
27.9	268	0.97	0.60	
30.1	268	0.93	0.58	
23.3	268	1.00±0.05	0.624	From tests at constant stress.

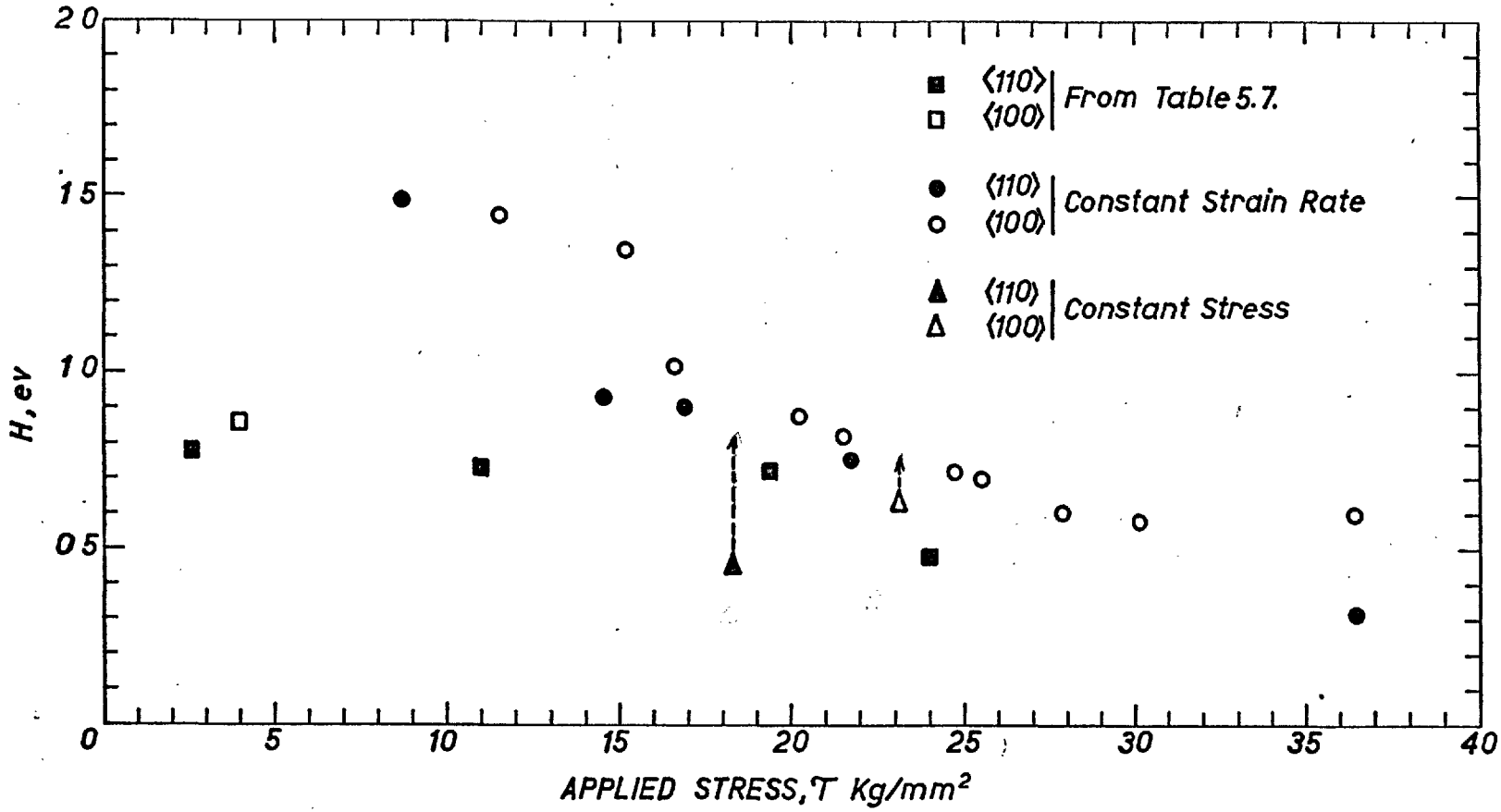

Figure 6.28. The stress dependence of the activation energy for the yielding and flow of molybdenum single crystals (assuming a single rate controlling mechanism).

also be pointed out that these values are consistent with the interpretation given by Conrad (1963) for the yielding and flow of the b.c.c. metals.

The fact that, for a given stress, the activation energies obtained in Chapter 5 are smaller than those calculated from the strain rate cycling tests is not really significant. The reason is that in Figure 6.28. the values of H are plotted versus the applied stress, whilst they should be plotted against effective stress if the results are to be compared.

It is far more important to realise that the activation energies obtained from temperature change experiments at constant strain rate do not agree with those obtained from temperature change experiments at constant stress. The disagreement is quite marked for the case of crystals with a ⟨110⟩ orientation, and it is certainly too large to be due to experimental errors. This result in itself, suggests that inconsistencies can occur in the method of calculation.

There have been reports of some cases for which no disagreement exists. For example Stone and Conrad (1964) determined the activation energies for the deformation of polycrystalline niobium from creep experiments and found values in good agreement

with those calculated from tests at constant strain rate.

Another point that should now be commented upon is the difference found between the ratio $\frac{\lambda_{293^\circ K}}{\lambda_{243^\circ K}}$ at constant stress and the ratio of the temperatures 293/243. This result implies that the activation volume, at constant stress, is a function of the temperature. Certainly some authors have arrived at a similar conclusion[+], but in the present case this has a greater significance. If the activation volume is an intrinsic function of the temperature, then the energy characteristic of the process that controls the deformation, U, should also be an intrinsic function of the temperature. This result would be in disagreement with the models of Seeger (1956) and Dorn and Rajnak (1964) for the Peierls mechanism, on which most of the interpretations of the behaviour of b.c.c. metals have been based (Conrad and Hayes 1963, Conrad 1963, Stone and Conrad 1964, Christian and Masters 1964). In both these models the energy for the nucleation of a pair of kinks is independent of the temperature.

Similar results to those reported here for molybdenum single crystals have also been obtained by Stone and Conrad (1964) for polycrystalline niobium, although these authors do not mention them explicitly.

[+]Thornton and Hirsch, 1958, Feltham and Copley 1960.

The variation of the strain rate sensitivity when the temperature is increased from 84.2°K to 92.6°K at a constant stress of 84.3 kg/mm^2 can be determined from the data shown in Figure 3 of Stone and Conrad's paper.[4] On doing this it is found that $\frac{\lambda\, 92.6^\circ K}{\lambda\, 84.2^\circ K} = 7$ whilst the temperature ratio is only 92.6/84.2 = 1.1. Therefore, in this case the interpretation of the values of the activation energies could also be objected.

The variation of λ with stress observed for crystals with a ⟨100⟩ orientation is another result that would be difficult to explain on the basis of a structure independent lattice friction alone.

The Activation Energy for Overcoming the Lattice Friction

According to the interpretation proposed in this thesis, the activation energy for the mechanism of overcoming the lattice friction should be calculated from the variation of τ_p^* with temperature and from the values of λ given in Figures 6.10. and 6.11.

The variation $\Delta\tau_p^*/\Delta T$ obtained from Figure 6.22. is about 0.05 kg/mm^2/°K, for temperatures between 400°K and 300°K, and almost negligible at lower temperatures. Values of the activation energies calculated at three different temperatures are given in

---

[4]Equation 24 of the Appendix is used for this calculation.

Table 6.5.

TABLE 6.5.

Stress kg/mm^2	Temp. ^oK	λ kg/mm^2	H		
			erg x 10^{-12}	e.V.	
0			2.65	1.65	Extrapolated
4	413	1.5	1.80	1.12	
7	353	2.4	0.85	0.51	
9	300	2.75	0.52	0.32	
11			0	0	Extrapolated

A linear extrapolation of the calculated values to $\tau_p^* = 0$ would give a value of 1.65 e.V for the activation energy of the process. By extrapolation to zero activation energy a stress of 11 kg/mm^2 is obtained.

The activation energy at zero stress is in the present calculation almost equal to that obtained from the variation of the applied stress with temperature (Figure 6.28.). However in the present case the activation energy decreases much more rapidly with increasing stress.

It must be pointed out that the results of Table 6.5. can not be satisfactorily explained in terms of Seeger's model of double kink nucleation (Seeger 1956). If the energy for the nucleation of

a pair of kinks, $2U_k$, is calculated from Equation 1.4. one obtains (with $\tau_o^* = 10$ kg/mm^2), $2U_k = 0.26$ e.V. This value is six times smaller than that obtained by extrapolation of the data of Table 6.5. to zero stress.

The significance of this disagreement is difficult to assess, and before it is used as an argument against the interpretation proposed in this thesis some considerations should be made. In the first place the variation $\Delta\tau_p^*/\Delta T$ obtained from Figure 6.22. is a crude approximation. Secondly, the lattice friction may not be solely due to the Peierls stress, but also to the presence of impurities. Finally, the length of the dislocation segment lying free between the jogs is relatively small, and therefore it is possible that Seeger's model of kink nucleation would require some modification in the present case.

The Activation Energy for the Non-conservative Movement of Jogs

The activation energy for the nor-conservative movement of jogs should be calculated from the variation of τ_j^* with temperature (Figure 6.22.) and from the value of w_j obtained in Section 6.7.2. For temperatures between 77°K and 300°K, $\Delta\tau_j^*/\Delta T = 0.16$ kg/mm^2/°K. The activation volume, in this range of temperatures is approximately $50b^3 = 10^{-21}$ cm^3 (Section 6.7.2.).

Table 6.6. shows the values of H (calculated from Equation 1.13.) and $U_j = H + w_j \tau_j^*$ at three different temperatures.

TABLE 6.6.

Stress τ_j^* kg/mm^2	Temp. ^oK	H		$U_j = H + w \tau_j^*$ e.V.
		erg x 10^{-12}	e.V.	
35	100	1.6	1.0	3.30
22	200	3.2	2.0	3.37
7	300	4.8	3.0	3.44
$\tau_j^* \simeq \tau_r - \tau_\mu$ $\tau_\mu \simeq 3$ kg/mm^2				

These values of U_j are in good agreement with the value of 3.6 e.V. which was taken as the energy for vacancy formation.

At temperatures higher than 300^{o}K the variation $\Delta\tau_j^*/\Delta T$ decreases, and therefore smaller values of U_j would be obtained if the same value of w_j were used in the calculation of the activation energy. However, at these temperatures, it is possible that the mean jog spacing and hence the activation volume may increase, and then values of U_j of the same order of magnitude as those of Table 6.6. could still be obtained.

6.7.9. The Effect of Orientation on the Proportional Limit and the Work-hardening Rate

The results reported in this chapter support the explanation given in Chapter 5 of the effect of orientation on the yield and flow stress of molybdenum single crystals. Some aspects of this effect which can now be understood in more detail will be discussed briefly in this section.

Crystals with <110> Orientation

For crystals with this orientation, a relatively small number of sites are available for thermal activation at the beginning of the deformation (see Section 5.6.3.), and this is reflected in a rapid increase of the stresses τ_p^* and τ_j^* in the micro-strain region.

After the yield point, when a large increase in the number of mobile dislocations has occurred, τ_p^* and τ_j^* attain an almost constant value, and this means that the concentration of jogs does not increase significantly with strain. Since at the same time the work-hardening rate after the yield point is small, one is tempted to conclude that the total dislocation density remains almost constant. The etch pit observations reported in Section 5.2.2. showed a rapid increase in the number of dislocation etch pits after the proportional limit had been reached,

but this technique is unable to show whether the dislocation density tends towards a saturation value or not. This is a problem which could probably be solved by transmission electron microscopy.

When the crystals deform at temperatures higher than 300°K the strain rate sensitivity, λ, decreases with increasing stress (and strain), and this is consistent with the corresponding decrease in τ_p^* with strain observed at these temperatures (see Figure 6.20.). This behaviour is similar to that exhibited by niobium single crystals deformed at room temperature (H. C. Kim, private communication), and by polycrystalline iron deformed above 150°K (Conrad and Frederick, 1962). The decrease in λ and τ_p^* with strain may arise from an increase in the total length of free dislocation segments as a result of the recovery phenomenon described in Section 5.6.8.

Crystals with <100> Orientation

Since a relatively large number of activated sites exist in crystals with this orientation, a sufficiently large number of dislocations can become mobile to produce macroscopic deformation at low stresses. Under these conditions both τ_p^* and τ_j^* are small, since at the proportional limit the plastic strain rate is also small. Continuous multiplication of dislocations also takes place at

low stress. As more dislocations become mobile the number of dislocation intersections increases, and hence the dynamic equilibrium spacing of jogs decreases. Then the stresses τ_p^* and τ_j^* increase for two reasons. One, and the most important is that the mean jog spacing becomes smaller; the other is that the plastic strain rate increases with strain.

The fact that τ_p^* increases at the same time as the total dislocation density may seem paradoxical. However this can be understood by realising that the magnitude of τ_p^* may be determined by the length of the free dislocation segments, and not by the total number of mobile dislocations. The reason for this is as follows:

The overall deformation rate is controlled by the speed at which the jogs move. This speed is given by

$$b\nu_p = b\nu' \exp\left(-\frac{U - Fb}{kT}\right)$$

where ν_p is the frequency of non-conservative jumps, ν' is a frequency factor, and F is the force on the jog. The force F is not constant, but varies with time, and decreases when the jog moves forward; since then the curvature of the dislocation segment decreases. Therefore the average value of F, and the number of non-conservative jumps per second, will also depend on the speed with which the curvature

of the dislocation line is restored, and hence on the magnitude of τ_p^*. Once the value of ν_p is fixed (by the imposed strain rate) the stresses τ_j^* and τ_p^* are not independent of each other, but must satisfy the condition that $\tau_j^* + \tau_p^*$ be a minimum. From this it follows that when the mean jog spacing varies there is a variation on both τ_j^* and τ_p^*.

At high strains, when a final equilibrium distribution of dislocations and jogs is almost reached, the work-hardening rate is small. Then τ_p^* and τ_j^* and their variation with temperature and strain rate is of the same order as for crystals with ⟨110⟩ orientation.

There are three different processes contributing to the work-hardening rate. The variations $d\tau_p^*/d\epsilon$ and $d\tau_j^*/d\epsilon$ both give rise to the thermal component of the work-hardening. There must exist also an athermal component $d\tau_\mu/d\epsilon$ which is only a function of the dislocation configuration, and which may arise from dislocation intersection processes and from a long range internal stress field. However the discussion of the nature of the stress τ_μ and its variation with strain is a subject which falls out of the scope of the present investigation.

When the crystals are deformed at temperatures

higher than 300°K, both the strain rate sensitivity and the stress τ_p^* decrease with increasing strain (Figures 6.11. and 6.21.). This effect which is associated with the recovery phenomenon, has already been discussed above for crystals with <110> orientation. The explanation given there is also applicable to the present case.

CHAPTER 7.

CONCLUSIONS AND SUGGESTIONS FOR FUTURE WORK

7.1. Conclusions

(1). The yield stress and the work-hardening rate of molybdenum single crystals grown by electron beam floating zone melting has been found to be very strongly orientation dependent.

Crystals deformed in the ⟨110⟩ direction at temperatures lower than 300°K exhibit a high proportional limit and a rounded yield point. The subsequent work-hardening rate is relatively low. At temperatures higher than 350°K the yield point disappears and the crystals experience a large uniform elongation.

The crystals deformed in the ⟨100⟩ direction exhibit a very low proportional limit and parabolic hardening. At temperatures above 350°K work-softening is observed, and the final elongation of the crystals is of the order of 30%.

At temperatures lower than 300°K, the crystals with the tensile axis orientated in a direction near the centre of the stereographic triangle behave like the crystals with ⟨100⟩ orientation. However when they are deformed at temperatures higher than 350°K

they exhibit three work-hardening stages rather similar in characteristics to those of the f.c.c. single crystals.

The transition in the deformation behaviour observed at temperatures between 300°K and 350°K has been termed 'recovery transition' and is believed to be due to a softening of the initially active slip systems.

(2). An explanation based on the non-conservative movement of jogs in screw dislocations has been proposed for the effect of orientation on the proportional limit of molybdenum single crystals.

This explanation also accounts for the fact that at high and very low temperatures no effect of orientation is observed.

(3). A study of the temperature and strain rate sensitivity of the flow stress has been carried out using a stress relaxation method. The results obtained indicate that the stress τ_r necessary to deform the crystals at a strain rate $<10^{-7}$ sec^{-1} is very strongly temperature dependent. At the same time the stress increment $(\tau - \tau_r)$ necessary to increase the strain rate from 10^{-7} sec^{-1} to 10^{-3} sec^{-1} is temperature independent at temperatures lower than 293°K.

(4). In order to understand these results an

explanation has been proposed assuming that the deformation is controlled by two simultaneous processes. One is the non-conservative dragging of jogs in screw dislocations; the other is the overcoming of the lattice friction opposing the movement of the free dislocation segments lying free between the jogs. In order to move a jogged screw dislocation at a steady macroscopic rate an effective stress $\tau^* = \tau_j^* + \tau_p^*$ is required. The component τ_j^* is the stress necessary to move the jogs non-conservatively, and τ_p^* is the stress needed to overcome the lattice friction.

The value of τ_j^* is approximately equal to $\tau_r - \tau_\mu$ and τ_p^* is approximately equal to the difference $\tau - \tau_r$.

The variation of τ_j^* with temperature, below 293°K, is large, whilst τ_p^* is almost constant. Above 293°K both stresses τ_j^* and τ_p^* are temperature dependent.

(5). By applying this model to the experimental results, it is concluded that the lattice friction stress at 0°K is about 10 kg/mm^2, and that the overcoming of the lattice friction is not a thermally activated process below 293°K (for $\dot{\epsilon}$ 10^{-3} sec^{-1}).

The temperature dependence of the flow stress below 293°K is due entirely to variations in τ_j^*, whilst the strain rate dependence of the flow stress at any temperature is equal to the strain

rate dependence of τ_p^*. The calculation of the activation energy from the variation of the applied stress with temperature and strain rate is therefore questionable.

(6). The activation energy for the mechanism of overcoming the lattice friction has been calculated from the variation of τ_p^* with temperature and strain rate. The value of the activation energy thus obtained, for $\tau_p^* = 0$, is 1.65 e.V. The activation volume varies from $10b^3$ (at $\tau_p^* = 11$ kg/mm^2) to $120b^3$ (at $\tau_p^* = 2$ kg/mm^2).

The activation energy for the non-conservative movement of jogs calculated from the variation of τ_j^* with temperature is 3.4 e.V., and is in agreement with the value of the energy for vacancy formation in molybdenum. At low temperatures the activation volume for this process is $50b^3$, and the mean jog spacing is 50b.

The model proposed explains also the effect of the orientation on the work-hardening rate, and the variation of the strain rate sensitivity with temperature and stress.

7.2. Suggestions for Future Work

Many of the ideas presented in this thesis to explain the effect of orientation in terms of two

thermally activated mechanisms need to be further developed. The implications of the explanation proposed (Section 6.7.3.), not only lend themselves to easy experimental verification, but also suggest that the study of the deformation mechanisms should be extended over a range of temperatures and strain rates from the region where τ_p^* is temperature dependent to that where τ_p^* is temperature insensitive.

It seems obvious that it would be profitable to apply the experimental methods used in this investigation to study the deformation of other b.c.c. metals, and it should be investigated whether the results obtained can also be explained in terms of the model proposed in this thesis.

The work contained in this thesis suggests a new method of approach to the problem of the effect of the interstitial impurity atoms on the yield and flow stress. For example, it is possible to investigate whether the impurity interstitial atoms affect the mobility of the jogs (i.e. the value of τ_j^*) or the magnitude of the lattice friction (i.e. the value of τ_p^*).

A detailed theoretical treatment of the movement of a jogged screw dislocation through a lattice with

a high frictional stress would also be desirable.

The recovery transition discussed in Section 5.6.8. is a problem which also requires further investigation. A comparative study of the dislocation structures by means of transmission electron microscopy in different b.c.c. metals would probably be a good approach to the problem.

APPENDIX

STRESS RELAXATION AND THE PLASTIC DEFORMATION OF SOLIDS

A C K N O W L E D G E M E N T S

I am extremely grateful to Professor P. L. Pratt for the supervision of this work and to Professor J. G. Ball for providing research facilities.

I would also like to record my thanks to Dr. A. A. Johnson for his advice in the early stages of this research; to Professors R. L. Bell and H. W. Paxton for many valuable discussions; to Dr. J. A. Wright for his critical comments on the manuscript, and to Mr. A. R. Khan and my colleagues in the Crystal Physics Group for the interest they took in this work.

The specialised assistance provided by the Workshop and photographic staff of the Department is gratefully acknowledged.

Finally I wish to thank the Central Electricity Generating Board for their generous financial assistance.

REFERENCES

ALEFELD,G.,1962,Z.Naturforschg. 17a,899.

ALLEN,N.P.,HOPKINS,B.E. and McLENAN,J.E.,1956,Proc.Roy. Soc. A234, 221.

AMELINCKX,S. and DEKEYSER,W.,1959,Solid State Physics, 8 , 327.

ANDRADE,A.N. and CHOW,Y.S.,1940,Proc.Roy.Soc.,A175,962.

AUST,K.T. and MADDIN,R.,1956,Acta Met., 4 , 632.

AVERY,D.H.,EBNER,M.L. and BACKOFEN,W.A.,1958,Trans. Met. Soc. AIME, 212, 256.

BARRET,C.S. and BAKISH,R.,1958,Trans AIME,212 , 122.

BASISNSKI,Z.S. and CHRISTIAN,J.W.,1960,Aust.J.Phys.13,299

BELK,J.A.,1959,Symp. on Electron Bombardment Techniques, S.E.R.L. Labs.,Baldock,Herts.,England.

BELK,J A. and CALVERLEY,A.,1961, Le Vide,Sept/Oct. p.270

BELL,R.L. and BONFIELD,W.,1964,Phil.Mag.,9 , 9.

BENSON,R.,THOMAS,G.and WASHBURN,J.,1962,Direct Observation of Imperfections in Crystals,Intersc.N.Y.,p.375.

BERLEC,I.,1962, J.Appl. Phys., 33 , 197.

BIRBECK,F.E. and CALVERLEY,A.,1959,J.Sci.Instr.,36,460.

BOLEF,D.I. and de KLERK,J.,1962,J.Appl.Phys.,33, 2311.

BROOM,N. and HAM,R.K.,1958,Vacancies and Other Point Deffects, Inst.Met.Monograph.

BROWN,N. and EKVALL,R.A.,1962, Acta Met., 10, 1101.

BUEHLER,E.,1958, Trans.Met.Soc. AIME, Oct.,p.694.

BUEHLER,B.and KUNZLER,J.E.,1961,Trans. AIME, 221,957.

CALVERLEY,A.,DAVIS,M. and LEVER,R.L.,1957,J.Sci.Instr., 34 , 142.

CARLSON,R.G.,1959, J.Electrochem.Soc., 106 , 49.

CARRINGTON,W.,HALE,K.F. and McLEAN,D.,1960,Proc. Roy. Soc., 257A , 203.

CELLI,V.,KABLER,M.,NINOMIYA,T. and THOMSON,R.,1963, Phys. Rev., 131 , 58.

CHEN,N.K. and MADDIN,R.,1951,Trans. AIME, 191, 461.

CHEN,N.K.,MADDIN,R. and POND,R.B.,1951,Trans. Met.Soc. AIME, June,p.461.

CHRISTIAN,J.W.,1964, Acta Met., 12 , 99.

CHRISTIAN,J.W. and MASTERS,B.C.,1964,Proc.Roy.Soc.,281A, 223 & 240.

CHURCHMAN,A.T.,1960, J.Inst.Met., 88 , 221.

COCHARDT,A.W.,SCHOECK,G. and WIEDERSICH,H.,1955, Acta Met., 3 , 533.

COLE,M.,BUCKLOW,I.A. and GRIGSON,C.W.B.,1961, Brit.J. Appl. Phys., 12 , 296.

COLE,M.,FISHER,C. and BUCKLOW,I.A.,1961,Brit.J.Appl.Phys. 12 , 577.

CONRAD,H.,1961,Acta Met.,9,367;1961a,J.I.S.I.,198,364; 1963,The Relation Between The Structure and Mechanical Properties of Metals,H.M.S.O., London, p.476.

CONRAD,H. and FREDERICK,S.,1962,Acta Met.,10 , 1013.

CONRAD,H. and HAYES,W.,1963,Trans.ASM., 56 , 249.

CONRAD,H. and SCHOECK,G.,1960, Acta Met.,8 ,791.

CONRAD,H. and WIEDERSICH,H.,1960,Acta Met., 8 ,128.

COTTRELL,A.H.,1948,Bristol Conf.Rep. on the Strength of Solids,Phys.Soc.,p.30;1953,Dislocations and Plastic Flow in Crystals,Oxford Univ. Press; 1957,Conf. on High Rates of Strain,I.Mech.E.; 1957 a,Dislocations and Mechanical Properties of Crystals,John Wiley & Sons Inc.;1963,The Relation Between the Structure and Mechanical Properties of Metals,H.M.S.O.,Lond.,p.456.

COTTRELL,A.H. and BILBY,B.A.,1949,Proc.Roy.Soc.,A62,49.

COTTRELL,A.H. and STOKES,R.J.,1955,Proc.Roy.Soc.,A233,17.

DAVIS,M.,CALVERLEY,A. and LEVER,R.F.,1956,J.Appl.Phys,27,195.

DEW-HUGHES,D.,1961,IBM J.and Res.Dev.,5,279; 1962, Phil.Mag.,7 , 1959.

DORN,J.E. and RAJNAK,S.,1964,Trans.Met.Soc.AIME,230,1052.

DRANGEL,I. and MURRAY,G.,1964,Materials Research Corp., Report to the Feb. AIME Meeting,New York.

DUAN,F.,NAY-BEN,M.,CHI,L.and TIAN-NAN,L.,1963,Scientia Sinica, 12 , 979.

EDMONDSON,B.,1961, Proc.Roy.Soc., A264, 145.

ELAM,C.F.,1935, The Distortion of Metal Crystals,Oxford.

EMEIS,R.,1954, Z.Naturforschg., 9 A , 67.

ERICKSON,J.S.,1962, J.Appl.Phys., 33, 2499.

EYRING,H.,1936, J. Chem. Phys., 4 , 283.

FARMER,M.H. and GLAYSHER,G.H.,1953,J.Sci.Instr,30, 9.

FELTHAM,P. and COPLEY,G.H.,1960,Phil.Mag., 8 , 649.

FERRIS,D.P.,ROSE,R.M. and WULFF,J.,1962,Trans.Met.Soc. AIME, 224 , 975.

FISHER,J.C.,1955,Trans. ASM., 47, 451.

FLEISCHER,R.L.,1962 a,Acta Met.,10,835; 1962 b,J.Appl. Phys.,33,3504; 1963,(Fleischer,R.L. and Hibbard,W.R.) The Relation Between the Structure and Mech. Prop. of Metals,HMSO, Lond.,p.261.

FOREMAN,A.J.,JASWON,M.A. and WOOD,J.K.,1951,Proc.Phys. Soc., A 64 , 156.

FRIEDEL,J.,1956, Les Dislocations,Gauthier-Villars,Paris.

GIBBS,G.B.,1964, phys.stat.sol., 5 , 693.

GILMAN,J.J.,1960, Aust.J. Phys., 13 , 327.

GREGORY,D.P., 1963, Acta Met., 11 , 455.

GREGORY,D.P. , STROH,A.N. and ROWE,G.H.,1963,Trans. Met. Soc. AIME.,227 , 678.

GRENINGER,A.B.,1937, Trans ASM.,25, 702.

HAASEN,P.,1957, Acta Met., 5 , 598.

HAHN,G.T., 1962, Acta Met., 10 , 727.

HESLOP,J. and PETCH,N.J.,1956, Phil. Mag., 1 , 866.

HIRSCH,P.B.,1960,Fifth Int. Congrss on Crystallography, Cambridge; 1962, Phil.Mag., 7 , 67.

HIRSCHHORN,J.S.,1963, J. Less-Common Met., 5 , 493.

HONDA,R.,1961, J.Phys.Soc.Japan, 16 , 1309.

HULL,D.,1960,Acta Met.,8,11; 1961,Acta Met.,9,191.

HUNT,A.L.,DAMM,C.C. and POPP,E.C.,1960,Univ. of Calif. Lawrence Rad. Lab.,Rep. No UCRL-5889.

HURWITT,S.D. and ADAMS,M.A.,1963,Metal Progr.,February.

HUTCHISON,M.M.,1963, Phil. Mag., 8 , 121.

JOHNSTON,W.G.,1962, J. Appl. Phys., 33 , 2050.

JOHNSTON,W.G. and GILMAN,J.J.,1959, J.Appl.Phys.,30,129; 1960, J. Appl. Phys., 31 , 632.

KECK,P.H. and GOLAY,M.J.E.,1958, Phys. Rev., 89 , 1927.

KEH,A.S., 1963, quoted by Mitchell et al.(1963).

KEH,A.S. and WEISSMANN,S.,1963,Electron Microscopy and Strength of Crystals,Intersc.,N.Y.,p.231.

KOO,R.C.,1963, Acta Met., 11 , 1083.

KUHLMANN-WILSDORF,D., 1960, Phys. Rev., 120 , 773.

LAWLEY,A.,VAN den SYPE,J. and MADDIN,R.,1962, J. Inst. Met., 91 , 23.

LAWLEY,A. and GAIGHER,H.L.,1963,Phil. Mag.,8, 1713; 1964, Phil. Mag., 10 , 15.

LEIBFRIED,G. and DIETZE,H.D.,1949,Z. Physik, 126, 790.

LI,J.C.M.,1962,Direct Observation of Imperfections in Crystals,Interscience,N.Y.,p.234; 1963, J. Aust. Inst. Met., 8 , 206.

LIVINGSTON,J.D., 1962, Acta Met. , 10 , 229.

LOTHE,J. and HIRTH,J.P.,1959, Phys. Rev., 115 , 543.

LOW,J.R. and TURKALO,A.M.,1962, Acta Met., 10 , 215.

LOW,J.R. and GUARD,R.W., 1959, Acta Met., 7 , 171.

MADDIN,R. and CHEN,N.K.,1953,Trans.AIME,Sept.,p.1131;

1954, Progr. Met. Phys., 5 , 53.

McLEAN,D.,1962,Mechanical Properties of Metals,John Wiley & Sons, p.120.

MITCHELL,T.E.,FOXALL,R.A. and HIRSCH,P.B.,1963,Phil. Mag., 8 , 1895.

MORDIKE,B.L.,1962, Z. Metallkde., 53 , 486.

MORDIKE,B.L. and HAASEN,P.,1962, Phil. Mag., 7 , 459.

MOTT,N.F. and NABARRO,F.R.N.,1940,Proc.Phys.Soc.,52, 86; 1948,Report on Strength of Solids,Phys.Soc.,p.1.

NABARRO,F.R.N.,1947, Proc.Roy.Soc., 59 , 256.

NABARRO,F.R.N.,BASINSKI,Z.S. and HOLT,D.B.,1964,Advances in Physics, 13 , 193.

NORTHCOTT,L.,1956,"Molybdenum",Butterworths Scientific Publications,London.

OHR,S.M. and BESHERS,D.N.,1964, Phil. Mag., 10 , 219.

ORAVA,R.N.,1963, Ph.D. Thesis, University of London.

OROWAN,E.,1936, Z. Phys., 98 , 386.

PEACOCK,D.E.,1961, Ph.D. Thesis, University of London.

PEIERLS,R.E., 1940, Proc. Roy. Soc., 52 , 34.

PFANN,W.G.,1952, Trans. AIME,194,747; 1957,Met.Rev.,2,29; 1958, Zone Melting,John Wiley & Sons,N.Y.

ROSE,R.M.,FERRIS,D.P. and WULFF,J.,1962,Trans.Met.Soc. AIME, 224 , 981.

SAADA,G.,1960,Acta Met.,8,200; 1961,Acta Met.,9,166; 1963,Electron Microscopy and Strength of Crystals, Intersc. Publ.,N.Y., p.651.

SCHADLER,H.W.,1962,Direct Observation of Imperfections in Crystals,Intersc. Publ. p.593; 1963, The Art and Science of Growing Crystals,John Wiley & Sons,N.Y.,p.343; 1964,Acta Met., 12 , 861.

SCHADLER,H.W. and LOW,J.R.,1962, General Electric Res. Lab.,Rep. No. 62-GC-206.

SCHÄFER,S.,ALEXANDER,H. and HAASEN,P.,1964,phys.stat.sol., 5 , 247.

SCHMID,E. and BOAS,W.,1950,Plasticity of Crystals, Hoghes & Co, Ltd.,London.

SCHOECK,G,, 1961, Acta Met., 9 , 382.

SCHOECK,G. and SEEGER,A.,1959, Acta Met., 7 , 469.

SEEGER,A.,1955,Phil.Mag.,46,1194;1956,Phil. Mag.,1,651.

SEEGER,A.,DONTH,H. and PFAFF,F.,1957,Disc.Faraday Soc., 23, 19.

SHAW,B.J. and SARGENT,G.A.,1964, Acta Met., 12 , 1225.

SLEESWYK,A.W.,1962,Acta Met.,10,803;1963,Phil. Mag.,8,1467.

SLEESWYK,A.W. and HELLE,J.N.,1963, Acta Met., 11 , 187.

SMITH,H.R.,1958,Vacuum Metallurgy,Reinhold Publ.Co.N.Y.,p.221

SNOEK,J., 1941, Physica, 8 , 711.

STEIN,D.F. and LOW,J.R.,1960, J. Appl. Phys., 31 , 362.

STONE,G.A. and CONRAD,H., 1964, Acta Met., 12 , 1125.

TAYLOR,G.L. and ELAM,C.F.,1926,Proc.Roy.Soc.,A112 ,337; 1928, Proc. Roy. Soc., A118 , 273.

TILLER,W.A.,1963,The Art and Science of Growing Crystals, John Wiley & Sons,N.Y., p.276.

THORNTON,P.R. and HIRSCH,P.B.,1958,Phil.Mag., 3 , 738.

TITCHENER,A.L. and DAVIES,G.J.,1963,J.Sci.Instr.,40,57.

TSIEN,L.C. and CHOW,Y.S.,1937,Proc. Roy. Soc., 163A, 19.

VAN TORNE,L.I. and THOMAS,G.,1963,Acta Met., 11 , 881.

VOGEL,F.L. and BRICK,R.M.,1953, Journal of Metals,May,p.700

VOTAVA,E., 1964, phys. stat. sol., 5 , 421.

WERNICK,J.H.,DORSI,D. and BYRNES,J.J.,1959, J. Electrochem. Soc., 106 , 245.

WINKLER,O., Met. Rev., 5, 1.

WRONSKI,A.S. and JOHNSON,A.A.,1962,Phil. Mag.,7, 213.

WULFF,J., 1957, Hochvacuumtecknik,M.Auwarter,Wissenschaftl. Verlags-Ges.,MBH,Stuttgart, p.272.

YOKOBORI,T., 1952, Phys. Rev., 88 , 1423.

YOUNG,F.W. and WILSON,T.R.,1961,Rev.Sci.Instr., 32 , 559.

phys. stat. sol. 6, 111 (1964)

Department of Metallurgy, Imperial College, University of London

Stress Relaxation and the Plastic Deformation of Solids

By
F. GUIU and P. L. PRATT

When a solid is plastically deformed in a hard testing machine and the cross-head is arrested, a continuous decrease of load is observed. An interpretation and analysis of this stress relaxation phenomenon is made. This effect can be used to study mechanisms of plastic deformation in solids, and details are given in the paper.

Wenn ein fester Körper in einer Härteuntersuchungs-Apparatur verformt und die Gleitbacke angehalten wird, wird eine kontinuierliche Abnahme der Belastung festgestellt. Es wird eine Deutung und Analyse dieser Spannungsrelaxation gegeben. Dieser Effekt kann zur Untersuchung des Mechanismus der plastischen Verformung in festen Körpern verwendet werden. Einzelheiten darüber werden in dieser Arbeit mitgeteilt.

1. Introduction

Two kinds of mechanical relaxation phenomena can be distinguished in solids. One type arises from the "anelastic" or imperfect elastic nature of real solids and is manifested even at very low values of the applied stress. Such an "anelastic" behaviour can be described by ZENER's "standard linear solid" model [1] which is characterized by an exponential time dependence of the relaxed strain and a characteristic relaxation time. This fact makes it possible to study the physical nature of the elastic imperfection by means of internal friction measurements [2].

A second kind of relaxation is observed when a solid is plastically deformed. The phenomenon is then associated with the movement of free dislocations and can not be described in terms of ZENER's model. The relaxed strain does not involve a time exponential but instead is logarithmic with time. In order to show this effect the solid must be deformed plastically in a hard testing machine by the application of a load. If then the movement of the cross-head of the machine is arrested a continuous decrease of the load is observed. The decrease in load is a consequence of the deformation of the solid. The term "relaxation at constant strain" which has been sometimes applied to this effect seems therefore rather unfortunate and it is better to refer to it simply as stress relaxation.

The purpose of this paper is to analyse the stress relaxation process and to show how it can be used to study some aspects of the plactic deformation of solids.

2. Analysis of the Test

Let us imagine that a specimen is deformed in a hard testing machine at a cross-head speed $\dot{y}$ and that on reaching the point $\sigma_0\, \varepsilon_0$ of the stress strain curve (Fig. 1) the plastic strain rate experienced by the specimen is $\dot{\varepsilon}_0$. If at that moment taken as $t = 0$ the movement of the cross-head is arrested, the specimen continues deforming under a decreasing stress and decreasing strain rate. From the record of load versus time the relaxation curve $\sigma = \sigma(t)$ can be obtained.

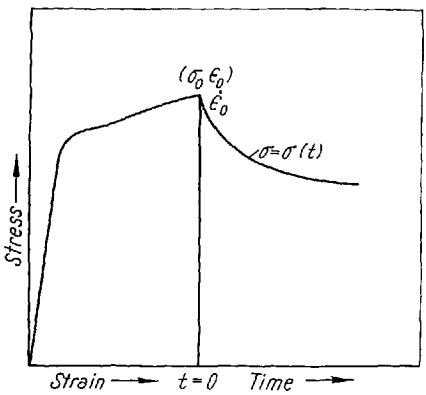

Fig. 1. Typical stress-strain curve and relaxation curve obtained at $\sigma_0\ \varepsilon_0$

Throughout the relaxation process the relation between the stress and strain is determined by the stiffness of the machine, and the geometry and elastic modulus of the specimen. This relation is obtained as follows:

The speed $\dot{y}$ at which the cross-head of the machine is moving is matched by the elastic plus plastic deformation rate of the specimen $\dot{l}_p + \dot{l}_e$ and the elastic extension rate of the different parts of the machine itself $\dot{z}$. Thus

$$\dot{y} = \dot{l}_p + \dot{l}_e + \dot{z} \,. \tag{1}$$

When the cross-head is arrested $\dot{y} = 0$ and then

$$\dot{l}_p + \dot{l}_e = -\dot{z} \,. \tag{2}$$

z is related to the stiffness of the testing machine given by

$$s = \frac{dP}{dz} \,, \tag{3}$$

which is practically constant in the small range of load, P, involved in the relaxation. Then, converting from deformation rates to strain rates, (2) can be written

$$\dot{\varepsilon}_p + \dot{\varepsilon}_e = -\frac{a_0}{l_0 s}\dot{\sigma} \,, \tag{4}$$

where l_0 and a_0 are the length and cross section of the specimen at time $t = 0$. Expressing $\dot{\varepsilon}_e$ in terms of the elastic modulus E of the specimen

$$\dot{\varepsilon}_e = \frac{\dot{\sigma}}{E} \tag{5}$$

the relation between the strain rate and the stress rate takes the form

$$\dot{\varepsilon}_p = -M'\,\dot{\sigma} \,, \tag{6}$$

where

$$M' = \frac{a_0}{l_0 s} + 1/E$$

can be assumed to be constant because the deformation introduced during relaxation is small compared with l_0. When a numerical constant α is introduced to

convert tensile strain and tensile stress into shear strain and shear stress (6) is written as

$$\dot{\gamma} = -M\,\dot{\tau} \tag{6a}$$

with $M = \alpha\, M'$.

The applied stress τ is the sum of the thermal component or effective stress τ^* and the long range internal stress τ_μ.

$$\tau = \tau^* + \tau_\mu\,. \tag{7}$$

During relaxation τ_μ is practically constant. It varies with strain as $d\tau_\mu = \theta\, d\gamma$ where θ is a work-hardening coefficient and from (6a) $d\tau_\mu = -\theta\, M\, d\tau$. In a hard machine M is of the order of 10^{-4} mm²/kg and therefore $d\tau_\mu$ is only a very small fraction of $d\tau$. Then (6a) becomes

$$\dot{\gamma} = -M\,\dot{\tau}^*\,. \tag{6b}$$

The strain rate sensitivity of the stress defined as $(\partial\tau^*/\partial \log \dot{\gamma})_T$ is easily obtained from the relaxation curve $\sigma = \sigma(t)$. Eq. (6b) shows that

$$\frac{d\tau^*}{d\log\dot{\gamma}} = \frac{d\,\tau^*}{d\log(-\dot{\tau}^*)} = \lambda(\tau^*)\,. \tag{8}$$

Therefore, if τ is plotted versus $\log(-\dot{\tau})$ the slope of the plot at any point gives the value of $\lambda(\tau)$.

An alternative way of analysing the relaxation curve which was originally used by FELTHAM [3] consists in plotting τ versus $\log(t + c)$, where c is a constant. It has been repeatedly verified [3, 4, 5, 6, 7] that in such a plot a straight line is obtained. This means that the relaxation equation is of the form

$$\sigma - \sigma_0 = \lambda' \log c - \lambda' \log(t + c) \tag{9}$$

or if shear stress is plotted instead of tensile stress,

$$\tau - \tau_0 = \lambda \log c - \lambda \log(t + c)\,. \tag{9a}$$

The constant c is chosen so as to give a linear plot from $t = 0$, and $-\lambda'$ or $-\lambda$ are the slopes of the straight line. (9) and (9a) are only valid for the interval $0 < t < t_1$ in which the experimental linear relation is established. The derivative of τ^* with respect to t calculated from (9a) is

$$\frac{d\tau^*}{dt} = -\frac{\lambda}{2.3\,(t + c)}\,. \tag{10}$$

Combining (6b) and (10), taking logarithms and differentiating, one obtains

$$\frac{d\log\dot{\gamma}}{dt} = -\frac{1}{2.3\,(t + c)}, \tag{11}$$

and from (10) and (11) it follows

$$\frac{d\tau^*}{d\log\dot{\gamma}} = \lambda\,. \tag{12}$$

The positive value of the slope of the logarithmic relaxation plot is the strain rate sensitivity of the stress. This result shows that $\lambda(\tau^*)$ as defined in (8) is constant and equal to λ and that the plot of τ versus $\log\dot{\tau}$ will also give a straight line.

The plastic strain rate at any time t during relaxation can be evaluated by combining (10) and (6b)

$$\dot{\gamma} = \frac{M\lambda}{2.3\,(t+c)} \tag{13}$$

or

$$\dot{\varepsilon}_p = \frac{M'\lambda'}{2.3\,(t+c)} \tag{13a}$$

if tensile strain is used.

The plastic strain rate $\dot{\varepsilon}_0$ at which the specimen is deforming under the imposed rate of extension of the machine, is determined by making $t = 0$ in (13) or (13a). The alternative way of calculating the strain rate is by measuring the slope $\dot{\sigma}$ of the relaxation curve and using (6).

The experimental relations (8) and (9) on which all the analysis has been based can be theoretically justified. If the deformation process can be described by the rate equation

$$\dot{\gamma} = A \cdot \exp - \left\{\frac{H - w\,\tau^*}{k\,T}\right\} \tag{14}$$

then (8) is immediately obtained from (14) if A, H and w are constant.[1])

Using (6b) the rate equation (14) can be integrated. Assuming again that A, H and w are constant, one obtains

$$\tau^* = \frac{H}{w} + \frac{k\,T}{w}\,l_n\left(\frac{M\,k\,T}{A\,w}\right) - \frac{kT}{w}\,l_n\,(t+c)\,, \tag{15}$$

which is of the same form as (9a). The integration constant c is given by

$$c = \frac{M\,k\,T}{A\,w}\exp\left\{\frac{H - w\,\tau_0^*}{k\,T}\right\}, \tag{16}$$

where τ_0^* is the effective stress at $t = 0$.

In both cases the well known relation

$$\lambda = \frac{2.3\,k\,T}{w} \tag{17}$$

between the strain rate sensitivity and the activation volume is obtained.

3. The Relation between Stress Relaxation and Creep

A creep experiment connected with the relaxation test can be carried out as follows: The specimen is deformed at a certain cross-head speed and, when the point $\sigma_0\ \varepsilon_0$ of the stress strain curve is reached, the speed of the cross-head is continuously varied in such a way as to maintain the applied stress constant. The amount dl that the specimen extends is entirely balanced by the displacement dy of the cross-head. This situation is described by (1) with the condition $\dot{l}_e = \dot{z} = 0$. Therefore, $\dot{y} = \dot{l}_p$ and it is possible to know the variation of l_p with time by following the variation of y.

---

[1]) A is a frequency factor including the entropy term, H the activation enthalpy, w the activation volume, k Boltzmann's constant and T absolute temperature.

It has been found experimentally [4] that the relation between strain and time during the creep process has the form

$$\varepsilon - \varepsilon_0 = -\delta' \log g + \delta \log (t + g) \tag{18}$$

or if shear strain γ is plotted instead of tensile strain

$$\gamma - \gamma_0 = -\delta \log g + \delta \log (t + g) . \tag{18a}$$

A relation between the relaxation parameter λ and the creep parameter δ has been derived by two different authors [4, 8]. They expressed the variation of the applied stress with time by the equation $d\tau/dt = (\partial\tau/\partial t)_\varepsilon + (\partial\tau/\partial\varepsilon)_t \, d\varepsilon/dt$. In their derivation both authors overlooked the condition that at constant strain $\partial\tau/\partial t$ must be zero; furthermore the equality $d\varepsilon/dt = 0$ was introduced as a condition during relaxation and it has already been made clear that during relaxation the strain is not constant.

To establish a satisfactory relation between stress relaxation and creep it is necessary to distinguish in the applied stress τ the thermal component τ^* and the long range internal stress τ_μ as in (7). For creep, $d\tau = 0$ and from (7) one obtains

$$d\tau^* = -d\tau_\mu . \tag{19}$$

Defining a work-hardening coefficient θ as $\theta = d\tau_\mu/d\gamma$ from (19) it follows that

$$d\gamma = -d\tau^*/\theta , \tag{20}$$

which with the relation derived from (18a),

$$\frac{d\gamma}{d \log (t + g)} = \delta , \tag{21}$$

yields

$$\frac{d\tau^*}{d \log (t + g)} = -\theta\delta . \tag{22}$$

The variation of the effective stress τ^* with $\log t$ given by (22) can be compared with that derived from (9a) to obtain

$$\lambda = \theta\, \delta . \tag{23}$$

Equation (23) simply states that the strain rate sensitivity measured from a relaxation test is the same as that measured from a creep test. This result is to be expected because in the proximity of the point $\sigma_0\, \varepsilon_0$ in the stress strain curve (not too large values of t) the same deformation process is taking place in both cases.

It is also evident, as Buck [8] already pointed out, that the coefficient θ would be equal to the work-hardening coefficient measured from the slope of the stress-strain curve if no thermally activated process contributes to the work-hardening.

If for the creep test the relation (18a) is experimentally verified then a plot of γ versus $\log \dot\gamma$ should give also a straight line of slope $-\delta$, for from the eqs. (12), (20) and (23) it follows that

$$-\frac{d\gamma}{d \log \dot\gamma} = \frac{d\tau^*}{\theta\, d \log \dot\gamma} = \frac{\lambda}{\theta} = \delta . \tag{24}$$

This linear relationship has also been experimentally established [9, 10].

A logarithmic creep equation of the same form as (18a) is obtained by integration of the rate equation (14). The relations (24) follow immediately from eq. (14). In both cases A, H and w in (14) must be assumed constant.

The relaxation test is rather easier to perform than the creep test, specially when an automatic load recording device is available, and it has been extensively used in our Department in the study of the plastic deformation of molybdenum single crystals. The few results that will be presented here are intended to show the practical application of the analysis, to discuss the sources of error, and to show how the errors can be accounted for.

4. Experimental Methods of Analysis

If a specimen is left to relax for a long time, the equilibrium state $\dot{\sigma} = 0$, $\dot{\varepsilon} = 0$ should be reached when $\tau = \tau_\mu$. It has been found, nevertheless, that in the case of molybdenum even after 14 hours no equilibrium has been attained. This result suggests that the possibility of a recovery process taking place should not be disregarded, and this would conflict with the hypothesis that τ_μ is constant during relaxation. To avoid this difficulty it is necessary to make the relaxation time as short as possible, and it has been found that a relaxation time of one minute is sufficient to obtain reliable results for molybdenum.

Plots of τ versus $\log (t + c)$ are shown in Fig. 2 and 3, with various values of c. The values of τ are corrected from the variation in cross section area during relaxation. It can be observed that a very good linear plot is obtained in some cases, whilst in other cases there is a departure from linearity at $t < 6$ s. In the same figures are also shown the plots of τ versus $\log t$ in order to illustrate the determination and effect of the constant c.

4.1 The effect of "machine relaxation"

If the relaxation test is reproduced with a stiff calibration piece replacing the specimen a certain amount of relaxation in some part of the machine takes place. The observed decrease in load with time has the following characteristic features: It increases with the applied load and with the speed of the cross-head, and is insensitive to work-hardening, i. e. it is always reproducible in magnitude.

When a test is performed at very low cross-head speeds (< 0.01 cm/min) the amount of machine relaxation is negligible, but at higher speeds (> 0.01 cm/min)

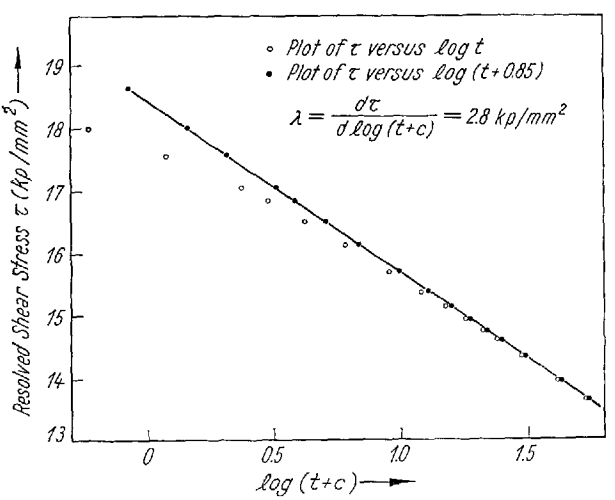

Fig. 2. Logarithmic representation of the relaxation curve obtained at the point A of the stress-strain curve represented in Fig. 5

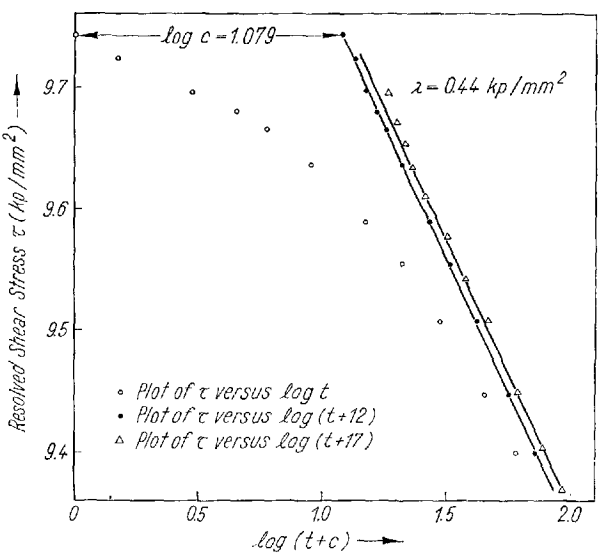

Fig. 3. Logarithmic representation of relaxation curves obtained at the same stress after straining at two different cross-head speeds.

○ and ● cross-head speed 0.01 cm/min, △ cross-head speed 0.1 cm/min.

A point △ with the coordinates (1.22; 9.75) must be added

can sometimes be relatively important compared with the relaxation of the specimen. In any case, after 3 to 6 s the amount of machine relaxation has become so small that it could be entirely neglected.[2])

As a result of this effect, in the first seconds of a relaxation test a certain amount of "anomalous" extension is superimposed on the extension of the specimen. If $\dot{p}$ is the variation in load produced by the machine relaxation then the relaxation rate of the machine is $\dot{p}/s$ and (4) should be written as

$$\dot{\varepsilon}_p + \dot{\varepsilon}_e = -\frac{\dot{P} - \dot{p}}{l_0 s} \tag{4a}$$

and instead of (6) one would obtain

$$\dot{\varepsilon}_p = -\left(M' - \frac{a_0}{l_0 s}\beta\right)\dot{\sigma}\,, \tag{6c}$$

where $\beta = \dot{p}/\dot{P} \leqq 1$ is the ratio between the variation in load due to machine relaxation and the observed variation in load during the test.

The variation in stress $\dot{\sigma}$ for a given deformation of the specimen (equation (6c)) is now larger than it would be in absence of any machine effects (equation (6)). The ratio $\beta = \dot{p}/\dot{P}$ which is variable with time and is zero after 3 to 6 s will destroy the linearity of (8) and (9). This is what is shown in one of the plots of Fig. 3. In this case, the constant c was chosen so as to fit a straight line from the smallest possible value of t. Whenever the ratio β is negligible at $t = 0$ no departure from the linearity is observed.

4.2 The strain rate sensitivity

For the calculation of the strain rate sensitivity, the relaxation method has clear advantages over the strain-rate-cycling test. Values of λ can be obtained in parts of the stress-strain curve that show a very large work hardening rate, and

[2]) The machine relaxation is less pronounced the softer is the machine, in accord with (6).

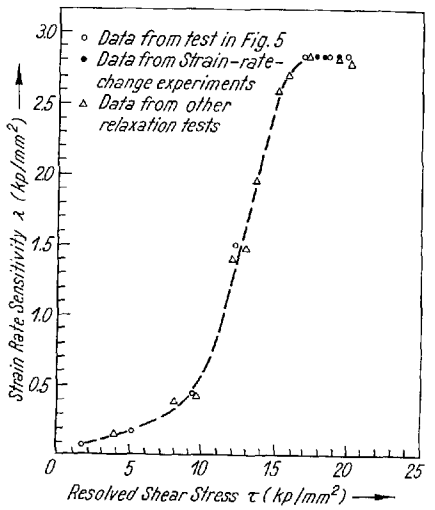

Fig. 4. Plot of strain rate sensitivity versus applied stress for molybdenum single crystals oriented in the ⟨110⟩ direction

even at stresses lower than the proportional limit. If the strain rate sensitivity is strongly stress dependent, with the relaxation test one obtains true values of λ instead of mean values. The amount of strain introduced in the determination of λ is very small and it is therefore possible to determine simultaneously the strain rate dependence and the temperature dependence of the flow stress.

In Fig. 4 are shown the values of λ as a function of the applied stress for a molybdenum single crystal with the tensile axis in the ⟨110⟩ direction, deformed at room temperature at a cross-head speed of 0.1 cm/min. The stress strain curve of this test (Fig. 5) shows the points at which the relaxation was carried out. Some values of λ obtained by the strain-rate-change method are also included in Fig. 4. The agreement between the values of λ determined by the two methods is always better than 1%.

Finite values of λ are obtained at stresses below the proportional limit, indicating that the specimen is undergoing some plastic deformation. The possibility of this relaxation at low stresses being produced by an anelastic process (for instance, reordering of interstitial atoms) does not seem likely since it is impossible to obtain a linear relation between t and $\log \tau$. This indicates that the relaxation is not described by an equation of the type

$$\tau - \tau_f = B \cdot \exp - \{t/t_0\}\,, \tag{25}$$

where B, τ_f and t_0 are constants, but by (9).

KEEFER and WERT [11] studying the reordering of interstitial N atoms in iron, used the relaxation method and found that the results could not be represented by (25). They could, nevertheless, separate the relaxation curve into a spec-

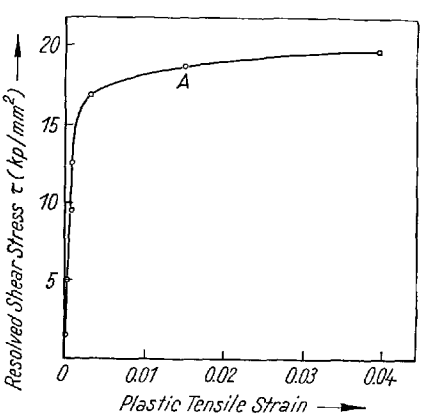

Fig. 5. Stress-strain curve of molybdenum single crystal oriented in the ⟨110⟩ direction, showing points where relaxation was carried out

trum of four different curves of the type of (25) each one characteristic of a different process. A similar procedure has not been tried with our results. The lowest values of the stress are not regarded as being significant, because deformation may have taken place at regions of high stress concentration. At higher values of the stress the large amount of relaxation observed can only be accomodated by plastic deformation.

4.3 The plastic strain rate

The plastic strain rate at any point in a stress-strain curve can be derived from the rate of variation of the load, the speed of the cross-head, and the constants of the testing machine. Combining (1), (3), and (5) one obtains for the plastic strain rate

$$\dot{\varepsilon}_p = \frac{\dot{y} - \dot{P}/s}{l_0} - \dot{P}/E\, a_0 \,. \tag{26}$$

The plastic strain rate calculated from the relaxation curve using (13a) at time $t = 0$ should be equal to that obtained from the stress-strain curve at the stress σ_0 chosen for relaxation.

When the test is carried out at cross-head speeds of the order of 0.01 cm/min, the values of the strain rate calculated from (13a) agree very well with those calculated from (26). The agreement is not so good for very low strains when the test is performed at cross-head speeds of the order of 0.1 cm/min.

There are two important sources of error in this last case. At low strains the ratio $\dot{P}/s$ can only be measured within an accuracy of $\pm$ 8%, but its value is so close to the value of $\dot{y}$ that the error of the difference $\dot{y} - \dot{P}/s$ is of the order of $\pm$ 30%. At the same time, at low strains and large cross-head speeds the ratio $\beta = \dot{p}/\dot{P}$ is rather large ($\sim$0.3) and too large values of c are obtained in the non linear logarithmic plot (Fig. 3). Equation (13a) gives then too small values of $\dot{\varepsilon}_p$. Here the sign of the error is known and $\dot{\varepsilon}_0$ can be obtained more accurately by measuring directly the slopes $\dot{P}$ and $\dot{p}$ of the relaxation curves at $t = 0$ and using (6c).

When the errors are taken into account, once again good agreement between the two methods is found.

The agreement between results obtained by the different experimental methods serves to confirm the validity of the analysis and interpretation given to the relaxation phenomenon.

Acknowledgements

The authors would like to thank Professor J. G. Ball for providing research facilities in the Department of Metallurgy and the C.E.G.B. and D.S.I.R. for generous financial support.

References

[1] C. Zener, Elasticity and Anelasticity of Metals, University of Chicago Press, Chicago 1948.
[2] K. M. Entwistle, Met. Rev. **7**, 175 (1962).
[3] P. Feltham, J. Inst. Metals **89**, 210 (1961).
[4] P. Feltham, Phil. Mag. **6**, 259 (1961).

[5] P. FELTHAM, Phil. Mag. **6**, 847 (1961).
[6] P. FELTHAM, phys. stat. sol. **3**, 1340 (1963).
[7] F. GUIU, unpublished results.
[8] O. BUCK, phys. stat. sol. **3**, 1903 (1963).
[9] H. CONRAD, L. HAYS, G. SCHOECK, and H. WIEDERSICH, Acta metall. **9**, 367 (1961).
[10] R. J. ARSENAULT, Acta metall. **12**, 547 (1964).
[11] D. KEEFER, and C. WERT, Acta metall. **11**, 489 (1963).

(Received April 8, 1964)